THE DEVELOPMENT AND MODELLING OF HIGH INTENSITY IMPINGING STREAM JET REACTORS FOR ENHANCED MASS TRANSFER IN GAS-LIQUID SYSTEMS

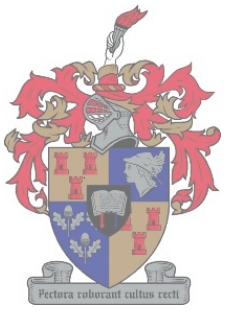

by

Anton W. Kleingeld

A thesis submitted in partial fulfilment of the requirements for the degree

Master of Science in Engineering
(Chemical Engineering)

at the Department of Chemical Engineering,
University of Stellenbosch

Supervisor: Prof. L. Lorenzen

STELLENBOSCH

DECEMBER 1999

DECLARATION

I, the undersigned, hereby declare that this thesis is my own original work, except where specifically acknowledged in the text. Neither the present dissertation, nor any part thereof, has previously been submitted for a degree at any university.

Anton W. Kleingeld
December 1999

SUMMARY

In the majority of gas-liquid contacting systems the kinetics of the heterogeneous chemical reaction is not limited by its intrinsic reaction rate, but by the transport of gas to the liquid phase and hence by the overall interfacial area available for mass transfer. These rates in turn limit productivity and are thus a critical design consideration. In view of this, novel high intensity impinging stream reactors have been developed at this institution for intensification of these mass transfer processes.

The reactors are characterised by small reactor volumes supplied with nozzles, which are directed towards one another. The gas and liquid feed streams are jetted through the nozzles into the reactor volume, resulting in a highly turbulent mixture of phases. Under these enhanced mixing conditions, mass transfer rates are increased dramatically.

Evaluation of mass transfer parameters exhibited by the three different reactor configurations investigated showed that the mass transfer coefficient (k_L) could be enhanced substantially by centrifugal acceleration of the fluid and more efficient promotion of turbulence in the round reactor chambers of the π- and σ-shaped reactors, compared to that of the kite-shaped reactor. However, it was also found that the jagged/angular reactor chamber of the kite-shaped reactor exhibited higher values of the interfacial area (a) due to more effective bubble break-up mechanisms and higher relative gas hold-ups. It was therefore concluded that an optimum reactor design would combine the kL-enhancing effects of the swirling flow in the σ-shaped reactor, with the bubble break-up and gas hold-up ability of the kite-shaped reactor.

Comparison of experimental results with literature data for conventional systems also revealed that, in terms of both the mass transfer coefficient and the value of the interfacial area per unit of energy dissipated in the reactor, the proposed reactors provide a significant improvement in mass transfer

performance. It is thus suggested that the newly developed impinging stream reactors have the potential to represent superior alternatives to conventional gas-liquid contacting equipment.

The fundamental model for the prediction of interfacial area production in the jet reactors originally proposed by *Botes* (1995) was also improved and expanded, resulting in more accurate prediction of trends in interfacial area as a function of various process variables.

The model, and its associated bubble breakage mechanism, was verified at the hand of additional absorption data and alternative bubble breakage mechanisms proposed in the literature. Very good results were obtained, so that it could be concluded that the model is very flexible and can be applied over a relatively wide range of hydrodynamic operating conditions, validating the potential application thereof in other turbulent gas-liquid systems.

Considering the above conclusions, recommendations could finally be made as to how the performance of the reactors could be improved further: liquid nozzles with larger orifices should be used for optimisation of the energy efficiency of the reactors. The use of gas nozzles with smaller orifices would additionally result in higher linear gas velocities, improving the efficiency of impingement of gas into liquid streams.

SINOPSIS

In die meerderheid gas-vloeistof kontaksisteme word die kinetika van die heterogene chemiese reaksie nie beperk deur die intrinsieke reaksietempo nie, maar deur die vervoer van gas na die vloeistoffase en derhalwe deur die totale interfase area beskikbaar vir massa-oordrag. Hierdie tempos beinvloed op hul beurt weer produktiwiteit en is dus 'n kritieke ontwerpsoorweging. In die lig hiervan is nuwe hoë intensitiet spuitreaktore by hierdie instituut ontwikkel vir die intensifisering van hierdie massa oordragsprosesse.

Die reaktore word gekaraktiseer deur klein reaktorvolumes wat toegerus is met spuitstukke wat opponerend ten opsigte van mekaar georiënteer is. Die gas en vloeistof voerstrome word deur die spuitstukke in die reaktorvolume ingespuit, met die gevolg dat daar 'n hoogs turbulente twee-fase mengsel ontstaan. Onder sulke turbulente vermengingskondisies word die tempo van massa oordrag aansienlik verhoog.

'n Evaluasie van die massa-oordragsparameters wat deur die drie verskillende reaktor konfigurasies vertoon is, het getoon dat die massa-oordragskoeffisient (k_L) aansienlik verbeter kan word deur sentrifugale versnelling van die vloeier en meer effektiewe bevordering van turbulensie in die ronde reaktor volume van die π- en σ-vormige reaktore, in vergelyking met die vlieër-vormige reaktor. Daar is egter ook bevind dat die hoekige vorm van die vlieër-vormige reaktor hoër waardes vir die interfase area (a) vertoon deur meer effektiewe borrel-breek meganismes en hoër relatiewe gas retensie volumes. Derhalwe is die gevolgtrekking gemaak dat die optimale reaktorontwerp die k_L-verbeteringsvermoë van die malende vloei in die σ-vormige reaktor en die borrel-breek en gas-retensie vermoë van die vlieër-vormige reaktor sal kombineer.

Vergelyking van eksperimentele resultate met data uit die literatuur vir konvensionele sisteme het verder getoon dat, in terme van beide die massa-

oordragskoeffisient en die interfase area per eenheid energie verbruik, die voorgestelde reaktore 'n aansienlike verbetering in massa oordragsvermoë bied. Dit word derhalwe voorgestel dat die nuwe spuitreaktore die potensiaal besit om uitstaande alternatiewe vir gas-vloeistof kontak te verteenwoordig.

Die fundamentele model vir die voorspelling van die interfase area produksie in die spuitreaktore soos voorgestel deur *Botes* (1995) is ook verbeter en uitgebou. So is meer akkurate voorspelling van die tendense in interfase area as funksie van verskillende prosesveranderlikes verkry.

Die model, en sy geassosieerde borrel-breek meganisme, is ook geverifieer deur middel van addisionele absorpsie data en alternatiewe borrel-breek meganismes soos voorgestel in die literatuur. Baie goeie resultate is verkry, sodat die gevolgtrekking gemaak kan word dat die model baie buigbaar oor 'n redelike wye gebied van hidrodinamiese bedryfstoestande is. Die potensiële toepassing daarvan in ander turbulente gas-vloeistof kontaksisteme is derhalwe gestaaf.

Met inagneming van die bogenoemde gevolgtrekkings, kon voorstelle ook gemaak word aangaande die verbetering van reaktor werkverrigting: vloeistof spuitstukke met groter openinge kan gebruik word vir optimering van die energy-effektiwiteit van die reaktore. Verder kan die gebruik van gas spuitstukke met kleiner openinge gebruik word vir hoër lineêre gas snelhede, wat die penetrasie van gas in vloeistof strome sal verbeter.

ACKNOWLEDGEMENTS

The work presented in this dissertation was carried out at the Department of Chemical Engineering of the University of Stellenbosch, South Africa.

I wish to express my most sincere appreciation to:

- SASOL, for their financial backing of myself and the project.
- My supervisor, Professor L. Lorenzen, for his guidance, motivation and support during the course of the project.
- All the technical and workshop personnel, in particular Mr J. Barnard and Mr A. Cordier, as well as Mrs H. Botha for her invaluable assistance in analyses of samples.
- My friends and colleagues, without whom this study would have been nothing else but work.
- The Lord, my God – most importantly.

DEDICATION

This dissertation is dedicated to my stepfather, Dr. W.B.H. Swanepoel, who died tragically on 9 June 1999. He was the only father I ever knew. *Dankie Pa.*

CONTENTS

Declaration i

Summary ii

Sinopsis iv

Acknowledgements vi

Dedication vii

Contents viii

List of tables xv

List of figures xvii

Nomenclature xxii

CHAPTER 1
INTRODUCTION

1.1 GAS-LIQUID CONTACTING 1
1.2 IMPINGING STREAM TECHNOLOGY 2
1.3 MODELLING OF GAS-LIQUID MIXING SYSTEMS 3
1.4 OBJECTIVES OF THIS STUDY 4

CHAPTER 2
LITERATURE REVIEW

2.1 CONVENTIONAL AND NOVEL GAS-LIQUID CONTACTING SYSTEMS 6
2.1.1 Venturi scrubbers 7
2.1.2 Centrifugal contactors 9
2.1.2.1 High intensity contactors 9

2.1.2.2 Gas-liquid cyclones 13
2.1.3 Jet loop absorbers 14
2.1.4 Impinging stream reactors 16
2.1.4.1 A short background to impinging streams 16
2.1.4.2 The essence of impinging streams 17
2.1.4.3 Impinging stream jet loop reactors (IS_JLR's) 17
2.1.4.4 Impinging stream absorbers 19

2.2 PREVIOUS RESEARCH ON IMPINGING STREAM CONTACTORS AT THIS INSTITUTION 23

2.3 MODELLING OF GAS-LIQUID PROCESSES 26
2.3.1 Fundamental modelling of processes 27
2.3.1.1 Population balances and Monte Carlo simulations 27
2.3.1.2 Kolmogoroff's theory of isotropic turbulence 29
2.3.1.3 Breakage and coalescence models 31
2.3.1.3.1 Bubble breakage models 31
2.3.1.3.2 Bubble coalescence models 36
2.3.2 Empirical modelling of design parameters 38
2.3.2.1 Bubble size 38
2.3.2.2 Interfacial area 41
2.3.2.3 Gas hold-up 42
2.3.2.4 Mass transfer coefficient 43
2.3.2.5 Volumetric mass transfer coefficient 45

2.4 FINAL REMARKS ON THE LITERATURE SURVEY 46

CHAPTER 3
EXPERIMENTAL

3.1 CHEMICAL SYSTEMS 51
3.1.1 Choosing a suitable chemical system 51
3.1.2 Chemical systems employed 53

3.1.2.1 Absorption of CO_2 53
3.1.2.2 Oxidation of sulphite solutions 55

3.2 ANALYSIS TECHNIQUES 57
3.2.1 CO_2 absorption 57
3.2.2 Oxidation of sulphite solutions 58

3.3 EXPERIMENTAL SET-UP AND PROCEDURE 59
3.3.1 Liquid feed preparation 59
3.3.1.1 CO_2 absorption 59
3.3.1.2 Sulphite oxidation 60
3.3.2 Gas feed preparation 60
3.3.2.1 CO_2 absorption 60
3.3.2.2 Sulphite oxidation 61
3.3.3 Experiment start-up and execution 61
3.3.3.1 CO_2 absorption 61
3.3.3.2 Sulphite oxidation 63
3.3.4 Reactor designs 64

CHAPTER 4
DETERMINATION OF THE MASS TRANSFER PARAMETERS

4.1 PRINCIPLES OF GAS ABSORPTION AND MASS TRANSFER 69
4.1.1 Diffusion and chemical reaction in quiescent liquids 69
4.1.2 Absorption models 72
4.1.2.1 The film model 72
4.1.2.2 'Still surface' models 73
4.1.2.3 Surface renewal models 74
4.1.2.4 Other models 76
4.1.3 Diffusion and chemical reaction in agitated liquids 77
4.1.3.1 The film model 77
4.1.3.2 Higbie model 79
4.1.3.3 Danckwerts model 80

4.2 REVIEW OF BOTES'S TECHNIQUE 81

4.3 VERIFICATION OF BOTES'S TECHNIQUE 83

4.4 CONCLUSIONS 86

CHAPTER 5
DISCUSSION OF EXPERIMENTAL RESULTS

5.1 THE BUBBLE SIZE AND GAS VOIDAGE FRACTION 87
5.1.1 CO_2 absorption 88
5.1.1.1 Determination of bubble size and gas voidage fraction 88
5.1.1.2 Gas voidage 90
5.1.1.3 Bubble size 92
5.1.2 Sulphite oxidation 93
5.1.2.1 Gas voidage 93
5.1.2.2 Bubble size 94
5.1.3 Comparison with literature data and conclusions 95

5.2 THE MASS TRANSFER COEFFICIENT 97
5.2.1 CO_2 absorption results 97
5.2.1.1 Interpretation of results 97
5.2.1.2 Comparison with literature data 105
5.2.1.3 Empirical correlation of k_L 107
5.2.2 Sulphite oxidation results 110

5.3 THE INTERFACIAL AREA 112
5.3.1 CO_2 absorption 112
5.3.2 Sulphite oxidation 117
5.3.3 Comparison with literature data 118
5.3.4 Empirical modelling 122

5.4 THE VOLUMETRIC MASS TRANSFER COEFFICIENT 125
5.4.1 CO_2 absorption 125
5.4.2 Sulphite oxidation 129
5.4.3 Comparison with literature data 130
5.4.4 Empirical modelling 133

5.5 CONCLUSIONS 135

CHAPTER 6
DEVELOPMENT AND EVALUATION OF A FUNDAMENTAL MODEL FOR THE PREDICTION OF INTERFACIAL AREA PRODUCTION IN HIGH INTENSITY REACTORS

6.1 MODEL DEVELOPMENT 137
6.1.1 The size of bubbles entering the reactor 138
6.1.2 Bubble break-up rates 141
6.1.2.1 The collision rate between bubbles and eddies 141
6.1.2.2 The collision efficiency between bubbles and eddies 144
6.1.2.3 Bubble breakage rate equations 146
6.1.3 Bubble coalescence rates 149
6.1.3.1 The collision rate between two bubbles 150
6.1.3.2 The coalescence efficiency between two bubbles 150
6.1.4 Bubbles exiting the reactor 151

6.2 MODEL IMPLEMENTATION 152
6.2.1 Declaration and calculation of the input parameters 153
6.2.2 Discretisation of bubble and eddy size distributions 155
6.2.3 Specifying the time interval 156
6.2.4 Simulation of interfacial area production 157
6.2.5 Repetition of the simulation cycle 158

6.3 MODEL EVALUATION 159

6.3.1 Evaluation of changes made to the model 160
6.3.1.1 Gas hold-up 160
6.3.1.2 Maximum stable bubble size 161
6.3.1.3 Bubble coalescence 162
6.3.2 Comparison between model and experimental data 163
6.3.2.1 Summing of bubble breakage events 163
6.3.2.2 Model verification with sulphite oxidation data 168
6.3.2.3 Model verification with alternative breakage rate equations 171
6.3.3 Sensitivity analysis 175
6.3.3.1 Performing the sensitivity analysis 175
6.3.3.2 The influence of physical properties on the model output 176
6.3.3.3 The influence of the flow conditions of the feed streams on the model output 177
6.3.3.4 The influence of the hold-up characteristics on the model output 178
6.3.3.5 The influence of the free parameters on the model output 179

6.4 CONCLUSIONS AND RECOMMENDATIONS 181

CHAPTER 7
CONCLUSIONS AND RECCOMENDATIONS

7.1 CONCLUSIONS DRAWN FROM THE CURRENT PROJECT 184

7.2 ACHIEVEMENT OF PROJECT OBJECTIVES 187

7.3 RECOMMENDATIONS REGARDING FURTHER RESEARCH 188
7.3.1 Future experimental research 188
7.3.2 Future model development 190

REFERENCES 193

APPENDIX A

ALGORITHM OF MODEL SIMULATION: APPROACH A

APPENDIX B

ALGORITHM OF MODEL SIMULATION: APPROACH B

APPENDIX C

TYPICAL EXAMPLE OF THE SIMULATION MODEL

APPENDIX D

PUBLICATIONS FROM THIS DISSERTATION

LIST OF TABLES

2.1	Comparison of mass transfer parameters for known absorption reactors and impinging jet absorbers	22
2.2	Comparison of the performances of the three final reactors	26
3.1	Range of operating conditions used for CO_2 absorption experiments	63
3.2	Range of operating conditions used for sulphite oxidation experiments	64
4.1	Explicit formulae for the enhancement factor E	84
4.2	An example of the correlation between enhancement factors predicted by Botes's and other methods	85
5.1	Bubble size correlations investigated	89
5.2	Gas voidages calculated for the reactors investigated	91
5.3	Gas voidages exhibited by the σ-shaped reactor for the sulphite oxidation system	93
5.4	Ranges of interfacial areas produced in the different reactors	112
5.5	Determining the functional dependence of the interfacial area on energy dissipation	120
5.6	Correlation of experimental data against energy dissipation and gas flow rate	123

5.7 Determining the functional dependence of the interfacial area on gas flow rate 124

5.8 Determining the functional dependence of k_La on energy dissipation and gas flow rate 133

5.9 Correlation of experimental k_La data against energy dissipation and gas flow rate 134

6.1 Comparison of bubble breakage rate equations based on the correlation between experimental and predicted interfacial areas 171

6.2 Comparison of bubble breakage rate equations based on the deviation (%) between experimental and predicted average bubble sizes 172

6.3 The response of a 10% change in the physical properties of the system on the predicted interfacial area and average bubble size 176

6.4 The response of a 10% change in the feed flow conditions of the system on the predicted interfacial area and average bubble size 177

6.5 The response of a 10% change in the hold-up characteristics of the system on the predicted interfacial area and average bubble size 179

6.6 The response of a 10% change in the free parameters specified in the system on the predicted interfacial area and average bubble size 180

LIST OF FIGURES

2.1	Venturi ejector reactor	8
2.2	Venturi/Bubble column combination	9
2.3	High intensity contactor	10
2.4	Gas-liquid hydrocyclone	13
2.5	Jet loop reactor	15
2.6	Impinging stream jet loop reactor	18
2.7	Investigating the intensification effects of impinging streams	20
2.8	Preliminary reactors	49
2.9	Final reactors	50
2.10	Energy distribution function $E(k,t)$ in the various wavenumber ranges	29
3.1	Experimental set-up	67
3.2	Reactors investigated	68
3.3	Possible flow patterns in the π-shaped reactor	65
4.1	Enhancement factors for a second-order reaction (film or Higbie models)	78

5.1 A comparison of the predicted values of the gas voidage as a function of the liquid flow rate 89

5.2 The effect of gas flow rate on the voidage fraction for the kite and π- and σ-shaped reactors 91

5.3 Comparison of average bubble sizes exhibited in the kite and π- and σ-shaped reactors as a function of the liquid and gas flow rates 92

5.4 Comparison of average bubble sizes exhibited in the σ-shaped reactor as a function of the liquid and gas flow rates 95

5.5 Comparison of generated data with data from the literature, based on energy consumption 96

5.6 The effect of liquid and gas flow rates on the value of the mass transfer coefficient for a pseudo-first order reaction 100

5.7 The effect of liquid and gas flow rates on the mass transfer coefficient in the kite-shaped reactor 101

5.8 The effect of liquid and gas flow rates on the mass transfer coefficient in the π-shaped reactor 101

5.9 The effect of liquid and gas flow rates on the mass transfer coefficient in the σ-shaped reactor 102

5.10 Comparison of the ranges of the mass transfer coefficients for different investigations as a function of the energy consumption of the system 106

5.11 Correlating the effect of energy dissipation on the mass transfer coefficient for a constant gas flow rate 108

5.12 Correlating the effect of energy dissipation on the mass transfer coefficient for a constant liquid flow rate 109

5.13 Investigating the effect of energy dissipation on the mass transfer coefficient 110

5.14 The effect of temperature on the mass transfer coefficient exhibited during the sulphite oxidation experiments 111

5.15 The effect of liquid and gas flow rates on interfacial area in the kite-shaped reactor 113

5.16 The effect of liquid and gas flow rates on interfacial area in the π-shaped reactor 113

5.17 The effect of liquid and gas flow rates on interfacial area in the π-shaped reactor 114

5.18 Comparison between the interfacial areas produced in the three reactors as a function of the energy dissipation rate 115

5.19 The effect of liquid and gas flow rates on the interfacial area in the σ-shaped reactor for the sulphite oxidation system 118

5.20 Comparison of experimental interfacial area results with data reported in the literature 120

5.21 The effect of liquid and gas flow rates on the volumetric mass transfer coefficient in the kite-shaped reactor 126

5.22 The effect of liquid and gas flow rates on the volumetric mass transfer coefficient in the π-shaped reactor 126

5.23 The effect of liquid and gas flow rates on the volumetric mass transfer coefficient in the σ-shaped reactor 127

5.24 Comparison between the volumetric mass transfer coefficients exhibited in the three reactors as a function of the energy dissipation rate 128

5.25 The effect of liquid and gas flow rates on the volumetric mass transfer coefficient for the sulphite oxidation system in the σ-shaped reactor 129

5.26 Comparison of experimental k_La values with those obtained from the literature 130

5.27 Comparison between absorbers 132

6.1 Illustration of the improvement in the model prediction of interfacial area trends with better specification of gas hold-up 160

6.2 Comparison of predicted trends in the maximum stable bubble diameter 162

6.3 Comparison of model and experimental data (π- and σ-shaped reactors) for summing of bubble breakage events (approach A) 164

6.4 Comparison of model and experimental data (kite-shaped reactor) for summing of bubble breakage events (approach A) 165

6.5 Comparison of model and experimental data for separate bubble breakage events in each class (approach B) 166

6.6 A typical example of a bubble size distribution as a function of the gas flow rate, generated by approach A 166

6.7 A typical example of a bubble size distribution as a function of the gas flow rate, generated by approach B 167

6.8 Comparison of model and experimental data for the sulphite oxidation system in the σ-shaped reactor (approach A) 169

6.9 Comparison of model and experimental data for the sulphite oxidation system in the σ-shaped reactor (approach B) 169

6.10 Bubble size distribution curves predicted by the bubble breakage rate model of Coulaloglou and Tavlarides (1977) 173

6.11 Bubble size distribution curves predicted by the bubble breakage rate model of Hesketh et al. (1991) 173

6.12 Bubble size distribution curves predicted by the bubble breakage rate model of Luo and Svendsen (1996) 174

NOMENCLATURE

a	Interfacial area per unit volume of reactor	m^2/m^3
A	Area	m^2
C	Concentration	mol/l
c	Arbitrary constant	-
C_A^*	Concentration of dissolved gas A at interface, in equilibrium with gas at the interface	mol/l
C_{AO}	Concentration of dissolved gas A in the bulk of the liquid	mol/l
C_{BO}	Concentration of dissolved reagent B in the bulk of the liquid	mol/l
d	Diameter	m
D	Diffusivity	m^2/s
D_A	Diffusivity of dissolved gas A in the liquid phase	m^2/s
D_B	Diffusivity of dissolved reagent B in the liquid phase	m^2/s
$d_{b,i}$	Diameter of bubbles entering the reactor	m
$d_{b,max}$	Maximum stable diameter of bubbles	m
e	Energy of one eddy	J
E	Enhancement factor	-
E_i	Enhancement factor for an instantaneous chemical reaction	-
E_1, E_2	Enhancement factors of the two experimental runs performed at the same operating conditions	-
$\overline{E}$	Average kinetic energy of eddies of a certain diameter	$kg.m^2/s^2$
$\dot{E}$	Rate of energy input into the reactor	kgm^2/s^2
E_c	Critical kinetic energy of an eddy needed to rupture a bubble	$kg/m^2/s^2$

F	Mass flux (net rate of transfer of a diffusant across a plane of unit area)	$kmol/m^2.s$
F	Force pressing two bubbles together	$kg.m/s^2$
f_{BV}	Bubble breakage fraction	-
h	Film thickness	m
h_o, h_f	Initial and final film thicknesses	m
H_{OL}	Height of an overall liquid transfer unit	m
k	Wavenumber	m^{-1}
k_1	First-order reaction rate constant	s^{-1}
k_2	Second-order reaction rate constant	l/mol.s
K_e	Constant parameter used for the calculation of the critical velocity, i.e. bubble break-up efficiency	-
K_f	Constant parameter used for the calculation of the size of bubbles entering the reactor	m
K_m	New constant parameter used for calculation of the maximum stable bubble diameter	m
k_L	Liquid film mass transfer coefficient	m/s
$\dot{m}$	Mass flow rate	kg/s
n	Number of eddies or bubbles per unit reactor volume	m^{-3}
$N_{b,e}$	Number of effective collisions, occurring during a chosen time interval, between bubbles and eddies, or two bubbles	-
$\dot{n}$	Absorption rate per unit volume of reactor	mol/l.s
$\dot{N}$	Absorption rate	mol/s
$n_{b,i}$	Number of bubbles entering the reactor in one simulation cycle	-

P	Pressure	Pa
P_B	Bubble breakage probability	-
P_R	Pressure inside the reactor	Pa
r	Radius	m
R	Chemical reaction rate per unit volume	mol/l.s
r_{12}	Equivalent radius of two coalescing bubbles	m
r_o	Orifice radius	m
s	fractional rate of surface renewal	s^{-1}
$S_{b,e}$	Collision cross-sectional area between bubbles and eddies	m^2
Sc	Schmidt number	-
t	Time	s
Δt	Incremental time	s
t_c	Coalescence time	s
T	Temperature	K
u	Velocity	m/s
$\overline{u^2}$	Average of the square of the velocity fluctuations	m^2/s^2
$U_{b\infty}$	Terminal rising velocity of a bubble	m/s
u_c	Critical velocity needed by an eddy to effect bubble break-up	m/s
$u_{G,O}$	Superficial orifice gas velocity	m/s
U_{sg}	Gas superficial velocity	m/s
υ_o	friction velocity	m/s
$\dot{V}$	Volumetric flow rate	m^3/s
V_G	Gas volume or gas hold-up	m^3
V_L	Liquid volume or liquid hold-up	m^3
V_R	Reactor volume	m^3
V_{total}	Combined volume of all the bubbles in the reactor	m^3

We	Weber number	-
$We_{critical}$	Critical Weber number	-
x	Arbitrary distance	m
Y	Fraction of eddies of a certain diameter with kinetic energy higher than the critical value needed for bubble break-up	-
z	Stoichiometric constant	-

Greek symbols

α	Arbitrary constant of Kolmogoroff's (-5/3)-law	-
α	Arbitrary exponent in a correlation	-
β	Arbitrary exponent in a correlation	-
ε	Energy dissipation rate per mass of liquid	m^2/s^2
θ	Collision rate per unit volume	$m^{-3}.s^{-1}$
θ	Time of exposure of liquid to gas	s
μ	Dynamic viscosity	kg/m.s
ν	Kinematic viscosity of the liquid	m^2/s
ρ	Density	kg/m^3
σ	Surface tension of liquid	kg/s^2
λ	Eddy diameter	m
Ω	Effective collision rate per unit volume	$m^{-3}.s^{-1}$
ω	Revolutions	s^{-1}
ϕ	Voidage fraction	-
ζ	Coalescence efficiency	-
τ	Bubble contact time	s
δ	Thickness of diffusion film	m

Λ	Average frequency of eddies arriving at a bubble surface	s^{-1}

Functions

E(k)	Spectral energy density function denoting distribution of energy over a spectrum of eddy wavelengths
N(k)	Number distribution function denoting the distribution of number of eddies over a spectrum of eddy wavelengths
$\chi(k)$	Energy density function denoting distribution of energy amongst eddies of the same diameter.

Subscripts

C,c	Continuous phase
D,d	Dispersed phase
G,g	Gas phase
L,l	Liquid phase
b	Bubble
e	Eddy

CHAPTER 1

INTRODUCTION

'A man must carry knowledge with him if he would bring home knowledge'

- Samuel Johnson, 1709 – 1784

In the light of this quotation, a thorough knowledge of the motivation behind any research project is essential for realisation of its objectives. Thus, it is the object of this chapter to introduce research in the field of impinging stream (IS) technology and motivate its use in the current investigation for intensification of gas-liquid contacting. Different modelling approaches applied for describing these systems will also be evaluated. Finally, the objectives set for this study will be presented.

1.1 GAS-LIQUID CONTACTING

Multiphase reactors, with special reference to gas-liquid systems, play a key role in chemical and biochemical process industries as is evident in the application of spray columns, packed columns and bubble columns in diverse processes such as gas scrubbing operations, liquid phase reactions (e.g. oxidation and sulfonation) and aerobic fermentations (*Gianetto and Silveston*, 1986).

In the majority of these systems the kinetics of the heterogeneous chemical reaction is not limited by its intrinsic reaction rate, but by the transport of gas to the liquid phase and hence by the overall interfacial area available for mass transfer. These rates in turn limit productivity and are thus a critical design consideration. In the light of this, a lot of research has been devoted to the design and development of reactors that promote intense, turbulent mixing of

phases whereby high shear rates are generated that promote interfacial area production and mass transfer due to enhanced bubble break-up and surface renewal. Although the introduction of venturis and various jet loop reactors have provided better results than conventional systems to some extent, they have as yet failed to fully realise the advantages of highly turbulent contacting of phases.

Research in the field of impinging stream jet reactors has, however, provided a means to do just this. Publications by *Elperin* (1961), *Herskowits et al.* (1990a and 1990b) and *Tamir* (1994) provide evidence of the intensification of mass and heat transfer processes in heterogeneous systems with the use of this technology, claiming that *'almost any process in chemical engineering can be carried out by applying impinging stream technology; most likely with a higher efficiency and a lower power input in comparison to conventional methods'* (*Tamir*, 1994). Of course, this will need to be evaluated at the hand of important factors such as the cost and availability of energy.

In the light of this, research into enhanced gas-liquid contacting using IS technology was initiated by *Botes* (1995) and *Botes et al.* (1998) at this institution. Investigating various reactor geometries and nozzle configurations, it was found that mass transfer coefficients and interfacial areas of orders of magnitude higher than those exhibited by conventional equipment could be realised. Continued research and development of these reactors were therefore warranted in the current investigation for further optimisation of the intensification effects inherent to these reactors. These aspects are discussed more broadly in *Chapters 3* and *5*.

1.2 IMPINGING STREAM TECHNOLOGY

Impinging stream technology has been implemented in what used to be known as the USSR since the mid 1960's in processes such as the drying of solid particles and solutions, combustion of gases, creation of emulsions and evaporative cooling of air (*Elperin*, 1961). Further research in Israel,

principally by *Tamir* (1994) and *Herskowits* (1990a and 1990b), has led to broader applications of this technology which is increasingly being developed and expanded into different configurations (based on performance and design considerations) such as swirling IS reactors (analogous to the working of a hydrocyclone) and jet loop reactors (*Gaddis* and *Vogenpohl*, 1992; *Prasad* and *Ramanujam*, 1995).

The essence of impinging streams lies in the penetration of particles into opposing streams, resulting in increased shear and relative velocities, increased particle (bubble) hold-up and mean residence times, as well as a higher probability for interparticle collisions due to multiple circulation of particles. This translates into a decrease in the geometric size of the system. Furthermore, due to the velocities of the entering streams, shear forces and pressure pulsations (in the continuous phase) result in increased bubble break-up, leading to increases in interfacial area and mass transfer rates, due to higher rates of surface renewal. These intensification effects inherent to IS technology, will be discussed in greater detail in *Chapter 2*.

1.3 MODELLING OF GAS-LIQUID MIXING SYSTEMS

Due to the complexity associated with the modelling of dispersion properties of gas-liquid systems such as bubble size distributions, interfacial area and bubble interaction rates, modelling of these processes have conventionally relied on empirical correlations. Although some of these are quite sound, others are indistinct and questionable, and cannot be confidently applied beyond the narrow range of operating conditions and geometries over which they were determined.

Fundamental modelling techniques which lend themselves to better understanding of these systems via modelling of single particle behaviour, have therefore received increasing attention. Fairly extensive research in the areas of bubble size and motion in bioreactors, bubble columns and stirred, aerated systems has been performed to gain insight into the interactions

between bubble break-up and coalescence mechanisms, which directly determine the equilibrium bubble size distribution and therefore interfacial area. Consequently, the results from research in these areas can be used and adapted to suit this specific application since the principles applicable to these areas of research share a common theoretical basis.

In this regard, population balances and Monte Carlo simulations have provided the simplest and most flexible tools for implementation of these mechanisms (*Ramkrishna*, 1981). Due to their ability to generate random numbers which can be substituted into calculated probability functions (e.g. whether a bubble will break up), Monte Carlo simulations in particular have extensively been used for description of gas-liquid dispersed phase properties.

In view of this, a fundamental model for the prediction of interfacial area production in the newly developed IS jet reactors was developed by *Botes* (1995) in the form of a Monte Carlo simulation – this has been improved and expanded in the current study. The development, implementation and evaluation of this model will be discussed in detail in *Chapter 6*. In addition to this, empirical correlation of design parameters is used for identification and verification of the effects of various operating parameters on reactor performance – these will be presented as part of the discussion of experimental results in *Chapter 5*.

1.4 OBJECTIVES OF THIS STUDY

Since the main aim of this study was the continued development and validation of the work performed by *Botes* (1995), the specific objectives set out for this project were as follows:

1. Further development of new reactor designs for optimum mass transfer efficiency, taking into account the conclusions made by *Botes* (1995)

regarding the most significant aspects of reactor configuration determining mass transfer performance.

2. Comparison of the newly developed jet reactors with conventional phase contacting equipment based on mass transfer performance and energy considerations. It was necessary to ascertain whether the higher relative energy consumptions associated with the proposed jet reactors indeed yielded superior mass transfer performance.

3. Improvement of Botes's fundamental model with specific reference to the size of bubbles entering the reactor, the gas hold-up and the incorporation of bubble coalescence.

4. Verification of the general applicability of the model against additional interfacial area data obtained via an alternative gas-liquid system. Alternative bubble breakage equations would also be used for further validation of the mechanism of bubble break-up proposed in the existing model.

5. Utilisation of digital video image analysis technology (or alternative non-intrusive methods) for direct determination of the bubble size distributions exhibited in the reactors. This would be used for comparison with size distributions predicted by the model.

CHAPTER 2

LITERATURE REVIEW

A survey of the fundamentals and state of the art in gas-liquid contacting was performed to obtain a thorough knowledge of this field of study. The aim thereof was two-fold, i.e. firstly, to investigate conventional and novel fluid contacting equipment and processes, paying particular attention to those employing aspects of high-intensity contacting; and secondly, to review current modelling techniques and strategies to provide information and new ideas regarding the mechanistic (and empirical) modelling of these processes.

2.1 CONVENTIONAL AND NOVEL GAS-LIQUID CONTACTING DEVICES

Most multiphase systems, specifically gas-liquid systems, are characterised by the fact that mass transfer rates are limited by the transport of gas to the liquid phase and hence by the overall interfacial area available for mass transfer. Therefore, systems which can induce high shear rates and generate small gas bubbles to increase the interfacial area, are continually being investigated.

For this purpose, mechanically agitated reactors, equipped with stirrers, multiple impellers or even turbine blades, have widely been applied as an alternative to conventional packed and bubble columns. The use of jets or venturis for mixing and agitation purposes have, however, become increasingly popular due to inherent advantages in their application from an operational and maintenance perspective, especially in corrosive (slurry) environments. For this reason, and the fact that the field of mechanically agitated gas-liquid reactors warrants an independent literature survey, the following study will only consider non-mechanically agitated systems.

Particular attention will be paid to so-called high-intensity gas-liquid contacting processes.

2.1.1 Venturi scrubbers

Although venturi scrubbers traditionally have been employed in dust and mist collection (pollution control) applications, they are increasingly being used in the field of gas-liquid contacting due to their simplicity and compactness. Typically, these scrubbers operate on the principle of an accelerated gas velocity in the throat of the venturi, where the gas is sprayed by a scrubbing liquor. The faster velocity of the gas stream results in both the atomisation of the liquor and promotion of shear forces at the phase interface, thereby promoting contact between the gas and liquid, leading to high interfacial areas and mass transfer rates.

Yet, in gas-absorption applications, venturi scrubber efficiencies are limited somewhat by the co-current flow of the two phases through the throat, since only a fraction of the kinetic energies of the streams is dissipated in the contacting process. For this reason the "ejector venturi scrubber" has been developed where the liquid is simply pumped through atomising spray nozzles, entraining the gas with it. No gas blower therefore needs to be employed.

Laurent et al. (1980) provide an example of such a venturi jet scrubber (*Figure 2.1*). The unit, with nominal diameter of 50 mm, was comprised of a standard venturi diffuser, 700 mm in length, and a throat diameter of 33 mm. Nozzles for liquid injection were designed so that the injected liquid is pulverised as a conical sheet entirely filling the cross section of the diffuser, resulting in good contact between gas and liquid. Typical values for the mass transfer parameters, determined by CO_2 absorption into NaOH solutions, were found to be in the region of $3 - 8 \times 10^{-4}$ m/s for the liquid side mass transfer coefficient and 0.5 – 1 m^2 (based on the volume of this system) for the effective interfacial area.

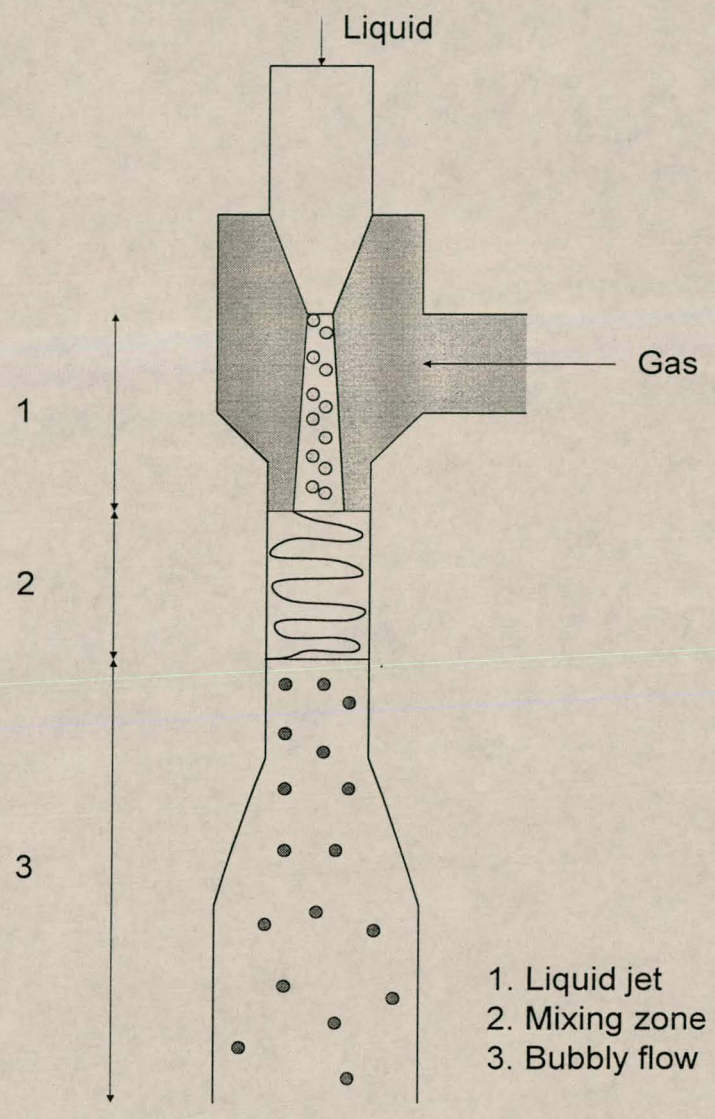

Figure 2.1 *Venturi ejector reactor (Laurent et al., 1980)*

On a different level, *Huynh et al.* (1991) employed a venturi to enhance the mass transfer characteristics of a conventional bubble column in a so-called "Venturi/Bubble Column Combination". Gas hold-up (and therefore interfacial area) was increased by 50 – 150%, and the overall volumetric mass transfer coefficient was tripled when the venturi was used as a "gas distributor" instead of a porous distributor. *Figure 2.2* provides a schematic diagram of this system.

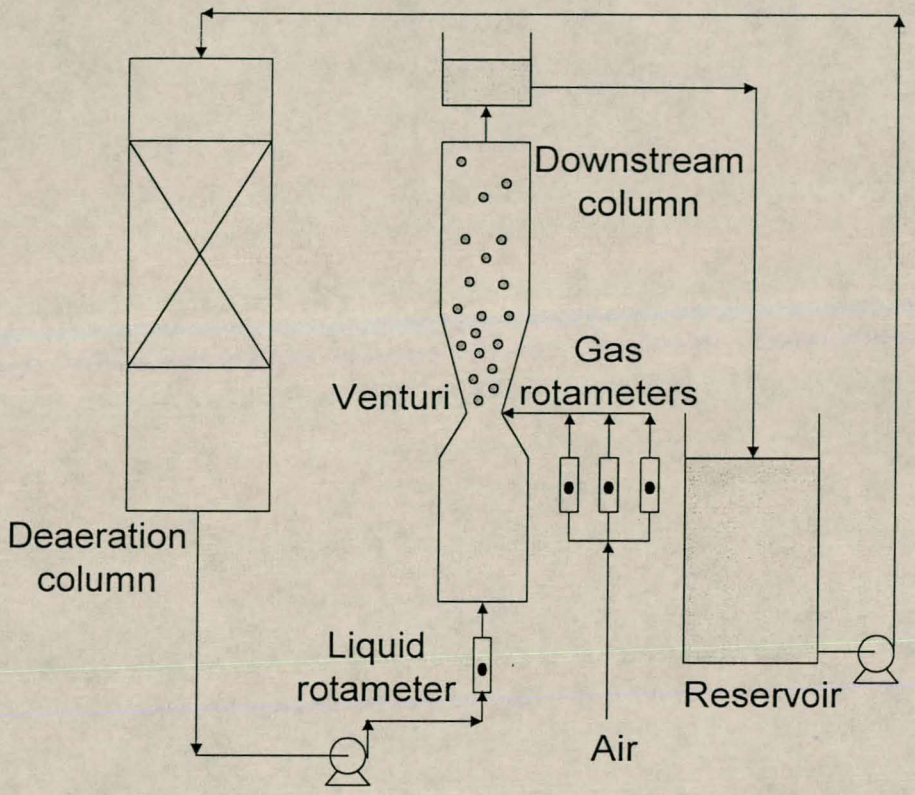

Figure 2.2 *Venturi/Bubble column combination (Huynh et al., 1991)*

2.1.2 Centrifugal contactors

2.1.2.1 High intensity contactors

Processes incorporating enhanced centrifugal acceleration fields for the generation of high liquid shearing forces (to promote bubble break-up), are also increasingly being employed for effective fluid contacting. Earlier centrifugal contactors typically consisted of a set of concentric rings, attached to a stationary plate, that intermesh with rings situated on a rotating disc. Liquid under a centrifugal force (generated by the spinning action of this disc) then moves through the mesh, where a thin liquid film is produced into which gas is absorbed.

Recent advances in this field has, however, lead to the development of a novel high intensity gas-liquid contactor (*Figure 2.3*) in which enhanced

centrifugal acceleration is achieved by liquid injection rather than by mechanical rotation (*Waldie*, 1995 and *Waldie and Harris*, 1998). In principle liquid is fed tangentially to form an annular spinning layer on the inside of a permeable tube through which gas passes inward as fine gas bubbles through the liquid. The centrifugal forces, $\omega^2 r$, promote the inward motion of the lower density gas and formation of a central gas core. Near-complete phase separation is therefore obtained, largely eliminating unwanted dispersed gas in the exiting liquid.

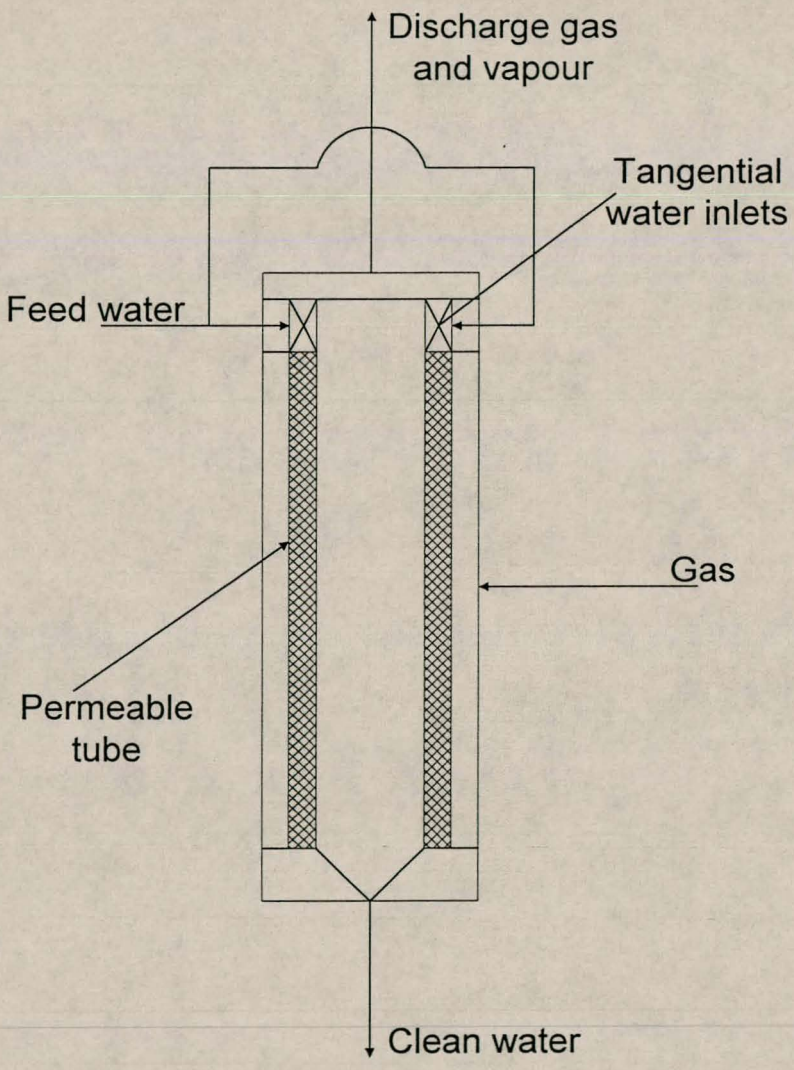

Figure 2.3 *High intensity contactor (Waldie, 1995)*

The potential for enhanced mass transfer by high centrifugal acceleration fields can be seen by considering the correlation of *Calderbank and Moo-Young* (1961) for liquid side mass transfer coefficients:

$$k_L = \frac{2D_L}{d_b} + 0.31Sc^{-2/3}\left[\frac{(\rho_L - \rho_G)\mu_L g}{\rho_L^2}\right]^{1/3} \quad \ldots (2.1)$$

If it can be assumed that the first term on the right hand side is relatively small (*Waldie and Harris,* 1998), then it can be seen that k_L increases approximately as (acceleration)$^{1/3}$. Considering that, for this contactor, liquid can be injected at velocities sufficient to give radial accelerations of the order of 100 – 1000g, there definitely exists potential for an increase of the mass transfer coefficient by 3 – 10 times.

Two applications of this novel contactor were found in the literature. In the first application the removal of oxygen from towns water by nitrogen stripping was studied in a prototype contactor with a permeable ceramic tube. Results were compared to that of a conventional column of Pall rings using the same water, gas and instrumentation. It was found that, in terms of H_{OL} (the height of an overall liquid transfer unit), the processing intensity of the new contactor was at least 20 times greater than that of the column, extending to 100x for high gas-liquid ratios. Compared to the bubble column, k_La values were some 100 – 150 times higher.

Another application involved assessing the potential of this novel contactor for providing a more compact means of removing the dissolved aromatic compounds from produced water on an oil or gas platform. Most of the produced water on such a platform contains dissolved aromatics such as benzene and toluene which, being sparingly soluble in the sea, are potentially harmful to marine life. The fact that more rigid legislation on the composition of water discharged to the sea is a possibility, practical means of improving on current water treatment equipment on platforms, e.g. hydrocyclones (only designed to remove dispersed or particulate oil), need to be considered.

Owing to the fact that produced water can be the largest tonnage output stream in oil or gas production, and the fact that older oil/gas fields start yielding ratios of water/oil flow rates of perhaps ten or more, the main objective was to determine whether dissolved aromatics could be removed by a high capacity, compact and light novel gas-liquid contactor, and, if so, what reduction in equipment size might be achieved relative to a packed column on the same aromatics removal duty. The expected insensitivity of the contactor to marine motion, opposed to that of the packed column, was seen to be of added advantage on the ever increasing amount of floating production systems used for new field developments.

The proposed process employed air as stripping gas which could be fed to the main gas turbines or other combustion engine on the platform to dispose of the aromatics by combustion. Once again results were compared to those of a conventional packed column. In terms of H_{OL} values, the new contactor yielded values of 7 – 10 times better than those of the packed column, especially with the use of salt water, due to the suppression of bubble coalescence. Values obtained for the volumetric mass transfer coefficient, k_La, were also several hundred times larger than those exhibited by the column. In terms of equipment size, it was shown that the internal contacting volume in the novel contactor could be over two orders of magnitude smaller than that of a packed column for equivalent energy duties. Reductions in overall equipment volumes could therefore be significant. However, these savings will need to be weighed up against operating and capital costs of the equipment.

It was pointed out that the substantial reduction in contacting volume and increase in the values of the mass transfer coefficients inevitably incurred an increase in the energy consumption over that for the packed column. It was, however, pointed out that this increase could be less pronounced if water were already available under pressure from the primary oil/water separators. Still, significantly higher values of k_La for a given energy input per volume of water treated, were reported.

2.1.2.2 Gas-liquid cyclones

According to *Van de Vusse* (1966), it is recognised that in many complex multiphase reactions, the values of the mass transfer coefficients may play a critical role in the overall selectivity realised in the process. Since the selectivity of a reaction often plays an important role in the economy of the process, new gas-liquid contactors, in which high values of k_L could be realised, needed to be developed. For this reason a gas-liquid cyclone reactor (GLCR) was developed by *Beenackers* and *Van Swaaij* (1976).

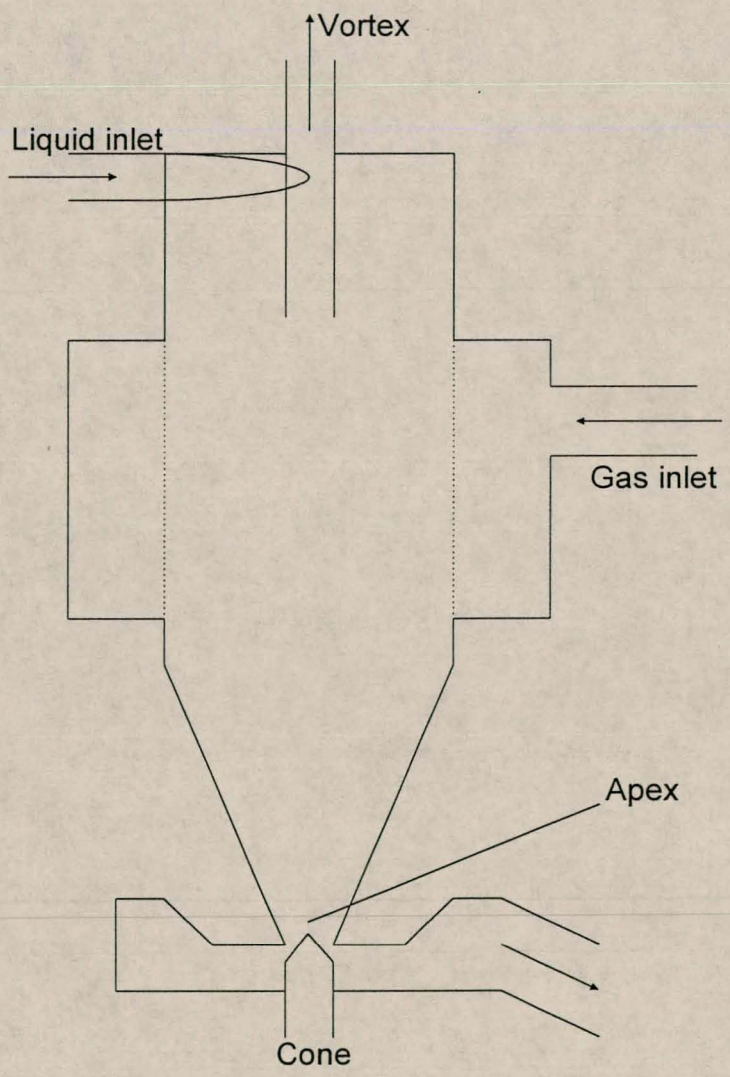

Figure 2.4 *Gas-liquid hydrocyclone (Beenackers and Van Swaaij, 1976)*

In essence the cyclone reactor (*Figure 2.4*) was designed analogous to a conventional cyclone, but with a longer cylindrical section (for promotion of phase separation) and a variable conical core trap in the apex to prevent gas entrainment. The liquid phase was fed tangentially to the reactor while gas was introduced through the porous stainless steel walls of the reactor. Using the chemical absorption of CO_2 into NaOH solutions, mass transfer coefficients of 8 - $10x10^{-4}$ m/s were obtained, compared to values for conventional equipment (agitated tanks, bubble columns and packed columns) of 0.64 – $2.85x10^{-4}$ m/s. Interfacial areas of 2000 – 5000 m^2/m^3 were also realised.

2.1.3 Jet loop absorbers

The extensive use of jet loop reactors (JLR's) in fields such as fermentation, wastewater treatment and catalyst testing, can be attributed to their many advantages, i.e. simple construction and operation, low investment and operational costs, definitely directed circulation flow, very fine gas dispersion, high mixing and mass transfer performance and relative energy efficiency.

Earlier JLR's consisted in principle of a smaller diameter cylinder, fitted inside a larger one, thereby effectively creating an inner draft tube and an annulus volume. A two-fluid nozzle, for injection of the gas and liquid into the reactor, was placed at the bottom of the reactor. This arrangement, however, provided operational problems when slurries were used, since blockage of the nozzle occurred.

These problems were eliminated with the introduction of a new design, the so-called reversed flow JLR (*Padmavathi* and *Remananda Rao,* 1993 and *Velan* and *Ramanujam,* 1991), which employs the two-fluid nozzle at the top of the reactor (*Figure 2.5*). This not only eliminates the problem of nozzle blockages, but also has some added advantages:

- Increase in the gas residence time as the bubbles are forced to move against buoyancy.
- Enhanced gas hold-up.

- Increase in the liquid residence time with the placement of the liquid outlet at the top of the reactor. Whereas only partial circulation of the liquid occurred in the set-up described previously, the new arrangement forces the entire liquid entering the reactor to travel down the draft tube and leave through the annulus at the top.

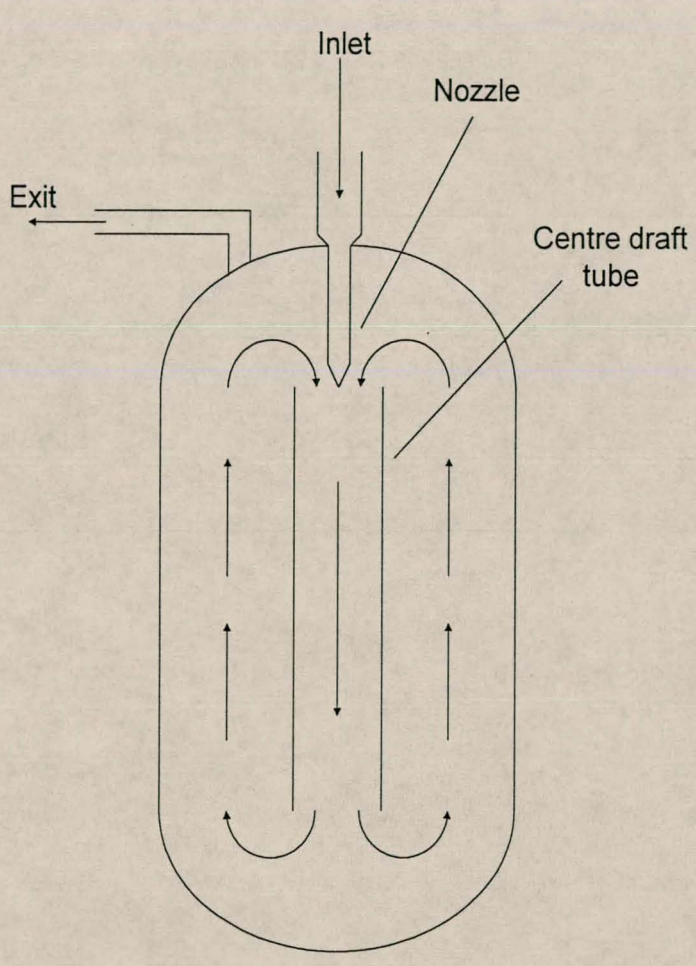

Figure 2.5 *Jet loop reactor (Padmavathi* and *Remananda Rao, 1993*)

Prasad and Ramanujam (1995) provide useful information regarding the mass transfer characteristics of such a modified reversed flow JLR using the physical absorption of oxygen (from air) into water. Values of the volumetric mass transfer coefficient, k_La, were reported to be in the range of 0.02 – 0.04 s^{-1}, compared to 0.005 – 0.015 s^{-1} for a conventional jet loop reactor. The following conclusions were made based on the results obtained from their investigation:

- The overall gas hold-up and k_La-values are found to be higher for the modified reversed flow JLR than in the conventional JLR and other conventional contacting devices.
- The reactor seems to deliver superior k_La values especially in the range of lower energy dissipation rates.
- The optimum draft tube to reactor diameter is found to be in the range of 0.4 – 0.5.

2.1.4 Impinging stream reactors

2.1.4.1 A short background to impinging streams

Tamir (1994) presents the idea of impinging streams as a unique and multipurpose configuration of a two-phase suspension, first suggested by *Elperin* (1961) in the early 1960's, which provides a tool for intensifying transfer processes in heterogeneous systems. *Tamir*'s experience in the field of impinging streams has been gained since 1980 in processes such as:

- absorption and desorption of gases from liquids in the presence of a chemical reaction,
- combustion of gas and coal,
- creation of emulsions,
- liquid-liquid extraction,
- dissolution of solids, and many more.

On the basis of such knowledge, and comparison of the above processes with conventional systems, he concludes that "almost any process in chemical engineering can be carried out by applying impinging streams; most likely with a higher efficiency and a lower power input in comparison to conventional methods". The underlying reasons for the successes of impinging streams are discussed in the following section.

2.1.4.2 The essence of impinging streams

The intensification of transfer processes in impinging systems is due to the following effects:

- An increase in the relative velocity between the penetrating particles and the opposed gas stream. Optimally a particle penetrating into an opposing gas stream could achieve a relative velocity twice that of the penetrated gas velocity, resulting in a decrease in the external resistance.
- An increase in the mean residence time of the particle in the system due to penetration and circulation in the opposing stream. This translates into a decrease in the geometrical size of the system.
- An increase in shear forces between the phases, which results in a break-up of the droplets/bubbles and an increase in the interfacial area. Surface rejuvenation rates are also accelerated, leading to an increase in mass transfer rates.
- Pressure pulsations and intense radial and axial velocity components in turbulent flow due to collision of the continuous phases of the opposed streams. Consequently, good mixing (homogenisation) of the mixture is achieved.

2.1.4.3 Impinging stream jet loop reactors (IS-JLR)

Impinging stream jet loop reactors were conceived as a further attempt to increase turbulence in jet loop reactors (*Gaddis and Vogenpohl*, 1992). *Figure 2.6* provides a schematic diagram of such a reactor. It can be seen that all the advantages exhibited by the previously mentioned jet loop reactors are complemented by the added benefits of three impingement zones:

- one head-on impingement zone of the gas-liquid mixture, and
- two perpendicular impingement zones at the exits of the nozzles.

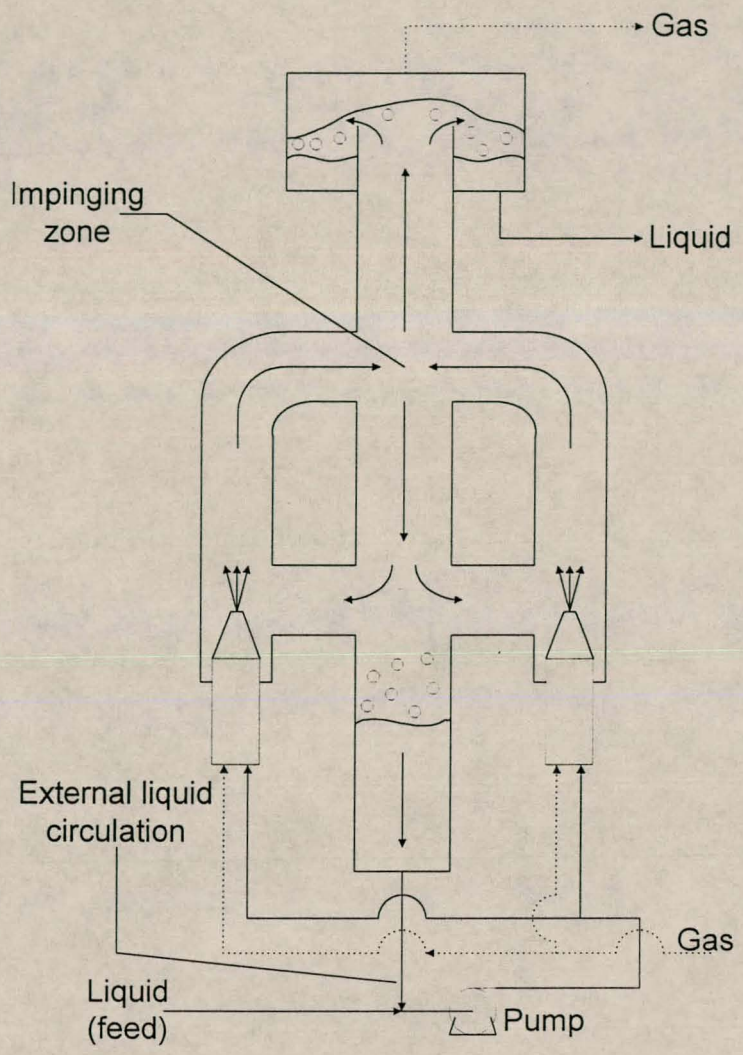

Figure 2.6 *Impinging stream jet loop reactor (Gaddis and Vogenpohl, 1992)*

Gaddis & Vogenpohl (1992) used the physical absorption of oxygen into water to characterise one of these reactors employing so-called critical nozzles, where premixed gas and liquid phases are jetted through the nozzles. Results were compared with those of alternative gas-liquid contacting devices.

It was found that the impingement zones are responsible not only for higher mass transfer coefficients than in other aerating systems, but also a high rate of increase of the mass transfer coefficient with increasing power dissipation. At low specific power input, the impinging velocity is not high enough to enhance mass transfer: the measured mass transfer rate is basically due to the influence of the above-mentioned nozzles. However, as the power input

increases, the impingement velocity increases (due to increased external recirculation velocity) to such an extent that the contribution of these intense mixing zones to mass transfer become more significant, even dominant. As a result of this it could be suggested that the benefits of more intensive phase mixing might well exceed the extra cost incurred from an increase in power input.

A power consumption-based comparison between the mass transfer performance of the new ISJLR and conventional contacting devices (mainly mechanically agitated tanks) revealed that, particularly for a coalescing system, the new reactor yielded very high mass transfer rates. Volumetric mass transfer coefficients of 0.1 – 1.0 s^{-1}, between power inputs of 0.4 – 2 kW/m^3, are reported, compared to values of 0.007 – 0.08 s^{-1} (in the same range of power inputs), for conventional equipment (*Bouaifi and Roustan,* 1998).

In a very similar piece of work by *Sprehe et al.* (1998), it was again found that at higher power consumption values, the exponent of the power input term in the following functional relationship,

$$k_L a \propto \varepsilon^{\alpha} \qquad \ldots (2.2)$$

ranged from 0.7 – 1.2, compared to values for conventional equipment of 0.4 – 0.6. It was also reported that the mass transfer coefficients in the impingement zone and main reactor tube were respectively, about 4 and 2.5 times higher than in the "rest of the reactor" at a high power dissipation.

2.1.4.4 Impinging stream absorbers

The most significant contributions to this relatively new field of study has been made by *D. Herskowits*, *V. Herskowits* and *A. Tamir* (1990a and 1990b) after the pioneering efforts by *Elperin* (1961). This section will highlight their most important experiments, results and conclusions.

The initial purpose of experimental work was to verify the enhancement of mass transfer by impinging streams. For this purpose the schematic set-ups demonstrated in *Figure 2.7* were employed, where the upper system represented the new impinging system; the lower system was simply obtained by operating each half separately, effectively eliminating the impingement effect. It was decided that, if R_2 would denote the absorption rate of gas in the two-impinging-streams (TIS) reactor, and R_1 the absorption rate of gas in the single stream absorber, that the TIS system would be considered as more efficient if:

$$\frac{R_2}{2R_1} > 1 \qquad \ldots (2.3)$$

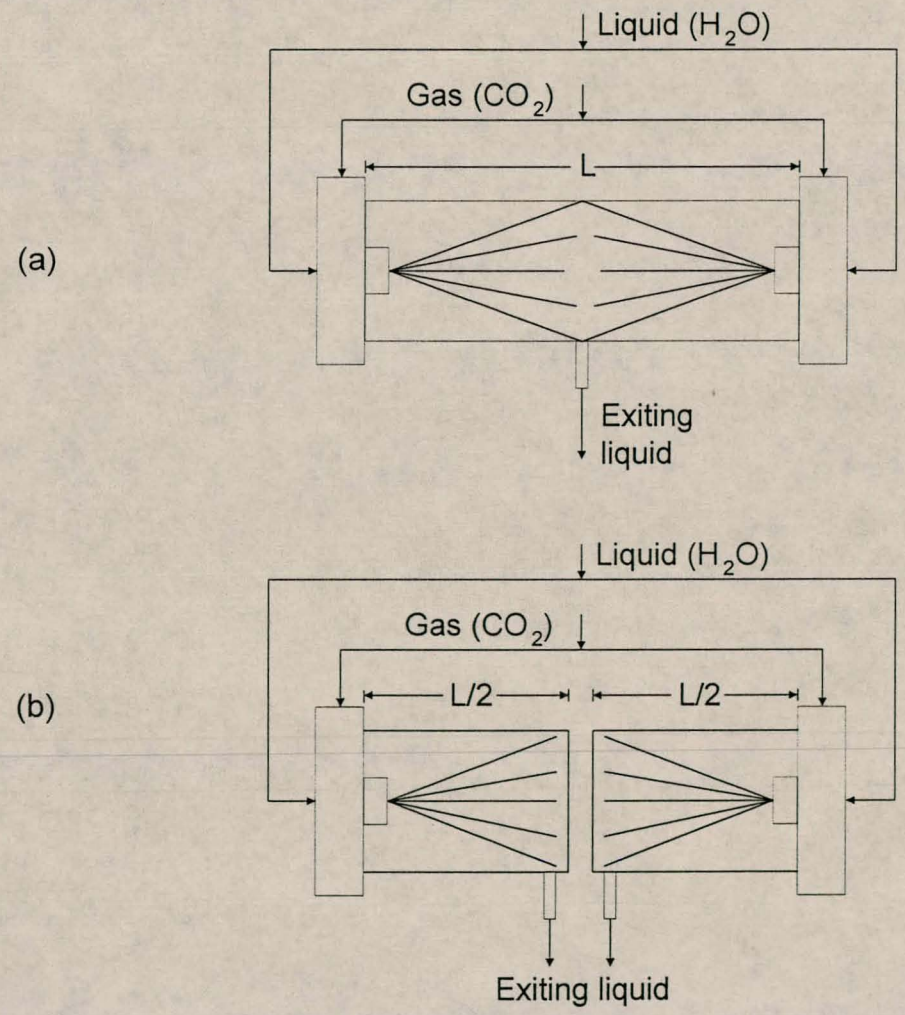

Figure 2.7 *Investigating the intensification effects of impinging streams*

Both set-ups (*Figures 2.7 a and b*) consisted of 2 nozzles placed on the same axis (*concentric configuration*), spraying against each other in counter-current flow. These nozzles were fixed at the extremities of a glass tube so that the reaction volume was clearly defined. Three chemical systems were used to determine absorption rates in the reactors:

- Physical absorption of CO_2 into water (bubble mode)
- Absorption of acetone from air into water (spray mode)
- Desorption of acetone from water by air (spray mode)

Results of the absorption and desorption intensification experiments proved that the above defined ratio ($R_2/2R_1$) was greater than unity and that the deviation from this value depended on different operating conditions. For CO_2 absorption a maximum value of 1.65 was achieved, thus a 65% improvement in absorption rate above the non-impinging system. For the absorption of acetone from air into water, results proved even more convincing: absorption rate ratios of between 2 and 4 were achieved. This phenomenon was explained by the characteristics of impinging streams discussed previously, namely the secondary atomisation of droplets due to inter-droplet collisions and shear forces (generated by the gas stream), as well as an increase in droplet residence time due to possible oscillatory behaviour.

By investigating the effect of a wide variety of operating parameters during the above mentioned absorption experiments, the following additional conclusions could be made. It was found that:

- For bubble-mode absorption, where the resistance to mass transfer lies mainly in the liquid phase, the effect of liquid flow rate on absorption rate is much more pronounced than for the gas flow rate. Vice versa, where gas-side resistance is controlling, the effect of gas flow rate is much more pronounced.
- Absorption rates were relatively independent of cell diameter for CO_2 absorption, though acetone absorption did show some degree of dependency until a critical cell diameter was reached.

- Absorption rates exhibited a so-called "two-maxima" behaviour as a function of internozzle distance. This is ascribed to two different enhancement effects:
  - ⇒ Short-range impingement effect due to secondary atomisation of droplets, and
  - ⇒ Long-range impingement effect due to an increase of the residence time of droplets through oscillations.
- The so-called "critical nozzle" type (*Caldyn* CSL nozzles), where gas and liquid is mixed inside the nozzle and ejected as a well-mixed two phase jet, exhibits superior performance, since absorption already commences within the nozzle. It must be noted, however, that the power inputs associated with this nozzle are significantly higher than for typical non-mixing nozzles.

The following table provides a summary of the most important results achieved in mass transfer experiments by Tamir and Herskowits using impinging stream reactors. These results are compared with corresponding values from conventional contacting devices.

Table 2.1 *Comparison of mass transfer parameters for known absorption reactors and impinging jet absorbers*

Type of reactor	**k_L** *(cm/s x 100)*	**a** *(m^2/m^3)*	**k_La** *(s^{-1} x 100)*	**Gas voidage**	**Power** *(kW/m^3)*
Packed columns	0.4 – 6	0.1 – 17	0.04 – 120	>0.95	0.01 – 0.2
Plate columns	1 – 20	1 – 4	1 – 40	>0.8	0.01 – 0.2
Bubble columns	1 – 4	0.5 – 6	0.5 – 24	<0.2	0.01 – 1
Spray columns	0.7 – 1.5	0.1 – 1	0.07 – 1.5	>0.8	n/a
Mechanically agitated reactors	0.3 – 4	1 – 20	0.3 – 80	<0.1	0.5 – 4
Hydrocyclones	10 – 30	0.2 – 0.5	2 – 15	n/a	n/a
Venturi	5 – 10	1.6 – 2.5	8 – 25	<0.5	10 – 700
Impinging jets	3 – 6.6	0.9 – 20.5	2.5 - 95	<0.5	0.8 – 140

Lastly, the literature survey yielded one other publication (*Unger et al.*, 1998) regarding an alternative impinging jet contactor configuration. However, it focussed mainly on the numerical characterisation of flow fields and mixing with the use of Computational Fluid Dynamics, and is therefore only mentioned here to complete the literature survey on impinging stream contactors in this sub-paragraph.

2.2 PREVIOUS RESEARCH ON IMPINGING STREAM CONTACTORS AT THIS INSTITUTION

The development of gas-liquid impinging stream jet reactors at this institution was an indirect result of research having been performed on the use of impinging streams for the intensification of cyanidation of ores in the gold leaching process (*Lorenzen et al.*, 1997; *Loftus,* 1999). Since it was proved that the intensification of mass transfer properties was possible by means of impinging streams, it was decided to further investigate the intensification of gas-liquid mass transfer processes in jet reactors. This section will consider the most significant results and conclusions achieved by *Botes et al.* (1998) in this regard.

Using the chemical absorption of CO_2 into NaOH-solutions, *Botes* initially tested a number of different reactors to determine the effects of reactor geometry and flow rates on the absorption efficiencies in IS reactors. In his research, three reactor configurations were used (*Figure 2.8*):

A. Opposing jets reactor
B. Spherical reactor
C. Hemispherical reactor

In addition to the different reactor geometries tested, nozzles could also be fitted in such a fashion that similar phase nozzles faced one another (the so-called *GG-configuration*) or so that dissimilar phase nozzles faced one another (the so-called *GL-configuration*). Therefore a wide variety of resulting reactor geometries and flow patterns could be investigated.

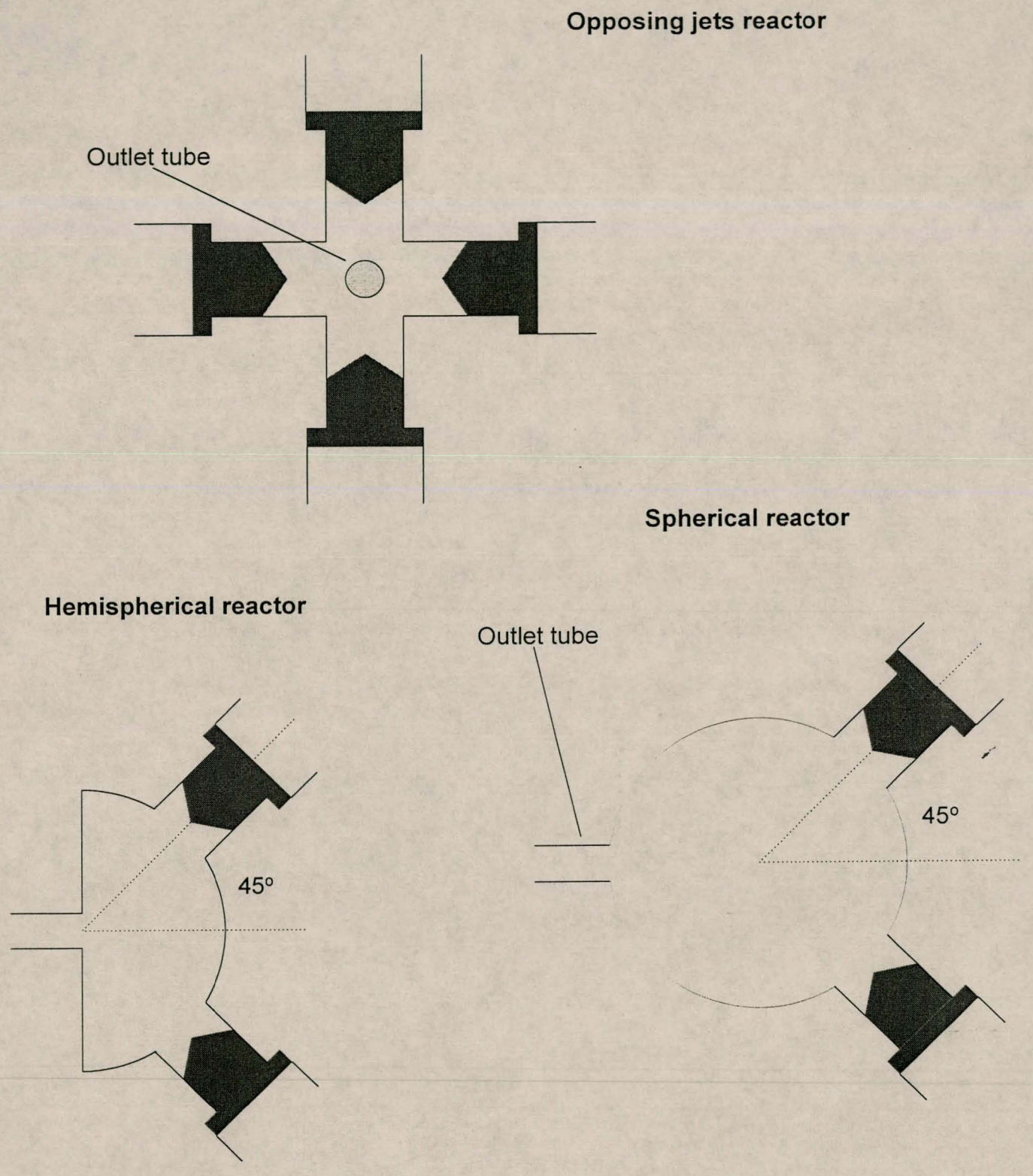

Figure 2.8 *Preliminary reactors (Botes, 1995)*

During the preliminary investigation, absorption efficiencies of the reactors were based simply on the conversion of hydroxide to carbonate. Although this did not yield an absolute measure of the efficiency of each reactor, relative performances could be ascertained. The following conclusions could be made from the results from these experiments:

- The opposing jets reactor in the GL-configuration proved to represent the most efficient geometry, due to a larger impingement effect between the gas and liquid feed streams.
- The arrangement of the nozzles plays a critical role in the efficiency of the reactors. It was found that nozzles should be positioned in such a fashion so as to create a forceful, directed flow pattern in the reactor. Liquid nozzles should be directed past gas nozzles, to effectively shear off bubbles from the entering gas stream. Dead zones are thus eliminated.
- Gas-liquid separation occurs as soon as the two phase mixture enters a plug flow region. For this reason nozzle placement must allow for the injection of feed streams from various directions to sustain high levels of turbulence throughout the reactor.

Employing the above observations, three final reactors were developed, each with a different angle of impingement to optimise the arrangement of nozzles (*Figure 2.9*):

A. Triangular reactor
B. Square reactor
C. Kite shaped reactor

The dimensions of the reactors, however, were such that all three reactors had the same reaction volume (0.00842 litres). In each case two gas and two liquid nozzles were used. Once again the absorption of CO_2 into sodium hydroxide solutions was used to determine the mass transfer parameters exhibited by the reactors.

Experimental results showed that the triangular and kite shaped reactors exhibited very similar trends in terms of interfacial area production and the value of the volumetric mass transfer coefficient, k_La. Increases in both the

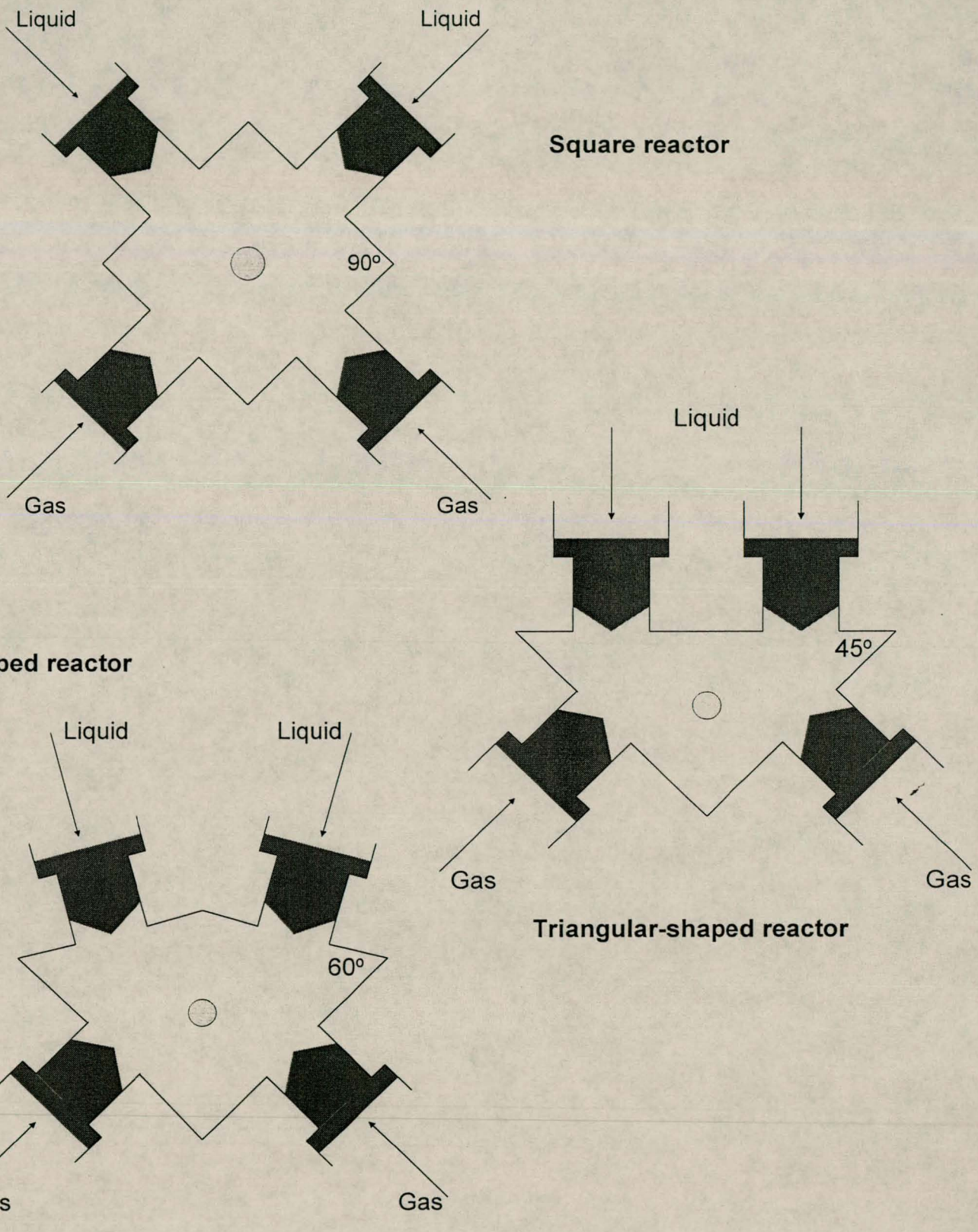

Figure 2.9 *Final reactors (Botes, 1995)*

liquid and gas flow rates resulted in an increase in the above parameters, although higher absolute values were always exhibited by the kite shaped reactor.

The superiority of this reactor (kite-shaped) was ascribed to a near-perfect angle of impingement between gas and liquid feed streams (liquid shearing off bubbles) and the fact that the liquid streams impact the reactor wall at an angle, so that they are reflected. Thus, the force of the liquid flow needed to distribute random turbulence throughout the reactor, is sustained. In the case of the triangular reactor, however, the liquid stream is not reflected very well so that a forceful macro flow pattern cannot be sustained. Only a fraction of the entire reaction volume is therefore used for intensification of mass transfer.

Results for the square reactor exhibited basically the same behaviour as that of the previously mentioned reactors, although the influence of gas pressure (and therefore flow rate) on the interfacial area was much more pronounced, and vice versa for the liquid flow rate. This was explained in terms of the following: no liquid nozzles were directed at gas nozzles to shear off gas bubbles, and gas could not penetrate effectively into the high velocity liquid streams due to their lack of momentum. Neither were random turbulence and vortices being created within the square geometry of the reactor to draw gas bubbles into the liquid stream. Dead volumes, created by lumps of gas in the vicinities of the gas nozzles, were therefore created, and poor mixing occurred. If, however, the gas pressure was increased, the gas penetrated more effectively into the liquid streams and gas bubbles were transported to the turbulent regions in the reactor where efficient mass transfer could take place. Therefore, the performance of the square reactor was improved by raising the inlet gas pressure.

Table 2.2 gives a brief summary of the mass transfer parameters obtained for the three final reactors:

Table 2.2 *Comparison of the performances of the three final reactors (Botes, 1995)*

Reactor	a (m^2/m^3)	k_La (s^{-1})
Triangular	1000 – 5000	1 – 8
Square	2500 – 6000	3 – 8
Kite shaped	2500 - 9000	4 – 14

To summarise, the following design philosophy was proposed by *Botes* for future design of effective impinging stream jet absorbers:

1. *"Liquid streams must effectively shear off bubbles from gas orifices and collide with the reactor wall in such a fashion that turbulence promotion is maintained in the bulk of the reactor"*
2. *"Plug flow regions must be avoided - the reactor geometry must support a homogeneous distribution of turbulence throughout the reactor"*

2.3 MODELLING OF GAS-LIQUID PROCESSES

A good process model provides an almost indispensable tool for the understanding of the system at hand – it not only serves as a mathematical description of the process, but also provides and predicts valuable information regarding the effects of various system inputs on the process output. For this reason a comprehensive literature study was performed on the state of the art modelling techniques applied in gas-liquid contacting. These techniques can, in principle, be divided into mechanistic and empirical modelling techniques.

2.3.1 Mechanistic modelling of gas-liquid contacting processes

Proper design of gas-liquid reactors not only requires a knowledge regarding the dynamic properties of the gas dispersion (bubble sizes and gas hold-up), but also a fundamental knowledge about the dynamic rate characteristics of bubble break-up and coalescence, since these mechanisms directly determine bubble size distributions. For this reason, mechanistic modelling techniques have been developed as an alternative to conventional empirical analysis. In this regard, population balances and Monte Carlo simulations have proved to be the most widely applied, especially for the case of dispersed systems. The following section will shortly highlight the main characteristics and advantages associated with these techniques.

2.3.1.1 Population balances and Monte Carlo simulations

Population balances, first introduced by *Hulburt* and *Katz* (1964) and subsequently developed by *Ramkrishna* and *Borwanker* (1973) and several other authors, arise from synthesis of information about single particle behaviour into a description of the behaviour of an entire population of such particles. The resulting system is characterised by a set of integrodifferential equations since conservation of the number of particles of a specific state is dependent on the cumulative contribution of particles of other states.

In much the same fashion, Monte Carlo simulations have been proposed as an alternative approach for the prediction of system characteristics through single particle behaviour. Examples thereof include the investigation of the effects of drop-mixing on reaction conversion in the dispersed phase of a liquid-liquid system (*Spielman* and *Levenspiel*, 1965) and the prediction of a stable drop size distribution in agitated liquid-liquid systems (*Zeitlin* and *Tavlarides*, 1972).

The advantages of Monte Carlo simulations above population balances are as follows:

- They eliminate the need for solving a complex set of integrodifferential population balance equations.
- Simulation results not only produce average results, but also provide information regarding fluctuations characteristic of small populations.
- They account for possible interaction effects between particles (such as in an agglomerating population), which are not accounted for by population balances.

The most significant difference between population balance models and Monte Carlo simulations, though, lie in the identification of probability functions which govern changes occurring in the system. The implementation of the simulation algorithm depends on generating random numbers which are substituted into the calculated probability functions, thus providing a prescription for the change to be introduced in the system. These changes are, however, still conditional on the state of the system at the stage at which the change is considered. Therefore, as stated by *Ramkrishna* (1981), Monte Carlo simulation procedures efficiently evaluate the solution by elimination of low probability events.

2.3.1.2 Kolmogoroff's theory of isotropic turbulence

As has been mentioned before, bubble size distributions in dispersed systems are in principle controlled by the interaction of bubble break-up and coalescence processes. In order to develop a mechanistic model for the prediction of the bubble size distribution, expressions for both these rates have to be determined. Due to the sheer complexity of this, simplifying assumptions have had to be made in order to make the problem tractable. In this regard, Kolmogoroff's theory of isotropic turbulence (*Kawase* and *Moo-Young*, 1990) has proved to be virtually indispensable. Since it will become clear in this study how widely this theory is applied in both fundamental and empirical models, it is worthy of a brief discussion. Thereafter a short review of breakage and coalescence models will follow.

As mentioned previously, the break-up and coalescence of bubbles is determined by their interaction with turbulent eddies. These eddies can be classified into 3 different classes of wavelengths:

- Primary eddies: these large eddies have the same wavelength as the dimensions of the main flow stream (produced by agitation) and merely 'move' the bubbles about. They are not isotropic (*isotropic* = turbulence is invariant with respect to orientation) and are unstable, disintegrating into smaller medium-sized eddies with a higher frequency.
- Intermediate size eddies: these eddies contain the main part of the kinetic energy of turbulent motion (the so-called "energy containing" eddies); their characteristic size is denoted by:

$$\eta_e = \left(1/k_e \right) \qquad \ldots (2.4)$$

where k_e is the wavenumber marking the range of energy-containing eddies (*Figure 2.10*). The wavenumber of an eddy is defined as the reciprocal of its radius ($k = r^{-1}$).

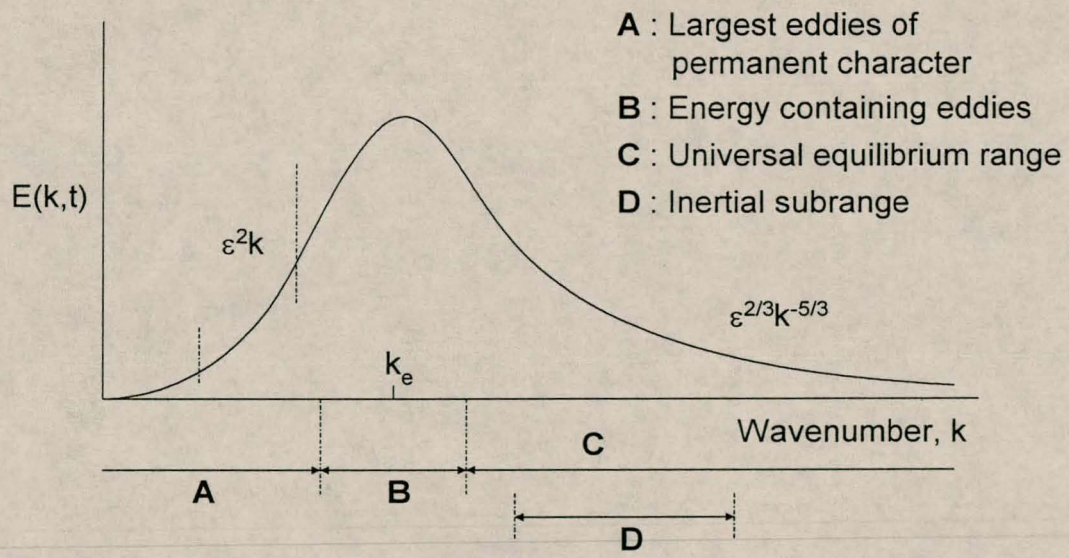

Figure 2.10 *Energy distribution function E(k,t) in the various wavenumber ranges (Kawase and Moo-Young, 1990)*

- Small terminal eddies: these eddies are formed by the break-up of the above mentioned medium sized eddies; they have completely lost their unidirectional nature and are therefore isotropic. Most of the energy

dissipation in the system takes place via these terminal eddies. Although the total energy associated with these eddies is not very large, they are continually recharged by momentum and kinetic energy transfer from the larger eddies. The size of the smallest eddy can be given by:

$$\eta_d = \left(1/k_d \right) \qquad \ldots (2.5)$$

where k_d is the wavenumber marking the size of the eddies that provide the main contribution to the total energy dissipation.

In terms of these definitions Kolmogoroff (*Kawase* and *Moo-Young*, 1990) proposed the following hypothesis:

" *At sufficiently high Reynolds numbers there is a range of high wavenumbers where the turbulence is statistically in equilibrium and uniquely determined by the parameters, the energy dissipation by turbulence per unit of mass, ε and the kinematic viscosity, ν. This state of equilibrium is universal.*"

In addition to this, his second hypothesis considered an "inertial subrange" in which viscous dissipation is unimportant. In other words, if the Reynolds number is sufficiently large, the energy spectrum in this subrange is independent of ν, and is solely determined by the energy dissipation. Therefore, the energy spectrum (or spectral energy density) function can be given in terms of ε alone:

$$E(k) = \alpha \varepsilon^{2/3} k^{-5/3} \qquad \ldots (2.6)$$

for the following wavenumbers: $k_e << k << k_d$

It is in this so-called inertial subrange that all eddies are assumed to be when applying Kolmogoroff's theory in modelling. This has become a standard approach in mechanistic modelling techniques. Practically speaking, the requirement for the above assumptions to be true is that the Reynolds number (defined as $Re = U\lambda/\nu$) should be larger than 1500, as stated by Stewart and Townsend (*Kawase* and *Moo-Young*, 1990). However, it has been shown

that, even when the flow field is not isotropic or homogeneous (for example in a bubble column), Kolmogoroff's theory of isotropic turbulence can still be applied with reasonable success (*Prince* and *Blanch*, 1990). This is due to the fact that isotropic turbulence might still be exhibited on a microscale even though the macroscale hydrodynamics of the fluid does not. Yet, it must be kept in mind that this theory is used as an approximation.

2.3.1.3 Breakage and coalescence models

2.3.1.3.1 Bubble breakage models

Various attempts have been made to predict mixing in dispersed phase vessels. For this purpose, *Curl* (1963) applied the first population balance model using the example of two immiscible liquid phases in a well stirred reactor. The proposed model consisted of the following simplifying assumptions:

- The dispersed phase consists of a large number of droplets, equal in size and constant in number.
- Binary coalescence occurs, the probability of coalescence being the same for all droplets.
- The droplets coalesce at a constant rate and upon coalescence, redisperse instantaneously to yield two new drops of equal size.

However, this model was a gross simplification of the phenomena exhibited in the reactor. Its greatest drawback was its inability to predict and use collision and coalescence rates – these rates had to be treated as free parameters which had to be specified externally.

Valentas et al. (1966) and *Valentas* and *Amundson* (1966) proposed a more comprehensive model, incorporating breakage and coalescence rates in a turbulent flow field. This population balance model seeked to include the effects of stirrer speed, temperature, surfactants and interfacial turbulence, but finally proved to be too empirical in terms of breakage and coalescence

frequencies, as can be seen from the following expression for their droplet break-up rate:

$$\frac{\Omega_B(d)}{n} = c_1 d^{c_2} \qquad \ldots (2.7)$$

where $\Omega_B(d)/n$ denote the specific break-up rate, i.e. the amount of collisions in a certain size class divided by the amount of bubbles/droplets in that class.

Since then a host of other authors have proposed models for bubble break-up, assuming that these processes are governed by their interactions with turbulent eddies. *Zeitlin and Tavlarides* (1972) simulated drop behaviour in a turbulent system by dividing the system into two zones, first a zone of high turbulence where drop break-up dominates, and a zone of low turbulence (circulation) where coalescence mainly occurs.

Narsimhan et al. (1979) proposed a model based on probability theory and the assumption that the arrival frequency of turbulent eddies at a droplet/bubble interface is constant, yielding the following expression for breakage rate:

$$\frac{\Omega_B(d)}{n} = \Lambda erfc\left(\frac{A\sigma^{1/2}}{\rho_c^{1/2}\varepsilon^{1/3}d^{5/6}}\right) \qquad \ldots (2.8)$$

where $A = [3(2^{2/3} - 1)]^{1/2}$. They also assumed that Λ was independent of drop size.

Lee et al. (1987) developed a bubble breakage model based on the above model, using dimensional analysis to obtain a form of an expression for the average frequency of eddies arriving at a bubble surface:

$$\frac{\Omega_B(d)}{n} = c_1\left(\frac{\varepsilon}{d^2}\right)^{1/3}\left[1 - \int_0^1 F\left(\frac{c_2\sigma}{\rho_d\varepsilon^{2/3}d^{5/3}l^{11/3}}\right)dl\right] \qquad \ldots (2.9)$$

where F( ) is the cumulative chi-square distribution function.

Finally, *Hesketh et al.* (1991) combined the natural oscillation mode of a sphere given by *Lamb* (1932) and a correlation for the maximum stable drop size in a stirred tank, to yield the following breakage rate expression:

$$\frac{\Omega(d)}{n} \approx 2.7\left(\frac{\rho_c^{0.1}\rho_d^{0.3}\varepsilon^{0.6}}{\varepsilon^{0.4}}\right) \qquad \ldots (2.10)$$

As seen from the preceding review, break-up models all share a common functionality (bubble break-up is governed by surface tension, density and energy dissipation effects), though they might differ in their final mathematical form. This can be attributed to a general approach towards the development of these models since all share the same basic phenomenological simplifications:

1. As mentioned previously, turbulence is usually assumed to be isotropic. Even for non-isotropic systems, like bubble columns, isotropic turbulence theory can be applied since theoretical considerations and experimental evidence have shown that the fine-scale structure of most actual non-isotropic turbulent flows is locally nearly isotropic (*Hinze*, 1955). Differences between results based upon the isotropic theory and actual results are often sufficiently small to be ignored compared to the uncertainty in data.
2. Binary breakage of fluid particles is assumed. Depending on the breakage type, bubbles or drops may break into two or more particles with equal or unequal volumes. Whereas turbulent fragmentation of bubbles leads to binary breakage, shear breakage leads to a bubble breaking up into several droplets due to viscous shear. However, since only turbulent dispersions are considered, and viscous forces can be neglected, bubble break-up is assumed to be binary only.
3. The occurrence of break-up is determined by the energy level of the arriving eddy. Only eddies with sufficient energy to induce particle

oscillations, can lead to bubble break-up. If it can be assumed that the particle oscillation frequency is higher than the arrival frequency of eddies, then eddies affect the particles independently, such that once an eddy of sufficiently high energy arrives, the particle will break.

4. The breakage volume fraction of the bubble is a stochastic variable. Although it is known that bubbles will break into some preferred range of daughter particle sizes depending on the flow conditions, no correlation could as yet be found between the size of the parent bubble and its daughter particles (*Hesketh et al.*, 1991), or the breakage volume fraction and eddy sizes (*Nambiar et al.*, 1992). Thus, an approximation of this breakage fraction always has to be made.

Models for breakage rates always consist of two parts: an expression for the bubble-eddy collision rate and an expression for the collision efficiency. The resulting breakage rate expression is then simply the product of the two expressions. Collision rates are typically functions of the following parameters:

- bubble and eddy sizes,
- bubble and eddy concentrations, and
- turbulent velocity.

These parameters are then combined in an expression such as the following by *Coulaloglou* and *Tavlarides* (1977):

$$\theta_{b,e}(d,\lambda) = \frac{\pi}{4} n_b n_e (d+\lambda)^2 \left(\overline{u_b^2} + \overline{u_e^2}\right)^{1/2} = C\varepsilon^{1/3} n_d n_\lambda (d+\lambda)^2 \left(d^{2/3} + \lambda^{2/3}\right)^{1/2} \quad \ldots (2.11)$$

where parameters such as the turbulent velocity can be determined with the aid of Kolmogoroff's theory of isotropic turbulence (ref. *equation 6.12*).

Since not all of the above collisions result in break-up, expressions for collision efficiencies also have to be determined. These expressions evolve from force or energy balances between the stabilising forces of a bubble and the disruptive forces of arriving eddies. For this purpose, two very similar approaches have been adopted.

The first approach utilises an expression for the Weber number, which relates the ratio of dynamic pressure forces to surface tension forces, to obtain a critical eddy velocity above which bubble break-up would occur:

$$We_{critical} = \frac{\rho_L u_c^2 d_b}{\sigma} = K \qquad \ldots (2.12)$$

$$\therefore u_c^2 = K\left(\frac{\sigma}{\rho_L d_b}\right) \qquad \ldots (2.13)$$

An energy distribution function, in most cases that proposed by *Angelidou et al.*, (1979), is then used to determine which fraction of eddies have a velocity in excess of this critical velocity:

$$\chi(E_c) = \frac{1}{\overline{E_e}} \exp\left(\frac{-E_e}{\overline{E_e}}\right) \qquad \ldots (2.14)$$

where E_e is simply the kinetic energy of an eddy. Taking the energy of an eddy as proportional to the square of its velocity, yields a function of the following form for the fraction of eddies with sufficient energy to cause rupture:

$$Y = \exp\left\{-\left(\frac{u_c^2}{\overline{u_e^2}}\right)\right\} \qquad \ldots (2.15)$$

The second approach determines whether break-up will occur by comparing the energy of an eddy to the minimum energy required by the surface area increase due to particle fragmentation, expressed as follows:

$$\bar{e}(\lambda) = \rho_c \frac{\pi}{6} \lambda^3 \frac{\overline{u_\lambda^2}}{2} \qquad \ldots (2.16)$$

and

$$\bar{e}_i(d) = \left[f_{BV}^{2/3} + \left(1 - f_{BV}^{2/3}\right) - 1\right]\pi d^2 \sigma \qquad \ldots (2.17)$$

where f_{BV} is the bubble breakage volume fraction.

The expression for the collision efficiency finally appears very similar to the previous expression for bubble breakage probability/efficiency:

$$P_B(f_{BV}, \lambda) = \exp\left\{-\frac{\bar{e}_i(d)}{\bar{e}(\lambda)}\right\} \qquad \ldots (2.18)$$

Note that in collision efficiency equations hydrodynamic properties of the fluid, such as surface tension and density, play an important role.

2.3.1.3.2 Bubble coalescence models

The rate of bubble coalescence may be accelerated or decelerated by turbulence, depending on the physical properties of the system. Although local velocity fluctuations will increase the rate of collisions between bubbles, very few of these collisions will actually result in coalescence events. This is due to the fact that two colliding bubbles need to stay in contact with one another for the processes of film drainage and film rupture to occur. If the velocity fluctuations cause the bubbles to re-separate during this process, no coalescence will obviously occur.

Bubble coalescence rates are modelled analogous to breakage rates: they are determined by both a collision frequency term and a coalescence efficiency term. For the collision rate term, the bubble collision rate expression can be used, substituting the eddy diameter (λ), with a second bubble diameter:

$$\theta_{B1,B2}(d_1, d_2) = \frac{\pi}{4} n_1 n_2 (d_1 + d_2)^2 \left(\overline{u_1^2} + \overline{u_2^2}\right)^{1/2} = C\varepsilon^{1/3} n_1 n_2 (d_1 + d_2)^2 \left(d_1^{2/3} + d_2^{2/3}\right)^{1/2}$$

$$\ldots (2.19)$$

Once again collision frequency is a function of bubble diameters, bubble densities and the energy dissipation rate. The expression for the coalescence efficiency between two bubbles is dependent on the criteria that the force which presses two bubbles together must act for a sufficient time to allow the encaptured film of liquid between the two bubbles to drain to a critical thickness so that film rupture and coalescence will take place. Therefore, it can be seen that coalescence will take place if the bubble contact time, τ, exceeds the necessary coalescence time of the bubbles, t_c. An expression for the efficiency will thus have the following form (*Coulaloglou* and *Tavlarides*, 1977):

$$\xi_{12} = \exp\left(-t_c/\tau\right) \qquad \ldots (2.20)$$

From Kolmogoroff's theory of isotropic turbulence it can be shown that the mean contact time between bubbles is (*Lee et al.*, 1987):

$$\tau = C\frac{(d_1 + d_2)^{2/3}}{\varepsilon^{1/3}} \qquad \ldots (2.21)$$

Using the parallel disc model, which assumes that the surfaces of the coalescing bubbles deform into parallel plates and a film is squeezed out from between these parallel plates during film thinning, an expression for the coalescence time can be obtained:

$$t_c = \left(\frac{r_{12}^3 \rho_l}{16\sigma}\right)^{1/2} \ln\frac{h_o}{h_f} \qquad \ldots (2.22)$$

where h_o and h_f are the initial and final (critical) film thicknesses, and r_{12} is given by:

$$r_{12} = \frac{1}{2}\left(\frac{1}{r_{b1}} + \frac{1}{r_{b2}}\right)^{-1} \qquad \ldots (2.23)$$

As can be seen from the above expressions, it is very difficult to calculate coalescence efficiencies due to the difficulties associated with estimating values for h_o and h_f. This issue will be addressed in a later chapter. The final bubble coalescence rate equation therefore, has a form analogous to the following:

$$\Omega_{B1,B2}(d_1,d_2) = C\varepsilon^{1/3} n_1 n_2 (d_1 + d_2)^2 \left(d_1^{2/3} + d_2^{2/3}\right)^{1/2} \exp\left(\frac{-t_c}{\tau}\right) \quad \ldots (2.24)$$

2.3.2 Empirical modelling of design parameters

Unfortunately, theoretical explanation has lagged behind traditional empiricism due to its inherent complexity. Owing to their simplicity, conventional empirical models have become a long-established norm in industrial practice. This has resulted in a magnitude of correlations to predict design parameters and has led to some confusion and misinformation as a result of divergent results. The following review will highlight some of the most important correlations for reactor design parameters, based on *Kolmogoroff's* theory of isotropic turbulence. This theory has found wide application in correlations due to its simplicity (as mentioned before): the fact that hydrodynamics in reactors can be accounted for by a single parameter, the energy dissipation rate.

2.3.2.1 Bubble size

As is the case with many other aspects to be considered in this section, bubble size has received a great deal of attention, but as yet there are no reliable general correlations available (*Kawase* and *Moo-Young*, 1990). This can be attributed to the fact that bubble size and bubble size distributions differ significantly depending on the region where the bubble finds itself (in different hydrodynamic regimes). Apart from bubbles being formed at an orifice or sparger, it can, however, generally be said that a balance between the rates of bubble break-up and coalescence determines the bubble size (distribution). For this case, Kolmogoroff's theory of isotropic turbulence is

generally accepted to be applicable. As has been mentioned earlier, Kolmogoroff (*Kawase* and *Moo-Young*, 1990) and *Hinze* (1955) suggested that the maximum stable bubble size in turbulence can be estimated by means of dimensional analysis based on the above mentioned theory. This yielded the following form of a relationship implying that bubble size is determined by a balance between the dynamic forces of liquid motion and surface tension forces:

$$D_p \approx \frac{\sigma^{3/5}}{\rho^{3/5}\varepsilon^{2/5}} \qquad \ldots (2.25)$$

This equation can also be derived from energy considerations between stabilising surface energy and the opposing turbulent energy (*Leng and Quarderer*, 1982). It should be noted that this equation can be considered as an estimation of the diameter of the largest bubble stable against break-up.

Due to the fact that this functional dependence was determined from dimensional analysis, it has widely been used to correlate data for average bubble size. Using this, *Calderbank* (1958) proposed the following correlation for dispersions of gas bubbles in solutions of electrolytes:

$$D_p = 2.25\frac{\sigma^{3/5}}{\rho^{3/5}\varepsilon^{2/5}}\phi_g{}^{0.4}\left(\frac{\mu_g}{\mu_l}\right)^{0.25} \qquad \ldots (2.26)$$

This clearly revealed that the mechanism of bubble formation in turbulent reactors is so complicated that the direct application of isotropic turbulence theory is not enough to describe it, and needs to be modified. Since then, many other correlations of approximately identical functional form have been proposed, such as the following by *Lee and Meyrick* (1970):

$$D_p = 4.25\frac{\sigma^{3/5}}{\rho^{3/5}\varepsilon^{2/5}}\phi_g{}^{0.5} \qquad \ldots (2.27)$$

Kolmogoroff's theory can also be applied to bubble coalescence to obtain an expression for the size of the smallest bubble stable against coalescence, as compared to the approach followed above for bubble breakup. *Sprow* (1967), *Coulaloglou and Tavlarides* (1977) and *Thomas* (1981) proposed that the force which presses a pair of bubbles together is related to turbulent pressure fluctuations, mathematically expressed as follows:

$$F \approx \rho u^2 l^2 \approx \rho \varepsilon^{2/3} D_p^{8/3} \quad \ldots (2.28)$$

Combined with an expression for the film drainage time, we have:

$$T \approx \frac{3}{32\pi} \mu \rho \varepsilon^{2/3} D_p^{8/3} \left(\frac{D_p}{\sigma h} \right)^2 \quad \ldots (2.29)$$

Equating the above with the following expression for the time scale t, gives:

$$t \sim l/u \sim \left(l^2/\varepsilon \right)^{1/3} \sim \left(D_p^{\,2}/\varepsilon \right)^{1/3} \quad \ldots (2.30)$$

The following expression was obtained for the size of the smallest bubble stable to coalescence:

$$D_p = 2.4 \left(\frac{\sigma^2 h^2}{\mu \rho \varepsilon} \right)^{1/4} \quad \ldots (2.31)$$

Alternatively, using a combination of the isotropic turbulence theory and coagulation theory, Metkin and Sokolov (*Kawase* and *Moo-Young*, 1990) derived the following theoretical correlation for D_p, analogous to the expressions obtained with bubble breakup equations:

$$D_p = 1.25 \frac{\sigma^{3/5}}{\rho^{3/5} \varepsilon^{2/5}} \phi^{0.37} \left(\frac{\rho}{\rho_g} \right)^{1/5} \quad \ldots (2.32)$$

Despite all the above correlations, substantial work still needs to be done on D_p to establish reliable correlations.

2.3.2.2 Interfacial area

Gas-liquid interfacial area plays an important role in the mass transfer rate, as can be seen from the expression for the volumetric mass transfer coefficient, k_La, the proportionality constant for the driving force behind mass transfer. For this reason many attempts have been made at prediction of this parameter, often with divergent results. *Calderbank* (1958) proposed an empirical correlation for *a*, namely:

$$a = 1.44 \frac{\varepsilon^{2/5} \rho^{3/5}}{\sigma^{3/5}} \left(\frac{U_{sg}}{U_{b\infty}} \right)^{0.5} \quad \ldots (2.33)$$

Again it can be observed from the functionality of this equation that it is based on Kolmogorov's theory of isotropic turbulence. Other expressions derived for the specific area include that of *Nagel et al.* (1979), who, using Kolmogorov's theory, stated that :

$$a \sim \varepsilon^{2/5} \phi_g{}^{\beta} \quad \ldots (2.34)$$

where β can vary between 0.4 and 1.0; and Kastanek (*Kawase* and *Moo-Young*, 1990), who obtained the following relationship:

$$a \sim \left(\frac{\rho}{\sigma} \right)^{3/5} U_{sg}{}^{2/5} \left(\frac{\mu_g}{\mu} \right)^{2/5} \left(1 - \phi_g\right)^{2/5} \phi_g{}^{0.6} \quad \ldots (2.35)$$

Note that the two latter mentioned expressions include a 'gas holdup' - term for prediction of the interfacial area. Since:

$$a = \frac{A}{V} \sim \frac{1}{D_p} \phi_g \quad \ldots (2.36)$$

this seems like a more worthwhile approach compared to the use of superficial gas velocities and bubble terminal rise velocities by *Calderbank*. There, however, exists a problem in that it is difficult to obtain reliable measurements of the specific interfacial area, since neither physical nor chemical methods produce high accuracy results. The validity of the above correlations will therefore only fully be realised once this problem has been addressed.

2.3.2.3 Gas hold-up

Gas hold-up is a very important parameter characterising the hydrodynamics of a reactor and is mainly determined by the gas velocity, power input and physical properties of the liquid. Although a wealth of information is available on gas hold-up, no generalised correlation could as yet be proposed due to the scatter in these data.

Keeping in mind that the gas hold-up is related to the average bubble size and interfacial area by the following equation:

$$a = \frac{6\phi_g}{D_p} \qquad \ldots (2.37)$$

a correlation for the gas holdup can be derived by the combination of correlations mentioned above. An example of such a correlation is as follows:

$$\phi_g = \left(\frac{U_{sg}\phi_g}{U_{b\infty}}\right)^{1/2} + 0.0216\frac{\varepsilon^{2/5}\rho^{3/5}}{\sigma^{3/5}}\left(\frac{U_{sg}}{U_{b\infty}}\right)^{1/2} \qquad \ldots (2.38)$$

Kudrewizki (*Kawase* and *Moo-Young*, 1990) derived a theoretical model for the gas holdup using Kolmogoroff's theory and expressions for the potential and kinetic energies of gas. Equating the latter two equations, and invoking Kolmogoroff's theory, the following equation was derived:

$$\frac{\phi_g}{1-\phi_g} = \frac{1}{2}\frac{U_{sg}^{2/3}}{(gl)^{1/3}}\frac{\rho}{\rho-\rho_g} \quad \ldots (2.39)$$

Note that this equation does not take into account the influence of mixing (no energy dissipation term), and is therefore of broader application in contactors such as bubble columns. Many gas hold-up correlations for bubble columns (such as the above mentioned model) are found in the literature. However, since these models do not account for the energy dissipated in the reactors, and are therefore strictly not applicable to highly turbulent systems, no further discussion of this subject is deemed necessary.

2.3.2.4 Mass transfer coefficient

Since most gas-liquid contacting systems are characterised by the fact that mass transfer rates are limited by the transport of gas to the liquid, extensive literature on mass transfer, and prediction thereof by means of empirical correlations, exist.

Calderbank and *Moo-Young* (1961) employed Kolmogoroff's theory of isotropic turbulence to predict mass transfer in turbulent stirred tanks, defining the Reynolds number, as proposed by Batchelor (*Kawase* and *Moo-Young*, 1990), as follows:

$$\mathrm{Re} = \frac{ul}{\nu} = \frac{\varepsilon^{1/6} l^{2/3}}{\nu^{1/2}} \quad \ldots (2.40)$$

This Reynolds number was used in stead of its conventional form in existing correlations for mass transfer. Assuming that $l \sim D_p$, the following correlation was obtained:

$$\frac{k_L D_p}{D} = 0.13\left(\frac{\mu}{\rho D}\right)^{1/3}\left(\frac{\varepsilon^{1/6} D_p^{2/3}}{\nu^{1/2}}\right)^{3/2} \quad \ldots (2.41)$$

which is equivalent to the following expression in terms of the energy dissipation rate:

$$k_L = 0.13(\varepsilon\nu)^{1/4} Sc^{-2/3} \quad \ldots (2.42)$$

This correlation has been verified by *Kawase* and *Moo-Young* (1987). It should at this stage be noted that the mass transfer coefficient seems to increase at a rate proportional to $\varepsilon^{1/4}$. Also, the above equation was derived using solid-liquid mass transfer data, and should therefore only be taken as applicable to small (rigid-sphere) bubbles.

Kulov et al. (1983) also derived a 'theoretical' correlation for k_L, applicable to small rigid sphere bubbles:

$$k_L = \frac{2(2)^{1/2}}{\pi}\left(\frac{v_O D^3}{\delta^3}\right)^{1/4} \quad \ldots (2.43)$$

which, assuming that the friction velocity υ_o, is approximately equal to the root mean square of the fluctuating velocity u, and that the thickness of the viscous sublayer δ, is equal to l, can be simplified to yield the following expression for the mass transfer coefficient in terms of the energy dissipation rate:

$$k_L = 0.267(\varepsilon\nu)^{1/4} Sc^{-3/4} \quad \ldots (2.44)$$

Combining Higbie's penetration theory and Kolmogoroff's isotropic turbulence theory, Kastanek (*Kawase* and *Moo-Young*, 1990) derived an expression for the mass transfer coefficient. Higbie's theory was used as a point of departure:

$$k_L = \frac{2}{\pi^{1/2}}\left(\frac{D}{t_e}\right)^{1/2} \quad \ldots (2.45)$$

The exposure time was calculated in terms of the energy dissipation rate via the following:

$$t_e = \frac{l}{u} = \left(\frac{\nu}{\varepsilon}\right)^{1/2} \quad \ldots (2.46)$$

The above equations were then substituted into one another to yield:

$$k_L = \frac{2}{\pi^{1/2}} (\varepsilon \nu)^{1/4} Sc^{-1/2} \quad \ldots (2.47)$$

It must, however, be noted that a certain amount of uncertainty exists regarding the direct application of Higbie's theory in this case. Indeed, it has been stated that both the functional form of the equation and the value of the proportionality constant is incorrect (*Lamourelle* and *Sandall*, 1972).

2.3.2.5 Volumetric mass transfer coefficient

Correlations for the volumetric mass transfer coefficient, k_La, is therefore easily obtained by the product of correlations developed so far for interfacial area and mass transfer coefficients. A typical example of such an equation would be that of *Kawase* and *Moo-Young* (1987):

$$k_L a = 0.452 \frac{\rho^{3/5} \nu^{1/4}}{\sigma^{3/5}} \varepsilon^{59/60} \frac{1}{D_c^{1/6} g^{1/2}} \left(\frac{\mu_g}{\mu}\right)^{1/4} Sc^{-1/2} \quad \ldots (2.48)$$

Equations of this type are, however, tedious to use and can be simplified to yield the following general form for k_La correlations:

$$k_L a \sim (\varepsilon)^a (U_{sg})^b \quad \ldots (2.49)$$

where the constants *a* and *b* reported in the literature vary from 0.4 – 0.8 and 0.25 – 0.5, respectively. Once again it can be noted that very accurate

correlations are not possible due to poor accuracy in interfacial area experiments.

2.4 FINAL REMARKS ON THE LITERATURE SURVEY

The purpose of any literature survey is to provide the reader with a thorough background to the field of study, so that discussions of results and models applied in this investigation can be put into perspective. This was done by presenting information from the literature under the following headings:

- Conventional and novel gas-liquid contacting equipment.
- Impinging stream technology.
- Previous research done at this institution.
- Mechanistic modelling concepts and techniques.
- Empirical modelling of design parameters.

Conventional and novel gas-liquid contacting equipment

It has been demonstrated how mixing devices have been developed towards a type of phase contacting device where intense turbulent mixing is increasingly being used to enhance interfacial area production and mass transfer. This is exemplified by the many papers presented in the literature on reactors such as venturi ejectors, jet loop reactors and reactors employing the centrifugal acceleration of fluid, such as the high intensity contactor proposed by *Waldie and Harris* (1998). In this chapter, each of these systems have been discussed to provide information regarding their principles of operation and inherent advantages to illustrate the train of thought leading towards the development of the reactors in this investigation.

Impinging stream technology

The increasing use of impinging stream jet loop reactors (*Spehe et al.*, 1998), as well as recent research performed in the field of impinging stream absorbers (*Herskowits et al.*, 1990 and *Tamir*, 1994) have signified an increased awareness of the advantages associated with impinging stream technology. This review has provided some insight into the intensification

correlations are not possible due to poor accuracy in interfacial area experiments.

2.4 FINAL REMARKS ON THE LITERATURE SURVEY

The purpose of any literature survey is to provide the reader with a thorough background to the field of study, so that discussions of results and models applied in this investigation can be put into perspective. This was done by presenting information from the literature under the following headings:

- Conventional and novel gas-liquid contacting equipment.
- Impinging stream technology.
- Previous research done at this institution.
- Mechanistic modelling concepts and techniques.
- Empirical modelling of design parameters.

Conventional and novel gas-liquid contacting equipment

It has been demonstrated how mixing devices have been developed towards a type of phase contacting device where intense turbulent mixing is increasingly being used to enhance interfacial area production and mass transfer. This is exemplified by the many papers presented in the literature on reactors such as venturi ejectors, jet loop reactors and reactors employing the centrifugal acceleration of fluid, such as the high intensity contactor proposed by *Waldie and Harris* (1998). In this chapter, each of these systems have been discussed to provide information regarding their principles of operation and inherent advantages to illustrate the train of thought leading towards the development of the reactors in this investigation.

Impinging stream technology

The increasing use of impinging stream jet loop reactors (*Spehe et al.*, 1998), as well as recent research performed in the field of impinging stream absorbers (*Herskowits et al.*, 1990 and *Tamir*, 1994) have signified an increased awareness of the advantages associated with impinging stream technology. This review has provided some insight into the intensification

mechanisms behind this technology, illustrating how it promotes increases in the:

- relative velocity between particles, leading to a decrease in the mass transfer resistance,
- mean residence time due to particle penetration into opposing streams and resulting oscillations, and
- shear forces between particles, leading to enhanced bubble break-up and surface renewal rates (and the mass transfer coefficient).

Previous research done at this institution

Since the work done in this investigation was a continuation of previous research performed in this field by *Botes et al.* (1998), it was important to highlight the most important results and conclusions made by this author. This would lead to a better understanding of the work in this investigation. *Botes* made the following important conclusions:

- The opposing jets reactor in the GL-configuration proved to represent the most efficient geometry.
- The arrangement of nozzles plays a critical role in the efficiency of the reactors.
- Nozzle placement must allow for the injection of feed streams from diverse directions to sustain high levels of turbulence throughout the reactor.

All the above considerations were taken into account in the design of two new impinging stream jet reactors. Results obtained for these reactors are discussed in Chapter 5.

Mechanistic modelling concepts and techniques

As part of their research, *Botes et al.* (1998) also developed a mechanistic stochastic model for the prediction of the interfacial area produced in the jet reactors. To put this into perspective, this part of the review has provided a concise summary and comparison of the two most important techniques for modelling of dispersed systems, namely Monte Carlo simulations and population balances. Since bubble break-up is assumed to be the result of interactions with turbulent eddies, typical equations (presented by various authors) describing the collision rate and collision efficiency between eddies

and bubbles are provided to serve as a background to those equations applied in the model. Many of these equations are based upon Kolmogoroff's theory of isotropic turbulence – the fundamentals behind this theory and the reason for its application in this work is therefore, also discussed.

Empirical modelling of design parameters

An additional aspect of the modelling done in this investigation was the empirical modelling of design parameters such as bubble size, mass transfer coefficients and interfacial areas. Due to the complexity associated with modelling of dispersed gas phase systems, this approach has conventionally been followed by most researchers, leading to a wide array of correlations in the literature. Therefore, typical functional forms of these correlations were provided in this chapter, focussing on different approaches adopted by various researchers in developing them. This would provide better understanding of the effects of various operating parameters on design variables when comparing experimental correlations with those presented in the literature.

Continuation of the development of high intensity impinging stream jet reactors is therefore justified in view of the above. Since a general need for better understanding of the interaction of mechanisms in dispersed phase systems continues to exist, development and improvement of descriptive mechanistic models for this purpose is also justified.

CHAPTER 3

EXPERIMENTAL

The quantification of the efficiency of a novel reactor system (for comparison with conventional systems) not only involves the development of the reactor, but also the use of a suitable chemical system for determining the appropriate mass transfer parameters. For this purpose the literature was once again surveyed to find a safe and simple system which allowed for accurate determination of these parameters. The following chapter will provide insight into the various strategies and chemical systems employed conventionally, with special regard to those used in this project. In addition to this, a description of the experimental set-up and procedure will be given.

3.1 CHEMICAL SYSTEMS

3.1.1 Choosing a suitable chemical system

In choosing a suitable chemical system, a number of key factors have to be considered. The most significant of these are:

- Both the reagents and products must be safe. Gases used must preferably be non-toxic; if toxic, as in the case of H_2S, chlorine and SO_2 gas, suitable measures should be taken to ensure safe concentration limits. Likewise, liquid solutions should present minimal harm to skin, etc.
- The reagents used must be cheap and readily available. These reagents should be as pure as possible, since the presence of impurities and surfactants in solutions have considerable effects on bubble phenomena such as coalescence.
- Chemical analyses of the products should be fast and simple, yet accurate. It is well known that analyses of products often account for the most strenuous part of many experimental investigations. In addition to

$$\therefore k_L a = \frac{\dot{n}_A}{\left(C_A^* - C_{AO}\right)} \qquad \ldots (3.2)$$

It is often necessary to know the values of these parameters seperately, to predict the absorption rate when physical absorption is actually accompanied by chemical reaction. Two different absorbers might exhibit the same value for $k_L a$, but under chemical absorption one system might outperform the other (due to the enhancement of k_L by certain other factors, eg. solute concentration, etc.). Therefore, chemical absorption processes seem to present the only viable option.

In the light of the above considerations, it was decided to use two chemically enhanced systems for the separate determination of the mass transfer parameters exhibited by the reactors under investigation. The primary system used was the chemical absorption (chemisorption) of carbon dioxide CO_2 into sodium hyroxide solutions. A secondary system was also employed for generation of additional data for the verification of model output data. This system involved the oxidation of sodium sulphite solutions in the presence of a cobaltous catalyst. The following section will briefly discuss the above two systems.

3.1.2 Chemical systems employed

3.1.2.1 Absorption of CO_2

The chemisorption of carbon dioxide in an aqueous solution of sodium hydroxide is a well-understood reaction for which comprehensive kinetic data is available (*Danckwerts* and *Sharma*, 1966). It is a simple and safe reaction, leading to a stable product which can be analysed easily.

The reaction in the liquid phase can be described by the following mechanisms:

$CO_2 + OH^- \Leftrightarrow HCO_3^-$ . . . (R3.1)

$HCO_3^- + OH^- \Leftrightarrow CO_3^{2-} + H_2O$ . . . (R3.2)

$CO_2 + H_2O \Leftrightarrow HCO_3^- + H^+$ . . . (R3.3)

$H^+ + OH^- \Leftrightarrow H_2O$ . . . (R3.4)

In the pH-range under consideration (pH > 7), only reactions R3.1 and R3.2 are of importance. At high hydroxide concentrations (pH > 12.5), hydrogen carbonate is instantaneously converted to carbonate ions, while with decreasing hydroxide concentration (9 < pH < 12), the concentration of hydrogen carbonate becomes more significant until it completely dominates at pH-values of 7 – 9. However, for the purpose of the experimental work, pH-values of 13+ were measured: reactions R3.1 and R3.2 were therefore considered as one:

$CO_2 + 2OH^- \Leftrightarrow CO_3^{2-} + H_2O$ . . . (R3.5)

It is thus, effectively, an irreversible second-order reaction (reaction equilibrium lies far to the right). Most of the experiments were conducted in this regime, with hydroxide concentrations in the order of 0.5M. However, some experiments were performed in the pseudo-first order regime: physically the situation is that the mass transfer coefficient is large enough so that the concentration of reactant is maintained virtually undepleted, with its bulk concentration holding right up to the surface (of the bubble). In this case hydroxide concentrations of ~2.5M were used to satisfy the condition for a pseudo first order reaction:

$$\sqrt{D_A k_1 C_{BO}} > 3k_L \quad \text{. . . (3.3)}$$

This corresponds to absorption with 'fast pseudo-first order reaction' where the enhancement factor, which will be discussed in greater detail in the next chapter, could be approximated by:

$$E = \sqrt{M} = Ha \qquad \ldots (3.4)$$

This greatly simplified the equations used for determining the mass transfer coefficient, k_L. Values obtained for k_L in this way were more stable than those calculated normally, as will be discussed in the next chapter.

3.1.2.2 Oxidation of sulphite solutions

In aqueous solution sulphite ions are oxidised by the absorbed oxygen according to the following overall reaction equation:

$$O_2 + 2SO_3^{2-} \Rightarrow 2SO_4^{2-} \qquad \ldots (R3.6)$$

The reaction is catalysed by the addition of various metallic ions, particularly copper and cobalt (typically as sulphates). Due to its relatively complex kinetics, many authors have published papers using this reaction; yet, the reaction mechanism has remained somewhat "badly" understood. For example, *De Waal* and *Okeson* (1966) and *De Waal* and *Beek* (1967) concluded that the reaction had a real first order character over a wide range of sulphite concentrations, while *Astarita* (1967) and *Wesselingh* and *Van't Hoog* (1970) proved that the reaction actually exhibited second order characteristics.

Measurements of oxygen absorption rates at different oxygen partial pressures using cobalt as a catalyst in a wetted wall column (*Reith* and *Beek,* 1973) have, however, to a great extent, eliminated this uncertainty. Under specific conditions it was found that the reaction is second-order with respect to oxygen, first order in cobalt and zero-order in sulphite. It was also found that the rate of reaction is very dependent on pH: continuous adjustment of

the pH is therefore necessary to keep the reaction rate constant as oxidation proceeds. The ionic strength of the solution also proved to play an important role: liquid should not be allowed to come into contact with brass or copper, as it will dissolve copper which, in the presence of cobalt, reduces the reaction rate. By changing the pH, temperature and catalyst concentration, it was found that the second order reaction rate constant could be varied between 2×10^5 m^3/kmol.s and 10^8 m^3/kmol.s.

Cobalt was also proved to be a better catalyst than copper, for various reasons. Cobalt is simply a more effective catalyst than copper, and yields more reproducible results during absorption experiments. Furthermore, it is quite difficult to determine exactly how much copper is present in solution as unreduced Cu^{2+}, as opposed to Cu^{+}, in a sulphite solution (*Barron* and *O'Hern*, 1966). For these reasons, all absorption experiments were catalysed with cobalt.

The conclusions made above were obtained from experiments performed within a specified range of parameters, which are as follows:

$$3 \times 10^{-5} \text{ kmol/m}^3 < C_{Co^{2+}} < 10^{-3} \text{ kmol/m}^3$$

$$15°C < T < 33°C$$

$$7.50 < pH < 8.50$$

$$0.4 \text{ kmol/m}^3 < C_{SO_3^{2-}} < 0.8 \text{ kmol/m}^3$$

$$p_{O_2} = 10^5 \text{ N/m}^2$$

These conditions have been applied by the majority of researchers when using the sulphite oxidation method for determining mass transfer parameters. They were therefore, also applied in the jet reactor experiments so that the data published for the sulphite oxidation reaction could be directly applied.

As is the case with CO_2 absorption experiments, this reaction can also be regarded as a pseudo-first order reaction. This approximation is valid at least up to the point where 50% of the amount of sulphite originally present

(~0.8M), is oxidised. If the sulphite concentration becomes too low, the reaction becomes second order; the absorption rate is then also determined by the sulphite concentration and the first order approximation is not valid. In the jet reactor experiments, sulphite concentrations were always maintained above 0.4M: therefore absorption data was analysed using the pseudo-first order approximation.

Although the above chemical system proved to be rather complicated, it was employed due to the fact that a vast amount of literature on the application of the method is available, facilitating easy comparison with other systems in terms of mass transfer parameters. The fact that oxygen, and not toxic chlorine or H_2S gasses, could be used, also seemed to present a safer option.

3.2 ANALYSIS TECHNIQUES

3.2.1 CO_2 absorption

For calculation of the absorption rate, accurate values of both the liquid feed and product stream hydroxide concentrations needed to be obtained. For this purpose, pH-electrodes have been used by other researchers; it was, however, found that they were rather inaccurate, especially at high pH-values. Therefore, titration of the liquid samples was used as a suitable and highly accurate analysis method.

Since only the hydroxide concentration needed to be determined, simple acid-base titrations were employed. Feed samples were titrated directly with a standardised acid, using phenolphtaleien or methyl red as an indicator:

$$OH^- + H^+ \Rightarrow H_2O \qquad \ldots (R3.7)$$

However, liquid product samples cannot be titrated this way. Carbonate ions present in the sample (produced in the absoprtion reaction) may interfere as the titration nears its endpoint, also reacting with the acid:

$$CO_3^{2-} + H^+ \Leftrightarrow HCO_3^- \quad \ldots (R3.8)$$

$$HCO_3^- + H^+ \Leftrightarrow H_2CO_3 \quad \ldots (R3.9)$$

Thus, similar to *Haimour and Sandall* (1983), an excess of barium chloride salt was added to the product sample immediately at sample-taking, effectively precipitating the carbonate (solubility of $BaCO_3$ ~ $1.2x10^{-4}$ mol/L):

$$CO_3^{2-} + Ba^{2+} \Leftrightarrow \underline{BaCO_3} \quad \ldots (R3.10)$$

The remaining clear liquid solution was then simply decanted off and titrated against acid, as with the feed samples.

3.2.2 Oxidation of sulphite solutions

Analogous to the method outlined above, sulphite ion concentrations of both the feed and product samples had to be determined for calculation of absorption rates. A literature survey on the subject produced a rather limited number of standard methods, most of which were rather complicated. Of these methods, the principle of iodimetric titration presented the simplest approach.

The method basically entailed pipetting a fixed amount of standardised iodine solution into a conical flask, whereafter it was acidified and diluted with water. A fixed amount of the sulphite solution was then added to this solution, effectively reducing the iodine to iodine ions:

$$SO_3^{2-} + I_2 + H_2O \Leftrightarrow SO_4^{2-} + 2H^+ + 2I^- \quad \ldots (R3.11)$$

The excess I_2, in the resulting solution, was then determined by back-titration with standard sodium thiosulphate ($Na_2S_2O_3$) solution, using sodium starch glycollate (*Jeffery et al.*, 1989) as an indicator. From this, the concentration of sulphite solution originally added, could be determined:

$$3I_2 + 6e^- \Leftrightarrow 6I^- \quad \text{. . (R3.12)}$$

$$6S_2O_3^{2-} \Leftrightarrow 3S_4O_6^{2-} + 6e^- \quad \text{. . (R3.13)}$$

$$3I_2 + 6S_2O_3^{2-} \Leftrightarrow 6I^- + 3S_4O_6^{2-} \quad \text{. . (R3.14)}$$

During these titrations special care was taken to minimise the exposure of the sulphite to air: the sample solution was pipetted into the iodine solution, keeping the tip of the pipette as close to the surface of the solution as possible.

3.3 EXPERIMENTAL SETUP AND PROCEDURE

Experimental results are of very little value if they have been produced by a system of experiments which do not conform to conventional standards. The following section will provide a discussion on experimental techniques employed, as well as a description of the experimental set-up. For reference, a schematic diagram of the set-up is provided in *Figure 3.1*.

3.3.1 Liquid feed preparation

3.3.1.1 CO_2 absorption

Most ions have a catalytic effect on this chemical reaction, and are therefore undesirable. For this reason only freshly distilled water, with a conductivity below 1.5 μmhos, was used for all experiments. The water was poured into a 210 litre plastic liquid feed mixing tank which was equipped with an overhead stirrer for effective mixing. Caustic soda pellets with a purity of 98.5% were then added to obtain the required concentration, after which the tank was

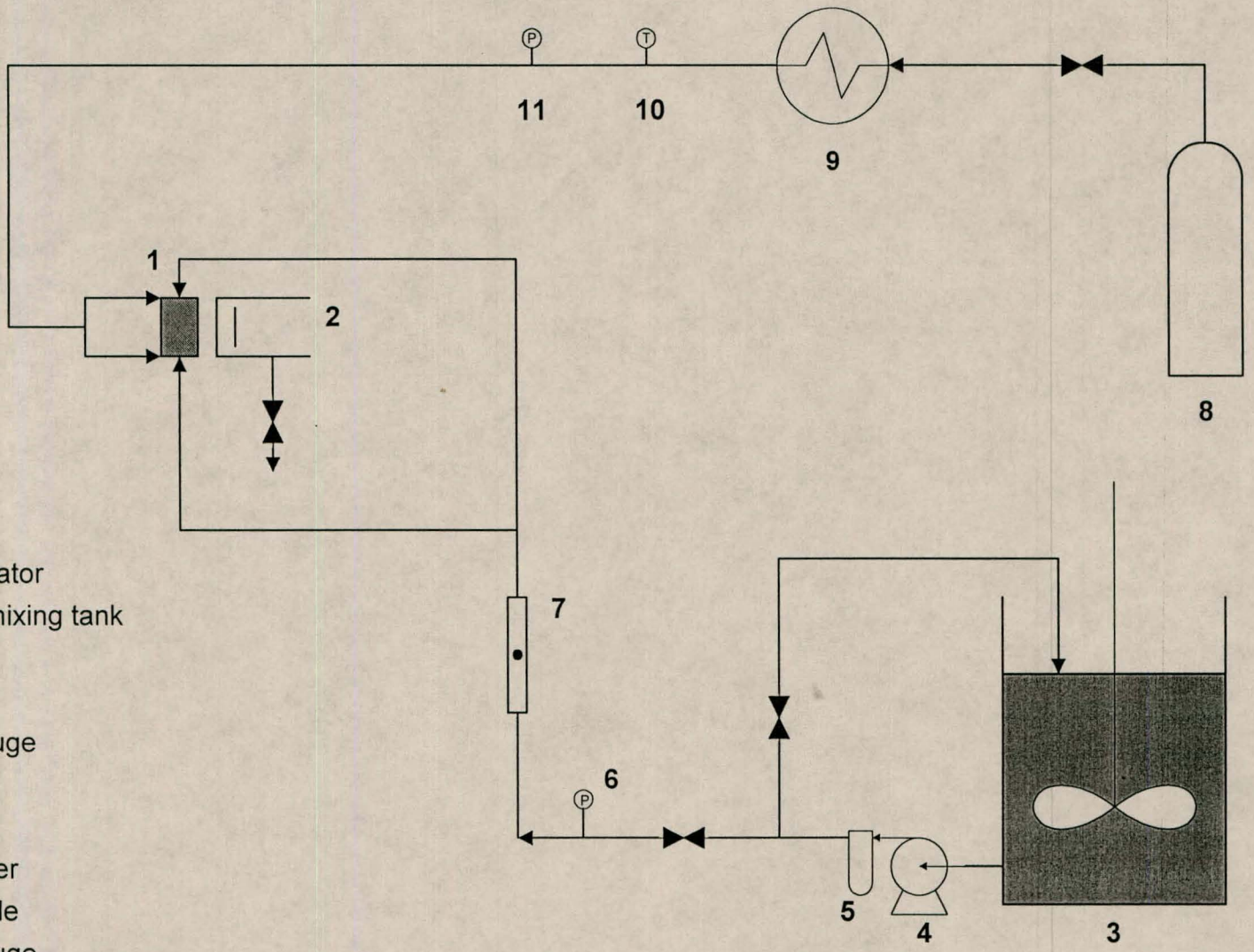

Key

1	Reactor
2	Phase separator
3	Liquid feed mixing tank
4	Liquid pump
5	Strainer
6	Pressure gauge
7	Rotameter
8	Gas cylinder
9	Gas preheater
10	Thermocouple
11	Pressure gauge

Figure 3.1 *Experimental set-up*

thoroughly mixed until all the caustic soda was dissolved. Then the liquid feed pump was started and the mixing of the tank continued under full pump recycle for at least 15 minutes, to ensure a homogeneous feed concentration.

3.3.1.2 Sulphite oxidation

Since the sulphite oxidation experiments did not require performing each set of experiments twice at different feed concentrations (this will be discussed in the next chapter), 20 litre distilled water cans were sufficient for use as feed tanks. According to the standard approach used for sulphite oxidation experiments (as discussed previously), 100 grams of 99.5% pure sodium sulphite was added per 1 litre of freshly distilled water (~0.8M). Analogous to the preparation of the sodium hydroxide feed, the liquid feed pump was then started and run at full recycle until all the sulphite was dissolved. While this was under way, the required amount of standardised cobalt sulphate catalyst solution was added from a burette. Finally, the pH of the feed solution was adjusted with 2M sulphuric acid from approximately 13.2 to 8.0 (within 0.5% accuracy).

3.3.2 Gas feed preparation

3.3.2.1 CO_2 absorption

Pure (99%) carbon dioxide, supplied from a cylinder, was used during the experiments to eliminate any gas-side resistance to mass transfer during the absorption reaction. The cylinder was fitted with both a pressure gauge and a gas flow gauge (calibrated from 0 – 20 L/min), which facilitated easy control of gas flow rates. The gas flow gauge was checked against a wet gas flow meter and found to be quite accurate. Due to the cooling of the gas as it expands through the valve, the CO_2 was fed through a coil submerged in a constant temperature water bath. The purpose of this bath served not only to heat the gas to a certain temperature, but also to ensure relatively constant gas feed temperatures during the extent of the experimental investigation. Therefore,

gas feed temperatures could be maintained between 24°C and 27°C, as measured by a thermocouple.

3.3.2.2 Sulphite oxidation

Gas feed preparation for these experiments were basically identical to that of the CO_2 absorption system. Pure oxygen was supplied from a gas cylinder and passed through the constant temperature water bath to ensure relatively constant feed temperatures. The oxygen cylinder, however, was not equipped with a gas flow gauge; therefore, gas flow rates had to be calibrated beforehand against gas pressures using a wet gas flow meter and gas rotameter. In this way, gas pressures indicated by the appropriate gauge could be associated with the corresponding gas flow rate.

3.3.3 Experiment start-up and execution

3.3.3.1 CO_2 absorption

Since experimental data for various liquid and gas flow rates (pressures) had to be obtained, a systematic experimental strategy was followed whereby each run was performed by varying the liquid flow rate between the operational settings for each given gas flow rate. This strategy was employed for each of the three gas flow rates investigated, until a complete set of data was generated. All runs were repeated in triplicate (at least) to ensure accurate values for the absorption rates.

In accordance with this, the gas flow rate was firstly set at the desired flow rate and allowed to pass through the (already heated) constant temperature water bath to achieve a steady state temperature. After this, the liquid feed valve to the reactor was opened. The liquid flow rate could be controlled by varying the amount of feed recirculated to the feed tank via this valve. A liquid rotameter and a liquid pressure gauge were used to measure the liquid flow rate and feed pressure, respectively. The liquid fed to the reactor was

contacted with the CO_2, where the product stream left the reactor as a two phase mixture.

The two phase mixture exiting the reactor immediately entered a phase separator which consisted of a cylindrical tube, supplied with a baffle. This two phase mixture sprayed against the baffle and separated quickly and completely into two phases. It was assumed that the extent of reaction taking place in the tranquil environment of the separator was negligible in comparison with the reaction taking place in the highly turbulent reactor. The reactor liquid effluent was collected in a suitable tank for disposal, while the gas was allowed to diffuse into the atmosphere.

A liquid sample was drawn for analysis from the separator for each operational setting. At least one minute was allowed between changing of the operational settings and the drawing of the sample. Considering the fact that the average residence time of liquid in the reactor was in the order of 0.5 seconds, this seemed like more than enough time for steady state conditions to set in (although this was not checked explicitly, no difference in sample concentrations taken at different elapsed times was detected). Each sample consisted of 100ml of liquid, drawn over an interval of one minute to negate the effect of small fluctuations in the liquid and gas flow rates. An excess of barium chloride, to precipitate the formed carbonate (as discussed previously), was immediately added whereafter the sample was vigorously shaken. Samples were kept overnight for complete precipitation of the barium carbonate crystals, and analysed the next morning. Samples of the liquid feed were also taken continuously at the recycle of the liquid pump.

The following operational parameters were noted for each run:

- The gas and liquid pressures at the inlet to the reactor. These values were important for determining the energy input into the reactor.
- The gas and liquid flow rates: essential for the determination of absorption rates.
- The temperature of the liquid exiting the reactor. This was measured either by a thermometer or a thermocouple. Since the reactor was viewed

as a perfectly mixed tank reactor, the temperature in the reactor was assumed to be equal to the temperature of the exiting stream.

The following table provides information regarding the range of operating conditions used in the experiments:

Table 3.1 *Range of operating conditions used for CO_2 absorption experiments*

Parameter	**Value**
NaOH inlet concentration *mol/L*	
Second order reaction	0.25 – 0.5
Pseudo first order reaction	2.25 – 2.5
Gas flow rate *L/min*	10 – 20
Gas inlet pressure *kPa*	135 – 240
Liquid flow rate *L/min*	1.21 – 2.04
Liquid inlet pressure *kPa*	120 – 589
Reaction temperature ^oC	23 – 28

3.3.3.2 Sulphite oxidation

The experimental procedure for this system varied minimally from the procedure described above. Once again, each run was performed by varying the liquid flow rate between the operational settings for each given gas flow rate. Liquid samples were also taken at each operational setting; to each of these samples a few drops of EDTA solution were added to form complexes with any metallic ions present in the solution which could catalyse the reaction between sulphite and air from the atmosphere. For this reason, samples were analysed as soon as possible.

The following table provides information regarding the range of operating conditions used in the experiments:

Table 3.2 *Range of operating conditions used for sulphite oxidation experiments*

Parameter	Value
Sulphite inlet concentration *mol/L*	~0.8
Gas flow rate *L/min*	3 – 5
Gas inlet pressure *kPa*	100 – 200
Liquid flow rate *L/min*	1.21 – 2.04
Liquid inlet pressure *kPa*	120 – 589
Reaction temperature ^{o}C	28 – 33

3.3.4 Reactor designs

One of the main objectives of this study, as had been the case for *Botes* (1998), was to investigate different reactor configurations in the search for an optimum design in terms of mass transfer performance. In this regard, *Botes* tested various reactor shapes and nozzle-configurations, finally presenting three reactor designs, of which the so-called 'kite-shaped' reactor (volume = 8.4 ml) exhibited superior performance (as discussed in *Chapter 2*).

This was the first reactor design investigated as part of this particular study (*Figure 3.2*), since it was necessary to verify experimental procedures and claimed experimental results. Good agreement was found between data generated by ourselves and that quoted by *Botes*.

In the design of the new π-shaped reactor (the nozzle configuration resembles an upside-down π symbol), the following conclusions made by Botes during his investigations, were kept in mind:

- The angle of impingement between gas and liquid streams is an important design consideration: each liquid spray must be directed slightly towards an opposing gas nozzle so as to shear off gas bubbles as they exit the nozzle, before colliding with another liquid stream or the reactor wall.

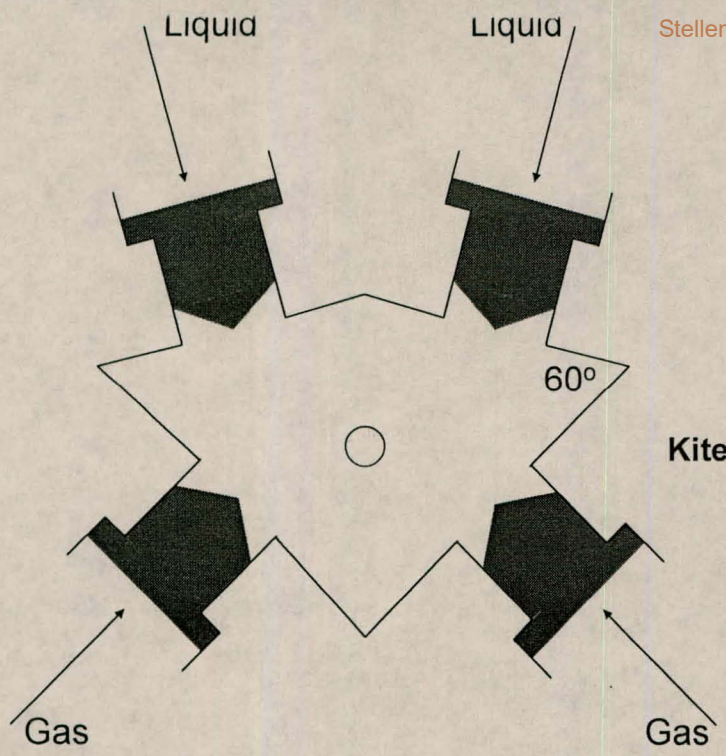

Kite-shaped reactor

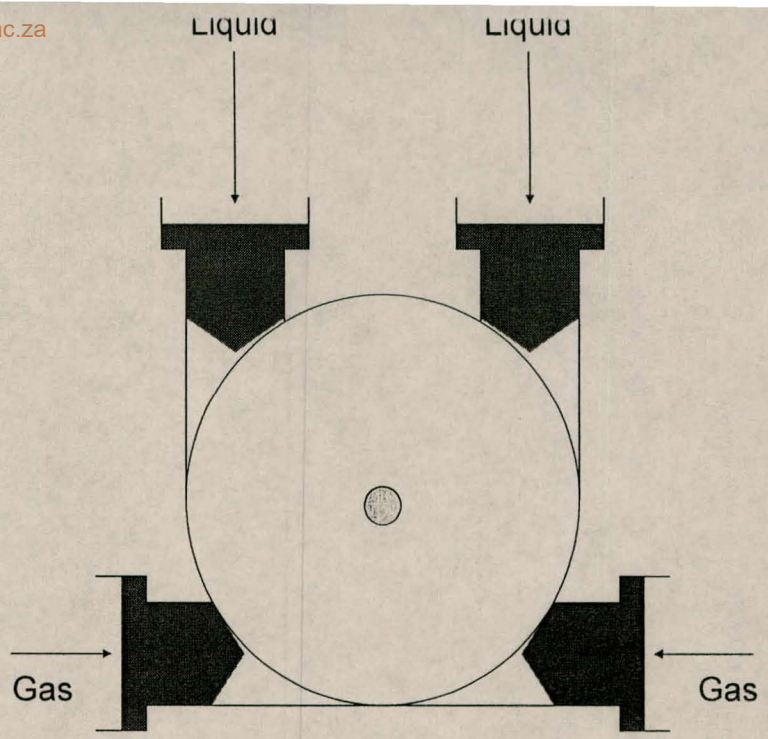

π - shaped reactor

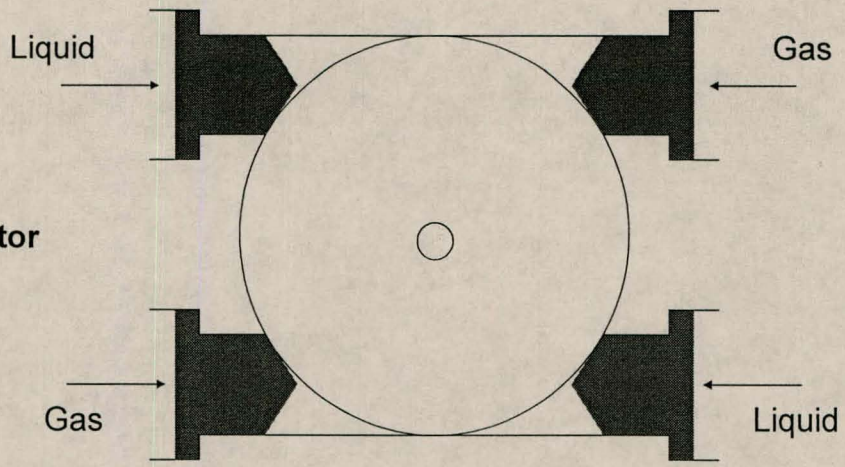

σ - shaped reactor

Figure 3.2 *Reactors investigated*

- The reactor geometry must allow for the reflection of these liquid and gas streams off its walls to sustain a homogeneous distribution of turbulence and momentum throughout the reactor, thereby avoiding the formation of any plug flow regions (where bubble coalescence has been seen to occur) in the reactor.

In terms of the first conclusion, the design strategy not only made provision for the shearing off of gas bubbles from their corresponding nozzles, but also for the head-on impingement of the resulting two-phase streams, which (theoretically) would result in extra intensification of mass transfer processes. In terms of the second conclusion, a circular reactor chamber (volume = 20 ml) was designed for efficient sustainment of turbulence. This larger reaction volume was used to improve upon the energy efficiency of the reactor. It was also thought that the extra shear effect between the two gas-liquid streams moving upwards after impingement (*Figure 3.3*), would result in additional bubble break-up and renewal of surface area.

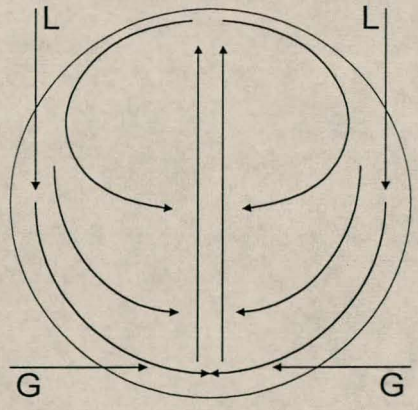

Figure 3.3 *Possible flow patterns in the π-shaped reactor*

The final reactor investigated was the so-called σ-shaped reactor (volume = 20 ml), so called due to the fact that the design resembled four overlapping σ symbols, each rotated 90 degrees relative to one another. This design improved upon the previous design by incorporating two impingement zones (as opposed to only one) and allowing more effective promotion and sustainment of turbulence. Due to the swirling motion of the liquid under the

influence of centrifugal acceleration, the potential also existed for enhancement of the mass transfer coefficient, as previously discussed in *Chapter 2*.

Despite their different reactor chamber geometries and nozzle configurations used, all the above reactors were basically identical. All incorporated four impinging streams (two gas and two liquid nozzles) and used the same nozzles. For gas injection, *Spraying Systems* TX-2 nozzles were used, while liquid injection was via *Spraying Systems* TG-1 nozzles. Only stainless steel nozzles were used due to their ability to withstand corrosive attack by caustic soda solutions used in the CO_2 absorption experiments.

Finally it must be noted that, whereas all of the above reactors were characterised by the CO_2 absorption system, only the σ-shaped reactor was characterised by both the CO_2 absorption and sulphite oxidation systems.

CHAPTER 4

DETERMINATION OF THE MASS TRANSFER PARAMETERS

Gas-liquid contactors are compared with one another based on their respective mass transfer coefficients and interfacial areas. The calculation of these mass transfer parameters, however, is not always simple, especially in the case of a chemically enhanced absorption system. This chapter will discuss the main models used for extraction of mass transfer parameters form absorption data, as well as a new technique proposed for this purpose. Special attention will also be given to the verification of this technique and its results.

4.1 PRINCIPLES OF GAS ABSORPTION AND MASS TRANSFER

The theory on gas-liquid reactions has been the subject of many publications by celebrated authors in this field of research, such as *Astarita* (1967), *Danckwerts* (1970) and *Charpentier* (1981). The following section aims to provide a concise summary of the principles underlying gas absorption and mass transfer and the determination of the mass transfer parameters according to these publications.

4.1.1 Diffusion and chemical reaction in quiescent liquids

Although the focus of this investigation has mainly been on highly turbulent liquids, a study of diffusion in quiescent liquids is important at this stage since it not only provides a simple approach to understanding mass transfer fundamentals in quiescent and agitated liquids, but also serves as a point of departure for various models for the process of absorption of gases into agitated liquids. These models will be discussed in a following section.

For the purpose of diffusion of gas into a stagnant liquid, a situation is considered in which the liquid has a free surface which is exposed to the gas. This surface is plane and the liquid for all practical purposes is infinitely deep, implying that, during the time considered, the diffusion process does not bring about any appreciable concentration changes in the body of the liquid. Applying Fick's law of diffusion to a one-dimensional system, assuming that the concentration of the diffusant is uniform over the plane perpendicular to the x-axis and the transport of the diffusant only takes place in the x-direction, the mass flux of the diffusant can be expressed as:

$$F = -D\frac{\partial C}{\partial x} \qquad \ldots (4.1)$$

In general, the concentration varies with position (along the x-ordinate) as well as with time. The partial differential equation relating concentration, time and position is established as follows: consider an element of differential thickness, *dx*, and of unit cross-sectional area, disposed perpendicular to the x-axis. Diffusant diffuses into and out of this control volume in the x-direction and is also depleted by chemical reaction. Applying the principle of conservation of mass over the element, the following equations can be written:

(diffusion in) – (diffusion out) = (accumulation) + (reaction) . . . (4.2)

or

$$-D\frac{\partial C}{\partial x} + D\left(\frac{\partial C}{\partial x} + \frac{\partial^2 C}{\partial x^2}dx\right) = \frac{\partial C}{\partial t}dx + Rdx \qquad \ldots (4.3)$$

By rearrangement of this equation, the general equation for diffusion with chemical reaction is given by:

$$D\frac{\partial^2 C}{\partial x^2} = \frac{\partial C}{\partial t} + R \qquad \ldots (4.4)$$

For the reaction $A + zB \Rightarrow yP$, assuming steady-state conditions, the following differential equations can therefore, be written:

$$D_A \frac{d^2 C_A}{dx^2} = R \qquad \ldots (4.5)$$

$$D_B \frac{d^2 C_B}{dx^2} = zR \qquad \ldots (4.6)$$

with boundary conditions:

$C_{AO} = 0$ (no dissolved gas in the bulk liquid)

$C_B = C_{BO}$, $x > 0$, $t = 0$

$C_B = C_{BO}$, $x = \infty$, $t > 0$

$\frac{\partial C_B}{\partial x} = 0$, $x = 0$, $t > 0$

A complete analytical solution of the above equations is not possible, but an approximate set of numerical and analytical solutions may be computed for a specified range of parameters. The results of these solutions are generally discussed in terms of the enhancement factor *E*, which accounts for the enhancement in absorption due to a chemical reaction. It is equal to the ratio of the amount of gas absorbed in a given time into a reacting liquid, to the amount of gas which would be absorbed if there were no reaction.

Both the chemical reactions employed in this investigation proceed according to a second order irreversible reaction mechanism (as discussed in *Chapter 3*). For this mechanism, Perry and Pigford (*Danckwerts*, 1970) and *Brian et al.* (1961) computed an approximate set of solutions and showed that they could be fitted by the following equation, of which the error does not exceed 12%:

$$E = \frac{\sqrt{\hat{M}\frac{E_i - E}{E_i - 1}}}{\tanh\sqrt{\hat{M}\frac{E_i - E}{E_i - 1}}} \qquad \ldots (4.7)$$

where,

$$\hat{M} = \frac{\pi}{4} k_2 C_{BO} t \qquad \ldots (4.8)$$

and E_I, is the maximum value for the enhancement factor for an instantaneous reaction, at which point chemical reaction cannot enhance absorption any further and the absorption process becomes completely mass transfer controlled. E_i is determined via the following equations:

$$E_i = \frac{1}{erf(\beta / \sqrt{D_A})} \qquad \ldots (4.9)$$

where β is defined by the implicit relation:

$$e^{\beta^2/D_B} erfc\left(\frac{\beta}{\sqrt{D_B}}\right) = \frac{C_{BO}}{2C_A^*}\sqrt{\frac{D_B}{D_A}} e^{\beta^2/D_A} erf\left(\frac{\beta}{\sqrt{D_A}}\right) \qquad \ldots (4.10)$$

All of the above equations have been developed for absorption into quiescent liquids, i.e. for the case where mass transfer is accomplished by diffusion alone. However, for absorption into an agitated turbulent liquid, both diffusion and convection play a role. For this purpose, simplified models of the absorption process have been proposed to establish a link between diffusive and convective mass transfer. The following section will briefly discuss the most significant of these models.

4.1.2 Absorption models

4.1.2.1 The film model

The film model, first proposed by Whitman (*Danckwerts*, 1970), originated from Nernst's idea (*Danckwerts*, 1970) of a so-called 'diffusion layer', and simplified models of heat transfer from solid surfaces to moving fluids. It

supposes a stagnant film of thickness δ, at the surface of the liquid next to the gas. While the rest of the rest of the liquid below the film boundary is kept uniform in composition by turbulent agitation, the concentration in the film falls from C_A^* at the interface, to C_{AO} at the inner edge of the film, that is, the bulk liquid. Convection is assumed absent in the liquid film, within which the transport of the soluble gas takes place via molecular diffusion alone. This simple model leads to:

$$\overline{R} = \frac{D_A}{\delta}\left(C_A^* - C_{AO}\right) \quad \ldots (4.11)$$

$$k_L = \frac{D_A}{\delta} \quad \ldots (4.12)$$

Hydrodynamic properties of the system are taken into account by the single parameter, δ, which depends on the geometry, liquid agitation and physical properties. Though the model is not very realistic (experimentally k_L is found to vary as $D_A^{0.5}$), predictions based on the film model are usually remarkably similar, sometimes even identical, to those based on more sophisticated models. Therefore, in view of its simplicity, it is often preferred in calculations.

4.1.2.2 'Still surface' models

'Still surface' models assume a progressive transition from a purely molecular (diffusive) transport to predominantly convective transport as the distance from the gas-liquid surface increases, compared to the discontinuity envisaged in the film model. King (*Danckwerts*, 1970) proposed a model whereby transport of the soluble gas is the combined result of molecular diffusivity and of an 'eddy diffusivity' which is proportional to some power, n, of the distance from the surface. In this case k_L may be proportional to any power of D_A, depending on the value of n. However, this model has added complexity, since it contains two parameters which relate k_L to the hydrodynamic parameters of the system, as opposed to only one (δ) used by the film model.

Andrew (*Danckwerts*, 1970) and *Danckwerts* (1955) discussed another still surface model, called the surface rejuvenation model, which supposes that diffusion takes place at a diminishing rate into a stagnant liquid, whereafter a convective disturbance then replaces the liquid up to a certain depth below the surface by liquid of the bulk concentration. Quiescent diffusion then recommences with a steeper concentration gradient (and a more rapid rate of absorption), and continues until the next disturbance. Although this model seems to present the most accurate description of the actual process, it is undesirably complicated: once again it will require at least two parameters for characterisation of hydrodynamic features and rejuvenation frequency.

4.1.2.3 Surface renewal models

Surface renewal models have as their essence the periodic replacement of elements of liquid at the gas-liquid interface from the interior, of mean bulk composition. Each element of liquid at the surface exposed to the gas absorbs gas as though it were quiescent and infinitely deep, where the rate of absorption is a function of the time of exposure of the element, being rapid (or infinite) initially and decreasing with time. The replacement of the liquid at the surface by fresh liquid from the bulk composition is achieved by the turbulent motion of the body of the liquid. Therefore, it can be seen that surface renewal models suggest a mosaic of different surface 'ages' for all of the exposed elements. Different versions of this model lead to different distributions of surface ages around the mean value.

Higbie (*Danckwerts*, 1970) proposed that every element of the surface is exposed to the gas for the same length of time, θ, before being replaced by liquid of the bulk composition. During this time, every element of the liquid absorbs the same amount Q of gas per area as if it were stagnant and infinitely deep, and the average rate of absorption is Q/θ. The relations between θ and k_L are derived from the equations for physical absorption into quiescent liquids:

$$Q = 2\left(C_A^* - C_{AO}\right)\sqrt{\frac{D_A\theta}{\pi}} \qquad \ldots (4.13)$$

$$\overline{R} = \frac{Q}{\theta} = 2\left(C_A^* - C_{AO}\right)\sqrt{\frac{D_A}{\pi\theta}} \qquad \ldots (4.14)$$

$$k_L = \frac{\overline{R}}{C_A^* - C_{AO}} = 2\sqrt{\frac{D_A}{\pi\theta}} \qquad \ldots (4.15)$$

The hydrodynamic properties of the system are accounted for by the exposure time θ; thus k_L is defined as the mean value of the mass transfer coefficient during the time interval from $t = 0$ to $t = \theta$. Note that k_L varies according to $D_A^{0.5}$, as predicted by experimental results.

Since the *Higbie* model rather unrealistically assumed an equal age for all liquid elements, Danckwerts (*Danckwerts*, 1955) proposed a new model which supposes that the probability of an element of surface being replaced by fresh liquid from the bulk, is independent of the length of time for which it has been exposed. This leads to a stationary distribution of surface ages in which the fraction of the surface which, at any given instant, has been exposed to the surface for times between θ and $(\theta + d\theta)$, is given by $se^{-s\theta}d\theta$. Here s, is a parameter analogous to *Higbie*'s θ, and is defined as the fraction of the area of surface which is replaced by fresh liquid. The following relations were therefore, developed:

$$\overline{R} = s\int_0^\infty R.e^{-s\theta}d\theta \qquad \ldots (4.16)$$

$$= \left(C_A^* - C_{AO}\right)s\sqrt{\frac{D_A}{\pi}}\int_0^\infty \frac{e^{-s\theta}}{\sqrt{\theta}}d\theta \qquad \ldots (4.17)$$

$$= \left(C_A^* - C_{AO}\right)\sqrt{D_A s} \qquad \ldots (4.18)$$

$$k_L = \sqrt{D_A s} \qquad \ldots (4.19)$$

Once again, the hydrodynamic properties of the system are accounted for by a single parameter *s*, which has the dimensions of reciprocal time.

4.1.2.4 Other models

A wide variety of other models have been proposed besides those mentioned above. For example, Dobbins (*Danckwerts*, 1970) and *Toor* and *Marchello* (1958) proposed a so-called 'film renewal' model, which supposes a stagnant film of definite thickness (as in the film model) which is replaced piecewise from time to time by liquid from the bulk. In addition to this, Marchello and Toor (*Danckwerts*, 1970) also proposed a model in which a liquid film of definite thickness is mixed to uniform concentration at intervals. Kishnevskii et al. (*Danckwerts*, 1970) developed a model in which turbulence is supposed to extend to the surface or interface, the rate of absorption being determined by a combination of molecular and eddy diffusivity.

All of these models are, however, rather complicated since k_L is characterised by two parameters or more. Seen in light of the fact that these models do not provide more accurate answers than the previously mentioned film and surface renewal models, their applications have been somewhat limited.

4.1.3 Diffusion and chemical reaction in agitated liquids

It has been shown how the models described above combine the molecular diffusion of gas in a quiescent liquid with the replenishment of fresh bulk liquid at the interface via agitation. By applying these models, the diffusion equation (*equation 4.3*) can be applied to the absorption of gas into agitated liquids. For the case of an irreversible second order reaction, this diffusion equation has been solved using the film and surface renewal models of Higbie and Danckwerts.

4.1.3.1 The film model

Analogous to the numerical solution of the diffusion equation by Perry and Pigford (Danckwerts, 1970) and *Brian et al.* (1961), *Van Krevelen* and *Hoftijzer* (*Danckwerts*, 1970) computed an approximate set of solutions and showed that they could be fitted within 10% by the following equation:

$$E = \frac{\sqrt{M\dfrac{E_i - E}{E_i - 1}}}{\tanh\sqrt{M\dfrac{E_i - E}{E_i - 1}}} \qquad \ldots (4.20)$$

where

$$M = Ha^2 = \frac{D_A k_2 C_{BO}}{k_L{}^2} \qquad \ldots (4.21)$$

and E_i is determined in exactly the same way as in equations (*4.9*) and (*4.10*).

The physical importance of the Hatta number (*Ha*) (or $\sqrt{M}$), is that it provides an important indication as to whether a large specific interfacial area or a large liquid holdup is required for a particluar reaction of rate constant *k*. This will be illustrated in the following situation.

As discussed in *Chapter 3*, some experiments were also conducted in the pseudo-first order regime, where, to a close approximation (*Figure 4.1*):

$$E = \sqrt{M} = Ha \qquad \ldots (4.22)$$

and

$$R = C_A^* \sqrt{D_A k_2 C_{BO}} \qquad \ldots (4.23)$$

for $\frac{1}{2}E_i > \sqrt{M} > 3$.

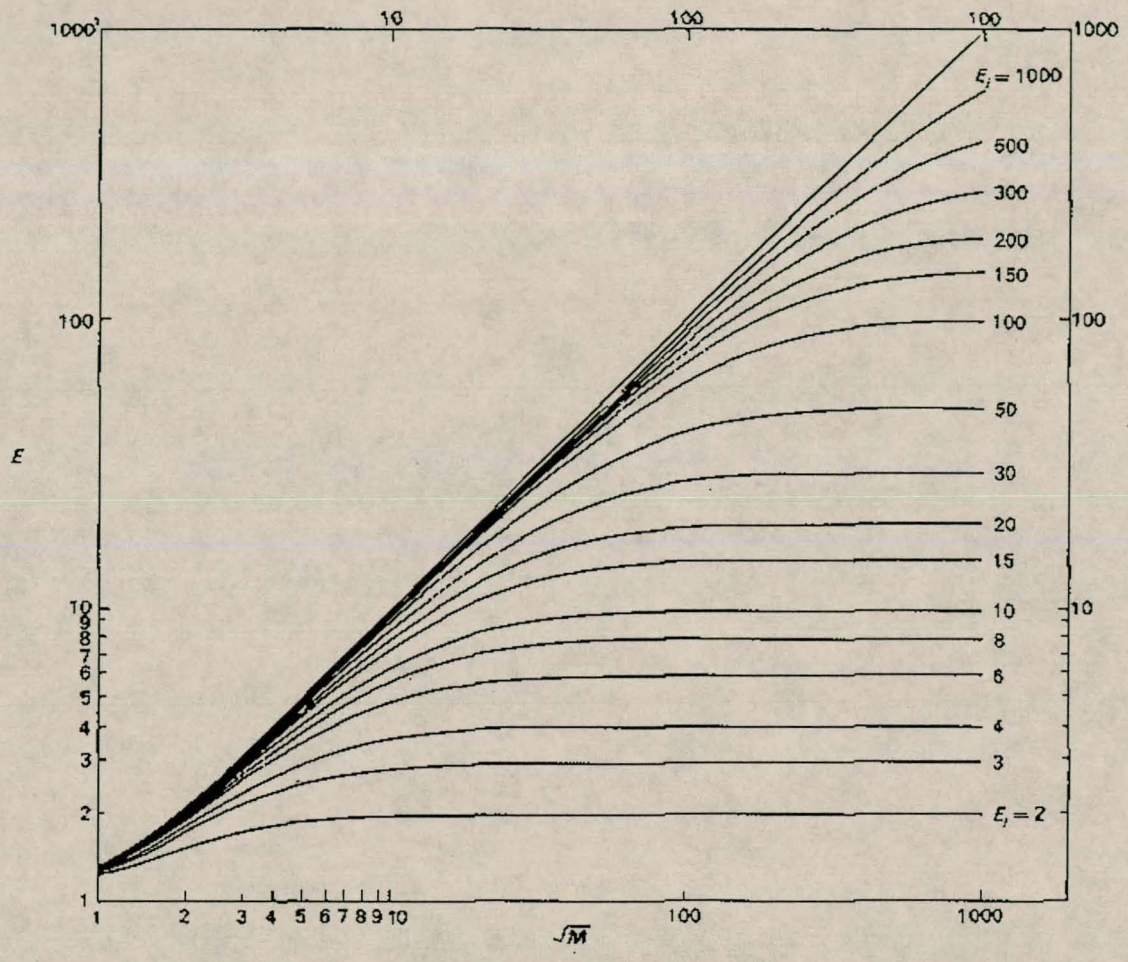

Figure 4.1 *Enhancement factors for a second-order reaction (film or Higbie models). Note the diagonal representing E =* $\sqrt{M}$ *for a pseudo-first order reaction.* Taken from *Danckwerts* (1970).

For this case the instantaneous enhancement factor, E_i, can simply be calculated by the following, in stead of using *equations (4.9)* and *(4.10):*

$$E_i \approx \sqrt{\frac{D_A}{D_B}} + \frac{C_{BO}}{zC_A^*}\sqrt{\frac{D_B}{D_A}} \qquad \ldots (4.24)$$

The physical significance of this situation is that reactant *B* (the solute) diffuses toward the surface of the film fast enough to prevent the reaction from

causing any significant depletion there, so that C_{BO} is kept virtually constant. In addition to this, all the dissolved gas reacts in the diffusion film as opposed to a slow process where a substantial amount of this gas has to be transferred unreacted to the bulk liquid. The rate of absorption can then be written as:

$$\overline{R} = aC_A^* \sqrt{D_A k_2 C_{BO}} \qquad \ldots (4.25)$$

It can be seen that the film thickness, or value of k_L, is irrelevant and does not appear in the expression for the average of absorption. However, the value of the interfacial area plays a critical role. Therefore, for such reactions, the rate of absorption will be large if the interfacial area is large. So a high interfacial area is required in the reactor, but the liquid holdup is relatively unimportant.

4.1.3.2 Higbie model

The average absorption rate for a contact time θ, is given in terms of the enhancement factor, i.e:

$$E = \frac{Q}{2C_A^*}\sqrt{\frac{\pi}{D_A\theta}} \qquad \ldots (4.25)$$

According to the *Higbie* model these values of E can be used to find the average rate of absorption into an agitated liquid:

$$\overline{R} = k_L C_A^* E \qquad \ldots (4.26)$$

It is noted by *Danckwerts* (1970) that the computed values of E for the *Higbie* and the film models are almost equal for given values of M and E_i.

4.1.3.3 Danckwerts model

The *Danckwerts* model does in general not deal conveniently with second-order reactions (or other reactions leading to non-linear differential equations).

However, the model can sometimes be used to find criteria for limiting types of behaviour.

One such an example is determining when a second-order irreversible reaction between A and B, can be regarded as a pseudo-first order reaction in A. Using the *Danckwerts* model, the following condition is obtained:

$$\sqrt{\left(1+\frac{D_A k_1}{k_L^{\,2}}\right)}-1 \;\langle\langle\; \frac{C_{BO}}{zC_A^{\,*}} \qquad \ldots (4.27)$$

compared to the following derived from the film model:

$$\frac{\sqrt{D_A k_1}}{k_L} \;\langle\langle\; 1+\frac{C_{BO}}{zC_A^{\,*}} \qquad \ldots (4.28)$$

The two conditions are equivalent if $\sqrt{(D_A k_1)}/k_L$ is substantially greater than one. For a more complete explanation and derivation of these equations, *Danckwerts* (1970) can be consulted.

It must be noted that all values for the liquid and gas diffusivities, reaction rate constants and gas solubilities in the above equations were taken from *Botes* (1995) for the CO_2 absorption system, and the publications of *Danckwerts* (1970) and *Reith* and *Beek* (1973) for the sulphite oxidation system, in the processing of absorption data.

This concludes the discussion on the theory and fundamentals behind gas absorption. A lot of attention has been devoted to the determination of the chemical enhancement factor *E*, since knowledge of this factor allows for the calculation of the other mass transfer parameters, *a* and $k_L a$. The following section will briefly discuss the new chemical technique proposed by *Botes et al.* (1998) for experimental determination of *E*, since it was also employed during this investigation. Verification of its results will also be presented.

4.2 REVIEW OF BOTES'S TECHNIQUE

The chemical technique for the determination of the mass transfer parameters proposed by *Botes et al.* (1998) is analogous to the approach followed by *Herskowits* (1990). Based on the standard definition for the enhancement factor (*section 4.1.1*), *Herskowits* absorbed carbon dioxide into water (physical absorption) and sodium hydroxide solutions (chemisorption) under identical operating conditions. Since it was assumed that the hydrodynamic behaviour of the two liquids was identical, and therefore had the same value for the mass transfer coefficient, the difference in absorption rates was attributed to the effect of chemical reaction. A value for the enhancement factor was thus obtained by dividing the chemical absorption rate by the purely physical absorption rate. The value of k_L could then be determined iteratively using *equation (4.20).*

Owing to the difficulty in the accurate determination of the concentration of a dissolved gas, and the inherent instability of these samples (due to temperature effects on solubility, etc.), a new chemical technique was developed whereby carbon dioxide was absorbed under identical operating conditions into two sodium hydroxide concentrations of different concentrations. It was, as in the case of *Herskowits*, assumed that the two solutions had similar hydrodynamic properties, which would theoretically yield a single mutual mass transfer coefficient. The difference in absorption rates of the two runs was ascribed to the difference in enhancement factors for the runs. Although absolute values of the enhancement factors could not be determined, the ratio of the *E*-values could be calculated from the two absorption rates:

$$\frac{E_1}{E_2} = \left(\frac{\dot{N}_1}{\dot{N}_2}\right)\left(\frac{C_{A2}^*}{C_{A1}^*}\right) \qquad \ldots (4.29)$$

Therefore, three unknown variables had to be accounted for to solve for the mass transfer parameters: E_1, E_2 and k_L. However, since E_1 and E_2 are

related through an experimentally determined ratio, only two independent variables needed to be solved. *Equations (4.20)* and *(4.21)* imply that the enhancement factor and the mass transfer coefficient are related by an implicit function of the form:

$$E = f(E,k_L) \qquad \ldots (4.30)$$

This equation could be applied to both experimental runs, yielding two independent governing equations. Since the system contained two independent variables governed by two independent equations, it was defined unambiguously in mathematical terms and would yield a unique solution of the variables.

For the solution of these equations an iterative mathematical strategy was used. To start, a value for k_L (identical for both runs) was assigned an initial value. The two implicit governing equations were then solved to yield values for E_1 and E_2 for this value of k_L. The ratio of these E-values was then compared to the experimentally calculated ratio, and a better value was assigned to k_L. This procedure was repeated until the calculated E-ratio agreed with the experimental ratio. The correct value of the mass transfer coefficient was thus obtained, after which E_1 and E_2 could be solved for.

It did, however, seem that the system yielded unstable results for the mass transfer coefficients: it was very difficult to achieve satisfactory reproducible results for this parameter between two identical experiments. To find an answer behind this phenomenon, a sensitivity analysis was performed on the above mathematical system. It showed that the technique is very sensitive to variations in the input parameters, amplifying small changes in these variables to major fluctuations in the mass transfer parameters.

The high sensitivity of the technique was found to be inherent to the functional relationship between E and k_L, i.e. using another chemical technique to determine the mass transfer parameters would not solve this problem, since all techniques would inevitably rely on this relationship. It was therefore, made

clear that the uncertainty in the values of the mass transfer parameters was not the result of poor experimental technique, but rather due to the notorious nature of mass transfer experiments.

Since this new chemical technique was also adopted during this investigation, it needed to be verified against existing correlations for E, which have been proposed by various authors in the field over the years. This is the topic of the following section.

4.3 VERIFICATION OF BOTES'S TECHNIQUE

Although the new chemical technique proposed by *Botes* theoretically made mathematical sense, it had to be verified in some way (*Botes* had not originally done this) to eliminate any uncertainty in the determination of the mass transfer parameters through the use of the enhancement factor. This was accomplished by comparing values for E, generated by Botes's method, with values obtained from other empirical and semi-empirical correlations for E, proposed by various authors. Five different correlations were used, summarised in *Table 4.1*.

Verification of the mass transfer parameters yielded by *Botes*'s method could be done in two ways, using these correlations:

- The Hatta number (or k_L-value) could be used as a base, and the enhancement factors generated by Botes's method and the above formulae, could be correlated, or vice versa:
- One or both of the enhancement factors could be used as a base for comparing the values of k_L generated by the two methods.

Table 4.1 *Explicit formulae for the enhancement factor E. All correlations taken from Gianetto and Silveston (1986).*

Authors	Formula	Validity domain
Yeramian et al. (1970)	$E = \frac{E_1^{\,2}}{2(E_i - 1)}\left(-1 + \sqrt{1 + \frac{4(E_i - 1)E_i}{E_1^{\,2}}}\right)$ where $E_1 = Ha/\tanh(Ha)$	$Ha > 1$
Kishnevskii et al. (1971)	$E = 1 + \frac{Ha}{\alpha}\left(1 - \exp\left(-0.65 Ha\sqrt{\alpha}\right)\right)$ where $\alpha = \frac{Ha}{E_i - 1} + \exp\left(\frac{0.68}{Ha} - \frac{0.45 Ha}{E_i - 1}\right)$	$Ha > 1$
De Coursey (1974)	$E = -\frac{Ha^2}{2(E_i - 1)} + \sqrt{\frac{Ha^4}{4(E_i - 1)^2} + \frac{E_i Ha^2}{E_i - 1} + 1}$	$Ha \geq 1$
Baldi & Sicardi (1975)	$E = 1 + (E_i - 1)\left(1 - \exp\left(-\frac{\sqrt{1 + Ha^2} - 1}{E_i - 1}\right)\right)$	$Ha \geq 1$
Karlsson and Bjerle (1980)	$E = \frac{\left(Ha^{-x} + E_i^{-x}\right)^{-(1/x)}}{\tanh\left(\left(Ha^{-x} + E_i^{-x}\right)^{-(1/x)}\right)}$ where $x = \frac{1}{2} + \frac{1}{m}$ and m = reaction order	$E_i \geq 2$

As mentioned in the previous section, one experimental run consisted of two hydrodynamically identical runs performed at different initial solute concentrations to obtain one mutual value of the mass transfer coefficient and two values (E_1 and E_2) of the enhancement factor. In light of this, and the fact that the above correlations are all presented as explicit functions of E, it was decided to use a set of experimental data, using their mutual k_L–value as a base, and compare values of E_1 and E_2 determined by Botes's method and the above formulae.

Results for one of the test sets are used as an illustration of the results obtained for the method of Botes and alternative methods:

Table 4.2 *An example of the correlation between enhancement factors predicted by Botes's and other methods*

Author	Run 1a (E_1)	Run 1b (E_2)	Average deviation %
Botes (1998)	1.051	1.091	-
Yeramian et al. (1970)	1.043	1.083	-0.75
Kishnevskii et al. (1971)	1.033	1.072	-1.69
De Coursey (1974)	1.074	1.130	2.86
Baldi & Sicardi (1975)	1.075	1.131	2.98
Karlsson & Bjerle (1980)	1.016	1.031	-4.38

This illustration clearly indicates that correlation between the method of Botes and other methods for the determination of E is very good: the average deviation between corresponding values is less than 5%. Taking into account the fact that Botes's method incorporates *equation (4.20)*, which is only accurate to within an error of 10%, the comparison looks better yet and it can be assumed that the values of E are identical.

Assuming, from a different perspective, that the method of Botes has provided proof of the accuracy of the above correlations, it can also be noted that the domains of validity of the proposed formulae above need not always apply. This was discovered when experimental data of which the Hatta numbers were smaller than one ($Ha < 1$) were substituted into the above formulae, most of which require Hatta to be larger than one ($Ha > 1$). Despite this discrepancy, good correlation was still obtained within a margin of 10%.

However, for correlations stipulating that $Ha > 3$, a very bad correlation was obtained (+200% deviation) for data which did not satisfy the necessary

criteria. This can be explained by the fact that, for *Ha* > 3, pseudo-first order conditions exist for which determination of *E* is much simpler, as discussed above: therefore, if data which does not represent the correct chemical regime, is substituted into these equations, gross over estimation of *E* occurs as it is assumed that $E = \sqrt{M}$.

4.4 CONCLUSIONS

This chapter has not only provided a fundamental background to the determination of mass transfer parameters from absorption data, but has also in essence proved that the method of *Botes et al.* (1998) for the determination of the mass transfer parameters, and therefore also *E*, is valid and accurate. This has been accomplished using correlations for *E* proposed by a wide variety of independent authors. It has also been described why the system using two hydrodynamically identical runs at different initial solute concentrations, presents a more accurate approach to the determination of *E* and k_L, than using the physical absorption of gas into water, as proposed by *Herskowits et al.* (1990).

In light of the above considerations, *Botes*'s new chemical technique has been used for the extraction of mass transfer parameters from absorption data. The discussion and comparison of these parameters with data from the literature will be the subject of the following chapter.

CHAPTER 5

RESULTS AND DISCUSSION

Experimental results represent the culmination of all the knowledge gained in previous chapters: characterisation of gas-liquid systems by way of a suitable chemical method, design of these reactors for optimum absorption efficiency and the extraction of mass transfer parameters from absorption data. The aim of this chapter is therefore, to present the mass transfer performance of the reactors investigated compared to alternative gas-liquid contacting systems presented in the literature.

Hydrodynamic mechanisms proposed by *Botes* (1995) for the explanation of experimental results will be used and adapted to the current investigation to provide insight into the respective absorption efficiencies of the three different reactors investigated. Complementary to this, attention will also be given to empirical modelling of the design parameters of these reactors (a, k_L and ϕ_g) to quantify the effects of various operating parameters on reactor performance.

5.1 THE BUBBLE SIZE AND GAS VOIDAGE FRACTION, ϕ_G

Fair comparison of the mass transfer performance between two gas-liquid contactors can only be made if their mass transfer coefficients or interfacial areas are compared on the basis of a mutual neutral parameter. This parameter is usually the energy dissipation in the reactor per unit volume of liquid, measured in W/m^3 or W/kg. It can therefore be seen that a thorough knowledge of the gas voidage in the reactor is required to make accurate assesments of the volume of liquid present in the reactor and therefore, also the energy dissipation.

5.1.1 CO_2 absorption

5.1.1.1 Determination of bubble size and gas voidage fraction

Since the bubble size distributions and gas voidages in the reactors could not be measured by physical methods such as video image analysis or ultrasonic tomography, these parameters had to be determined via chemical techniques. The chemical systems used for the characterisation of the mass transfer parameters of the reactors already yielded values for the interfacial area, so the values for the average bubble size and gas voidage could be determined via the following equation:

$$\phi = \frac{ad_{bs}}{6 + ad_{bs}} \qquad \ldots (5.1)$$

where d_{bs} and a denote the average bubble size (Sauter mean diameter) and interfacial area respectively.

It was therefore necessary to calculate either the value of d_{bs} or ϕ to fully describe the system in terms of average bubble size and gas voidage. A review of the literature revealed that correlations for the prediction of the average bubble size were more readily available and more accurate than those for the estimation of the gas voidage. In light of this, it was decided to use approximated values of the bubble size to obtain values for the gas voidages in the reactors.

In total six different correlations for the calculation of d_{bs} (summarised in *Table 5.1*) were compared with one another to find one which yielded the most representative results. Comparison was made using a set of data for interfacial areas at constant gas flow rate for the σ-shaped reactor, based on each correlation's predicted gas voidage. As can be seen from the correlations applied, the value of d_{bs} is dependent on both the values of the gas voidage and the energy consumption, which in turn is dependent on the gas voidage. Due to this interdependence of variables, an iterative solution for

the bubble size was obtained by changing the gas voidage until the constraints specified by *equation (5.1)* were satisfied.

Table 5.1 *Bubble size correlations investigated*

Author	Correlation
Calderbank (1958)	Chapter 2 – *equation (2.26)*
Calderbank & Vermeulen (1958)*	$d_{bs} = 0.045\frac{\sigma^{3/5}}{\rho^{3/5}\varepsilon^{2/5}}\phi_g^{0.5} + 0.0009$
Bhavaraju et al. (1978)	$d_{bs} = 0.7\frac{\sigma^{3/5}}{\rho^{3/5}\varepsilon^{2/5}}\left(\frac{\mu}{\mu_g}\right)^{0.1}$
Metkin & Sokolov (1985)*	Chapter 2 – *equation (2.32)*
Lee & Meyrick (1970)	Chapter 2 – *equation (2.27)*
Bouaifi & Roustan (1998)	$d_{bs} = 0.0101(\varepsilon)^{-0.2}$

* Taken from *Kawase* and *Moo-Young* (1990).

The results of this investigation can be illustrated by the following graph.

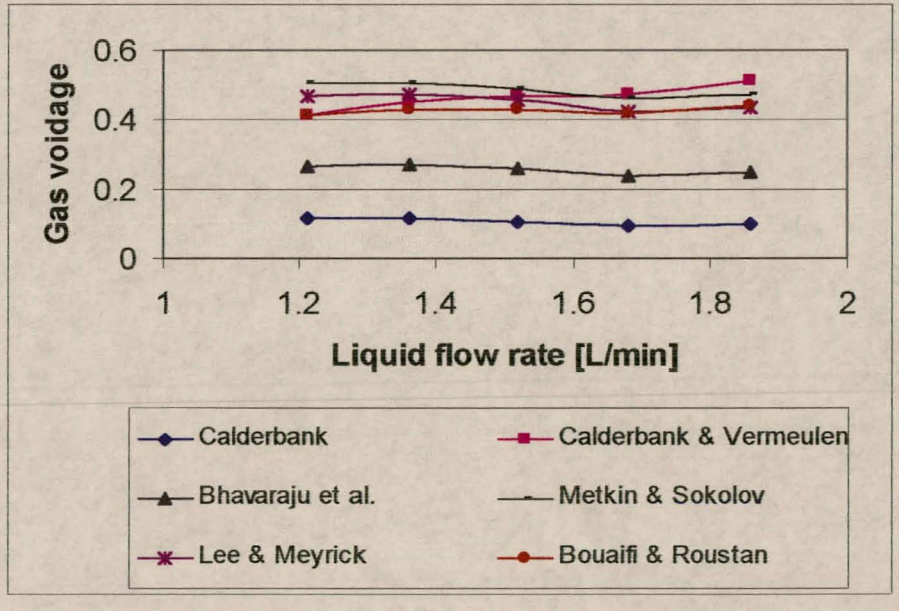

Figure 5.1 *A comparison of the predicted values of the gas voidage as a function of the liquid flow rate*

It was found that the correlations predicted very similar values of the gas voidage, except those proposed by *Calderbank* (1958) and *Bhavaraju et al.* (1978). Ignoring these correlations, anyone of the four remaining correlations could be used with reasonable confidence for the determination of gas voidages for various operating parameters in the different reactors investigated. Due to the relative simplicity thereof, and the fact that it represents the most recent correlation available for estimation of d_{bs}, the correlation of *Bouaifi & Roustan* (1998) was chosen for this purpose. During these calculations it was assumed that the gas voidage remained constant for variations in the liquid flow rate, as illustrated by the trends in *Figure 5.1.*

It must, however, be pointed out that all of the above correlations were obtained from data generated under much lower energy dissipation rates ($\varepsilon <$ 1.0 kW/m^3) than those exhibited in the new jet reactors ($106 < \varepsilon < 386$ kW/m^3), since literature data on prediction of bubble sizes at these high energy dissipation rates is simply not available. Therefore, it must be kept in mind that the bubble sizes determined during this investigation could only be considered as estimations or approximations of their real values. In light of the above, the discrepancy in the values predicted by *Calderbank* (1958) and *Bhavaraju et al.* (1978), can most probably be attributed to the fact that these particular correlations were developed under a very limited scope of energy dissipation rates which, when extrapolated, yielded distorted values of the gas voidage.

5.1.1.2 Gas voidage

Using the techniques described above, the following results could be obtained for the gas hold-up in the three reactors investigated. Since the π- and σ-shaped reactors were operated under identical gas flow and energy dissipation rates and exhibited very similar values for interfacial area, it was assumed that the gas voidage fractions in these reactors could be taken as identical.

Table 5.2 *Gas voidages calculated for the reactors investigated*

Reactor configuration	Gas flow rate *L/min*	Gas voidage ϕ
Kite-shaped	10	0.47
	15	0.53
	20	0.58
π- and σ-shaped	10	0.29
	15	0.36
	20	0.43

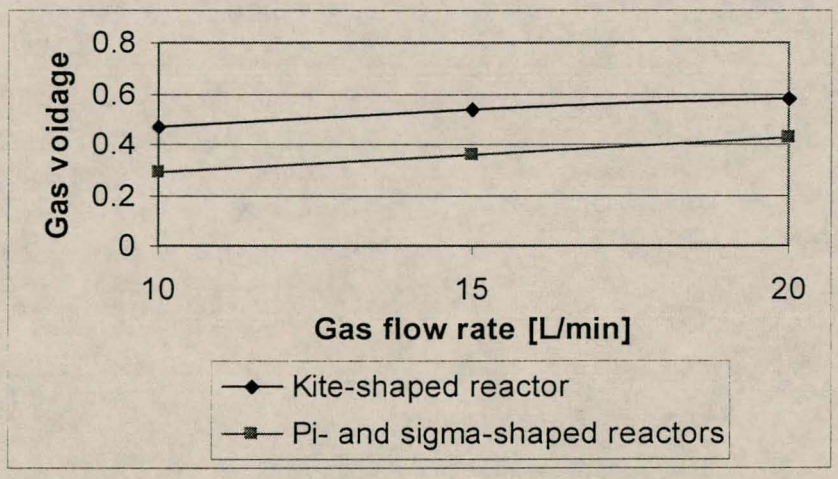

Figure 5.2 *The effect of gas flow rate on the voidage fraction for the kite and π- and σ-shaped reactors*

As expected, results show that an increase in the gas flow rate results in an increase of the gas voidage. It was also found that the gas voidages exhibited by the kite-shaped reactor was consistently higher than that of the other two reactors. This was also expected since both reactors were operated under identical flow rates, while the reactor volume of the kite-shaped reactor was smaller than that of the other two (8.25 vs 20 *mL*). More physical volume would therefore be taken up by the same amount of gas in the kite-shaped reactor than in the other reactors, leading to a higher relative voidage fraction.

5.1.1.3 Bubble size

Determination of the gas voidage fraction, as discussed above, implicitly allowed for the simultaneous determination of the average bubble size in the reactors, as a function of the gas and liquid flow rates and therefore, the energy dissipation rate. Once again it was assumed that the average bubble size exhibited in the π- and σ-shaped reactors were identical. The results obtained for the average bubble size are summarised in Figure 5.3, where the values in brackets in the legend, refer to gas flow rates in *L/min*.

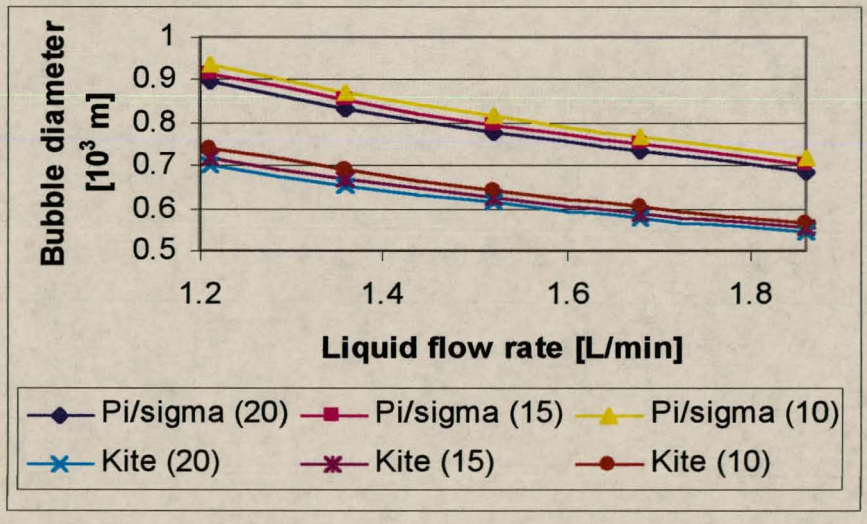

Figure 5.3 *Comparison of average bubble sizes exhibited in the kite and π- and σ-shaped reactors as a function of the liquid and gas flow rates.*

Figure 5.3 shows two distinct bands of average bubble sizes represented by the kite-shaped reactor and the π/σ-shaped reactors. It can clearly be seen that the bubble diameters exhibited by the latter mentioned reactors are larger than those exhibited by the kite-shaped reactor, due to a higher energy dissipation rate in the kite-shaped reactor (approximately 3.5 times) than that in the other reactors. This higher energy dissipation rate is the result of two factors. Firstly, the kite-shaped reactor is operated under identical liquid flow rates to that of the π- and σ-shaped reactors, but has a volume of less than half that of the other two, so that the specific energy input into this reactor is higher. Secondly, the relatively larger gas hold-ups exhibited by the kite-

shaped reactor (on average 50% higher) leads to a further increase in the energy dissipation rate per unit volume or mass of liquid in the reactor.

In addition to this it is obvious that the average bubble diameter decreases with an increase in liquid flow rate. This is to be expected, since an increase in this flow rate results in an increase in the energy dissipation in the reactor, resulting in the decrease in average bubble size due to more effective break-up of bubbles. A further discussion of the effect of energy dissipation on bubble size will be given in *section 5.1.3*, where data generated in this investigation will be compared with data from the literature.

5.1.2 Sulphite oxidation

5.1.2.1 Gas voidage

Gas voidage for the sulphite oxidation system was determined using the same strategy as outlined above. *Table 5.3* provides a summary of the results obtained for the σ-shaped reactor, the only reactor used for these experiments.

Table 5.3 *Gas voidages exhibited by the σ-shaped reactor for the sulphite oxidation system*

Gas pressure *kPa*	Gas voidage ϕ
100	0.114
150	0.136
200	0.156

Since the sulphite oxidation runs had to be performed within a very narrow range of oxygen pressures (due to the senistivity of the reaction system), the variation between minimum and maximum gas flow rates was not as large as for the CO_2 absorption system. For this reason the voidage fractions exhibited

for the different gas flow rates do not differ very significantly: whereas the CO_2 absorption system displayed a 50% variation in ϕ, the sulphite oxidation system displayed only a 25% variation. Due to the fact that the oxygen pressure in the reactor chamber had to be maintained as close as possible to 1 bar, gas flow rates employed also had to be kept relatively low: therefore flow rates of 3 – 5 L/min were used. This is the reason behind the lower values of voidage fractions (0.114 – 0.156 vs 0.29 – 0.43). However, it can be seen that an increase in the gas flow rate translates into an increase in the gas voidage.

5.1.2.2 Bubble size

In the previous section it was explained why the spread in the gas voidage data was very limited. Due to these reasons, the average bubble size between different gas flow rates did not vary significantly, as illustrated in *Figure 5.4*. However, the decrease in bubble size with an increase in liquid flow rate and energy dissipation is clearly illustrated. Comparison of average bubble sizes exhibited by the two chemical systems shows that bubble sizes for the sulphite oxidation system are consistently larger than for the CO_2 absorption system. This can once again be ascribed to lower energy dissipation rates for the former system: it is operated at similar energy input conditions, but yields a lower value for the energy dissipation rate per unit mass of liquid due to a lower gas hold-up.

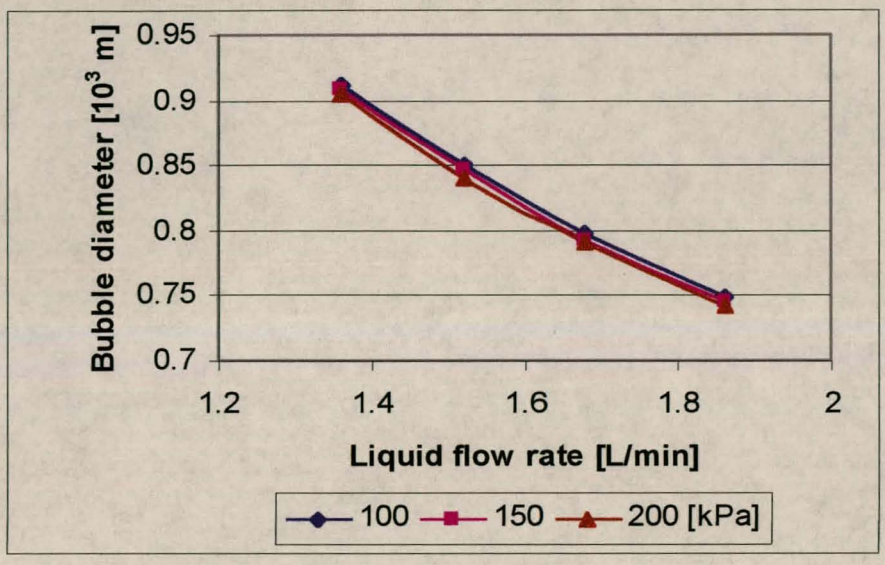

Figure 5.4 *Comparison of average bubble sizes exhibited in the σ-shaped reactor as a function of the liquid and gas flow rates, where the legend refers to oxygen pressures.*

5.1.3 Comparison with literature data and conclusions

Gas voidage is a function of the energy dissipation and gas flow rates in a reactor and is usually correlated by an expression of the following form (*Kawase* and *Moo-Young*, 1990):

$$\phi = C\varepsilon^{\alpha}U_{sg}{}^{\beta} \qquad \ldots (5.2)$$

where α and β range between 0.3 – 0.5 and 0.25 – 0.7, respectively. Most of the results for gas voidage are, however, not published as functions of the energy dissipation in the reactors, but as functions of linear gas velocity (U_{sg}), especially for the case of bubble columns. This makes comparison of gas voidage results with literature data very difficult, since linear gas velocities for the reactors under investigation, could not be determined. Due to this, and the fact that gas voidage fractions are typically very specific to the ratio of reactor volume to gas flow rates employed, it was decided to rather focus on bubble size as a basis for comparison of results.

Since bubble sizes in this investigation were not measured experimentally, but simply calculated from a correlation, results could only be checked for their consistency with data from other publications. *Figure 5.5* provides an illustration of this.

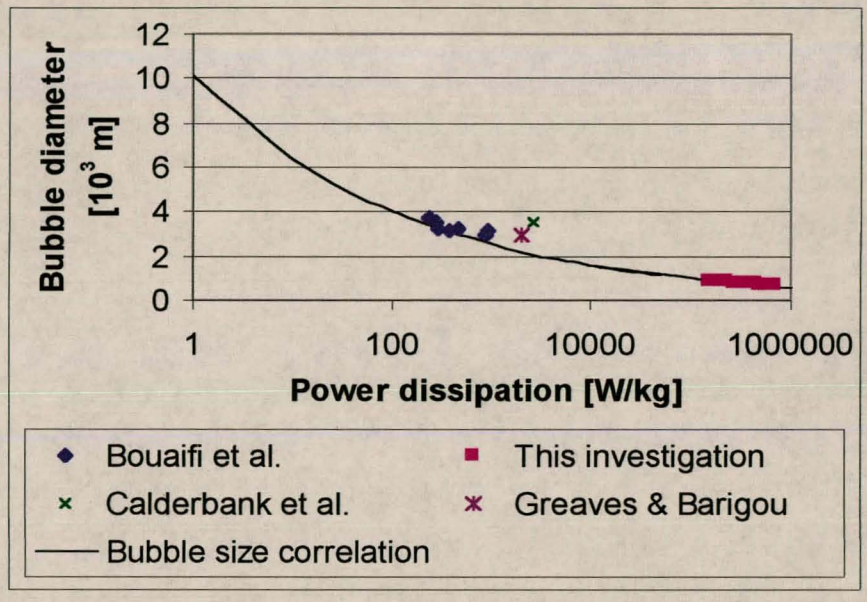

Figure 5.5 *Comparison of generated data with data from the literature, based on energy dissipation*

Once again it proved very difficult to find suitable data from the literature which related average bubble size to energy dissipation rates. In the majority of cases bubble sizes were plotted either as functions of the impeller speed in an agitated sparged tank or gas pressure, which made comparison virtually impossible. However, the publications of *Bouaifi & Roustan* (1998), *Lopes de Figueiredo & Calderbank* (1979) and *Greaves & Barigou* (1988) provided data which could be used for comparison. Since the correlation used for the determination of average bubble sizes in this investigation was based on the data of *Bouaifi & Roustan* (1998), excellent agreement is found, as can be seen in *Figure 5.5.* It can, however, also be seen that data reported by the other authors compare reasonably well with data generated from the correlation; therefore, it can be be concluded that bubble sizes determined in this fashion are valid. It must, however, be re-iterated that these bubble sizes can at best only be considered as approximations to their real values.

Finally, it is interesting to note that, although some of the correlations listed in *Table 5.1* predict an increase in bubble size with an increase in gas voidage, results obtained during this investigation yielded exactly the opposite trend: a decrease in the average bubble size with an increase in the gas voidage. This is most probably due to the very high energy dissipation rates employed in this investigation. Whereas the gas flow rate, and therefore gas voidage, played a significant role in determining average bubble sizes under the relatively low energy dissipation rates used for generation of these correlations, it can be argued that this effect is completely dominated and negated by the higher relative energy dissipation rates used in this investigation, yielding smaller bubble sizes (and larger interfacial areas) than anticipated. This phenomenon is a good example of the potential advantages associated with operating systems under relatively higher energy inputs.

5.2 THE MASS TRANSFER COEFFICIENT, k_L

5.2.1 CO_2 absorption results

5.2.1.1 Interpretation of results

In *Chapter 4* the chemical technique for the determination of the mass transfer parameters was described (*Botes*, 1995). It was, however, mentioned that this particular technique led to uncertainty in the values of the mass transfer coefficients to the extent that the effect of liquid and gas flow rates on k_L could not be determined since no trends in these values could be observed. This uncertainty was not the consequence of poor experimental technique, but was the result of various factors. Impurities in the sodium hydroxide feed and demineralised water introduced foreign ions and organic matter into the system which not only acted as catalysts in the chemical system, but also behaved as surfactants at the gas-liquid interface, affecting interfacial area production. Values of the diffusivities of carbon dioxide gas and hydroxide ions and reaction rate constants were also at best approximated from data available in the literature. Finally, the accuracy of the processed results was

also dependent on the accuracy of the functional realtionship (*equation 4.20*) between the enhancement factor and the mass transfer coefficient. Not only was this relationship an approximation (accurate within 12%) to the numerical solution of differential equations governing convective mass transfer enhanced by chemical reaction, but it also amplified variations in the input parameters: for instance, a one percent change in the outlet hydroxide concentration resulted in a change of 11% in the value of the mass transfer coefficient. It was also noted that mass transfer operations were notorious for their sensitivity to contaminants and their inability to produce highly reproducible results.

In the light of the above uncertainties, this new chemical technique was verified against existing correlations for E and k_L, and found to be very accurate, as discussed in *Chapter 4*. It was therefore decided to continue using this technique for the extraction of E and k_L from absorption data, but to do the following:

- Use only freshly distilled water to minimise the presence of surfactants and foreign ions in solution.
- Use higher purity (99.5%) sodium hydroxide feed pellets.
- Repeatedly perform absorption experiments until noticable trends in the mass transfer parameters, with specific reference to the mass transfer coefficient, were observed.

After completion of more than 250 runs (to obtain 50 data points), certain trends and results became evident. Whereas *Botes* (1995) concluded that "k_L is not heavily dependent on either the liquid or the gas flow rate", it was found that the mass transfer coefficient did exhibit a marked dependence on the gas flow rate. Indeed, it proved that the gas pressure (and therefore flow rate) had a greater effect on k_L, than the liquid flow rate. This can be explained in terms of the dependence of k_L on the energy dissipated in the reactor (see *Chapter 2* for correlations relating k_L to ε). If the gas flow rate to the reactor is raised, the gas voidage inside the reactor would increase and the liquid holdup would decrease. Since the rate at which kinetic energy is introduced to the reactor remains constant, while the mass of liquid inside the reactor decreases, the

rate of energy dissipation per unit mass of liquid is higher. Taking into account the fact that a change in gas voidage from 0.29 to 0.43 (see *section 5.1*) translates into an increase in energy dissipation of approximately 25%, it is obvious that a change in gas flow rate should yield a definitive change in the value of the mass transfer coefficient.

The dependence of k_L on the liquid flow rate could, however, not be ascertained as easily or accurately. From the above explanation relating k_L to the energy dissipation in the reactor, it should be obvious that an increase in the liquid flow rate, and therefore an increase in the specific (rate of) energy entering the reactor, would result in an increase in the value of the mass transfer coefficient. The extent to which k_L would be 'enhanced', however, needed to be determined. For this purpose approximately 60 CO_2 absorption runs were performed in the pseudo-first order regime since it was noted by *Botes* and other authors that "changing the concentration of the dissolved reagent results (only) in a change in the enhancement factor, but has no effect on the mass transfer coefficient, because k_L is only dependent on the hydrodynamics of the absorption process". Since the determination of the mass transfer parameters in the pseudo-first order regime is considerably less complicated and more stable than for a pure second order system, it was anticipated that following this approach would provide some indication as to both the effect of the liquid flow rate on k_L. Results obtained for these experiments (only performed in the σ-shaped reactor) can be seen in the following graph, where the liquid flow rate is simply represented by the rotameter reading and the values in the legend refer to the gas flow rate:

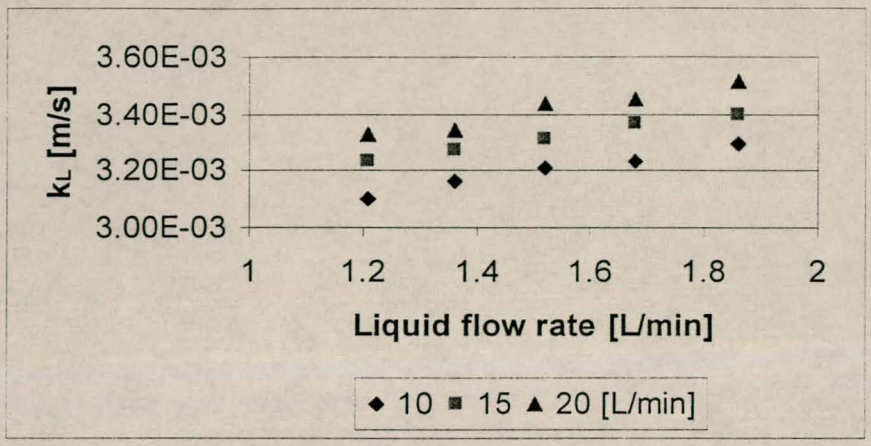

Figure 5.6 *The effect of liquid and gas flow rates on the value of the mass transfer coefficient for a pseudo-first order reaction.*

Not only can it be seen that the graph provides proof of the considerable increase in k_L due to an increase in gas flow rate, but that an increase in the liquid flow rate also results in an increase in the value of the mass transfer coefficient, although this effect is less prominent. Analysis of this data revealed that the value of k_L, increased with approximately 10 – 15% from the lowest to the highest liquid flow rate setting. Since high reaction temperatures and heat transfer coefficients were exhibited during these runs, due to the high feed concentrations of NaOH used to obtain pseudo-first order conditions, calculations were done to ascertain the possible effect of temperature on the values of k_L (the effect of temperature on the gas diffusivity was evaluated). It was, however, found that temperature effects were negligible and that variations in the value of the mass transfer coefficient were purely due to variations in the hydrodynamics of the fluid in the reactor. If it could therefore be assumed that the value of the mass transfer coefficient followed trends analogous to the above in all three of the reactors investigated, the following graphs could be obtained to illustrate the effect of both gas and liquid flow rates on the mass transfer coefficient.

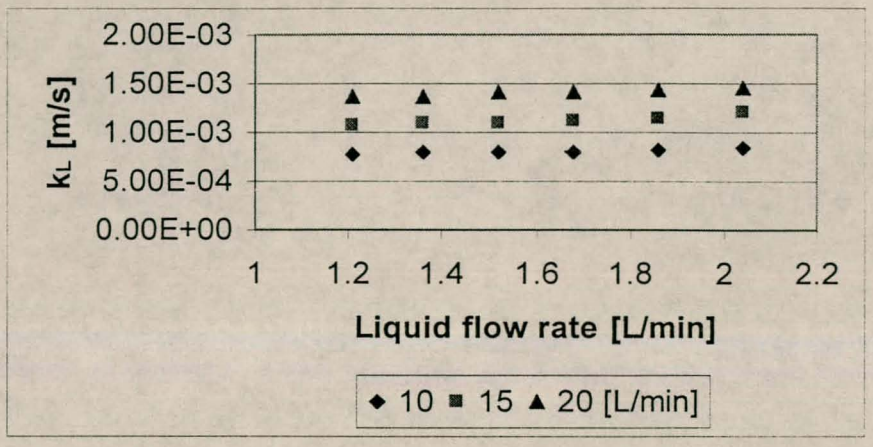

Figure 5.7 *The effect of liquid and gas flow rates on the mass transfer coefficient in the kite-shaped reactor*

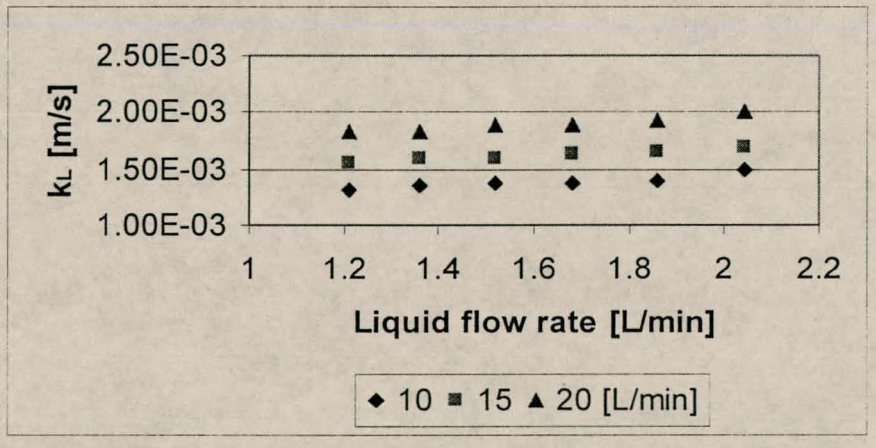

Figure 5.8 *The effect of liquid and gas flow rates on the mass transfer coefficient in the π-shaped reactor*

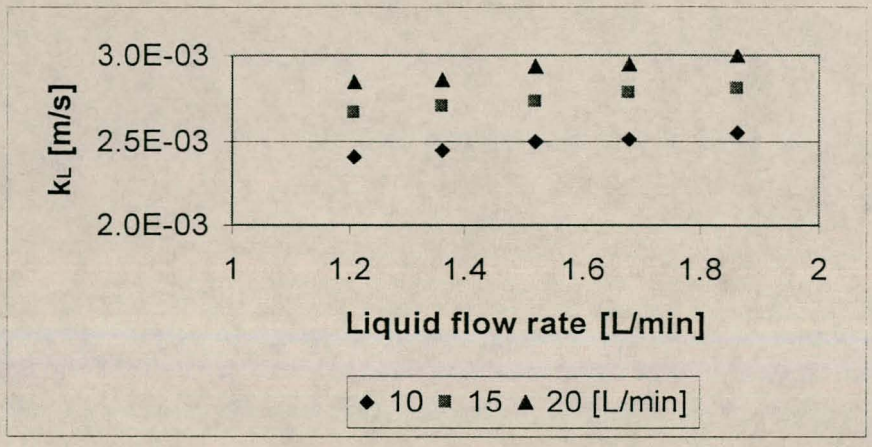

Figure 5.9 *The effect of liquid and gas flow rates on the mass transfer coefficient in the σ-shaped reactor*

At this stage it is interesting to note that the values obtained for k_L via a pseudo-first order reaction (*Figure 5.6*) and via a second order reaction (*Figure 5.9*) do not agree: whereas the pseudo first order reaction yielded values between 3.0×10^{-3} and 3.5×10^{-3} *m/s*, the second order reaction could only achieve values in the range of 2.4×10^{-3} to 3.0×10^{-3} *m/s*. Assuming that the small differences in the density and viscosity of the two feed solutions could not have a significant effect on the hydrodynamics of the system, the assumption that k_L remained constant with a change in concentration of the dissolved reagent seemed erroneous. However, it must be kept in mind that for a fast pseudo-first order reaction, at sufficiently high values of the solute concentration (and therefore the Hatta number), the enhancement factor reaches a limiting value where k_L becomes dependent on C_{BO} (*Figure 4.1*). But, since the first order reactions performed employed similar NaOH concentrations (< 5% variation), it could be assumed that, in this particular range of experiments, C_{BO} was relatively constant so that the results obtained for these reactions were still valid in the sense that they provided an indication of the effects of the gas and liquid flow rates on the value of the mass transfer coefficient.

To re-iterate, a fair degree of uncertainty is associated with the extraction of mass transfer coefficients from absorption data using *Botes*'s chemical technique. In order to gain a better understanding of the effects of both gas

and liquid flow rates on the value of k_L, runs were also performed under pseudo-first order conditions as a tool to collect more stable results. Although the mass transfer coefficients obtained from these experiments were higher than those extracted by way of *Botes*'s technique, the aim of the exercise was still accomplished since trends in k_L versus liquid and gas flow rates were obtained. However, for the purpose of fair comparison of the mass transfer coefficients exhibited by the different reactors investigated, only those k_L-values determined by way of *Botes*'s method will be considered in the remaining discussion of results.

Comparison of *figures 5.7* to *5.9* shows that there is a definitite distinction between the ranges of the mass transfer coefficients exhibited for the different reactors. While the kite-shaped reactor achieved values of k_L in the range of $8x10^{-4}$ to $1.5x10^{-3}$ *m/s*, the π- and σ-shaped reactors exhibited values of between $1.3x10^{-3}$ – $2x10^{-3}$ *m/s* and $2.4x10^{-3}$ – $3.0x10^{-3}$ *m/s*, respectively. Taking into account the fact that the kite shaped reactor's volume was less than half that of the other two reactors (8.25 vs 20 mL), but was operated under identical liquid feed (and therefore energy input) conditions, it is surprising to find that this reactor yielded lower values for k_L under higher (almost double) relative energy dissipation rates. This phenomenon can be explained via the following mechanisms:

- turbulence promotion,
- centrifugal acceleration of the fluid, and
- impingement zones.

As concluded by *Botes* (1995), the reactor geometry and nozzle configuration of any jet reactor should be such that high levels of turbulence can be sustained throughout the reactor. In terms of this, it can be argued that the round reactor chambers of the π- and σ-shaped reactors provide better promotion of turbulence than the angled/jagged shape of the kite-shaped reactor. Whereas a significant amount of the kinetic energy of the fluid in the kite-shaped reactor may be dissipated through collisions with the reactor wall, most of the energy dissipated in the other reactors can be applied to the

break-up of bubbles since a minimum amount of energy is wasted in changing the direction and momentum of the fluid stream.

As has been discussed in *Chapter 2*, the centrifugal acceleration of the liquid in the round reactor geometries of the π- and σ-shaped reactors also provides enhancement of the value of the mass transfer coefficient above that of the kite-shaped reactor, as illustrated by the following relation (*Calderbank*, 1967):

$$k_L \propto \left(\frac{(\rho_L - \rho_G)\mu_L g}{\rho_L^{\,2}} \right)^{1/3} \qquad \ldots (5.3)$$

where g can be replaced by the acceleration of the fluid due to its centrifugal acceleration. The enhancement of k_L, due to this mechanism, is absent in the kite-shaped reactor where the fluid flow in the reactor chamber is largely random.

The final mechanism responsible for the superior mass transfer coefficients exhibited by the π- and σ-shaped reactors is the enhancement effect of head-on impingement of gas into liquid streams. In the discussion of the essence of impinging streams in *Chapter 2*, it was pointed out that one of the intensifying mechanisms of impinging streams was an increase in the shear rate between gas and liquid, resulting not only in increased bubble break-up, but also an increase in the surface rejuvenation. Mass transfer is thus enhanced. The nozzle configuration of the kite-shaped reactor did not allow for the head-on impingement of liquid and gas streams – liquid streams were rather directed at opposing gas nozzles so as to shear off exiting gas bubbles. Although it can be argued that this mechanism also results in an increase in shear between gas and liquid phases, experimental results seem to indicate that the head-on impingement effect in the π- and σ-shaped reactors is more effective. In addition to this, the other intensification mechanisms associated with impinging streams, e.g. the increase in relative velocity between phases and increased residence time of bubbles due to their oscillations in the liquid stream, could also contribute to the relatively higher values of the mass transfer coefficient.

Much the same mechanisms as discussed above can be adduced to explain the relatively higher k_L values exhibited by the σ-shaped reactor ($2.4x10^{-3}$ – $3.0x10^{-3}$ *m/s*), compared to that of the π-shaped reactor ($1.3x10^{-3}$ – $2.0x10^{-3}$ *m/s*). In terms of turbulence promotion, it can be visualised that the swirling flow field in the σ-shaped reactor results in more effective promotion of turbulence than that of the π-shaped reactor where the momentum of the liquid flow is somewhat impeded by the head-on collision of the two phase fluids in the impingement zone. Due to this superior promotion of momentum and turbulence in the σ-shaped reactor, higher tangential velocities can be obtained, resulting in greater centrifugal acceleration of the fluid and the subsequent enhancement of the mass transfer coefficient via *equation (5.3)*. Finally, it can be noted that the superiority of the σ-shaped reactor can be attributed to the fact that, whereas the π-shaped reactor employs only one impingement zone, the σ-shaped reactor has two head-on impingement zones. Theoretically, this would mean a higher degree of bubble break-up and surface rejuvenation and thus a higher value of the mass transfer coefficient.

5.2.1.2 Comparison with literature data

Although the literature is abound with reported data for the volumetric mass transfer coefficient, k_La, it is very seldom found that authors provide independent values for the mass transfer coefficient, principally due to the difficulty in obtaining accurate and reproducible results for this mass transfer parameter (as discussed in the previous section). Finding mass transfer coefficient data for the CO_2 absorption system further limits the frame of reference, since most of the articles concerning the characterisation of gas-liquid contactors report mass transfer coefficients for the physical absorption of air (or oxygen) into water. Despite these restrictions, some data reported by *Herskowits et al.* (1990b) can be used as a basis for comparison of mass transfer coefficients. For their two-impinging stream absorber, values for the interfacial area and k_La were reported to be in the range of 0.03 – 0.52 m^2 and 0.025 – 1.22 s^{-1}, respectively, translating into values for the mass transfer coefficient in the range of $1.4x10^{-4}$ to $1.3x10^{-3}$ *m/s*. Mass transfer coefficients

reported by *Botes et al.* (1998) were also in the region of $2.6 \times 10^{-4} - 2.2 \times 10^{-3}$ *m/s*.

In light of the above data it might seem that the mass transfer coefficients obtained for the three reactors under investigation are superior to those presented in the literature. However, since k_L is a function of the energy dissipation in the reactors (as is the case with a and k_La), a fair comparison can only be made on the basis of this energy dissipation. *Figure 5.10* provides a rough comparison of the k_L-values as a function of the energy consumption in the respective reactors.

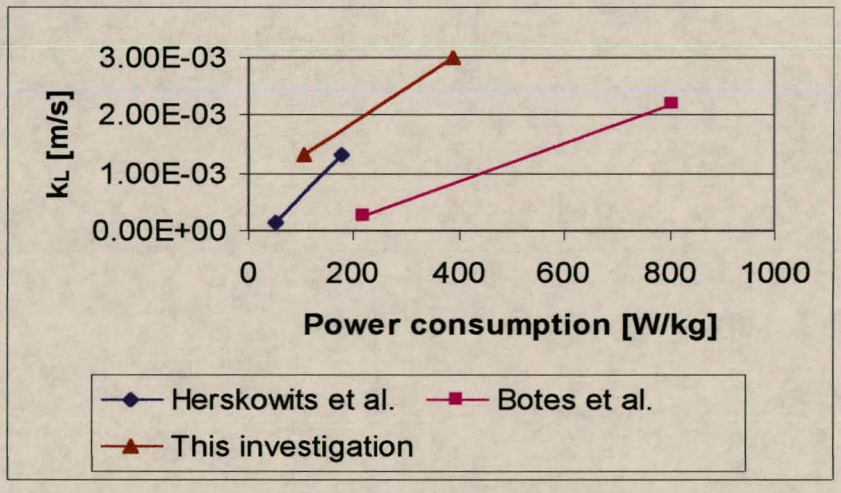

Figure 5.10 *Comparison of the ranges of the mass transfer coefficients for different investigations as a function of the energy consumption of the system.*

From this graph it can be seen that the mass transfer coefficients obtained by *Botes et al.* (1998) compare very poorly to those obtained by *Herskowits et al.* (1990b) based on energy consumption considerations, though they initially (at face value) seemed to be on par. It can also be seen that the values of k_L obtained in this investigation, compared relatively well with those of *Herskowits et al.* (1990b). However, it must be kept in mind that this graph should only be considered as a rough comparison of the relative values of k_L, since many assumptions had to be made in calculating the values of the mass transfer coefficient and power consumption for the system used by *Herskowits et al.* (1990b). Despite this, and considering the inherent enhancement of

mass transfer via impinging streams technology, it can be concluded with a reasonable amount of confidence that the mass transfer coefficients exhibited by the reactors under investigation represent a potential improvement over those of conventional gas-liquid contacting equipment.

5.2.1.3 Empirical correlation of k_L

In *Chapter 2* various empirical models for the correlation of k_L were presented. These correlations do not only serve as tools for the prediction of mass transfer coefficients under certain operating conditions, but can also be employed to verify results obtained in an experimental investigation. Since it has been mentioned how difficult it is to make a direct comparison between experimental data and literature data, k_L-correlations can be used to provide some indication as to the validity of results.

It has been shown that all correlations for k_L follow the following basic functional form (*Kawase* and *Moo-Young*, 1990):

$$k_L = C(\varepsilon\nu)^{1/4} Sc^{-\alpha} \qquad \ldots (5.4)$$

where α has been reported as $\frac{1}{2}$, $\frac{2}{3}$ and $\frac{3}{4}$. If it can be assumed that the value of the Schmidt number (ν/D_{AB}) does not vary significantly during a set of experiments, *equation (5.4)* can be rewritten to yield a simple relationship between k_L and the energy dissipation rate:

$$k_L = C_2 \varepsilon^{1/4} \qquad \ldots (5.5)$$

It can therefore be seen that k_L should vary as ε varies to the power 0.25. This simple condition was applied to check the validity of the trends in the mass transfer coefficient. *Figure 5.11* shows the typical variation in k_L at a constant gas flow rate, taken from data for the σ-shaped reactor.

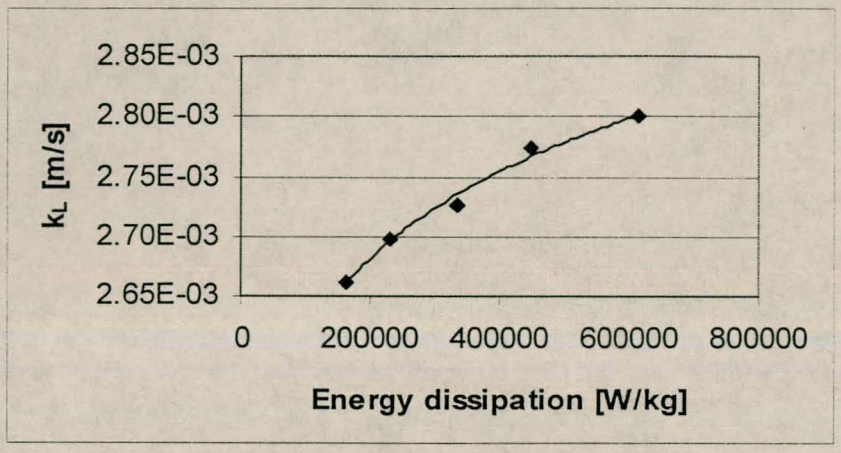

Figure 5.11 *Correlating the effect of energy dissipation on the mass transfer coefficient for a constant gas flow rate*

For this data, based on a constant gas flow rate, the following correlation (*equation 5.6*) was obtained, which showed that k_L is virtually independent of the energy dissipation rate and does not follow the relationship specified above:

$$k_L = 0.0017\varepsilon^{0.04} \quad \ldots (5.6)$$

This can most probably be ascribed to the relatively limited scope of liquid flow rates (and therefore energy dissipation rates) investigated in the reactor. Varying the flow rate over a greater range will possibly illustrate the effect of ε on k_L better.

Investigation of the effect of energy dissipation on the value of k_L for constant liquid flow rate, on the other hand, showed that the energy dissipation rate did have a significant effect on k_L, as illustrated in *Figure 5.12* and the following correlation:

$$k_L = 4.10^{-7}\varepsilon^{0.70} \quad \ldots (5.7)$$

In this case it seems that the effect of energy dissipation rate on the mass transfer coefficient is more pronounced than expected, since the value of the

exponent of the ε-term is 75% higher than anticipated (0.7 vs 0.4). This could either be a result of the very high power inputs into the system, leading to exceptional bubble break-up (as mentioned in section 5.1.3) and surface renewal, or could quite simply be attributed to the uncertainty in the values of k_L.

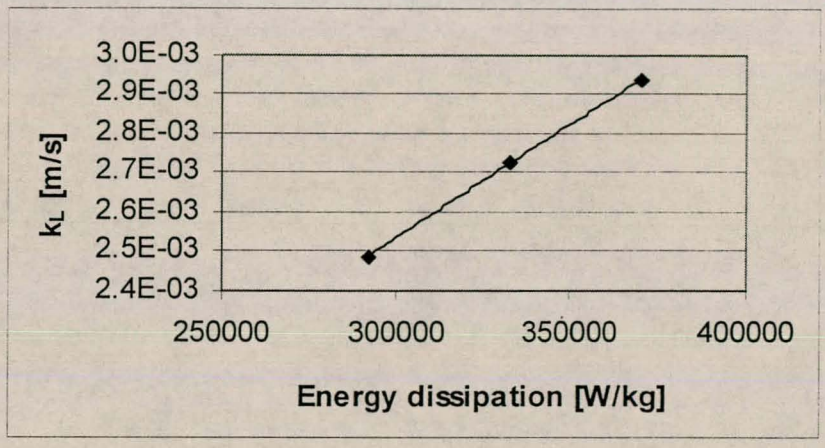

Figure 5.12 *Correlating the effect of energy dissipation on the mass transfer coefficient for a constant liquid flow rate*

In an attempt to make sense out of the conflicting observations regarding the effect of ε on k_L, a standard correlation for the mass transfer coefficient was fitted over the experimental data to determine to which extent the experimental data proved to be compatible with expected trends. This is illustrated in *Figure 5.13*. Reasonably good agreement between the minimum and maximum values of k_L in the range of energy dissipation rates investigated was obtained, although a lot of scatter around the expected trend was exhibited. It could therefore be concluded that, although it seemed possible that the trends in experimental k_L-data compared well with expected trends, the spread in the data was too great to make any definite conclusions. Once again this could be attributed to the difficulty in obtaining accurate and reproducible results for the mass transfer coefficient.

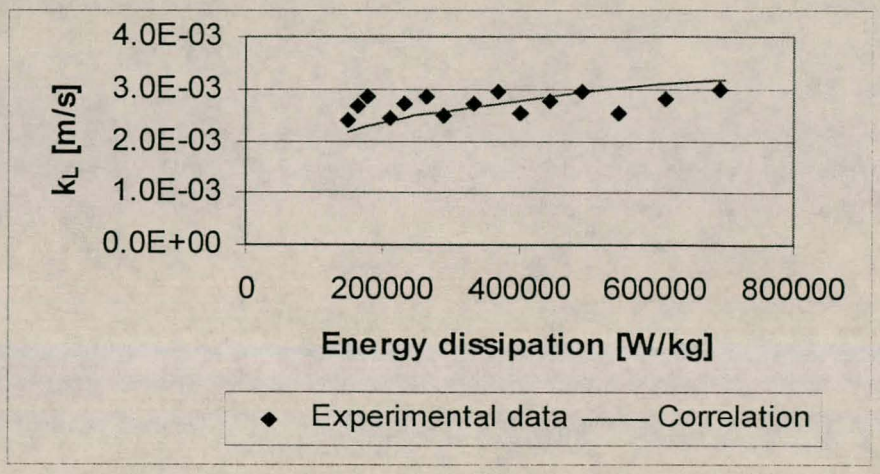

Figure 5.13 *Investigating the effect of energy dissipation on the mass transfer coefficient.*

5.2.2 Sulphite oxidation results

The aim of the sulphite oxidation experiments was to collect additional data on the interfacial area production in the reactors for verification of the fundamental model, the development and results of which will be discussed in the next chapter. Therefore, only a brief discussion of the results obtained for the mass transfer coefficient exhibited by this system will suffice.

As has been discussed in *Chapters 3* and *4*, the sulphite oxidation experiments were performed in the fast-pseudo first order regime, analogous to the standard approach followed by previous researchers. This theoretically allowed for a more stable and accurate determination of the mass transfer coefficient. It was however, found that no specific trends in these values could be identified since the effect of the reaction temperature on the reaction rate constant, and therefore the mass transfer coefficient, seemed to overshadow the hydrodynamic effects of varying gas and liquid flow rates. Taking into account the very small difference in gas voidages (0.114 – 0.156) between the three gas flow rates investigated, the difference in energy dissipation per unit mass of liquid in the reactor was not sufficient to yield definitive changes in the value of k_L with a change in gas flow rate. It was therefore assumed that

the value of the mass transfer coefficient remained relatively constant throughout the range of operating conditions.

The effect of temperature on the value of the mass transfer coefficient can be illustrated by the following graph:

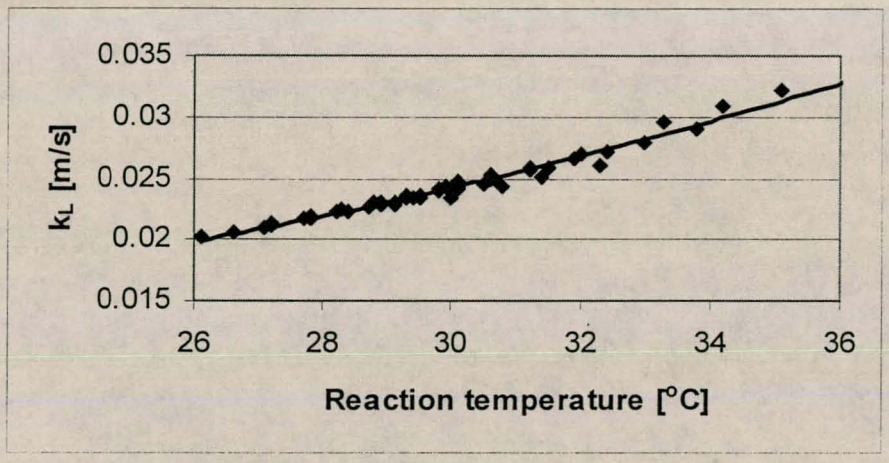

Figure 5.14 *The effect of temperature on the mass transfer coefficient exhibited during the sulphite oxidation experiments.*

Taking into account the fact that the model for which this data had been generated was based on a temperature of 25°C, the trend in the above data was extrapolated to yield a value of the mass transfer coefficient of 0.019 *m/s* at this particular temperature.

Comparison of this value with data from the literature was virtually impossible due to the sheer dependence of this parameter on the specific operating parameters used. Nowhere in the literature could suitable results be found that were obtained under experimental conditions similar to those employed in the current investigation. It was therefore accepted that the mass transfer performance of the newly developed jet reactors, specifically in terms of the mass transfer coefficient, had already been established with sufficient proof by the data from the CO_2 absorption experiments.

5.3 THE INTERFACIAL AREA, *a*

The object of this study was not only to characterise the reactors under investigation, but also to provide data for the development of a mechanistic model for the prediction of the interfacial area production in these new reactors. Therefore it could be said that the most important mass transfer parameter under consideration was the interfacial area. The following section will discuss the results obtained for this design parameter and compare it with data from the literature. Brief attention will also be given to the empirical modelling of the interfacial area.

5.3.1 CO_2 absorption

In *section 5.2.1.1* it was discussed how the chemical technique proposed by *Botes* (1995) yielded values for the mass transfer coefficient which were rather inaccurate and difficult to reproduce. Since interfacial areas were simply calculated by dividing k_La-values by corresponding k_L-values, it seemed as though determining accurate values for the interfacial area would also be very difficult. However, realising that the value of the interfacial area and k_La was much less sensitive to a variation in input parameters than k_L (~5% vs. 11%), reasonably accurate values could be obtained for this mass transfer parameter. The following table and graphs provide a summary of the results obtained for the three reactors investigated.

Table 5.4 *Ranges of interfacial areas produced in the different reactors*

Reactor configuration	**Interfacial area produced** m^2/m^3
Kite-shaped reactor	6650 – 16 000
π-shaped reactor	2700 - 6300
σ-shaped reactor	2600 - 6900

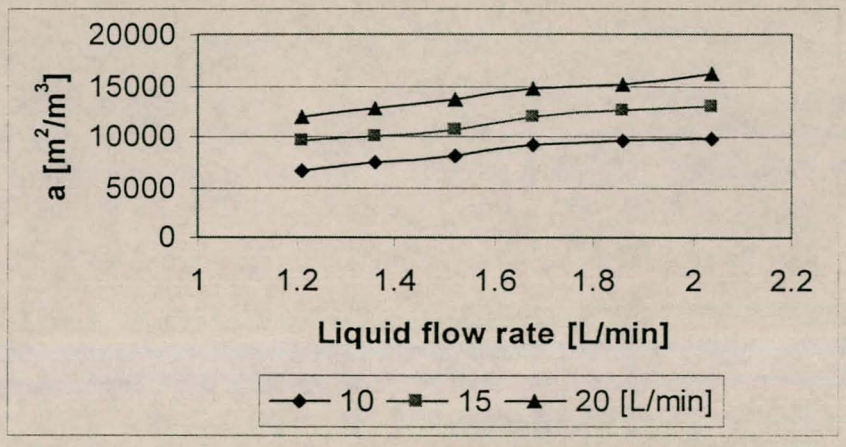

Figure 5.15 *The effect of liquid and gas flow rates on interfacial area in the kite-shaped reactor*

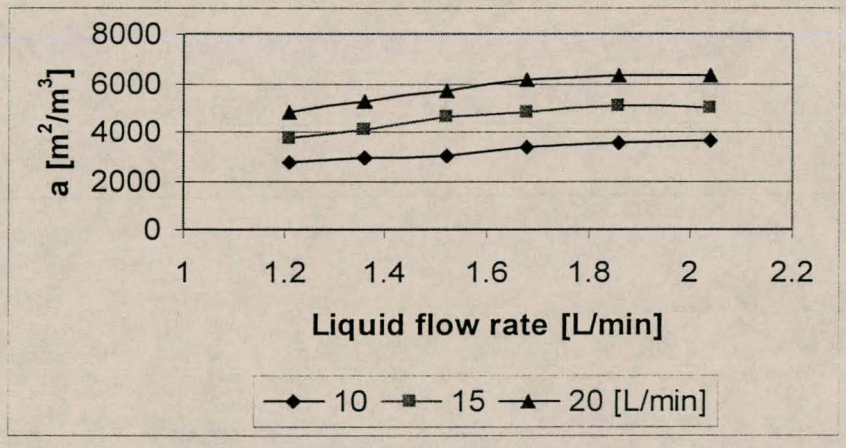

Figure 5.16 *The effect of liquid and gas flow rates on the interfacial area in the π-shaped reactor*

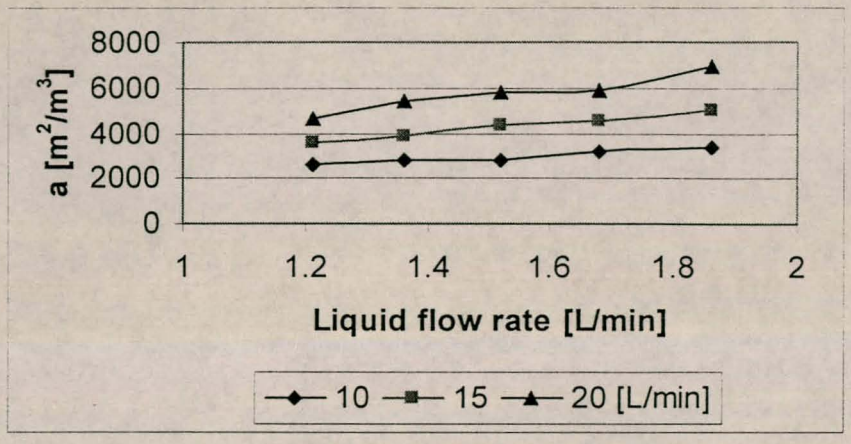

Figure 5.17 *The effect of liquid and gas flow rates on the interfacial area in the σ-shaped reactor*

It can be seen that the trends in the interfacial areas produced in the reactors are very similar to those exhibited by the mass transfer coefficients, since both are governed by the mutual mechanism of bubble break-up. In *section 5.2.1.1* it was explained how increased turbulence (due to impingement zones etc.) leads to an increase in the shear rate between bubbles and the bulk liquid, resulting in more effective bubble break-up. This effect not only leads to a higher surface renewal rate, yielding higher values of the mass transfer coefficient, but also to an increase in the interfacial area due to an increase in the number of bubbles for a constant gas hold-up.

Much as was the case with the mass transfer coefficient, it was found that an increase in both the liquid and gas flow rates resulted in an increase in the interfacial area produced. However, it was also found that the gas flow rate had a more significant effect on the interfacial area than the liquid flow rate. This is to be expected since an increase in the gas flow rate not only leads to a larger volume of gas in the reactor, but also to an increase in the energy dissipation rate in the reactor, resulting in more intensive turbulence and bubble break-up. An increase in the liquid flow rate simply translates into an increase in the energy input into the reactor, having little effect on the amount of gas held up in the system.

Comparison of the values of the interfacial areas exhibited by the reactors under investigation, as seen in *Table 5.4*, seems to indicate that the kite-shaped reactor represents the most effective system for interfacial area production. Although this might be true in absolute terms, a fair assesment of its efficiency can only be made on the basis of its energy consumption relative to that of the other reactors. *Figure 5.18* provides an illustration of the relative performances of the reactors in terms of energy consumption.

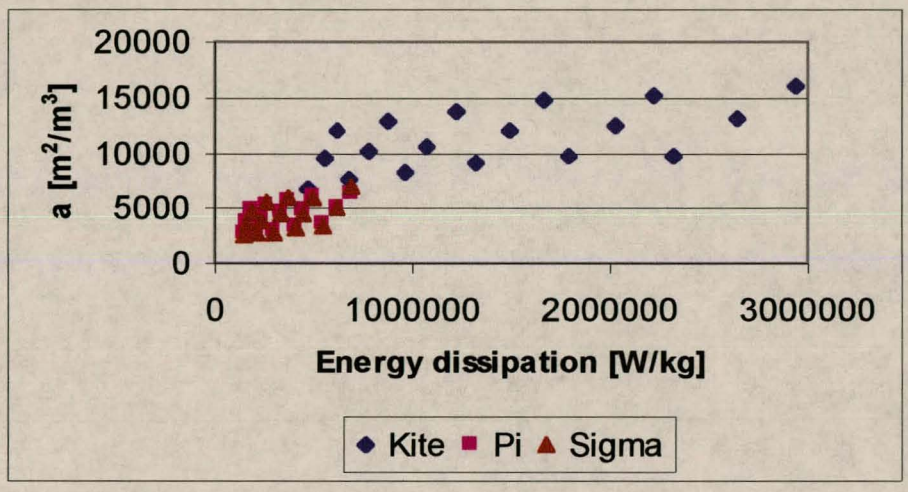

Figure 5.18 *Comparison between the interfacial areas produced in the three reactors as a function of the energy dissipation rate.*

From this graph it can clearly be seen that the interfacial areas exhibited by the kite-shaped reactor are, in fact, higher for a specific energy dissipaton rate (where a comparison is possible). Whereas for the kite-shaped reactor it was found that the mass transfer coefficient compared very poorly based on energy dissipation considerations, experimental results have proven that the interfacial areas exhibited in this reactor represent a significant improvement over the values exhibited by the other reactors. This phenomenon is most probably due to the following two factors:

- Reactor configuration, and
- Flow fields.

In *section 5.2.1.2* the comparatively low k_L-values exhibited by the kite-shaped reactor were attributed to poor sustainment and promotion of

turbulence in this reactor, due to the angular/jagged shape thereof. It was said that a significant amount of the kinetic energy of the fluid in the reactor was dissipated through collisions with the reactor wall. Conversely, it can be argued that a significant enhancement in bubble break-up (and therefore interfacial area production) occurs due to the break-up of entrained bubbles in the liquid bulk as the fluid collides with a portion of the reactor wall. This can be visualised when looking at the reactor geometry of the kite-shaped reactor: after having sheared off bubbles exiting the gas nozzles, the liquid spray collides with the reactor wall after which it is reflected back into the reaction chamber. Therefore, although the reactor does not promote effective promotion of turbulence (and therfore exhibits low k_L-values), it does provide an additional mechanism for effective bubble break-up, thereby increasing the interfacial area produced.

The flow fields in the kite-shaped reactor are also very random: the reactor does not exhibit any directed flow patterns, as is the case with the round reactor chambers of the π- and σ-shaped reactors. It is therefore possible that a large amount of gas (in the form of bubbles) is entrained in the bulk liquid which circulates randomly in the reaction chamber before exiting, as opposed to the flow fields in the other two reactors where the flow field basically directs the fluid to the exit of the reactor. Due to this entrainment of bubbles a larger volume of gas is held up in the reactor, resulting in higher interfacial areas. Although these proposed mechanisms cannot be verified via the chemical systems used, they could be observed visually through the perspex wall of the reactor.

Further comparison of the values of the interfacial areas exhibited by the π- and σ-shaped reactors show that these reactors yield very similar results, which is to be expected since both reactors share the same reaction volume and are operated under identical conditions. However, it can be noted that the σ-shaped reactor has some advantage over the π-shaped reactor at high flow rates, and vice versa at low flow rates. In terms of flow fields, this is not what is expected, since with the σ-shaped reactor an increase in the flow rates, especially that of the liquid rate, would lead to the formation of a central core

of gas in the middle of the reactor due to the centrifugal forces of the liquid pushing bubbles out towards a less dense area, analogous to a hydrocyclone. Since the outlet of the reactor is in its centre, it would therefore be expected that gas could escape more easily, yielding a lower gas hold-up and resulting interfacial area.

It could, however, also be argued from a hydrodynamic point of view that at high flow rates the two impingement zones in the σ-shaped reactor become more effective (due to deeper penetration of the gas into the liquid) so that higher shear rates are generated, leading to more effective bubble break-up and higher values for the interfacial area. To which extent these opposing mechanisms determine the production of interfacial area can, however, not be determined. In the light of this, and considering a certain degree of uncertainty in the experimental results, it is assumed that the π- and σ-shaped reactors yield reasonably similar values for the interfacial area.

To conclude, therefore, experimental evidence seems to suggest that the kite-shape reactor represents the most efficient configuration for interfacial area production due to its ability to enhance bubble break-up through collisions of the bulk fluid with the reactor wall and its random flow pattern which results in larger gas holdups. Values for the interfacial area exhibited in the π- and σ-shaped reactors are otherwise very similar. *Section 5.3.3* will provide some insight as to how the interfacial areas produced in these reactors compare with literature data, while *Section 5.3.4* will investigate the effects of gas and liquid flow rates quantitatively through empirical correlations.

5.3.2 Sulphite oxidation

The sulphite oxidation reactions were performed only in the σ-shaped reactor since their objective was simply to provide additional data for verification of the model and not to characterise the reactors. The following graph illustrates the results obtained for this reactor, where the legend refers to gas inlet pressures.

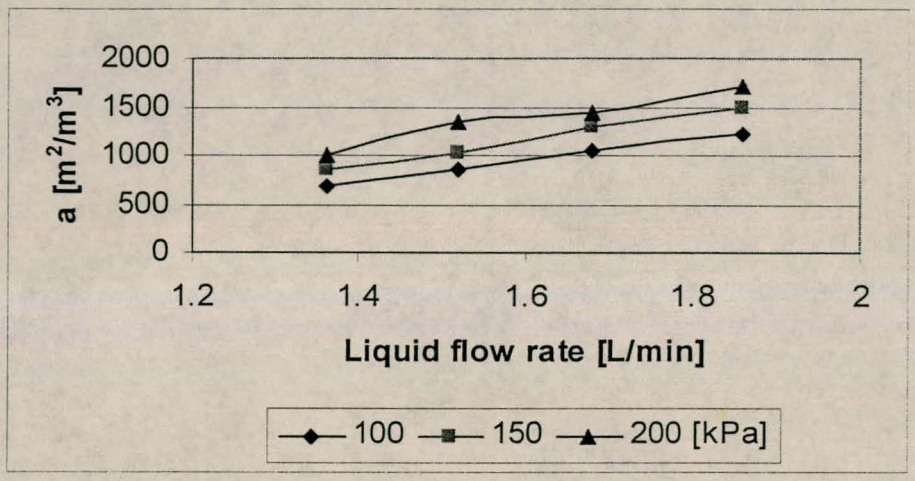

Figure 5.19 *The effect of liquid and gas flow rates on the interfacial area in the σ-shaped reactor for the sulphite oxidation system.*

Analogous to the results obtained for the CO_2 absorption system, the sulphite oxidation system exhibits an increase in interfacial area with an increase in both gas and liquid flow rates. Once again it can be seen that the effect of the gas flow rate is more pronounced than for the liquid flow rate, although less significant than for the CO_2 absorption system. This can simply be attributed to the smaller gas voidages in the reactors (due to lower gas flow rates employed) so that the difference in energy dissipation rates between minimum and maximum gas and liquid flow rates is less severe.

Chapter 6 will provide insight into how the values obtained for this system compare with those for the CO_2 system when the evalution of the model is discussed. Since the interfacial areas exhibited for this system were very low in comparison with those of the CO_2 absorption system (700 – 1300 vs 3300 – 6900 m^2/m^3), the data provided for validation of the model over a wide range of gas flow and energy dissipation rates.

5.3.3 Comparison with literature data

Comparison of experimental results with data from the literature for interfacial area proved to be much easier than for bubble sizes and mass transfer

coefficients. Whereas data for bubble sizes were relatively difficult to find and were only reported as functions of gas pressures or superfical gas velocities and not energy dissipation rates, mass transfer coefficients are relatively specific with regard to the chemical system used (especially within certain chemical regimes) and therefore cannot be compared with many other systems. If it can be assumed that all aqueous systems share basically similar values of general physico-chemical parameters such as density, viscosity and surface tension, systems can be compared with one another based on energy dissipation rates alone.

However, interfacial area data in the literature are generally reported for agitated tank contactors which conventionally employ considerably lower energy dissipation rates than those exhibited in the newly developed jet reactors. Therefore, to be able to make a comparison of the interfacial areas based on energy dissipation rates, these values had to be extrapolated. Although this approach is not very accurate, it is the only way in which some sort of comparison can be made between data generated in different regimes of energy dissipation. Since the functional relationship between interfacial area and energy dissipation rate is not linear, the literature first needed to be surveyed to obtain the exponent α for the energy dissipation rate in the following equation (*Kawase* and *Moo-Young*, 1990):

$$a = C\varepsilon^{\alpha} \qquad \ldots (5.8)$$

Table 5.5 provides a summary of the values obtained for α:

Trom this table it can be seen that α varies widely between 0.25 and 0.5, around an average of approximately 0.4. This scatter in α-values can greatly be ascribed to very poor accuracy in both physical and chemical methods for determining interfacial areas, as stated by *Kawase & Moo-Young* (1990). However, taking 0.4 as the most representative value of the data, comparison between interfacial areas determined in different energy dissipation regimes can now be made.

Table 5.5 *Determining the functional dependence of the interfacial area on energy dissipation*

**Note: Based on Kolmogoroff's theory of isotropic turbulence*

Authors	Value of α
Lopes de Figueiredo and Calderbank (1979)	0.25
Breman et al. (1996)	0.286
Bouaifi and Roustan (1998)	0.32 – 0.5
Calderbank (1958)*	0.4
Nagel et al. (1979)*	0.4

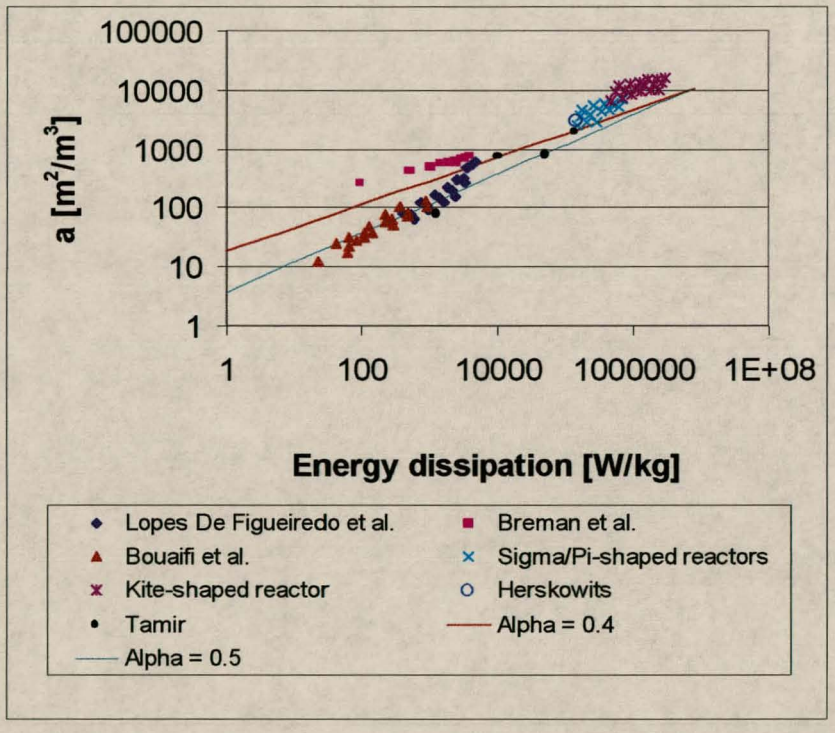

Figure 5.20 *Comparison of experimental interfacial area results with data reported in the literature*

Figure 5.20 provides a graphic representation of the data of a number of authors for interfacial area for comparison with results obtained in this investigation. Although in some instances interfacial areas had to be

calculated from k_La and gas hold-up values, care was taken to ensure that these values were as accurate as possible (for fair comparison).

Firstly, focussing on data reported for agitated tanks, it can clearly be seen that the data reported by *Lopes De Figueiredo & Calderbank* (1979) and *Bouaifi & Roustan* (1998) compare very well, while the data reported by *Breman et al.* (1996) yielded significantly higher values for the interfacial area per rate of energy dissipation. This was due to the fact that the latter mentioned authors investigated the enhancement of gas-liquid contact in a novel multi-stage agitated contactor (MAC), whereas the other two authors simply considered conventional impeller-agitated tank systems. In this sense it can be seen that the MAC already represents an improvement over conventional equipment, so that the data of *Lopes De Figueiredo & Calderbank* (1979) and *Bouaifi & Roustan* (1998) can be considered as the basis upon which the newly developed jet reactors will be evaluated.

Figure 5.20 also features data obtained by *Herskowits et al.* (1990b) and *Tamir* (1994) for different impinging stream reactors. These results are included in the graph to provide some indication as to how the impinging stream reactors in this investigation compare to other reactors employing the same technology. Although only one data point is given for the system proposed by *Herskowits et al.* (1990b), it can be taken as representative of the maximum interfacial area obtained during their investigation.

In addition to the plotted data, two lines representing the functional relationship between energy dissipation rate and interfacial area are also provided to facilitate easy comparison between the data generated in this investigation and expected values, extrapolated from conventional data.

Taking the value of α as equal to 0.4 in equation (5.8) and fitting this line through the *maximum* values obtained by *Lopes De Figueiredo & Calderbank* (1979) and *Bouaifi & Roustan* (1998), it can be concluded that in terms of energy dissipation rate, both the kite and π- and σ-shape reactors represent a significant improvement over interfacial area production in conventional gas-

liquid contactors, although this is more significant for the kite-shaped reactor (as discussed previously). Furthermore it can be seen that the interfacial areas obtained by *Herskowits et al.* (1990b) also represent some degree of improvement over conventional systems, while the data presented by *Tamir* (1994) appears to be very much on par with expected trends.

Taking only the data of *Lopes De Figueiredo* & *Calderbank* (1979) and *Bouaifi* & *Roustan* (1998) as basis for comparison, and extrapolating this data using a higher value of α equal to 0.5 (which represents a 'stricter' comparison due to a higher rate of increase in interfacial area with increase in energy dissipation rate), it can still be seen that reactors in this investigation represent an improvement over conventional contacting systems. Although it must be re-iterated that this is a very crude way to make a comparison between different reactor systems, evidence points strongly towards the potential improvement of gas-liquid interfacial area production in these newly developed impinging stream reactors. Even compared to other impinging systems, these reactors seem to represent a better alternative.

5.3.4 Empirical modelling

As shown in *Chapter 2*, interfacial area is typically correlated against energy dissipation rate and superficial gas velocity or gas hold-up. Since a superficial gas velocity could not be determined for the reactors investigated, and gas hold-up was simply calculated from interfacial area and gas flow rate, it was decided to rather correlate interfacial area as a function of the energy dissipation rate and the gas flow rate. This approach was also followed by *Tamir* (1994) for empirical modelling of his impinging stream absorbers.

Table 5.6 provides a summary of the correlations obtained for the different reactor configurations and chemical systems employed.

Table 5.6 *Correlation of experimental data against energy dissipation and gas flow rate*

Reactor / Chemical system	Correlation
CO_2 absorption:	
Kite-shaped reactor (R^2 = 0.99)	$a = 37.7.10^3 \varepsilon^{0.28} Q_g^{\ 0.58}$
π- and σ-shaped reactors (R^2 = 0.98)	$a = 19.2.10^3 \varepsilon^{0.35} Q_g^{\ 0.72}$
Sulphite oxidation:	
σ-shaped reactor (R^2 = 0.97)	$a = 5.4.10^3 \varepsilon^{0.5} Q_g^{\ 0.8}$

In *section 5.3.3* a literature survey was performed to find the dependence of the energy dissipation rate on the interfacial area. This also needed to be done for the gas flow rate to establish whether trends exhibited by the experimental results obtained during this investigation were consistent with those reported in the literature. If the following general form of a correlation relating interfacial area to energy dissipation and gas flow rates can be assumed:

$$a = C\varepsilon^{\alpha} Q_g^{\ \beta} \qquad \ldots (5.9)$$

Typical values of β obtained from the literature are presented in *Table 5.7*:

In this case it can be seen that β varies widely between values of 0.25 and 0.6, yielding an average value of approximately 0.5. This value will be compared to values obtained from experimental data in this investigation.

Table 5.7 *Determining the functional dependence of the interfacial area on gas flow rate*

Authors	Value of β
Meister et al. (1979)	0.248
Van't Riet (1979)	0.5
Yagi and Yoshida (1975)	0.28
Breman et al. (1996)	0.57
Bouaifi and Roustan (1998)	0.6
Tamir (1994)	0.26 – 0.52
Calderbank (1958)	0.5

It has been mentioned that the empirical correlations obtained from experimental data are simply used as tools to establish whether the trends exhibited in our data are consistent with conventional systems. From this perspective it can be seen that with regard to the energy dissipation rate, values obtained for α compare well with published data. Values obtained for this exponent (0.28 and 0.5) from experimental data fall neatly into the range of values found in the literature.

However, with regards to the effect of gas flow rate on interfacial area, it can be noted that experimental values of β are higher than values reported in the literature: whereas the literature presents values in the range of 0.25 – 0.6, experimental values range between 0.6 – 0.8. Results therefore, seem to indicate that the effect of gas flow rate on interfacial area in the newly developed reactors is more pronounced than in conventional systems. Thus, operating the reactors at higher gas loadings present the potential to yield a higher rate of increase in the interfacial area. Since the enhancement of interfacial area production (via smaller bubble sizes) due to increase in the energy dissipation rate with an increase in the gas flow rate has already been accounted for the the energy dissipation term in the correlation, it can only be concluded that this effect is due to more effective hold-up of gas in the reactor. Considering that mass transfer rates are generally limited by the

transport of gas to the liquid phase, a larger relative gas hold-up represents a considerable advantage.

In essence it can therefore be said that the interfacial correlations obtained from experimental data compare very well with those presented in the literature, establishing that trends exhibited in the investigated reactors are consistent those presented in the literature. It has also been shown how these reactors provide higher than expected interfacial areas due to more effective hold-up of gas.

5.4 THE VOLUMETRIC MASS TRANSFER COEFFICIENT, k_La

The volumetric mass transfer coefficient is an absolute indication of the contacting and mass transfer performance exhibited by any gas-liquid contactor. Since it is simply the product of the mass transfer coefficient and the interfacial area, the mechanisms proposed for the trends in these parameters can simply be combined to explain trends in the values of k_La. In the light of the fact that these mechanisms are explained in detail in the appropriate sections, this section will rather focus on the comparison of the reactors under investigation and other contactors in the literature, based on k_La values.

5.4.1 CO_2 absorption

Results obtained for the volumetric mass transfer coefficient in each of the three reactors investigated are given in *Figures 5.21 – 5.23*. Once again the numbers in the legends refer to the gas flow rates.

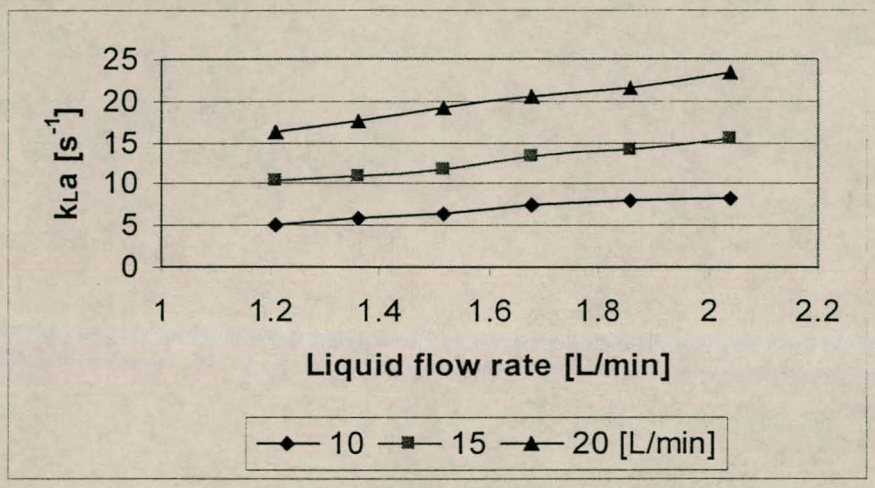

Figure 5.21 *The effect of liquid and gas flow rates on the volumetric mass transfer coefficient in the kite-shaped reactor*

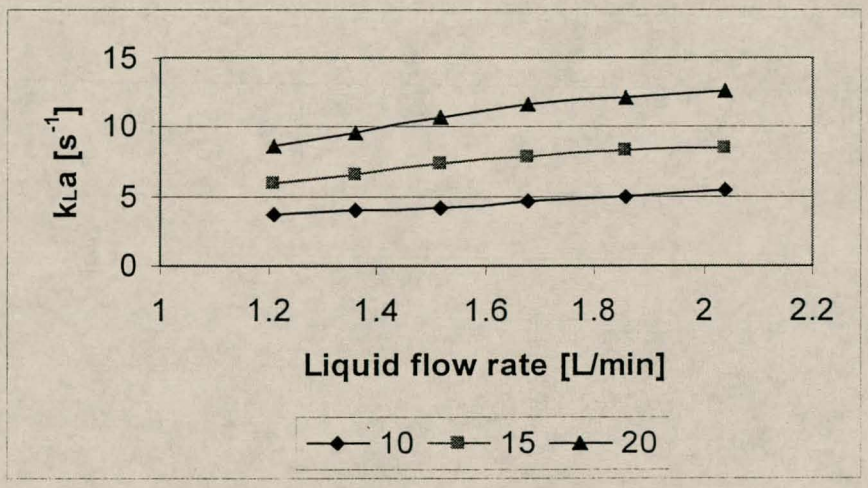

Figure 5.22 *The effect of liquid and gas flow rates on the volumetric mass transfer coefficient in the π-shaped reactor*

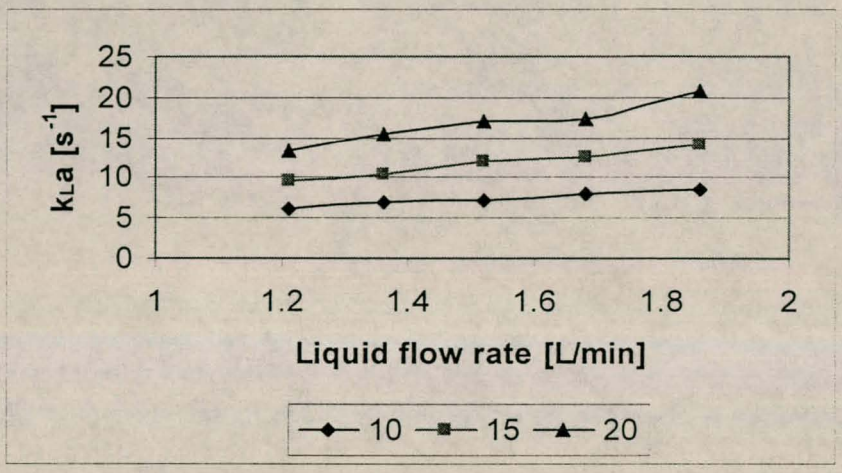

Figure 5.23 *The effect of liquid and gas flow rates on the volumetric mass transfer coefficient in the σ-shaped reactor*

As could be expected, it can be seen that the value of k_La increases with both an increase in the liquid and gas flow rates, due to an increase in the energy dissipation rate in the reactor. It is interesting to note that the gradient of the constant-gas-flow-rate lines increase with an increase in liquid and gas flow rates, since the values of both k_L and a exhibit an increase with an increase in these flow rates. This seems to suggest that it would be advantageous to run the reactor at higher gas flow rates for a higher rate of increase in the value of k_La. Since the additional energy associated with this is negligible compared to the energy introduced to the system via the liquid, this seems a viable option.

Comparing the k_La-values exhibited by each of the reactors, it can be seen that the σ-shaped reactor exhibits values virtually equal to those of the kite-shaped reactor, which is operated under more than double the energy dissipation rate. It can, therefore, immediately be concluded that the σ-shaped reactor represents the best design in terms of energy considerations. However, the k_La-values exhibited by the π-shaped reactor are significantly lower than those exhibited by the kite-shaped reactor so that it is neccesary to make a comparison based on energy dissipation rates in the reactors. *Figure 5.24* provides a graphic illustration of this. From this graph it can be seen that at low gas flow rates, the π-shaped reactor compares well with the kite-shaped reactor: virtually identical values of k_La per unit of energy is obtained.

However, at higher gas flow rates, the kite-shaped reactor starts exhibiting higher values of k_La. This can most probably be explained via the superior bubble breakage efficiency and interfacial area production ability of this reactor, as discussed previously.

Based on the above it can be concluded that the kite-shaped reactor represents a better design than the π-shaped reactor, based on the volumetric mass transfer coefficient. *Figure 5.24* also confirms that the σ-shaped reactor yields significantly higher values of k_La than the kite-shaped reactor: it represents an average increase of 30% in this parameter at equal energy dissipation rates.

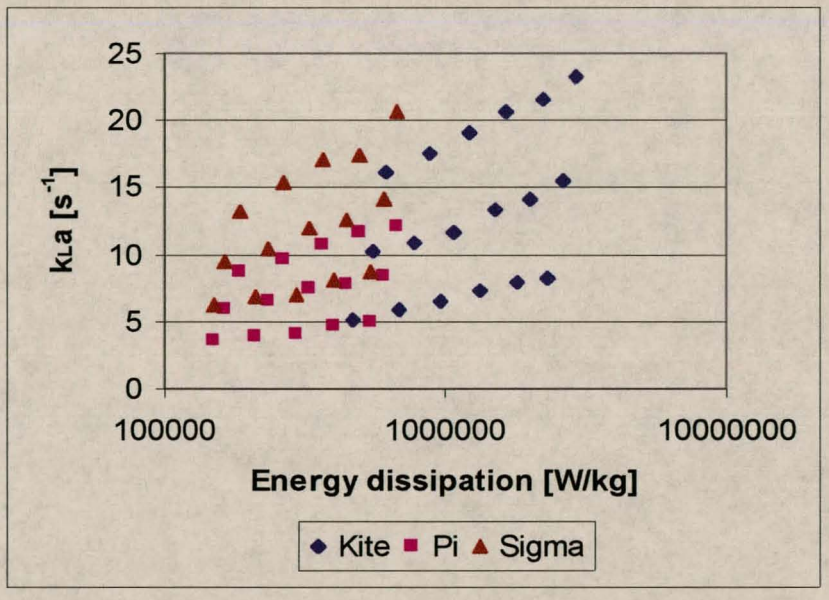

Figure 5.24 *Comparison between the volumetric mass transfer coefficients exhibited in the three reactors as a function of the energy dissipation rate.*

It can therefore be concluded that the σ-shaped reactor represents the best design, due simply to its ability to produce high values of the mass transfer coefficient via centrifugal acceleration of the fluid. However, the kite-shaped reactor represents a better design than the π-shaped reactor due to its ability to produce a high degree of bubble break-up (and therefore interfacial area production), the effect of which surpasses the relatively higher values of k_L in the π-shaped reactor.

Thus, it can be seen that the performance of a reactor is a result of the combination of its ability to produce high values of the mass transfer coefficient and interfacial areas. In terms of this, it seems that an optimum reactor design would incorporate the mass transfer enhancing benefits of a round reactor chamber with the bubble break-up ability of a jagged/angular reactor chamber.

5.4.2 Sulphite Oxidation

Since the object of the sulphite oxidation experiments were simply to provide additional data for verification of the fundamental model, not much attention will be given to the results of k_La for this system. Once again it was found that k_La increases with an increase in both liquid and gas flow rates, reaching a maximum at 15 s^{-1}. However, it can be seen that the gradients of the constant-gas-flow-rate lines do not increase with an increase in gas flow rates (as exhibited above) since a constant value of k_L was used throughout (*section 5.2.2*). Due to the fact that these experiments were only performed in the σ-shaped reactor, no comparison of the three reactor designs can be made based on this chemical system. *Figure 5.25* provides a summary of the results obtained in the σ-shaped reactor.

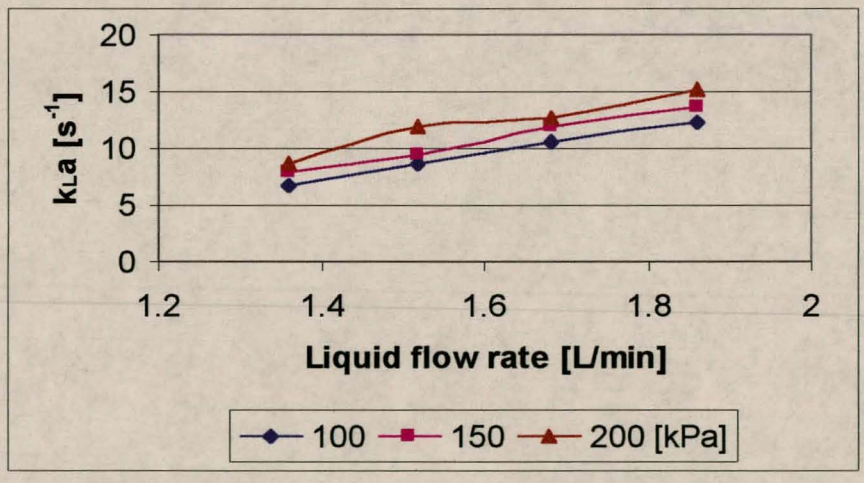

Figure 5.25 *The effect of liquid and gas flow rates on the volumetric mass transfer coefficient for the sulphite oxidation system in the σ-shaped reactor*

5.4.3 Comparison with literature data

As mentioned in *section 5.2.1.2*, care must be taken when comparing the k_L values of different systems, since these values are often dependent on the chemical regimes in which they were determined. Since the values of the volumetric mass transfer coefficients are directly determined from these values, exactly the same argument applies for k_La. However, the literature does present a relatively wide range of data for comparison of experimental k_La-values with those exhibited by conventional systems. This is facilitated by the following relationship (based on the penetration theory), which can be used to estimate k_La for gas-liquid systems other than those applied in this investigation:

$$\frac{(k_La)_1}{(k_La)_2} = \sqrt{\frac{D_1}{D_2}} \qquad \ldots (5.10)$$

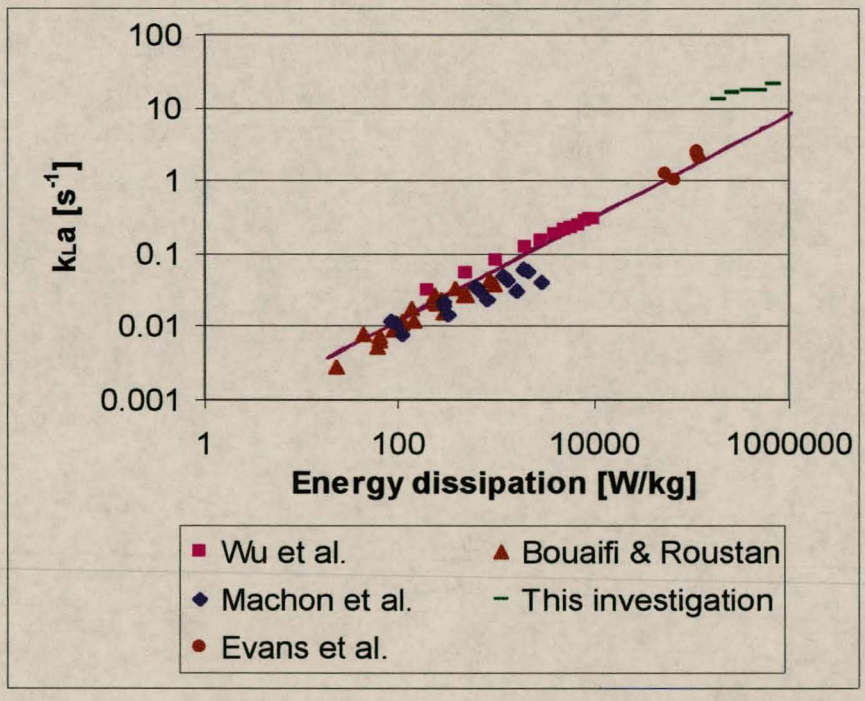

Figure 5.26 *Comparison of experimental k_La values with those obtained from the literature.*

Figure 5.26 shows that the data reported by *Wu et al.* (1998), *Bouaifi* and *Roustan* (1998) and *Machon et al.* (1988) compare very well. However, as was the case for interfacial areas in *section 5.3.3*, these k_La values were also obtained at relatively low energy dissipation rates compared to those exhibited in the experimental reactors. Therefore, the dependence of k_La on the energy dissipation rate once again needed to be determined to enable the extrapolation of the data to the regime of energy dissipation rates used during the experimental investigation. A survey of the literature (which will be discussed in more detail in the following section) revealed that the value of α in the following equation ranged between 0.4 –0.7:

$$k_La = C\varepsilon^{\alpha} \qquad \ldots (5.11)$$

Since the data of the above authors, featured in *Figure 5.26*, was best fitted using α = 0.7, this exponent for the energy dissipation rate was used in *equation (5.11)* for extrapolation of the data. In terms of this equation, represented in *Figure 5.26* by the smooth line, it can be seen that the data presented by *Evans et al.* (1999) for a plunging liquid jet bubble column is accurately predicted, even at energy dissipation rates significantly higher (orders of magnitude) than those employed by the three other authors. But it can also be seen that the values of k_La exhibited in experimental reactors are underpredicted. Therefore, taking the smoothed line as representative of the majority of data provided in the literature, it can be concluded that in terms of the volumetric mass transfer coefficient, the reactors in this investigation provide a significantly higher degree of phase contact and mass transfer than conventional systems.

In his book on impinging streams reactors, *Tamir* (1994) utilised dimensionless numbers for the energy dissipation rate and volumetric mass transfer coefficient to evaluate the performance characteristics of various absorbers by eliminating the effects of density and viscosity differences between chemical systems via the following equations:

$$k_L a^* = k_L a \left(\frac{\nu_L}{g^2} \right)^{1/3} \quad \ldots (5.12)$$

and

$$\varepsilon^* = \varepsilon \left(\nu_L \rho_L{}^3 g^4 \right)^{-1/3} \quad \ldots (5.13)$$

The following figure is an adaptation of the graph he presented to illustrate the the superior mass transfer performance of his proposed impinging stream absorbers; the dimensionless $k_L a$ values obtained for the reactors in this investigation are added for comparison with both conventional stirred tanks and other proposed impinging stream reactors.

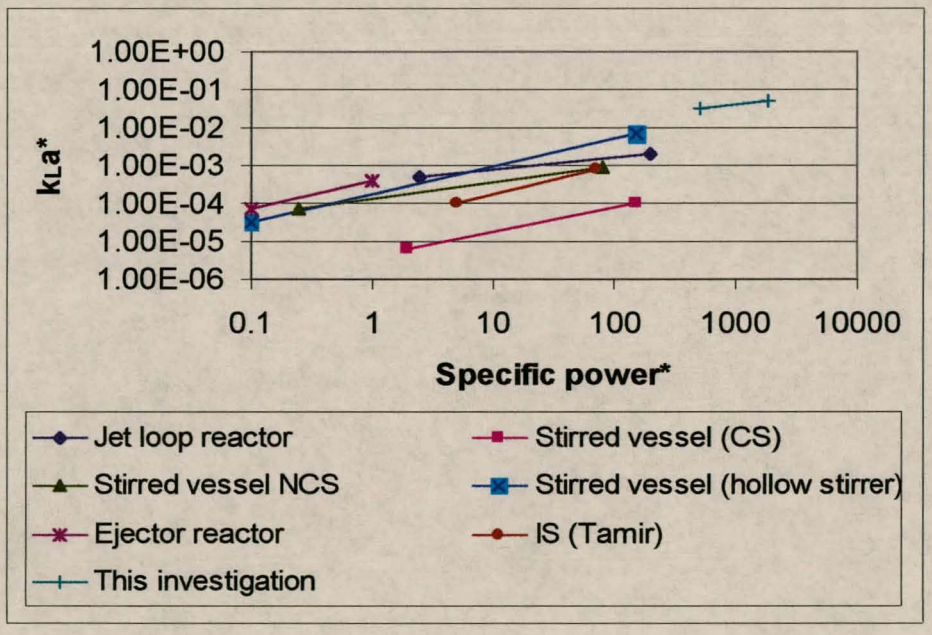

Figure 5.27 *Comparison between absorbers. Adapted from Tamir (1994).*

From this and the previous figure, it can be concluded that the newly developed impinging stream reactors have the potential to yield comparatively better mass transfer performance, based not only on conventional systems, but other high intensity systems too, e.g. jet loop and ejector reactors.

5.4.4 Empirical modelling

Due to the sheer importance of the volumetric mass transfer coefficient as a basis for comparison between different reactors, various correlations for this mass transfer parameter are available in the literature. Although many different combinations of variables are used to correlate k_La, the most common are the energy dissipation rate and the superficial gas velocity. Since no superficial gas velocity could be determined for the experimental reactors (as explained in *section 5.3.4*), this parameter was simply replaced by the gas flow rate to yield an equation of the following form:

$$k_L a = C\varepsilon^{\alpha} Q_g^{\beta} \qquad \ldots (5.13)$$

Once again a literature survey was performed to find typical values of the exponents α and β. Note that the form of *equation (5.13)* is identical to the corresponding correlation for the interfacial area, since k_L is basically a function of the energy dissipation rate alone. The values of β presented here will therefore be identical to those in *section 5.3.4.*, while values for α will be approximately equal to the sum of the exponents for ε in the correlations for k_L and a.

The values for these exponents are summarised in the following table:

Table 5.8 *Determining the functional dependence of k_La on energy dissipation and gas flow rate*

Author	α	β
Wu et al. (1998)	0.58 – 0.67	0.56 – 0.70
Bouaifi and Roustan (1998)	0.50	0.60
Meister et al. (1979)	0.80	0.25
Lopes de Figueiredo et al. (1979)	0.58	0.75
Van't Riet et al. (1979)	0.4	0.5

Despite very divergent values for α and β, average values of 0.6 and 0.5 – 0.6 can be assumed for the respective parameters against which experimentally determined exponents can be evaluated. *Table 5.9* provides a summary of the correlations obtained for the different reactors:

Table 5.9 *Correlation of experimental k_La data against energy dissipation and gas flow rate.*

Reactor configuration	Correlation
Kite-shaped reactor	$k_La = 2166\varepsilon^{0.36}Q_g^{1.18}$
π-shaped reactor	$k_La = 818\varepsilon^{0.32}Q_g^{1.07}$
σ-shaped reactor	$k_La = 1303\varepsilon^{0.32}Q_g^{1.07}$

Analogous to the case of interfacial area, it can once again be seen that values obtained for α (0.32 – 0.36) fall neatly into the range of values found in the literature, although slightly lower than the average value. Again it can also be seen that, with regard to the effect of gas flow rate, experimental values of β are much higher (almost double) than those reported in the literature.

Therefore, the same conclusions made as in the case of interfacial area, can be applied here: the k_La-correlations obtained from experimental data compare very well with those presented in the literature, establishing that trends exhibited in the investigated reactors are consistent those presented in the literature. Also, as mentioned in *section 5.3.4*, the very high experimetal β-values seem to suggest that reactor performance can be improved upon by operating the reactors at higher gas loadings, since an increase in gas flow rate increases the rate of increase in the interfacial area.

5.5 CONCLUSIONS

The objective of this investigation, as summarised in its title, was the development and modelling of high intensity impinging stream reactors for enhanced mass transfer. In this chapter, the results obtained from experiments were presented and discussed, and compared with data from the literature to determine to which extent the developed reactors provided enhanced mass transfer performance. Empirical modelling of these results were also done to promote understanding of the influence of operating parameters on the efficiency of the reactors. The most significant conclusions made during this investigation are summarised in terms of the following three mass transfer parameters.

Mass transfer coefficient

Contrary to the conclusion made by *Botes et al.* (1998) that the value of the mass transfer coefficient is relatively independent of the liquid and gas flow rates, it was found that both these variables have a significant effect on this parameter. This is due simply to an increase in energy dissipation rate with an increase in each of these flow rates. Comparison of the values of k_L exhibited by each of the three reactor configurations investigated showed that the mass transfer coefficient could be enhanced substantially by centrifugal acceleration of the fluid and more efficient promotion of turbulence in the round reactor chambers of the π- and σ-shaped reactor, compared to the kite-shaped reactor. It was also concluded that the head-on impingement effect employed in the π- and σ-shaped reactors was more efficient than the shearing off of bubbles from gas nozzles (as proposed by *Botes*), leading to higher surface renewal rates and higher mass transfer coefficients. Finally, it was found that experimental k_L values compared very well with values exhibited by other impinging stream reactors and conventional contacting equipment.

Interfacial area

Comparison of the interfacial areas produced in the different reactors showed that the kite-shaped reactor yielded the highest values of this parameter for a fixed energy dissipation rate. From this it could be concluded that the

jagged/angular reactor chamber design provided for more efficient break-up of bubbles, due to collisions of the two-phase fluid with the reactor walls. In addition to this the random flow patterns exhibited in this reactor resulted in higher relative hold-up of gas compared to the π- and σ-shaped reactors, resulting in larger interfacial areas. Comparison of experimental results with literature data also showed that the newly developed jet reactors provided significantly higher degrees of interfacial area production than obtained in conventional equipment, even the impinging jet absorbers proposed by *Herskowits et al.* (1990).

Volumetric mass transfer coefficient

Owing to its ability to exhibit high values of the mass transfer coefficient compared to the other two reactors (via the mechanisms discussed above), the σ-shaped reactor proved to exhibit the highest values of k_La. However, it was found that, despite its relatively lower k_L-values, the kite-shaped reactor outperformed the π-shaped reactor due its ability to create high levels of interfacial area. From these results it could be concluded that an optimum reactor design would combine the k_L-enhancing effects of the swirling flow in the σ-shaped reactor, with the bubble break-up and gas hold-up ability of the kite-shaped reactor.

Finally, by comparing correlations determined from experimental data with those published in the literature, it could be concluded that the trends exhibited by the various experimental reactors were consistent with those presented in the literature. It could, however, be seen from the relatively high exponents of the gas flow rates in these correlations that the potential exists to improve reactor performance even further by operating the reactors at higher gas loadings since an increase in gas flow rate increases the rate of increase in the interfacial area and therefore also k_La.

Based on all the above considerations it could therefore be concluded that the newly developed impinging stream reactors exhibit the potential to enhance mass transfer significantly.

CHAPTER 6

IMPROVEMENT AND EVALUATION OF A FUNDAMENTAL MODEL FOR THE PREDICTION OF THE INTERFACIAL AREA IN HIGH INTENSITY REACTORS

In industrial practice, conventional modelling and design theories have relied heavily on empirical correlations. Although some of them are reasonably sound, most of these methods cannot be confidently applied beyond the narrow range of operating conditions and geometries over which they were determined. Little understanding of the physical processes occurring in the reactors are also obtained. However, with the advent of fast and effective computing power, researchers have increasingly begun to employ theoretical models such as population balances and Monte Carlo simulations for describing and predicting process behaviour in gas-liquid contactors. By characterising the dispersion properties (bubble size distribution and bubble interaction rates) in these reactors, better understanding of these systems has been facilitated.

In view of the above, further development of a basic fundamental model for the prediction of the interfacial area in the jet reactors (*Botes*, 1995) was performed. This chapter will focus on the development of this model, and evaluation thereof against experimental data.

6.1 MODEL DEVELOPMENT

Analogous to many other conventional gas-liquid contactors (bubble columns, ejector reactors, jet loop reactors etc.), the reactors in this investigation were operated in the so-called *bubble regime*, where gas bubbles exist in a continuous liquid phase. Thus the interfacial area produced in the reactors can simply be determined from the combined surface area of these bubbles.

The sizes (and distribution of sizes) of these bubbles are determined by a balance between the rates of bubble coalescence and bubble break-up, which in turn is governed by the interactions of turbulent eddies. The following sections will focus on how these mechanisms have been combined into a fundamental model for the prediction of the bubble size distribution in the form of a Monte Carlo simulation, using Kolmogoroff's theory of isotropic turbulence (as discussed in *Chapter 2*).

This bubble size distribution was predicted by accounting for the size of the bubbles entering the reactor, the size of bubbles in the reactor and the size of the bubbles exiting the reactor. The size of bubbles in the reactor was determined as functions of bubble break-up and coalescence rates.

6.1.1 The size of bubbles entering the reactor

Since gas was fed into the reactors through nozzles, an expression for the bubble size at such a gas orifice needed to be obtained. Since no literature on the formation of bubbles under turbulent conditions could be found, *Botes* (1995) surveyed the literature on bubble formation in liquid cross flow. However, publications on this subject presented rather complex models that were only applicable to a clearly defined flow field. In view of this, it was decided to use the following simple statistical correlation presented by *Marshall et al.* (1993) for the approximation of the bubble size at a gas orifice:

$$r_b = 0.48 r_o^{0.826} \left(\frac{u_{G,o}}{u_L} \right)^{0.36} \qquad \ldots (6.1)$$

where the superficial orifice gas velocity is defined as:

$$u_{G,o} = \frac{\dot{V}_G}{\pi r_o^{\,2}} \qquad \ldots (6.2)$$

Adapting the numerical coefficient for non-perfect cross flow and incorporating with it the r_o term (since only one type of gas nozzle was used during the experiments), *equation (6.1)* could be simplified to yield the following:

$$r_b = K\left(\frac{\dot{V}_G}{u_L}\right)^{0.36} \quad \ldots (6.3)$$

Since it is very difficult to estimate the flow velocity of the liquid past the gas nozzle orifice, it was assumed that this velocity is directly proportional to the volumetric flow rate of the liquid into the reactor, so that the final form of *equations (6.2)* and *(6.3)* could be given as:

$$d_{b,i} = K_f\left(\frac{\dot{V}_G}{\dot{V}_L}\right)^{0.36} \quad \ldots (6.4)$$

where K_f is a free parameter and has to be specified externally when the model is applied. This compares well with the following equations proposed by *Bhavaraju et al.* (1978) and *Davidson and Schuler* (1960), respectively:

$$d_{b,i} = C\dot{V}_G^{1/3} \quad \ldots (6.5)$$

and

$$d_{b,i} = 1.11\left(\frac{\dot{V}_G^{\,2}}{g}\right)^{1/5} \quad \ldots (6.6)$$

However, careful examination of the role of this equation in the existing model prompted its replacement in the improved model during this investigation. Since it was determined that bubble coalescence did not occur in the highly turbulent environment of the reactors (this will be discussed in a later section),

the maximum possible bubble size would be this entering bubble size. Therefore, this equation not only needed to approximate the entering bubble size but, more importantly, also determine the maximum stable bubble size in the reactor for specific hydrodynamic conditions. Considering that experimental results showed a decrease in the average bubble size with an increase in gas flow rate, which is contradictory to the trend predicted by *equation (6.4)*, and taking into account that the final bubble size distribution is very sensitive to the maximum stable bubble size, it was decided to rather determine the maximum stable bubble size more accurately via an equation employing the energy dissipation rate in the reactor. A study of the literature yielded the following expression, proposed by *Walter and Blanch* (1986) who modelled bubble break-up in gas-liquid bioreactors:

$$d_{b,\max} = 1.12 \frac{\sigma^{0.6}}{\varepsilon^{0.4} \rho^{0.2}} \left(\frac{\mu_e}{3\mu_g} \right)^{0.1} \quad \ldots (6.7)$$

Since the meaning of μ_e in the viscosity correction term in this equation was described very vaguely, the literature was scrutinised further to find an alternative to this term. The following equation supplied by *Lee* and *Tsui* (1999) provided for this:

$$d_b = C \frac{\sigma^{0.6}}{\varepsilon^{0.4} \rho^{0.2}} \left(\frac{\mu_G}{\mu_L} \right)^{0.25} \quad \ldots (6.8)$$

Therefore, combining these two equations, the following equation was obtained which was used in the model for determination of the maximum stable bubble size:

$$d_{b,\max} = K_m \frac{\sigma^{0.6}}{\varepsilon^{0.4} \rho^{0.2}} \left(\frac{\mu_G}{\mu_L} \right)^{0.25} \quad \ldots (6.9)$$

where, as in the previous equation, K_m is a free parameter which has to be specified externally. This parameter replaces K_f in the original model.

Note that this equation is derived from Kolmogoroff's theory of isotropic turbulence. Since the most basic assumption of the proposed model implies homogeneous isotropic turbulence, it was believed that this equation would predict trends in the maximum bubble sizes accurately.

6.1.2 Bubble break-up rates

It has been stated that bubble break-up occurs through interactions with turbulent eddies, since bubbles and eddies collide with each other due to their movement in a turbulent system. If the concerned eddy contains sufficient energy, the bubble will break up. As has been shown in *Chapter 2*, expressions for bubble break-up rates always consist of two parts: firstly, an expression will de derived for the collision rate between bubbles and eddies of respective arbitrary diameters, and secondly, an expression for the collision efficiency will be derived to evaluate whether a particular collision results in bubble break-up.

The following sections will discuss the model proposed by *Coulaloglou and Tavlarides* (1977), as used by *Botes* (1995) and in this investigation. Thereafter, two modern breakage rate models proposed by *Hesketh et al.* (1991) and *Luo* and *Svendsen* (1996) for verification of and comparison with this model will briefly be discussed.

6.1.2.1 The collision rate between bubbles and eddies

In accordance with the assumptions usually employed in models of this sort, as discussed in *Chapter 2*, is it accepted that turbulence is homogeneous and isotropic and that the eddies responsible for bubble break-up are all in the inertial subrange. Even if turbulence is not strictly isotropic, the assumption is still reasonable if isotropy exists at the length scale of the involved eddies. Indeed, isotropic turbulence theory has been applied with high degrees of success for the modelling of bubble columns, where macroscale turbulence is far from isotropic.

According to *Coulaloglou and Tavlarides*, the mechanism of collision between bubbles and eddies can be modelled analogous to the mechanism of particle collision in an ideal gas (*Kennard*, 1938). Under this assumption, the collision rate between bubbles (*b*) of size *d* and eddies (*e*) of size λ can be expressed as:

$$\theta_{b,e} = n_b n_e S_{b,e} \left(\overline{u_b^2} + \overline{u_e^2} \right)^{1/2} \quad \ldots (6.10)$$

where n_b and n_e refer to the respective concentrations of involved bubbles and eddies and $S_{b,e}$ is the collision cross-sectional area which is defined by:

$$S_{b,e} = \frac{\pi}{4}(r_b + r_e)^2 \quad \ldots (6.11)$$

The velocity of the bubbles and eddies can be determined from the following expression for the average of the square of the velocity fluctuations in a turbulent system, given by *Hinze* (1955), using the concerned bubble and eddy diameters, respectively:

$$\overline{u^2} = 2\varepsilon^{2/3} d^{2/3} \quad \ldots (6.12)$$

By substituting *equations (6.11)* and *(6.12)* into *equation (6.10)* and rearranging, the following expression for the collision rate between bubbles and eddies as a function of their respective concentrations and diameters and the energy dissipation rate, is obtained:

$$\theta_{b,e} = \frac{\pi}{8\sqrt{2}} \varepsilon^{1/3} n_b n_e (d + \lambda)^2 \left(d^{2/3} + \lambda^{2/3} \right)^{1/2} \quad \ldots (6.13)$$

The concentration of eddies, belonging to a certain size interval, can be calculated using the following relationships, where *E(k)* is the energy density function and *N(k)* is defined as the number of eddies, per unit mass of liquid, with wavelengths between *k* and (*k* + *dk*):

$$E(k) = \alpha\varepsilon^{2/3}k^{-5/3} \quad \ldots (6.14)$$

and

$$E(k) = e.N(k) \quad \ldots (6.15)$$

where the kinetic energy of one eddy, *e*, as equal to:

$$e = \frac{1}{2}\left(\frac{1}{6}\pi\lambda^3\rho_L\right)\overline{u^2} \quad \ldots (6.16)$$

and recalling that $\lambda = 2k^{-1}$, an expression for *N(k)* can be obtained by equating *equations (6.14)* and *(6.15)*:

$$\alpha\varepsilon^{2/3}k^{-5/3} = N(k)\frac{2\pi\rho_L\overline{u^2}}{3k^3} \quad \ldots (6.17)$$

to yield the following, using the correct values for all the above constants (*Azbel*, 1981):

$$N(k) = 0.1\frac{k^2}{\rho_L} \quad \ldots (6.18)$$

For a given eddy diameter interval with boundaries λ_{low} and λ_{high}, and corresponding wavenumbers k_2 and k_1, this equation can be multiplied by the density of the liquid and integrated over the span of the interval to yield the number of eddies per unit volume of liquid, n_e, in *equation (6.13)*:

$$n_e = \rho_L\int_{k_1}^{k_2}0.1\frac{k^2}{\rho_L}dk = 0.1\left(k_2^{\,3} - k_1^{\,3}\right) \quad \ldots (6.19)$$

or

$$n_e = \frac{0.8}{3}\left(\lambda_{low}^{-3} - \lambda_{high}^{-3}\right) \quad \ldots (6.20)$$

Finally this value is multiplied by the ratio of the liquid hold-up to the reactor volume (to convert it to the number of eddies per unit reactor volume) before substitution into *equation (6.13)*.

6.1.2.2 The collision efficiency between bubbles and eddies

All the above collisions are, however, not effective and only a certain amount of them are likely to result in bubble break-up. To determine whether break-up will occur, the energy of the eddy is compared to the surface tension forces of the bubble: the disruptive hydrodynamic stress on the bubble surface is a result of the dynamic pressure ($\rho_L u^2$) of the liquid while the surface tension force per unit area (σ/d), tends to stabilise the bubble. The balance of these disruptive and cohesive forces is generally expressed in terms of the dimensionless Weber number, as described in *Chapter 2*:

$$We = \frac{u^2 d \rho_L}{\sigma} \quad \ldots (6.21)$$

As the turbulent velocity fluctuations of the liquid increase (with an increase in the energy dissipation rate), this Weber number increases until it reaches a critical value above which bubble break-up will occur. This is represented by the following equation:

$$We_{crit} = \frac{u_c^{\,2} d \rho_L}{\sigma} = K \quad \ldots (6.22)$$

where K is an arbitrary constant. Rearranging this equation, the critical velocity needed to rupture a bubble, referred to as the critical velocity, can be solved for:

$$u_c^{\,2} = K\left(\frac{\sigma}{\rho_L d}\right) \qquad \ldots (6.23)$$

Providing for viscosity effects as proposed by *Walter and Blanch* (1986), analogous to the expression for the maximum stable bubble diameter, the critical velocity can finally be determined from the following:

$$u_c^{\,2} = K_e\left(\frac{\sigma}{\rho_L d}\right)\left(\frac{\mu_L}{\mu_G}\right)^{1/6} \qquad \ldots (6.24)$$

where K_e, as in the case of K_f and K_m, is a free parameter which has to be specified externally when the model is applied.

Knowledge of this critical velocity is very important, since the fraction of collisions between bubbles and eddies of respective sizes that result in bubble break-up, is assumed to be equal to the fraction of eddies with velocities in excess of the critical velocity. To determine this fraction a function describing energy distribution amongst eddies of the same diameter, is needed. If one assumes a random distribution of energy amongst eddies of the same diameter, the following energy density function proposed by *Angelidou et al.* (1979) can be used:

$$\chi(E_e) = \frac{1}{\overline{E_e}}\exp\left(\frac{-E_e}{\overline{E_e}}\right) \qquad \ldots (6.25)$$

where E_e is the kinetic energy of a particular eddy and $\overline{E_e}$ is the average energy of the eddies of a certain diameter. If E_c denotes the critical energy needed to rupture a bubble, the fraction of eddies with energy in excess of E_c will be:

$$Y = \frac{\int_{E_c}^{\infty} \chi(E_e)dE}{\int_{0}^{\infty} \chi(E_e)dE} = \exp\left(-\frac{E_c}{\overline{E}}\right) \quad \ldots (6.26)$$

Taking the energy of an eddy as proportional to the square of its velocity yields a function of the following form for the fraction of eddies with sufficient energy to cause bubble rupture (*Coulaloglou* and *Tavlarides*, 1977):

$$Y = \exp\left(-\frac{u_c^{\,2}}{\overline{u_e^{\,2}}}\right) \quad \ldots (6.27)$$

where $\overline{u_e^{\,2}}$ can be determined via *equation (6.12)*. *Equation (6.27)* therefore represents the expression for the bubble breakage efficiency.

6.1.2.3 Bubble breakage rate equations

Combining the final expressions for the eddy-bubble collisions rates and collision efficiencies derived above, the following bubble breakage rate equation, according to *Coulaloglou and Tavlarides* (1977) was obtained:

$$\Omega_{b,e}(d,\lambda) = K_e \frac{\pi}{8\sqrt{2}} \varepsilon^{1/3} n_b n_e (d+\lambda)^2 \left(d^{2/3} + \lambda^{2/3}\right)^{1/2} \exp\left(-\frac{u_c^{\,2}}{\overline{u_e^{\,2}}}\right) \quad \ldots (6.28)$$

As mentioned in *section 6.1.2*, two additional breakage rate equations were also applied in the model for the purpose of comparison and verification of results obtained via the above equation.

Luo and *Svendsen* (1996) proposed a bubble break-up model analogous to that of *Coulaloglou* and *Tavlarides* (1977), assuming that the arrival frequency of eddies on the surface of bubbles, is equivalent to the collision frequency between the same eddies and fluid particles. Since the motion of eddies is

generally considered random, the following equation for this collision frequency is obtained:

$$\theta_{b,e}(d) = \frac{\pi}{4}(d+\lambda)^2 \overline{u_e} \dot{n}_e n_b \qquad \ldots (6.29)$$

In this case the mean turbulent velocity ($\overline{u_e}$) of eddies with size λ was determined using an expression supplied by *Kuboi et al.* (1972):

$$\overline{u_e} = \left(\frac{8\overline{u^2}}{3\pi}\right)^{1/2} = \left(\frac{8\tilde{\beta}}{3\pi}\right)^{1/2} (\varepsilon\lambda)^{1/3} = \beta^{1/2}(\varepsilon\lambda)^{1/3} \qquad \ldots (6.30)$$

where the constant, $\tilde{\beta}$ = *(3/5)Γ(1/3)*α. Here, α is considered to be a universal constant, as given by *Batchelor* (1982), based on turbulence theory. The measured value of $\tilde{\beta}$ is 2.0, according to *Kuboi et al.* (1972).

Analogous to the approach followed by *Coulaloglou and Tavlarides* (1977), the concentration of eddies was determined via the expression for the energy density function, *E(k)*:

$$\dot{n}_e \rho_c \frac{\pi}{6}\lambda^3 \frac{\overline{u_e^2}}{2} d\lambda = E(k)\rho_c(1-\phi)(-dk) \qquad \ldots (6.31)$$

Substituting the well known *equation (6.14)* into this equation and taking $k = 2\pi/\lambda$, the number of eddies of size λ and (λ + dλ) per unit reactor volume, or number density of eddies, is given by:

$$\dot{n}_e = \frac{c_3(1-\phi)}{\lambda^4} \qquad \ldots (6.32)$$

where

$$c_3 = \frac{9\alpha}{2(2\pi)^{2/3}\widetilde{\beta}} = \frac{15}{2(2\pi)^{2/3}\Gamma(1/3)} \approx 0.822 \quad \ldots (6.33)$$

Consequently, the bubble-eddy collision frequency between eddies of size λ and bubbles of size d, can be expressed as:

$$\theta_{b,e}(d) = c_4 (d+\lambda)^2 n_b \varepsilon^{1/3} \frac{(1-\phi)}{\lambda^{11/3}} \quad \ldots (6.34)$$

Using the same approach as that followed by *Coulaloglou and Tavlarides* (1977) for evaluating the collision efficiency, the expression for the bubble break-up rate could be written as:

$$\Omega_{b,e}(d) = K_e (d+\lambda)^2 n_b \varepsilon^{1/3} \frac{(1-\phi)}{\lambda^{11/3}} \exp\left(-\frac{u_c^{\,2}}{u_e^{\,2}}\right) \quad \ldots (6.35)$$

Note that this expression is very similar to that of *Coulaloglou and Tavlarides*, keeping in mind that the eddy concentration term is contained implicitly.

Hesketh et al. (1991) combined the natural oscillation mode of a sphere given by *Lamb* (1932) and a correlation for the maximum stable drop size in a stirred tank, and obtained the following bubble breakage rate:

$$\Omega_{b,e}(d) = 2.7 n_b \left(\frac{\rho_c^{\,0.1} \rho_d^{\,0.3} \varepsilon^{0.6}}{\sigma^{0.4}}\right) \quad \ldots (6.36)$$

Since it was assumed that the hydrodynamic and physicochemical parameters such as densities and surface tension did not vary significantly during application of the model, this model could be simplified even further to yield the following:

$$\Omega_{b,e}(d) = K_e n_b \varepsilon^{0.6} \quad \ldots (6.37)$$

where K_e once again needs to be specified externally during model application. Note that this model is the only one in which the exponent of the energy dissipation term is 0.6 and not 1/3.

Although this model proved to be highly empirical, it was applied due to its sheer simplicity, since it only considers the properties of the bubbles and does not take into account those of the bombarding eddies. If it could be shown that a simple expression such as *equation (6.30)* yielded results of comparable accuracy to those determined via the complex *equation (6.28)*, potential savings in simulation time could be realised.

6.1.3 Bubble coalescence rates

The effect of electrolytes on bubble coalescence is discussed by *Craig et al.* (1993). In these publications, it is stated that certain electrolytes have an inhibiting effect on bubble coalescence to such an extent that, above a certain transition concentration, the electrolytes stabilise the bubbles completely, effectively eliminating bubble coalescence. Since it was found that the sodium hydroxide concentrations used during the experimental runs always exceeded these so-called critical concentrations, it was assumed that no bubble coalescence took place and was therefore disregarded by the model.

However, it was decided to incorporate bubble coalescence into the model during the course of this investigation, since the purpose of development of the model was to provide a general tool for the prediction of the interfacial area in any gas-liquid system. Due to the fact that bubble coalescence was found not to occur in the jet reactors (see *section 6.3*), derivation of the expressions relating to bubble collision rate and coalescence efficiency will only be discussed briefly.

6.1.3.1 The collision rate between two bubbles

The expression for the collision rate between two approaching bubbles is analogous to that of the collision rate between a bubble and an eddy (*equation 6.13*), as proposed by *Coulaloglou* and *Tavlarides* (1977). In this case the respective eddy diameter and concentration is simply replaced by that of the second bubble:

$$\theta_{b_1,b_2} = \frac{\pi}{8\sqrt{2}} n_{d_1} n_{d_2} (d_1 + d_2)^2 \varepsilon^{1/3} \left(d_1^{2/3} + d_2^{2/3} \right)^{1/2} \quad \ldots (6.38)$$

6.1.3.2 The coalescence efficiency between two bubbles

As in the case of bubble break-up, only a fraction of bubble-bubble collisions will lead to coalescence events. To determine this coalescence efficiency, the following expression of *Coulaloglou* and *Tavlarides* (1977) is used:

$$Y = \exp\left(-\frac{t_{12}}{\tau_{12}} \right) \quad \ldots (6.39)$$

where t_{12} is the time required for coalescence of bubbles, while τ_{12} is the contact time between the two bubbles.

Coalescence of two bubbles in turbulent flow occurs in three steps. First, bubbles collide, trapping a small amount of liquid between them. This liquid then drains until the liquid film separating the bubbles reaches a critical thickness. At this point, film rupture occurs, resulting in coalescence. In view of this, the bubble coalescence time (t_{12}) can be regarded as the time needed for this liquid disc to thin to a critical thickness and is given by:

$$t_{12} = \left(\frac{r_{12}^{\,3} \rho_L}{16\sigma} \right)^{1/2} \ln \frac{h_o}{h_f} \quad \ldots (6.40)$$

Here h_o is the initial film thickness and h_f the critical film thickness where rupture occurs. Values of these parameters are typically $1x10^{-4}$ *m* and $1x10^{-8}$ *m*, as given by *Kirkpatrick* and *Locket* (1974) and *Kim* and *Lee* (1987), respectively. The equivalent bubble size (r_{12}), used to account for unequal bubble sizes, is given by *Chesters* and *Hoffman* (1982):

$$r_{12} = \frac{1}{2}\left(\frac{1}{r_1} + \frac{1}{r_2}\right)^{-1} \quad \ldots (6.41)$$

The contact time between two bubbles, on the other hand, is dependent on the bubble size and the energy dissipation rate. *Levich* (1962) provides an estimate of the contact time in turbulent flows:

$$\tau_{12} = \frac{r_b^{2/3}}{\varepsilon^{1/3}} \quad \ldots (6.42)$$

Since this equation was derived solely from dimensional considerations, the choice of the characteristic length denoted by r_b can be considered to be an adjustable variable, representative of the average bubble size in the reactor. In the application of the model this parameter is denoted as K_r : as is the case for the free parameter K_e, K_r has to be specified externally when the model is applied.

6.1.4 Bubbles exiting the reactor

To maintain steady state conditions and constant gas hold-up in the reactor, the model naturally also had to account for the bubbles exiting the reactor. In accordance with the assumption of an ideal mixed tank reactor, every bubble in the reactor has an equal chance of leaving the reactor, since it is assumed that they are distributed homogeneously through the reactor volume.

Therefore, bubbles were chosen to leave the reactor according to their weighted probability, which was calculated as the number of bubbles in that

class divided by the total number of bubbles in the reactor. The number of bubbles in the chosen bubble class was then reduced by one and the total volume of the bubbles re-calculated:

$$V_{total} = \sum_{b=1}^{50} \left(\frac{\pi}{6} d_b^{\,3} n_b \right) \qquad \ldots (6.43)$$

where d_b and n_b refer to the average bubble size and concentration per bubble class. If the combined volume of these bubbles was greater than the specified gas hold-up, another bubble was chosen to leave the reactor. This process was repeated until the total bubble volume approximated the gas hold-up.

6.2 MODEL IMPLEMENTATION

In *Chapter 2* the advantages associated with the modelling of dispersed phase properties via population balances and Monte Carlo simulations were described. Due to their inherent flexible and fundamental nature, this approach has also been followed in the modelling of the interfacial area through prediction of the bubble size distribution. Since the implementation of this model depends strongly on the generation of random numbers to satisfy calculated probability functions, it is in essence a Monte Carlo simulation. Since the source code of the original model proposed by *Botes* (1995) was compiled in *Turbo Pascal*, it was run in a 16-bit *Delphi*-environment during this investigation for faster processing of results.

In this computer program the values of the parameters required by the simulation are firstly specified or calculated. The respective bubble and eddy size distributions are then discretised, after which the actual simulation is executed and repeated to yield a stable value for the interfacial area. These aspects of the model implementation will be addressed in the following sections.

6.2.1 Declaration and calculation of the input parameters

As is the case with any model, certain parameters need to be fixed beforehand to specify the range of operating conditions for which prediction of data is required. Generally these include hydrodynamic, physicochemical and other free parameters. Hydrodynamic properties to be specified were the volumetric flow rates of the gas and liquid streams, as well as the pressures of these streams for calculation of energy dissipation rates (to be discussed later). The reactor volume also needed to be specified.

Physicochemical properties specified were the respective dynamic viscosities of the gas and liquid, as well as the surface tension and density of the liquid. Since the experimental runs were generally conducted at temperatures in the region of 25°C, all these properties were evaluated at the same temperature for optimum correlation of data. Typically the density of the liquid was assumed to be equal to that of water. This was taken as a reasonable approximation since these values differed by less than 5% from one another. However, the liquid viscosities and surface tensions of the respective sodium hydroxide and sodium sulphite solutions were specified accurately (from literature sources), since the values of these parameters differed quite substantially from one another and distilled water (> 25%) and had a significant impact on the output of the model (especially in terms of bubble break-up efficiencies: ref. *equation (6.24)*). This represented a significant improvement over the original model proposed by *Botes* (1995).

Three free parameters also had to be specified. K_m, the parameter replacing K_f in the original model, was needed for the determination of the maximum stable bubble size (i.e. bubbles entering the reactor through gas orifices), while K_e provided for the estimation of the critical amount of energy needed to rupture a bubble, i.e. estimation of the bubble break-up efficiency. K_r, analogous to K_e, was needed for the estimation of the bubble coalescence efficiency. Since it is virtually impossible to estimate these parameters theoretically, they were treated as free parameters in the model which could be adjusted for optimum correlation of experimental and model data.

However, all these values must be considered as universal constants, since they define fundamental phenomena taking place in any reactor, regardless of its geometry or volume. Therefore, the values of the three free parameters were kept constant for simulation of the three different reactor designs investigated. In addition to parameters such as these which could simply be specified in the model as above, others needed to be calculated before execution thereof. These included the gas hold-up, energy dissipation rate and pressure in the reactor.

As mentioned in the discussion of results, it is necessary to know what the gas hold-up in the reactor is to be able to determine the energy dissipation rate per unit mass of liquid. Since an excess of gas was fed to the reactor, only a small fraction of this was absorbed so that it could be assumed that the gas hold-up in the reactor remained constant. This was determined by *Botes* (1995) via the following equation:

$$V_G = \phi V_R = \left(\frac{\dot{V}_G}{\dot{V}_G + \dot{V}_L} \right) V_R \qquad \ldots (6.44)$$

However, this equation yielded highly inaccurate results of the gas hold-up since it can only be applied for the mixing of non-compressible fluids: typically values for ϕ_g of approximately 0.9 were obtained, compared to experimentally determined values of 0.3 – 0.5. In view of this, gas hold-ups were rather specified according to experimentally determined values in the improved model, and not calculated.

Arguably the most important parameter of the simulation, the energy dissipation rate per unit mass of liquid in the reactor, could now be determined. Analogous to the approach followed by *Tamir* (1994), the rate at which the liquid stream transports energy to the reactor via the nozzle was calculated as follows:

$$\dot{E} = (P_L - P_R)\dot{V}_L \qquad \ldots (6.45)$$

where $(P_L - P_R)$ is the difference between the liquid pressure in the feed line and the pressure inside the reactor. Since it was determined by *Botes* (using the Bernoulli equation) that the pressure inside the reactor did not deviate by more than 10% from atmospheric pressure, it was assumed the term P_R could always taken as atmospheric in the model (this will be validated during the sensitivity analysis in the next section). The energy dissipation rate, as used in the model, could then simply be determined from the following equation:

$$\varepsilon = \frac{\dot{E}}{\rho_L V_L} \qquad \ldots (6.46)$$

6.2.2 Discretisation of bubble and eddy size distributions

The use of any population balance model or Monte Carlo simulation necessitates the discretisation of bubble and eddy size distributions. Therefore, bubble sizes were divided into 50 classes of equal size, stretching from a maximum size as determined by *equation (6.9)* to a minimum size arbitrarily chosen as 0.1 mm. The midpoint of each interval was chosen as the representative bubble diameter of that class.

The range of eddy sizes stretched from the largest bubble diameter to one tenth of the diameter of the smallest bubble (chosen arbitrarily). As mentioned previously in *Chapter 2*, during the discussion of Kolmogoroff's theory of isotropic turbulence, eddies with diameters above this range would simply transport the bubbles rather than rupture them, whereas eddies with sizes below this range would not have sufficient energy to rupture any of the bubbles in the reactor. Here it is interesting to note that an eddy of diameter 20% of the bubble diameter possesses only 0.5% of the kinetic energy associated with an eddy equivalent to the bubble in size (*Prince* and *Blanch*, 1990). Eddy sizes were divided into 200 equal classes, their midpoint once again representing their respective diameters. The number of eddies in each

of these classes were determined via expressions such as those presented in *equations (6.20)* and *(6.32)*.

The approach outlined above was adopted from the original model of *Botes* (1995).

6.2.3 Specifying the time interval

In contrast to the conventional approach of assigning a simulation time interval, the model utilised its knowledge of the gas hold-up and entering bubble size to calculate a suitable time step, according to the following equation:

$$\Delta t = \frac{n_{b,i}\pi d_{b,i}^3}{6\dot{V}_G} \qquad \ldots (6.47)$$

where $n_{b,i}$ denotes the number of bubbles entering the reactor, usually taken as equal to two since two gas nozzles were used. Care had to be taken in determination of this time step since shorter time intervals would inevitably mimic reality better, but would also result in more calculation cycles before a stable bubble size distribution is obtained. In addition to this, some of the variables calculated during the simulation have to be rounded off to integer values before they are applied in further procedures (e.g. the total number of collisions taking place during one simulation cycle). If the time interval is too short, these variables will have such small values that, rounding them off to the nearest integer, would change their values appreciably.

It was, however, shown by *Botes* (1995) that the final results of the simulation was not significantly influenced by this time interval. This approach was therefore also used in the improved model.

6.2.4 Simulation of interfacial area production

In *section 6.1* it was shown how the bubble size distribution in a jet reactor could be accounted for by considering the processes of bubbles entering the reactor, bubble break-up and coalescence and bubbles leaving the reactor. Although these processes proceed simultaneously in reality, they are decoupled and treated in succession in the model. For each pre-determined time interval (or simulation cycle) these processes are simulated in isolation, after which the bubble size distribution is updated to present a new distribution as basis for the next step in the simulation.

The eddy size distribution was calculated before commencement of the simulation and remained constant throughout the duration thereof. An initial bubble size distribution was also specified: it was taken as all the bubbles entering the reactor, having the size of maximum stable diameter and number equal to the gas hold-up divided by the volume associated with each of these bubbles.

For bubble breakage, a two-dimensional matrix was set up with the number of rows and columns equal to the number of bubble and eddy classes, respectively: each of these matrix elements represented the number of effective collisions between the corresponding bubbles and eddies, calculated according to:

$$N_{b,e} = \Omega_{b,e}(d,\lambda) V_R \Delta t \qquad \ldots (6.48)$$

where $\Omega_{b,e}(d,\lambda)$ is calculated according to the breakage rate models outlined in *section 6.1.2.3*.

After the value of each matrix element had been calculated, the values of all the elements were summed to find the total number of effective collisions, which was rounded off to an integer value. Bubble break-up was then simulated by choosing a bubble class according to its weighted probability,

which was equal to the number of effective collisions involving bubbles of that particular class divided by the total number of effective collisions. Every time a certain class was chosen, the number of bubbles in that class was reduced by one. It was assumed that bubbles break up into two random fractions; the number of bubbles to which these daughter bubbles belonged, were then increased by one.

The approach of summing collisions and using weighted probabilities, was followed to reduce the number of computations per cycle. Since it needed to be determined whether this 'shortcut' was valid, an alternative procedure was written in which bubble break-up occurred separately in each bubble class, immediately after determination of the number of effective collisions in that class. The uncertainty in using weighted probabilities in determining the amount of bubble break-up events per bubble class was thus eliminated. Although this did indeed increase the simulation time, valuable conclusions could be made from this comparison. These will be discussed in the following section on model evaluation.

Bubble coalescence was treated analogous to bubble break-up, applying the latter approach of coalescing bubbles separately in each class without determining the amount of effective coalescence events beforehand.

Finally, bubbles exiting the reactor were simulated according to the procedure described in *section 6.1.4*.

6.2.5 Repetition of the simulation cycle

After every simulation cycle, the value of the interfacial area was calculated from the bubble size distribution. This value changed rapidly during the first stages of the simulation, where the bubble size shifted towards the lower spectrum of bubble classes, but slowed down as the bubble size distribution neared a stable (equilibrium) value.

Since the interfacial area calculated during the simulation never really converged to a single value, but rather oscillated around a final value, the simulation program employed a fixed number of iterations to yield a final solution, and not a conditional loop as would typically be the case. It was, however, always checked that the allowed amount of iterations exceeded the amount of iterations needed by the simulation to reach a stable value: typically 20 000 iterations were allowed per simulation of one data point. A sample of the output generated by a typical simulation will be shown in the next section to illustrate this point.

6.3 MODEL EVALUATION

In the preceding discussion regarding the development and implementation of the model, improvements on the original model proposed by *Botes* (1995) were highlighted. These changes essentially included the following:

- Accurate specification of the gas hold-up.
- Determination of the maximum stable bubble size via energy dissipation rates.
- Incorporation of bubble coalescence.
- Separate execution of bubble break-up in each class (no lumping).
- Application of two additional bubble breakage rate equations for verification and comparison with the model of *Coulaloglou* and *Tavlarides* (1977).

The first three of these changes will be discussed and their results compared to those obtained by *Botes* (1995). Taking these changes (or alternatives) into account, model and experimental data will then be compared and verified with data generated by the sulphite oxidation system and alternative breakage rate equations from the literature. Finally a sensitivity analysis will be used to identify the most important parameters determining model output – these results will then be used as a basis for conclusions as to the effectiveness of the model.

6.3.1 Evaluation of changes made to the model

6.3.1.1 Gas hold-up

From a sensitivity analysis on his model, *Botes* (1995) concluded that the model output is very much dependent on the value of the gas hold-up. Since it was conceded that the values determined for this parameter in the model were rather inaccurate, the recommendation was made that it be measured experimentally for better prediction of results. Although this was not done during this investigation (no residence time distribution investigations were performed), relatively accurate values of the gas hold-up were obtained through knowledge of the interfacial area and correlations for the average bubble size (as described in *Chapter 5*). As mentioned in *section 6.2*, values for the gas hold-up as functions of the gas flow rate were therefore specified in the improved model, and not calculated. The following graph (plotted at a constant liquid flow rate) illustrates how more accurate values for the gas hold-up result in better prediction of trends in interfacial area.

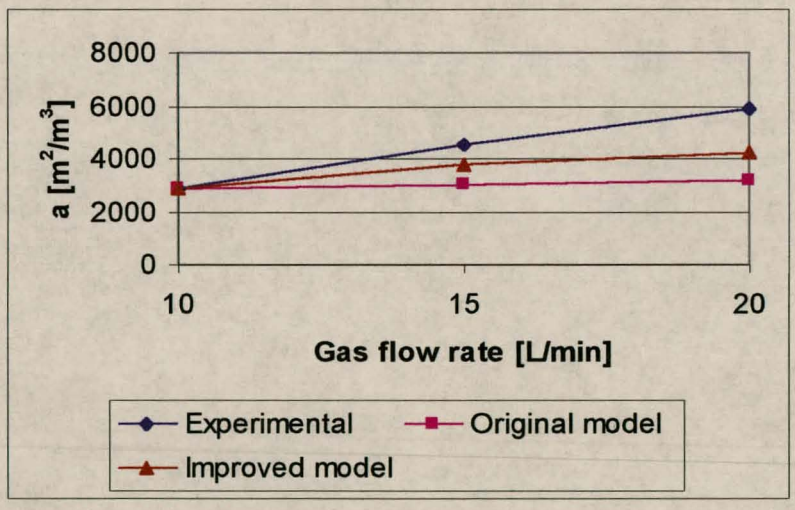

Figure 6.1 *Illustration of the improvement in the model prediction of interfacial area trends with better specification of gas hold-up*

From this graph it can clearly be seen that, in terms of predicted trends in the interfacial area production as a function of gas flow rate (and therefore gas hold-up), the improved model represents a significant improvement over the original. This can be ascribed to the manner in which the gas hold-ups were calculated in the original model via *equation 6.44*. For the range of gas flow rates employed, this equation predicted an increase of only 7% in the gas hold-up (between minimum and maximum flow rates), compared to an experimentally determined value of 33%, due to the dominance of the gas flow rate terms over that of the liquid flow rate term in this particular equation. Therefore, the expected rate of increase in gas hold-up with an increase in gas flow rate was underpredicted, which in turn led to an underprediction of the effect of energy dissipation rate on the interfacial area production.

It could therefore be concluded that specifying the gas hold-up according to experimentally determined values yielded better correlation of model data.

6.3.1.2 Maximum stable bubble size

In *section 6.1.1* it was discussed why the need existed for a more accurate equation for determining the size of bubbles entering the reactor, i.e. the maximum stable bubble size in the reactor. This is illustrated effectively in *Figure 6.2*.

Once again it can be seen that the improved model predicts trends in the maximum stable bubble diameter as a function of gas flow rate much better than the original. Indeed, it can be seen that the original model predicts exactly opposite trends to what are expected. This is once again due to the functional form of *equation (6.4)* which predicts an increase in bubble size with an increase in gas flow. Although this is certainly the case for bubble formation from sparger holes or nozzles, it is certainly not representative of bubble behaviour in a turbulent environment. Therefore, *equation (6.9)* presents a better alternative, since the value of the maximum stable bubble size has a significant effect on the bubble size distribution and average bubble size.

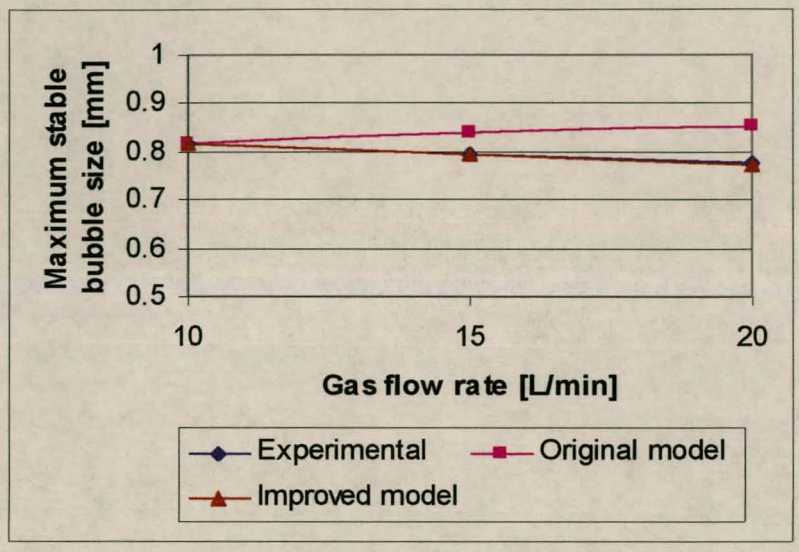

Figure 6.2 *Comparison of predicted trends in the maximum stable bubble diameter*

6.3.1.3 Bubble coalescence

Although it could be assumed with reasonable certainty that bubble coalescence did not occur for the chemical systems employed in this investigation (see *section 6.1.3*), bubble coalescence was incorporated into the model to allow for general application thereof in any turbulent gas-liquid system. Therefore, if it could be assumed that bubble coalescence would potentially occur in the reactor (for example an air-water system), this procedure was implemented in the simulation and K_r adjusted until bubble coalescence was found to occur.

It was found that bubble coalescence events only occurred at hypothetical *Kr* values greater than approximately 0.1. Considering the fact that *Kr* (or r_b) in *equation (6.42)* represented a characteristic length equal to the length scale of an average bubble diameter, it can be concluded that, even for a non-electrolyte system, bubble coalescence could not occur: bubble sizes of 0.1 *m* (100 *mm*) simply could not be exhibited.

It could therefore be concluded that bubble coalescence could not occur in the reactors for any chemical system, since the contact time between any two bubbles was orders of magnitude smaller (due to the highly turbulent nature of the liquid in the reactor) than the required contact time for film thinning and rupture in the coalescence process. The coalescence procedure in the simulation was therefore ignored in the remaining simulations for faster computation of results.

6.3.2 Comparison between model and experimental data

As described in *sections 6.1* and *6.2* the bubble breakage rate model proposed by *Coulaloglou and Tavlarides* (1977) has primarily been used in the Monte Carlo simulation. The first two sections considering this discussion on the comparison of model and experimental data focuses on this model, whereas the last section will consider comparison thereof with two alternative breakage rate equations presented in *section 6.1*.

6.3.2.1 Summing of bubble breakage events

In *section 6.2.3* it was discussed how the original model proposed by *Botes* (1995) used the technique of summing or lumping effective bubble breakage events and effecting bubble break-up after one complete cycle of the simulation, to reduce the number of computations per cycle. In this investigation this technique was checked by considering bubble break-up as soon as a effective collision event was identified. In other words, bubble break-up and re-calculation of the bubble size distribution took place after every collision in a particular class. These two approaches, designated *A* and *B* respectively, will be used to discuss and evaluate the predictive performance of the improved model.

Figures 6.3 and *6.4* provide a graphic comparison of experimental and predicted data for the π- and σ-shaped and kite-shaped reactors obtained via approach *A*, where the respective gas flow rates of 10, 15 and 20 *L/min* are plotted for every liquid flow rate setting between 16 and 26 *cm* on the rotameter. As has been shown previously (*section 6.3.1.1*), the improved model predicts trends in the gas flow rate well. It can, however, be seen that it overpredicts the influence of the liquid flow rate on the interfacial area produced. This is evident if the two lines corresponding to predicted and experimental values for a constant gas flow rate of 10 *L/min*, are compared: the gradient in the model output data is larger than that exhibited by the experimental data, leading to growing difference (maximum 27%) in values with an increase in liquid flow rate. Yet, despite this discrepancy, it can be noted that, especially for the π- and σ-shaped reactors, the model predicts the range of minimum and maximum values of interfacial area, exceptionally well.

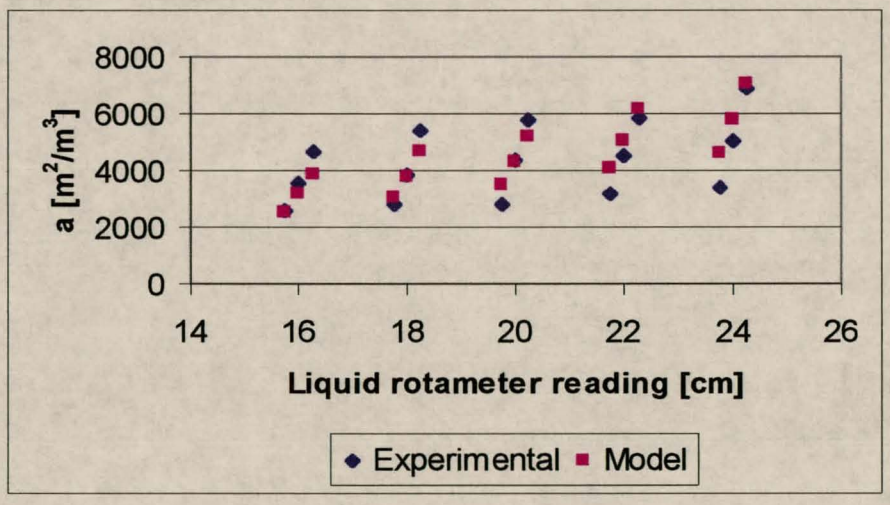

Figure 6.3 *Comparison of model and experimental data (π- and σ-shaped reactors) for summing of bubble breakage events (approach A), where the liquid rotameter readings at 16, 18, 20, 22 and 24 denote flow rates of 1.21, 1.36, 1.54, 1.68 and 1.86 L/min respectively.*

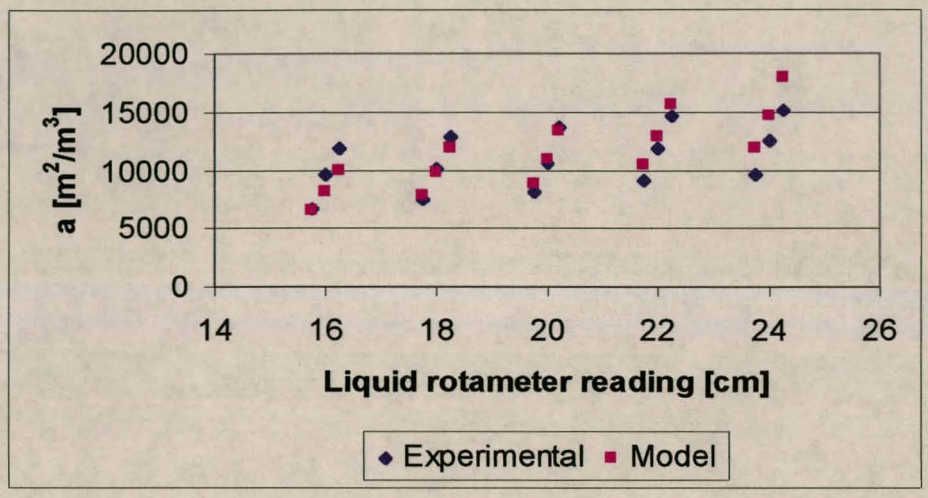

Figure 6.4 *Comparison of model and experimental data (kite-shaped reactor) for summing of bubble breakage events (approach A)*

Making the same comparison using values predicted via approach *B, Figure 6.5* shows that very much opposite trends, in terms of the influence of gas and liquid flow rates on interfacial area, are exhibited. In this case, the effect of gas flow rate is overpredicted, whereas the effect of liquid flow rate on interfacial area production was predicted very well (as seen by comparing predicted and experimental values for a constant gas flow rate of 10 *L/min*). Once again it could be noted that the minimum and maximum values of experimental data were predicted reasonably accurately to within 10%.

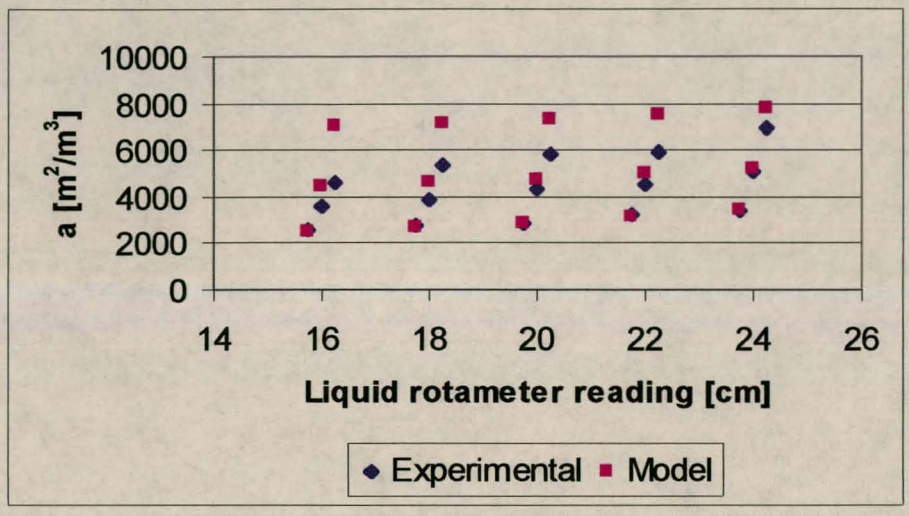

Figure 6.5 *Comparison of model and experimental data for separate bubble breakage events in each class (approach B)*

To provide some degree of insight into these contrasting results, typical bubble size distributions generated by each of these two approaches were investigated. These are shown graphically in *Figures 6.6* and *6.7*.

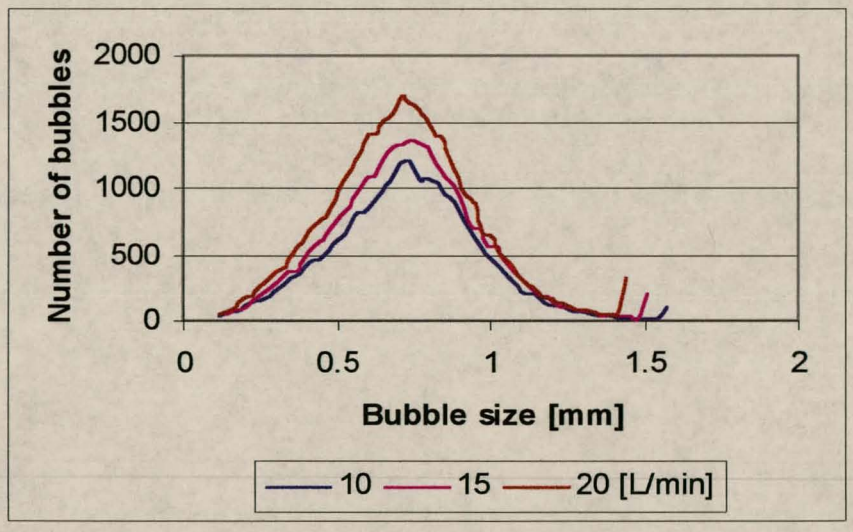

Figure 6.6 *A typical example of a bubble size distribution as a function of the gas flow rate, generated by approach A*

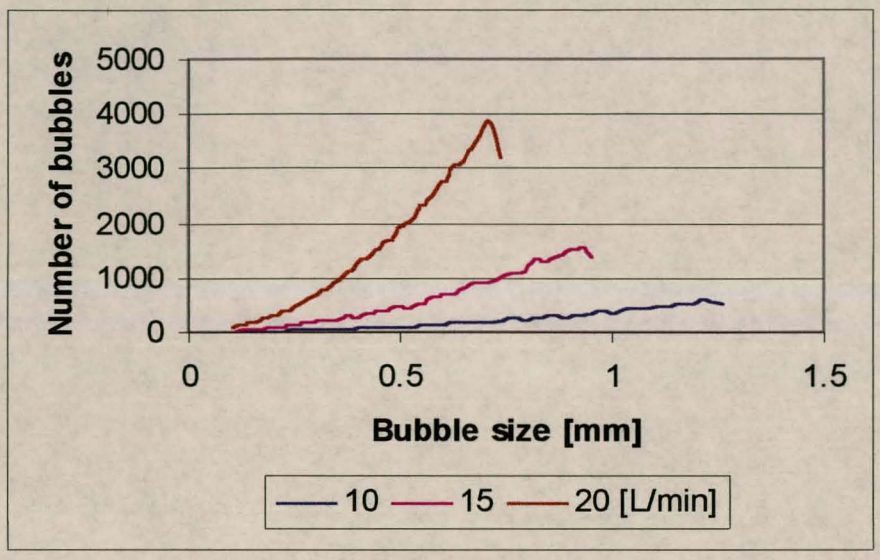

Figure 6.7 *A typical example of a bubble size distribution as a function of the gas flow rate, generated by approach B*

From these graphs a possible explanation for the overprediction of the effect of gas flow rate on interfacial area production via approach *B* can be found. Comparison of *figures 6.6* and *6.7* show that this approach predicts a much faster rate of decrease in the average bubble size with an increase in gas flow rate than that predicted by approach *A*. This is due to the fact that, as shown by the skewness of the bubble size distribution curves in *figure 6.7*, approach *B* tends to result in the continual break-up of the smaller sized bubbles into even smaller sizes, failing to also effectively break up larger sized bubbles. This inevitably results in a higher relative concentration of very small bubbles, as can be seen by comparing the values of the y-axes in each of the two graphs. Therefore, for a constant gas hold-up (as specified in the model), the rate of increase in interfacial area is overpredicted.

The reason for the overprediction of the effect of liquid flow rate on the interfacial area via approach *A*, can however, not be explained by these graphs. Since the energy dissipation rate in the reactor is determined strictly by the liquid flow rate, it can be argued that the exponent of the energy dissipation rate term in the bubble breakage rate equation ($^1/_3$) is too high, leading to an overprediction of the effect of liquid flow rate on interfacial area.

Since this theoretically should also be the case for approach *B*, which it is not, it must be kept in mind that this is only one of many possible explanations. However, it can be argued that this effect is offset by the overprediction of the interfacial area via approach *B*, resulting in more representative results.

From these results it can be concluded that both of the approaches contrasted above are able to satisfactorily predict trends in interfacial area production. Since both approaches exhibit certain advantages in the prediction of particular trends, these models can be combined to yield very good prediction of experimental data: approaches *A* and *B* can be used for prediction of the effect of gas flow rate and liquid flow rate respectively. In this way the value of the predicted interfacial area can be bracketed effectively.

Finally it needs to be said that, contrary to what was expected, approach *B* actually yielded a stable solution faster than approach *A*. Although the computation of one simulation cycle via approach *B* did take longer than for approach *A* (up to 5 times longer), a stable solution was reached much faster, i.e. after much fewer iterations. For example, approach *A* needed 6000 iterations in 100 seconds to reach a particular result, while approach *B* only employed 450 iterations in 35 seconds. Therefore it can be concluded that, in terms of computational time, approach *B* (ironically) represents the better alternative: convergence of results can be achieved in less than half the time needed by approach *A*.

6.3.2.2 Model verification with sulphite oxidation data

In *Chapters 3* and *5* it was discussed why an alternative chemical system was employed for verification of the proposed model. The results obtained for this system is compared to model predictions in the following graphs:

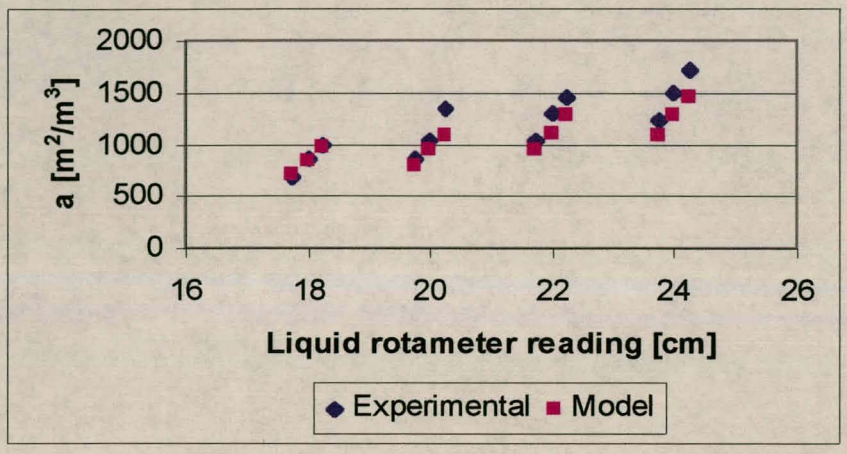

Figure 6.8 *Comparison of model and experimental data for the sulphite oxidation system in the σ-shaped reactor (approach A)*

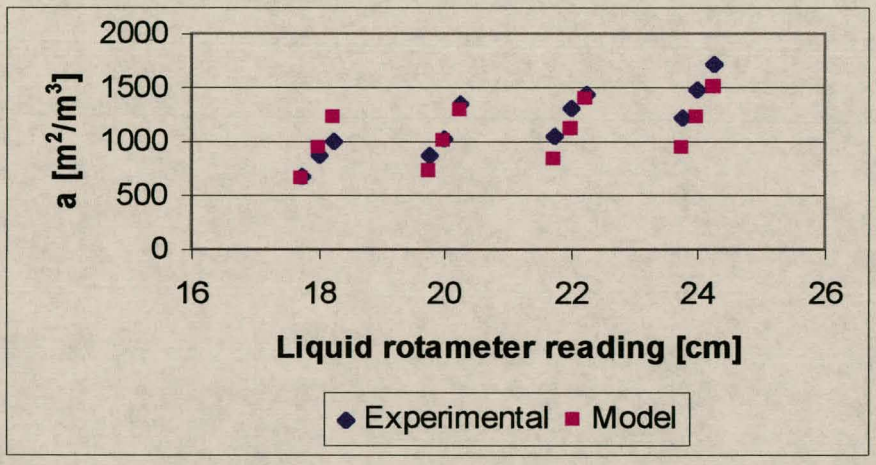

Figure 6.9 *Comparison of model and experimental data for the sulphite oxidation system in the σ-shaped reactor (approach B)*

From these graphs it can be seen that both the proposed models provide satisfactory prediction of trends with respect to the effects of both liquid and gas flow rates. Considering the fact that these experiments were performed at much lower gas flow rates and gas hold-ups (and therefore energy dissipation rates) than for the CO_2 absorption experiments, it can be said that the model is very flexible over a wide range of these operating parameters.

Comparison of the trends in these graphs with those exhibited by the CO_2 absorption system in *figures 6.3* and *6.5*, once again shows that approach *B* predicts a greater effect of the gas flow rate on the interfacial area than approach *A*: in this case, however, it does not lead to an overestimation, but rather a better approximation of experimental data, especially at higher flow rates.

In contrast to what was observed in *figures 6.3* and *6.5*, it can be seen that approach *B* tends to underpredict the effect of the liquid flow rate on the interfacial area, as is evident in a comparison of experimental and model data for the lowest gas flow of 3 *L/min*. This is also true for the case of approach *A*, where overprediction of this data should occur according to observations made from the CO_2 absorption data. However, it can still be seen that approach *A* predicts a less severe increase in the value of the interfacial area than approach *B*: better correlation of experimental data via approach *A* is simply due to a higher rate of increase in the interfacial area with an increase in liquid flow rate for this particular system.

Finally it can be noted that, irrespective of the approach used, the model tends to underpredict the values of the interfacial area, especially at increasing gas and liquid flow rates. This contrasts with the data obtained for the CO_2 absorption system where data was seldom underpredicted, but rather slightly overpredicted. Although this could very simply be due to inaccuracies in the values of the experimental data (as discussed in *Chapter 5*), it can be argued that at the relatively lower energy dissipation rates in this particular system, the enhancement of shear rates and resulting bubble break-up due to impingement zones in the reactor results in an improvement over the expected value of the interfacial area. For the higher energy dissipation rates, it can be argued that the increase in interfacial area production due to these effects is not as pronounced at the very high ranges of turbulence already present in the CO_2 absorption system. However, this explanation must be verified by incorporating it into the existing model. A possible suggestion as to how this could be implemented can be found in the following chapter, where recommendations will be made as to the further improvement of the model.

In conclusion, analogous to the conclusions made from the CO_2 absorption data, it can be said that both the approaches provide reasonably satisfactory prediction of experimental data. Again, each of these approaches have their advantages, so that a combination of the two have the potential to provide very good prediction of interfacial area data. In addition to this, it has already been concluded that the model is very flexible over a wide range of operating parameters, such as gas and liquid flow rates. Great potential therefore exists for the model's general applicability in other turbulent gas-liquid systems.

6.3.2.3 Model verification with alternative breakage rate equations

In *section 6.1* two alternative bubble breakage rate equations were presented which was used for verification and comparison of data predicted by the main model applied in this study (*Coulaloglou* and *Tavlarides*, 1977). The results obtained from this comparison can be summarised in the following tables:

Table 6.1 *Comparison of bubble breakage rate equations based on the correlation between experimental and predicted interfacial areas. (Figures for K_e in brackets represent optimal values)*

Author	**R^2**
Coulaloglou and *Tavlarides* (1977) [K_e = 5]	0.937
Hesketh et al. (1991) [K_e = 12]	0.965
Luo and *Svendsen* (1996) [K_e = 21]	0.963

Table 6.2 *Comparison of bubble breakage rate equations based on the deviation (%) between experimental and predicted average bubble sizes*

Author	CO_2 absorption %	Sulphite oxidation %
Coulaloglou and *Tavlarides* (1977)	10.3	7.5
Hesketh et al. (1991)	8.0	5.95
Luo and *Svendsen* (1996)	8.4	6.44

From *tables 6.1* and *6.2* it can be seen that all three breakage rate models employed provide accurate prediction of both the interfacial area production, as well as the average bubble size associated with each of these conditions. It can, however, further be noted that despite its relative simplicity compared to the other two models, the model proposed by *Hesketh et al.* (1991) results in the best fit of interfacial area and average bubble size data. This represents a great advantage in terms of computational time, since a simpler model will obviously result in shorter simulation cycle times.

At this point it is interesting to compare the respective bubble size distributions generated by each of these models (using approach *A*). This is illustrated in the following three graphs, represented by data from the CO_2 absorption system:

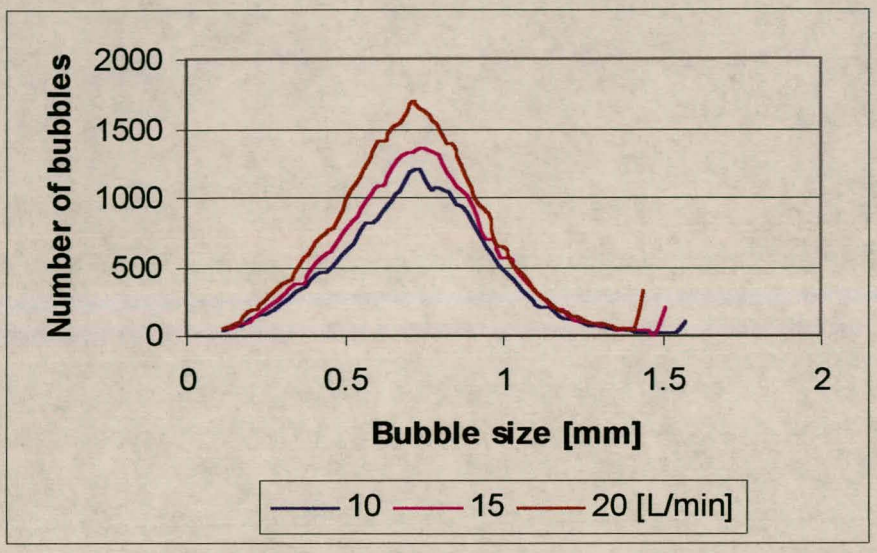

Figure 6.10 *Bubble size distribution curves predicted by the bubble breakage rate model of Coulaloglou and Tavlarides (1977).*

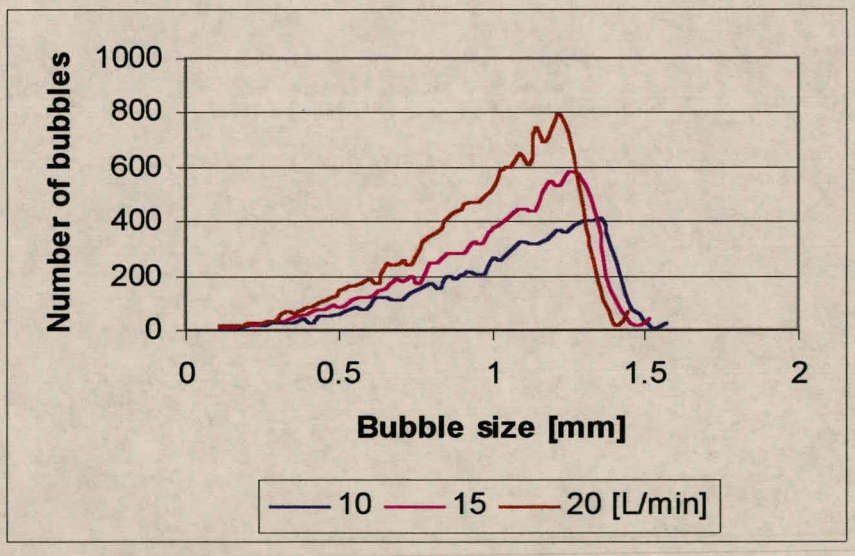

Figure 6.11 *Bubble size distribution curves predicted by the bubble breakage rate model of Hesketh et al. (1991).*

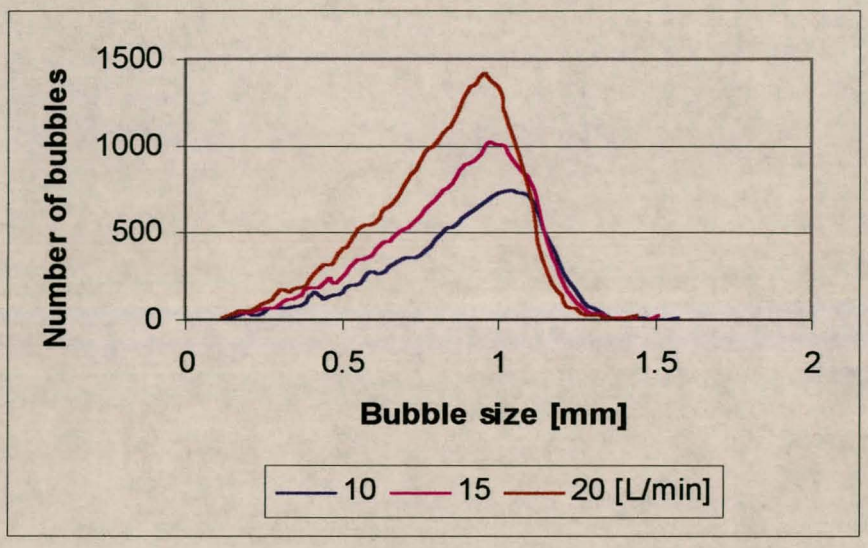

Figure 6.12 *Bubble size distribution curves predicted by the bubble breakage rate model of Luo and Svendsen (1996).*

From these graphs it can be seen that various shapes of bubble size distributions can be generated and still yield relatively similar predictions of the interfacial area. The bubble size distribution predicted by *Coulaloglou* and *Tavlarides* (1977) has the most normal distribution, where the model of *Hesketh et al.* (1991) produces the skewest bubble size distribution of all, very similar to what would be expected for the model of *Coulaloglou* and *Tavlarides* (1977) employing approach *B*. Finally it seems that the bubble size distribution predicted by *Luo* and *Svendsen* (1996) represents a combination of these two extremes.

However, no comparison could be made as to which of these bubble breakage models represented the best example of experimental data, since bubble size distributions could not be measured during this study. Therefore, it can only be concluded that all of the bubble breakage models analysed here yield very similar results in terms of interfacial area prediction, although it has been shown that the model of *Hesketh et al.* (1991) represents a better alternative in terms of simplicity and computing time. The model of *Coulaloglou* and *Tavlarides* (1977) for the prediction of interfacial area trends

has therefore been verified. Indeed, this was the main purpose of the present analysis.

6.3.3 Sensitivity analysis

6.3.3.1 Performing the sensitivity analysis

Despite the fact that many key changes and improvements have been made to the original model proposed by *Botes* (1995), the same strategy employed by him in performing a sensitivity analysis could be employed in this study since both the original and improved models share a common functional basis. Conclusions made in that study could therefore be compared more effectively with those obtained in the present investigation.

Therefore, a sensitivity analysis was performed by changing the value of an input parameter by 10%, whilst keeping the other parameter values constant. The effect of this change on both the interfacial area and average bubble size was recorded to determine the independent effects of each input variable on these parameters.

Having performed a sensitivity analysis at various operational settings and found that the sensitivity of the model to changes in any given parameter is in general not affected by the operational setting at which the sensitivity was evaluated, a sensitivity analysis was only performed at one operational setting. This setting, representative of the 'midpoint' of the range of experimental conditions, was at a gas flow rate of 15 *L/min* and a liquid rotameter setting of 20 *cm* (1.52 *L/min*). Since it was also concluded by *Botes* (1995) that the sensitivity analysis yielded similar results for both an increase and a decrease of 10% in the value of the input parameter, this study only considered the case of an increment in input variables. However, it must be kept in mind that, despite these simplifications, the results of the sensitivity analysis remains valid for any given operational setting.

Finally, as presented by *Botes* (1995), some parameters of the model simulation were specified arbitrarily such as the time increment for one simulation cycle, the number of bubble and eddy classes and the minimum bubble and eddy diameters. Since it was found that the model simulation was very insensitive to these parameters, they were disregarded during the sensitivity analysis.

6.3.3.2 The influence of physical properties on the model output

The response of the model output to changes in the physical properties of the system is presented in *table 6.3*.

Table 6.3 *The response of a 10% change in the physical properties of the system on the predicted interfacial area and average bubble size*

Parameter	Interfacial area %	Average bubble size %
ρ_L	2.1	-1.9
μ_L	-0.4	0.6
μ_G	1.9	-2.0
σ	-5.4	5.8

From this table it is evident that the viscosities of the gas and liquid phases, as well as the liquid density, do not have a significant influence on the output of the model. It can, however, be seen that the liquid surface tension does have a marked effect on the model output. This is due to the important role played by this parameter in stabilising the surface of a bubble against eddy bombardment, effectively determining the efficiency of a bubble-eddy collision. In the light of this, it is once again illustrated that the presence of surfactants in solution have the potential to influence the bubble size and interfacial area dramatically. The need to use very pure distilled water and

feed reagents in the experiments is therefore emphasised. It can also be suggested that the performance of the jet reactors might be enhanced by adding inert substances to the reactor feed which reduce the surface tension of the liquid, thereby reducing bubble stability and promoting bubble break-up.

6.3.3.3 The influence of the flow conditions of the feed streams on the model output

The influence of the flow conditions of the feed streams, i.e. the gas and liquid flow rates and pressures, on the model output is given in the following table.

Table 6.4 *The response of a 10% change in the feed flow conditions of the system on the predicted interfacial area and average bubble size*

Parameter	Interfacial area %	Average bubble size %
$\dot{V}_L$	5.3	-5.1
P_L	7.3	-6.9
ε	5.3	-5.1
$\dot{V}_G$	-0.6	0.7
P_G	~0.0	~0.0

From the results presented in *table 6.4*, it is clear that an increase in both the liquid flow rate and pressure results in a significant increase in the interfacial area and a decrease in the average bubble size. This was to be expected, since these parameters directly determine the rate at which energy is supplied to the reactor (as shown by *equations (6.45)* and *(6.46)*), resulting in higher degrees of bubble break-up due to an increase in the number of bubble-eddy collisions via *equation (6.13)*. It can also be seen that the effects of gas flow

rate and pressure is negligible in comparison to that of the above parameters. This can simply be ascribed to the fact that the effect of gas flow rate on the simulation was negated by direct specification of the gas hold-up in the reactor. The slight negative response of the interfacial area is explained by the fact that an increase in the gas flow rate translates into an increase in the bubble pressure in the reactor, resulting in more stable bubbles resistant to bubble break-up.

At this stage it is interesting to note that *Botes* (1995), based on conclusions made from the results of his sensitivity analysis of the feed flow conditions, recommended that the efficiency of the jet reactors could be enhanced further with the use of liquid nozzles with smaller orifices and gas nozzles with larger orifices – it was postulated that higher liquid pressures (due to smaller orifices) would result in higher energy dissipation rates, while higher gas flow rates at equivalent pressures (due to larger orifices) would improve gas hold-up and interfacial area effects. Although both of these recommendations have merit, it must be emphasised that results obtained from this investigation do not agree with them. Liquid nozzles with larger orifices should rather be used for optimisation of the energy efficiency of the reactors, while gas nozzles with smaller orifices should be used for generation of higher gas velocities for better impingement of gas into opposing liquid streams. Since the additional power associated with higher gas pressures would be negligible to the power dissipated through liquid nozzles, this seems to be a valid point. These two aspects of reactor optimisation will be discussed at greater length in the next chapter.

6.3.3.4 The influence of the hold-up characteristics on the model output

Table 6.5 presents the results of the sensitivity analysis on these parameters.

Table 6.5 *The response of a 10% change in the hold-up characteristics of the system on the predicted interfacial area and average bubble size*

Parameter	Interfacial area %	Average bubble size %
ϕ_g	14.7	-3.9

As stated earlier, the gas hold-up was specified and not calculated in the improved model due do its high dependence on this parameter. This is justified by the pronounced increase in the interfacial area with a change in this input parameter, as shown above. Indeed, it is the only parameter which as yet exhibits an amplified (> 10%) change in the value of the interfacial area. Therefore, further experimental work on the accurate determination of the gas hold-up, through residence time analysis or light scattering techniques, is justified so that the element of uncertainty associated with calculation of this parameter from experimental interfacial area and bubble size data is eliminated.

Once again the effect of gas-hold up on the energy dissipation rate per unit volume of liquid in the reactor is illustrated by the trend exhibited by the average bubble diameter. Since d_{bs} is basically a function of the energy dissipation rate alone, it can be seen that this value decreases slightly with an increase in gas hold-up. This is in good agreement with experimental data.

6.3.3.5 The influence of the free parameters on the model output

The response of the model output to changes in the free parameters specified in the system is presented in *table 6.6*.

Table 6.6 *The response of a 10% change in the free parameters specified in the system on the predicted interfacial area and average bubble size*

Parameter	Interfacial area %	Average bubble size %
K_e	-10.6	12.0
K_m	0.5	-0.6
K_f (original model)	0.0	0.0

The effect of K_e on the bubble breakage efficiency and therefore bubble breakage rate is clearly illustrated in the above results. An increase in the value of this parameter translates into an increase of the critical eddy velocity, which is a measure of the critical amount of energy needed to rupture a bubble. If a greater amount of energy is needed to rupture a bubble, bubbles are more stable. Therefore less bubble break-up of bubbles occurs, resulting in higher average bubble sizes and lower interfacial areas.

From the pronounced effect of K_e on bubble sizes and interfacial areas shown above, it can be argued that further optimisation of the value of this parameter be done for optimal correlation of experimental data. However, satisfactory predictive results were obtained by the model so that further time spent on this subject was not warranted.

In contrast to the significant effect of K_e on the model output (especially average bubble size), it can be seen that the model is relatively insensitive to changes in K_m. This corresponds well with results obtained by *Botes* (1995) for K_f in the original model. Since this parameter directly determines the value of the maximum stable bubble size in the reactor, the assumption made during modification of equation *(6.4)* that d_{bs} was strongly influenced by $d_{b,max}$, was not accurate. However, better correlation of average bubble size trends were obtained through the modification of this equation (*equation 6.9*) so that improvement thereof was justified.

It is concluded that the value of K_m only needs to be specified within a correct range of values to yield representative values of the maximum bubble size – highly accurate values need not be specified.

6.4 CONCLUSIONS AND RECOMMENDATIONS

In *Chapter 2* and in the introduction to this chapter, it was discussed how development of a fundamental model for prediction of the dispersed phase properties of the system would enhance understanding of the inter-dependent phenomena taking place in the jet reactors. By evaluating several changes made to the original model proposed by *Botes* (1995) and performing a sensitivity analysis on the improved model, this was realised.

During evaluation of the changes made to the original model it was concluded that the direct specification of the gas hold-up in the model, as determined from experimental data, resulted in more accurate prediction of the rate of increase in the interfacial area with increasing liquid flow rate. This was echoed by results obtained from the sensitivity analysis which showed that the gas hold-up had the most dramatic effect on the value of the predicted interfacial area of all the input parameters tested. It is therefore recommended that further work be done on the experimental determination of this parameter via RTD-analyses or light scattering techniques to eliminate any degree of uncertainty associated with the calculation of this parameter from experimental data.

Better correlation of average bubble sizes was also obtained by replacement of the original equation for calculation of the maximum bubble size via gas and liquid flow rates by an equation relating bubble size to the energy dissipation rate. This was done on the assumption that bubble coalesence did not occur in the highly turbulent environment of the jet reactors. By incorporating bubble coalescence into the model analogous to bubble break-up, this was indeed proved to be true, even for non-electrolyte systems.

A comparison of two approaches (designated *A* and *B* in the discussion) for treatment of bubble break-up in the model was also done. Whereas approach *A* utilised the summing of breakage events to effect bubble break-up once at the end of each simulation cycle, approach *B* effected bubble break-up immediately after identification of every bubble break-up event in every bubble class, effectively updating the bubble size distribution each time. Results obtained for these two approaches lead to the conclusion that both exhibited inherent advantages with regard to prediction of the effect of liquid and gas flow rates on the interfacial area, respectively. Ironically, it was also proven that approach *B*, despite longer individual simulation cycle times, resulted in faster prediction of a stable result through less simulation cycles than needed by approach *A*.

Verification of the model via prediction of additional sulphite oxidation results and alternative breakage rate equations presented in the literature also yielded very good results. It was concluded that the model is very flexible and can be applied over a wide range of hydrodynamic operating conditions in terms of flow rates and gas hold-up. The potential for the application thereof in many other turbulent gas-liquid systems, therefore exists. The model was further verified by the high degree of correlation between predicted and model trends in the interfacial area via the two alternative breakage rate equations. Since no assesment could be made as to which model most accurately predicted the bubble size distribution (due to a lack of experimental data in this regard) it is recommended that bubble sizes be measured experimentally in conjunction with the gas hold-up, as mentioned above.

From the sensitivity analysis, additional conclusions regarding the influence of system variables on interfacial area production could also be made. Since it was found that the value of the surface tension of the liquid had a significant effect on the interfacial area, it is recommended that the effect of the addition of surface agents to the reactor feed solution be investigated – in this way the degree to which surface tension decreases bubble stability and increases bubble break-up, can be quantified.

Contradictory to recommendations made by *Botes* (1995) regarding further use of nozzles, conclusions made from the results in this chapter and *Chapter 5* indicated that liquid nozzles with *larger* nozzle diameters should rather be used for optimisation of the energy efficiency of the reactors. In addition to this it was concluded that nozzles with *smaller* orifice diameters be used for generation of higher linear gas velocities to increase the efficiency of the impingement of these streams into opposing liquid streams.

Finally a need for the incorporation of this impingement effect into the existing model was identified by the model's inability to fully predict the increase in interfacial area production with an increase in the liquid flow rate. Knowledge of this mechanism would additionally not only facilitate better understanding of the under- and overprediction of trends exhibited by the current model, but also provide some means of differentiating between the interfacial production efficiencies of the π- and σ-shaped reactors. In the next chapter a brief strategy will be outlined for the incorporation of this model into the existing model.

CHAPTER 7

CONCLUSIONS AND RECOMMENDATIONS

'Enough research will tend to support your theory'

- Anon

The character of research (and researchers) is such that a project is never considered fully completed – the refinement of new or existing processes, in order to increase their efficiency, is indeed the most important task of the engineer and scientist. It is therefore the purpose of this chapter to present the most significant conclusions drawn from this investigation and compare them with conclusions made previously by *Botes* (1995). Based on these conclusions, recommendations regarding future research will be presented.

7.1 CONCLUSIONS DRAWN FROM THE CURRENT PROJECT

Literature survey

In *Chapter 2* it was discussed how mixing devices have been developed towards a type of phase contacting device where intense turbulent mixing is increasingly being used to enhance interfacial area production and mass transfer. It was shown how impinging stream reactors provide a tool for the intensification of these processes, exhibiting high mass transfer parameters and possessing the benefits of simple construction, low equipment cost, ease of operation and relatively small geometrical size. Considering these advantages and the significant successes achieved by *Botes* (1995) in this regard, the continuation of the development of high intensity impinging stream jet reactors at this institution was justified.

A survey of the literature concerning modelling of gas-liquid mixing systems also revealed a growing trend towards the fundamental modelling of these

systems (as opposed to empirical modelling), since a general need for better understanding of the interaction of mechanisms in dispersed phase systems continues to exist. The continued improvement of the original model proposed by *Botes* for the prediction of interfacial area production in the jet reactors, in the form of a Monte Carlo simulation, was therefore proved to be warranted.

Determination of the mass transfer parameters

In *Chapter 4*, the new chemical technique proposed by *Botes* for the determination of mass transfer parameters from absorption data was evaluated and proved to be accurate and valid using correlations for the enhancement factor *E,* proposed by a wide variety of independent authors. Therefore continued use of this method in this investigation was justified.

Discussion of experimental results

Evaluation of the mass transfer parameters exhibited by the newly developed reactors in *Chapter 5* revealed that the value of the mass transfer coefficient is indeed significantly influenced by both the liquid and gas flow rates, contrary to the conclusion made by *Botes et al.* (1998) that it is independent of these variables. Comparison of the different k_L-values exhibited by the reactor configurations investigated showed that the mass transfer coefficient could be enhanced substantially by centrifugal acceleration of the fluid and more efficient promotion of turbulence in the round reactor chambers of the π- and σ-shaped reactors, compared to the kite-shaped reactor. However, it could also be concluded that the jagged/angular reactor chamber of the kite-shaped reactor configuration provided for more efficient break-up of bubbles than the π- and σ-shaped reactors, due to collisions of the two-phase fluid with the reactor walls. In addition to this the random flow patterns exhibited in this reactor resulted in higher relative hold-up of gas compared to the other reactors, resulting in larger interfacial areas.

In addition to the above mentioned mechanisms, it was also concluded that the utilisation of impinging streams in these reactors indeed provided for process intensification. Comparison of mass transfer coefficient values

exhibited between the kite- and π/σ-shaped reactors seemed to suggest that the head-on impingement of gas and liquid streams was more efficient than the shearing off of bubbles from gas nozzles (as proposed by *Botes*), while slightly higher values of interfacial area in the σ-shaped reactor compared to the π-shaped reactor could be accounted for by the difference in the amount of impingement zones in each of these reactors.

Owing to its ability to exhibit high values of the mass transfer coefficient compared to the other reactors, it was found that the σ-shaped reactor exhibited the highest value of k_La and therefore represented the best alternative in terms of mass transfer performance. However, it was found that the kite-shaped reactor outperformed the π-shaped reactor due to its ability to exhibit comparably high interfacial areas so that the reactors could ultimately be classified as follows, based on performance:

σ-shaped > kite-shaped > π-shaped

Therefore, it was concluded that an optimum reactor design would combine the k_L-enhancing effects of the swirling flow in the σ-shaped reactor, with the bubble break-up and gas hold-up ability of the kite-shaped reactor.

Finally, by comparing experimental results with data obtained from the literature for conventional systems, it was shown that, in terms of both the mass transfer coefficient and the value of the interfacial area per unit of energy dissipation, the proposed reactors provided a significant improvement in mass transfer performance in certain applications, depending on the cost of energy.

It could therefore be concluded that the newly developed impinging stream jet reactors have the potential to represent superior alternatives to conventional gas-liquid contacting equipment.

Modelling

In *Chapter 6* it was shown how necessary improvements or changes made to the model with regard to gas hold-up, maximum stable bubble size and the treatment of effective collision events resulted in more accurate prediction of the trends in interfacial area as a function of various process variables.

Verification of the model via prediction of additional sulphite oxidation results and alternative breakage equations also yielded very good results. It was concluded that the model is very flexible and can be applied over a wide range of hydrodynamic operating conditions, validating the potential application thereof in other turbulent gas-liquid systems.

It was also concluded that the performance of the reactors might further be increased via the use of liquid nozzles with larger diameters for optimisation of the energy efficiency of the reactors. In addition to this, the use of gas nozzles with smaller orifices would result in higher linear gas velocities, improving the efficiency of impingement of these streams into opposing liquid streams.

Finally the need for incorporation of the impingement effect into the existing model was identified for better prediction and understanding of trends in interfacial area. This is addressed in *section 7.3*.

7.2 ACHIEVEMENT OF PROJECT OBJECTIVES

It is important to compare the initial project objectives to those which were actually realised, so that an accurate assessment of recommendations for further study in this project can be made. The project objectives specified in *Chapter 1* can be generalised to yield the following basic objectives:

1. To establish enhanced gas-liquid contact via impinging streams and high levels of turbulence.
2. To gain further insight into gas-liquid mixing by investigating alternative jet reactor designs.

3. To improve and verify the existing model for prediction of the interfacial area production in the jet reactors.

It can be said that all of the above objectives were realised to a large extent. Through the development and testing of two new alternative reactor designs, significant improvements in the mass transfer coefficient and interfacial area production over that exhibited by conventional phase contacting equipment, were achieved. Deep insight was also gained into various parameters that generate these process intensification effects. However, a few conclusions regarding the further optimisation of the efficiency of the proposed reactors were also made during this investigation: only after these have been implemented and tested, a final assessment can be made as to whether the reactors have been fully optimised.

Correlation of model data with experimental results has also been improved through the incorporation of various improvements to the model. The general applicability thereof in alternative gas-liquid systems, as well as the bubble breakage mechanism assumed by the model, has also been verified. However, direct verification of bubble sizes predicted by the model via non-intrusive measurement of bubble sizes in the reactors has not been done due to a lack of time and available resources. In terms of this, objective # 5 set out in *Chapter 1* has not been realised. It is therefore essential that this be done in the continuation of this study before the model can be accepted as fully valid and representative. In view of the above, recommendations concerning further research can now be done.

7.3 RECOMMENDATIONS REGARDING FURTHER RESEARCH

7.3.1 Future experimental research

During the comparison of results between the newly proposed jet reactors and conventional gas-liquid contactors, it was pointed out that, apart from higher exhibited mass transfer parameters, the new reactors have the additional

benefits of having no moving parts and being of simple construction. In view of this, there is limited scope in significantly improving reactor performance further. However, a number of possible improvements have been identified:

1. *Nozzles*. It has been shown how liquid nozzles with larger orifices have the potential for further optimisation of the energy efficiency of the reactors, while gas nozzles with smaller orifices will result in better impingement of gas streams into opposing liquid streams. In addition to these alternatives, so-called critical nozzles (as used by *Herskowits et al.* (1990) and *Tamir* (1994)), where gas and liquid are premixed in the nozzle body before injection into the reactor volume, can also be employed. Although these nozzles exhibit slightly higher relative pressure drops, they have been proved to exhibit superior gas-liquid mixing performance.

2. *Nozzle and reactor chamber geometry*. It has been shown how an optimal reactor configuration would combine the k_L-enhancing effects of swirling liquid in a round reactor geometry, with the bubble break-up ability of an angular/jagged shape. Additionally, the reactor design must be such that as many as possible head-on impingement zones between entering gas and liquid streams are incorporated.

3. *Reactor walls*. Since it was observed visually through the Perspex reactor that the movement of bubbles in the vicinity of its walls were impeded by a slight degree of clinging, it is suggested that the walls of the reactors be '*roughened*' to improve turbulence characteristics around them. Impeded bubble motion would thus be minimised.

In addition to possible improvement of the reactors themselves, additional experimental strategies must also be followed:

1. *Bubble size measurement and gas hold-up*. The importance of the accurate measurement of these parameters has already been stated. It is therefore recommended that methods for the direct determination of these parameters be investigated. Due to the very small reactor volumes used,

non-intrusive techniques such as video image analysis of bubbles and light scattering (e.g. laser-doppler) techniques must be used. Residence time distribution and tracer techniques might also be used for accurate determination of the gas hold-up.

2. *Surface active agents*. It has been shown how inert chemicals added to the liquid feed can reduce the surface tension of the solution which in turn will lead to decreased bubble stability and increased bubble break-up, resulting in higher interfacial areas. This mechanism for potential improvement of reactor performance must be investigated.

3. *Operating conditions*. A wider range of operating conditions will ensure that trends in the experimental data become more prominent, so that it will not be obscured by any scatter in the data. This is especially necessary in the case of the mass transfer coefficient.

4. *Scale-up*. After these recommendations have been implemented, the reactor system can be scaled up to a bank of reactors for testing on a industrial application. An ideal example of this would be the absorption of CO_2 from SASOL process gas, which is currently being done with highly dangerous and toxic MEA and DEA. Current research at this institution in the field of ozonation of wine cellar effluent water also poses a great opportunity for critical evaluation of these reactors on an industrial scale.

7.3.2 Future model development

It has been demonstrated how the original model proposed by *Botes* (1995) has been improved by addition and modification of various procedures and variables. Although this has resulted in significantly better correlation between experimental and model data, areas in which further improvements can be made have been identified as:

1. *Hydrodynamic and physicochemical properties.* The model should be tested to determine whether or not it compensates satisfactorily for changes in these properties. For instance, experiments can be performed with ethylene glycol added to the liquid feed which will effect changes in the hydrodynamics of the system (surface tension, density and viscosity) without affecting the rate of chemical reaction. Correlation of these results with model data will determine the applicability of the model over a wide range of liquid reagents. This has already been done to a limited extent in the sulphite oxidation experiments.

2. *Modelling of the mass transfer coefficient.* If more accurate values of k_L can be obtained, an attempt should be made to model the mass transfer coefficient by means of the surface renewal theory (as described in *Chapter 4*) or other relevant theories. If this can successfully be coupled with the existing model for prediction of the interfacial area, it would be one of the first practical, fundamental models for prediction of the value of k_La in turbulent systems. Considering the work involved in this, it is recommended that it be done as a independent study, using existing experimental data.

3. *Incorporation of impingement zones.* In *Chapter 6* a need for the incorporation of the effect of liquid-gas impingement into the model was identified since the existing model only allows for the prediction of bubble break-up under 'normal' turbulent conditions and not 'intensified' conditions generated in impingement zones. This would provide some means of differentiating between the interfacial areas produced in the π- and σ-shaped reactors respectively and serve as a first step into including the effect of reactor geometry on mass transfer performance. A brief (preliminary) strategy for implementation of this recommendation can now be given.

If it can be assumed that the total reactor volume can be divided into regions of so-called 'normal' and 'intensified' turbulent conditions, the volume of the reactor can mathematically be expressed as:

$$V_{total} = V_{normal} + nV_{\text{int}\,ense} \quad \ldots (7.1)$$

where n refers to the number of impingement zones in each reactor and $V_{intense}$ can be given by the following ratio:

$$V_{\text{int}\,ense} = rV_{total} \quad \ldots (7.2)$$

For these designated impingement zones, the relative velocity of the associated bubble or eddy can be given by the following, analogous to *equation (6.12)*:

$$\overline{u^2}_{\text{int}\,ense} = K_i\left(2\varepsilon^{2/3}d^{2/3}\right) \quad \ldots (7.3)$$

where the parameter K_i can be adjusted between 1 and a maximum of 2, which represents the increase in relative velocity between impinging gas and liquid streams:

$$u_{rel} = u_{liq} - \left(-u_{gas}\right) \quad \ldots (7.4)$$

An increase in this velocity will not only lead to an increase in the number of collisions between bubbles and eddies, but also increase the efficiency of bubble break-up. The increase in shear rates associated with impinging streams (as described in *Chapter 2*) is thus simulated well.

Therefore two additional free parameters, r and K_i, will be needed to describe the effect of impingement zones in the reactors. Although this will inevitably result in an increase in the complexity of the model, it can be considered as a reasonable basis for further development and simplification of this idea in the model.

REFERENCES

1. Angelidou, C., Psimopoulos, M. and Jameson, G.J. (1979). Size distribution functions of dispersions. *Chemical Engineering Science*, **34**, 671.

2. Astarita, G. (1967), Mass transfer with chemical reaction. Amsterdam, The Netherlands: Elsevier Science, pp. 33 – 42 and 144 – 151.

3. Azbel, D. (1981). Two-Phase Flows in Chemical Engineering. Cambridge, UK: Cambridge University Press.

4. Barron, C.H. and O'Hern, H.A. (1966). Reaction Kinetics of Sodium Sulphite Oxidation by the Rapid-mixing Method. *Chemical Engineering Science*, **21**, 397 – 404.

5. Batchelor, G.K. (1982). The Theory of Homogeneous Turbulence. Cambridge, UK: Cambridge University Press.

6. Beenackers, A.A.C.M. and Van Swaaij, W.P.M. (1976). Mass transfer and Chemical Reaction in a Gas-Liquid Cyclone Reactor. *Proceedings of the 4th International 6th European Symposium on Chemical Reaction Engineering*, Frankfurt, 260 – 270.

7. Bhavaraju, S.M., Russell, T.W.F and Blanch, H.W. (1978). The Design of gas Sparged Devices for Viscous Liquid Systems. *AIChE Journal*, **24**, 454 – 466.

8. Botes, F.G. (1995). The Development and Modelling of Impinging Stream Jet Reactors. *Masters Dissertation*. Department of Chemical Engineering, University of Stellenbosch, RSA.

9. Botes, F.G., Lorenzen, L. and Van Deventer, J.S.J. (1998). The Development of High Intensity Gas-Liquid Jet Reactors. *Chemical Engineering Communications*, 170, 217 – 224.

10. Bouaifi, M. and Roustan, M. (1998). Bubble Size and Mass Transfer Coefficients in Dual-Impeller Agitated Reactors. *The Canadian Journal of Chemical Engineering*, **76**, 390 – 397.

11. Breman, B.B., Beenackers, A.A.C.M., Bouma, M.J. and Van der Werf, M.H. (1996). The Gas-Liquid Mass Transfer Coefficient (k_La) in the Gas-Liquid Multi-Stage Agitated Contactor (MAC). *Transactions of the Institution of Chemical Engineers*, **74**, 872 – 881.

12. Brian, P.L.T., Hurley, J.F. and Hasseltine, E.H. (1961). Penetration Theory for Gas Absorption Accompanied by a Second Order Chemical Reaction. *AIChE Journal*, **7**, 226 – 231.

13. Calderbank, P.H. (1958). Physical Rate Processes in Industrial Fermentation, Part I.: The Interfacial Area in Gas-Liquid Contacting with Mechanical Agitation. *Transactions of the Institution of Chemical Engineers*, **36**, 443 – 463.

14. Calderbank, P.H. (1967). Mixing Theory and Practice, Volume II. New York, USA: Academic Press.

15. Calderbank, P.H. and Moo-Young, M.B. (1961). The Continuous Phase Heat and Mass Transfer Properties of Dispersions. *Chemical Engineering Science*, **16**, 39 – 54.

16. Charpentier, J. (1981). Advances in Chemical Engineering, **11**. New York, USA: Academic Press, pp. 2 – 65 and 102 – 126.

17. Chesters, A.K. and Hoffman, G. (1982). Bubble Coalescence in Pure Liquids. *Applications of Scientific Research*, **38**, 353.

18. Coulaloglou, C.A. and Tavlarides, L.L. (1977). Description of Interaction Processes in Agitated Liquid-Liquid Dispersions. *Chemical Engineering Science*, **32**, 1289.

19. Craig, V.S.J., Ninham, B.W. and Pashley, R.M. (1993). The effect of electrolytes on bubble coalescence in water. *The Journal of Physical Chemistry*, **97**, 10192 – 10197.

20. Curl, R.L. (1963). Dispersed Phase Mixing: I. Theory and Effects in Simple Reactors. *AIChE Journal*, 9, 175 – 181.

21. Danckwerts, P.V. (1955). Gas Absorption Accompanied by Chemical Reaction. *AIChE Journal*, **1**, 456 – 463.

22. Danckwerts, P.V. (1970). Gas-Liquid Reactions. New York, USA: McGraw-Hill Book Company.

23. Danckwerts, P.V. and Sharma, M.M. (1966). The Absorption of Carbon Dioxide into Solutions of Alkalis and Amines. *The Chemical Engineer*, **202**, CE244 – CE278.

24. Davidson, J.F. and Schuler, B.O.G. (1960). Bubble Formation at an Orifice in a Viscous Liquid. *Transactions of the Institution of Chemical Engineers*, **38**, 144.

25. De Waal, K.J.A. and Beek, W.J. (1967). A Comparison between Chemical Absorption with Rapid First-Order Kinetics and Physical Absorption in one Packed Column. *Chemical Engineering Science*, **22**, 585.

26. De Waal, K.J.A. and Okeson, J.C. (1966). The Oxidation of Aqueous Sodium Sulphite Solutions. *Chemical Engineering Science*, **21**, 559 – 572.

27. Elperin, I.T. (1961). Heat and Mass Transfer in Opposing Currents. *Journal of Engineering Physics*, **6**, 62 – 86.

28. Evans, G.M. and Machniewski, P.M. (1999). Mass Transfer in a Confined Plunging Liquid Jet Bubble Column. *Proceedings of the 4th International Conference on Gas-Liquid and Gas-Liquid-Solid Reactor Engineering*, Delft, The Netherlands, 4981 – 4990.

29. Gaddis, E.S. and Vogenpohl, A. (1992). The Impinging Stream Reactor: A High Performance Loop Reactor for Mass Transfer Controlled Chemical Reactions. *Chemical Engineering Science*, **47**, 2877 – 2882.

30. Gianetto, A. and Silveston, P.L. (1986), Multiphase Chemical Reactors: Theory, Design, Scale-Up. Washington, USA: Hemisphere Publishing Company.

31. Greaves, M. and Barigou, M. (1988). The Internal Structure of Gas-Liquid Dispersions in a Stirred Reactor. *Proceedings of the 6th European Conference on Mixing, Pavia, Italy*, 313 – 320.

32. Haimour, N. and Sandall, O.C. (1983). Gas Absorption Accompanied by an Irreversible Second Order Reaction in Turbulent Liquids. *AICHE Journal*, **29**, 277 – 281.

33. Herskowits, D., Herskowits, V., Stephan, K. and Tamir, A. (1990a). Characterisation of a Two-Phase Impinging Jet Absorber – I. Physical Absorption of CO_2 in Water. *Chemical Engineering Science*, **43**, 2773 – 2780.

34. Herskowits, D., Herskowits, V., Stephan, K. and Tamir, A. (1990b). Characterisation of a Two-Phase Impinging Jet Absorber – II. Absorption with Chemical Reaction of CO_2 in NaOH Solutions. *Chemical Engineering Science*, **45**, 1281 – 1287.

35. Hesketh, R.P., Etchells, A.W. and Russell, T.W.F (1991). Bubble Breakage in Pipeline Flows. *Chemical Engineering Science*, **46**, 1.

36. Hinze, J.O. (1955). Fundamentals of the Hydrodynamic Mechanism of Splitting in Dispersion Processes. *AIChE Journal*, **1**, 289 – 295.

37. Hulburt, H.M. and Katz, S.L. (1964). Some Problems in Particle Technology: A Statistical Mechanical Formulation. *Chemical Engineering Science*, **19**, 555 – 574.

38. Huynh, L.X., Briens, C.L., Large, J.F., Catros, A., Bernard, J.R. and Bergougnou, M.A. (1991). Hydrodynamics and Mass Transfer in an Upward Venturi/Bubble Column Combination. *The Canadian Journal of Chemical Engineering*, **69**, 711 – 722.

39. Jeffery, G.H., Bassett, J., Mendham, J. and Denney, R.L. (1989). Vogel's Textbook of Quantitative Chemical Analysis, 5th Edition. New York, USA: McGraw-Hill, pp. 384 – 389.

40. Kawase, Y. and Moo-Young, M. (1987). Theoretical Prediction of Volumetric Mass Transfer Coefficients in Bubble Columns for Newtonian and Non-Newtonian Fluids. *Chemical Engineering Science*, **42**, 1609 – 1616.

41. Kawase, Y. and Moo-Young, M. (1990). Mathematical Models for Design of Bioreactors: Applications of Kolmogoroff's Theory of Isotropic Turbulence. *The Chemical Engineering Journal*, **43**, B19 – B41.

42. Kennard, E.H. (1938). Kinetic Theory of Gasses. New York, USA: McGraw-Hill.

43. Kim, W.K. and Lee, K.L. (1987). Coalescence behaviour of Two Bubbles in Stagnant Liquids. *The Journal of Chemical Engineering of Japan*, **20**,449.

44. Kirkpatrick, R.D. and Locket, M.J. (1974). The Influence of Approach Velocity on Bubble Coalescence. *Chemical Engineering Science*, **29**, 2363.

45. Kleingeld, A.W., Lorenzen, L. and Botes, F.G. (1999). The Development and Modelling of High-Intensity Impinging Stream Jet Reactors for Effective Mass Transfer in Heterogeneous Systems. *Chemical Engineering Science*, **54**, 4991-4995.

46. Kuboi, R., Komasawa, I. and Otake, T. (1972). Behaviour of Dispersed Particles in Turbulent Liquid Flow. *The Journal of Chemical Engineering of Japan*, **5**, 349.

47. Kulov, N.N., Nikolaishvili, E.K., Barabash, V.M., Braginski, L.N., Malayusov, V.A. and Zhavoronkov, N.M. (1983). Dissolution of Solids in Agitated Vessels. *Chemical Engineering Communications*, **21**, 259 – 271.

48. Lamb, H. (1932). Hydrodynamics, 6th Edition. Cambridge, UK: Cambridge University Press.

49. Lamourelle, A.P. and Sandall, O.C. (1972). Gas Absorption into a Turbulent Liquid. *Chemical Engineering Science*, **27**, 1035 – 1043.

50. Laurent, A., Fonteix, C. and Charpentier, J.C. (1980). Simulation of a Pilot Scale, Liquid Motivated, Venturi Jet Scubber by a Laboratory Scale Model. *AIChE Journal*, **26**, 282.

51. Lee, C., Erickson, L.E. and Glasgow, L.A. (1987). Bubble Break-up and Coalescence in Turbulent Gas-Liquid Dispersions. *Chemical Engineering Communications*, **59**, 65 – 84.

52. Lee, J.C. and Meyrick, D.L. (1970). Gas-Liquid Interfacial Area in Salt Solutions in an Agitated Tank. *Transactions of the Institution of Chemical Engineers*, **48**, T37 – T45.

53. Lee, S. and Tsui, Y.P. (1999). Succeed at Gas-Liquid Contacting. *Chemical Engineering Progress*, July, 23 – 49.

54. Leng, D.E. and Quarderer, G.J. (1982). Drop Dispersion in Suspension Polymerisation. *Chemical Engineering Communications*, **14**, 177 – 201.

55. Levich, V.G. (1962). Physicochemical Hydrodynamics. New Jersey, Prentice Hall Publishers.

56. Loftus, B. (1999). The Design of a Jet Leaching Reactor for the Treatment of Gold Ores. *Masters Dissertation*. Department of Chemical Engineering, University of Stellenbosch, RSA.

57. Lopes de Figueiredo, M.M. and Calderbank, P.H. (1979). The Scale-up of Aerated Mixing Vessels for Specified Oxygen Dissolution Rates. *Chemical Engineering Science*, **34**, 1333 – 1338.

58. Lorenzen, L.L., Loftus, B.M., Petersen, K.R.P. and Van Deventer, J.S.J. (1997). The Effect of Jet Reactors on the Leaching of Gold from Ores. *Minerals Engineering*, 10, 909 – 917.

59. Luo, H. and Svendsen, H.F. (1996). Theoretical Model for Drop and Bubble Break-up in Turbulent Dispersions. *AIChE Journal*, **42**, 1225 – 1233.

60. Machon, V., Vlcek, J. and Hudcova, V. (1988). Multi-Impeller Gas-Liquid Contactors. *Proceedings of the 6th European Conference on Mixing, Pavia, Italy*, 351 – 360.

61. Marshall, S.H., Chudacek, M.W. and Bagster, D.F. (1993). A Model for Bubble Formation from an Orifice with Liquid Cross-Flow. *Chemical Engineering Science*, **48**, 2049 – 2059.

62. Meister, D., Post, P., Dunn, I.J. and Bourne, J.R. (1979). Design and Characterisation of a Multistage, Mechanically Stirred Column Absorber. *Chemical Engineering Science*, **34**, 1367 – 1374.

63. Nagel, O., Kurten, H. Hegner, B, Durst, F., Tsiklauri, G.V. and Afgan, N.H. (1979). Two-Phase Momentum Heat and Mass Transfer in Chemical Processes and Engineering Systems, Volume 2. Washington D.C., USA: Hemisphere Publishing.

64. Nambiar, D.K.R., Kumar, R., Das, T.R. and Gandhi, K.S. (1992). A New Model for the Breakage Frequency of Drops in Turbulent Stirred Dispersions. *Chemical Engineering Science*, **47**, 2989.

65. Narsimhan, G., Gupta, J.P. and Ramkrishna, D. (1979). A Model for Transitional Breakage Probability of Droplets in Lean Liquid-Liquid Dispersions. *Chemical Engineering Science*, **34**, 257 – 265.

66. Padvamathi, G. and Remananda Rao, K. (1993). Influence of Geometry on Gas Hold-ups in a Reversed Flow Jet Loop Reactor. *The Canadian Journal of Chemical Engineering*, **71**, 94 – 100.

67. Prasad, K.Y. and Ramanujam, T.K. (1995). Gas Hold-up and Overall Volumetric Mass Transfer Coefficient in a Modified Reversed Flow Jet Loop Reactor. *The Canadian Journal of Chemical Engineering*, **73**, 190 – 195.

68. Prince, M.J. and Blanch, H.W. (1990). Bubble Coalescence and Break-up in Air-Sparged Bubble Columns. *AIChE Journal*, **36**, 1485 – 1499.

69. Ramkrishna, D. (1981). Analysis of Population Balance – IV. The Precise Connection Between Monte Carlo Simulation and Population Balances. *Chemical Engineering Science*, **36**, 1203 – 1209.

70. Ramkrishna, D. and Borwanker, J.D. (1973). A Puristic Analysis of Population Balance. *Chemical Engineering Science*, **28**, 1423 – 1435.

71. Reith, T. and Beek, W.J. (1973). The Oxidation of Aqueous Sodium Sulphite Solutions. *Chemical Engineering Science*, **28**, 1331 – 1339.

72. Spielman, L.A. and Levenspiel, O. (1965). A Monte Carlo Treatment for Reacting and Coalescing Dispersed Phase Systems. *Chemical Engineering Science*, **20**, 247 – 254.

73. Sprehe, M., Gaddis, E. and Vogenpohl, A. (1998). On the Mass Transfer in an Impinging Stream Reactor. *Chemical Engineering Technology*, **21**, 19 – 21.

74. Sprow, F.B. (1967). Drop Size Distributions in Strongly Coalescing Agitated Liquid-Liquid Systems. *AIChE Journal*, **13**, 995 – 998.

75. Tamir, A. and Herskowits, D. (1985). Absorption of CO2 in a New Two-Impinging-Streams Absorber. *Chemical Engineering Science*, **40**, 2149 – 2151.

76. Tamir. A. (1994). Impinging-Stream Reactors: Fundamentals and Applications. Amsterdam, The Netherlands: Elsevier Science.

77. Thomas, R.M. (1981). Bubble Coalescence in Turbulent Flows. *International Journal of Multiphase Flow*, **8**, 709 – 717.

78. Toor, H.L. and Marchello, J.M. (1958). Film Penetration Model for Mass and Heat Transfer. *AIChE Journal*, **4**, 97 – 101.

79. Unger, D.R., Muzzio, F.J. and Brodkey, R.S. (1998). Experimental and Numerical Characterisation of Viscous Flow and Mixing in an Impinging Jet Contactor. *The Canadian Journal of Chemical Engineering*, **76**, 546 – 555.

80. Valentas, K.J., Bilous, O. and Amundson, N.R. (1966). Analysis of Breakage in Dispersed Phase Systems. *Industrial and Engineering Chemistry Fundamentals*, **5**, 271 – 279.

81. Valentas, K.J. and Amundson, N.R. (1966). Breakage and Coalescence in Dispersed Phase Systems. *Industrial and Engineering Chemistry Fundamentals*, **5**, 533 – 542.

82. Van de Vusse, J.G. (1966). Consecutive Reactions in Heterogeneous Systems: I – The Effect of Mass Transfer on Selectivity. *Chemical Engineering Science*, **21**, 631 – 643 .

83. Van't Riet, K. (1979). Review of Measuring Methods and Results in Non-Viscous Gas-Liquid Mass Transfer in Stirred Vessels. *Industrial Engineering Chemistry Process Development*, **18**, 357 – 363.

84. Velan, M. and Ramanujam, T.K. (1991). Hydrodynamics in Down Flow Jet Loop Reactors. *The Canadian Journal of Chemical Engineering*, **69**, 1257 – 1261.

85. Waldie, B. (1995). Novel High Intensity Gas-Liquid Contactor. *Proceedings of the 1st International Conference on Science, Engineering and Technology of Intensive Processing*, University of Nottingham, 5 – 8.

86. Waldie, B. and Harris, W.K. (1998). Removal of Dissolved Aromatics From Water: Comparison of a High Intensity Contactor with a Packed Column. *Transactions of the Institution of Chemical Engineers*, **76**, 562 – 570.

87. Waldie, B., Johnston, T., Harris, W.K. and Bell, C. (1999). Bubble Characteristics in a High Intensity Gas-Liquid Reactor. *Chemical Engineering Science*, **54**, 5319 – 5327.

88. Walter, J.F. and Blanch, H.W. (1986). Bubble Break-up in Gas-Liquid Bioreactors: Break-up in Turbulent Flows, *The Chemical Engineering Journal*, **32**, B7 – B17.

89. Wesselingh, J.A. and Van't Hoog (1970). Oxidation of Aqueous Sodium Sulphite Solutions: A Model Reaction for Measurements in Gas-Liquid Dispersions. *Transactions of the Institution of Chemical Engineers*, **48**, T69 – T74.

90. Wu, H., Arcella, V. and Malavasi, M. (1998). A Study of Gas-Liquid Mass Transfer in Reactors with Two Disc Turbines. *Chemical Engineering Science*, **53**, 1089 – 1095.

91. Yagi, H. and Yoshida, F. (1975). Gas Absorption by Newtonian and Non-Newtonian Fluids in Sparged Agitated Vessels. *Industrial Engineering Chemistry Process Design and Development*, **14**, 488.

92. Zeitlin, M.A. and Tavlarides, L.L. (1972). Fluid-Fluid Interactions and Hydrodynamics in Agitated Dispersions: A Simulation Model. *The Canadian Journal of Chemical Engineering*, **50**, 207 – 214.

APPENDIX A

ALGORITHM OF MODEL SIMULATION: APPROACH A

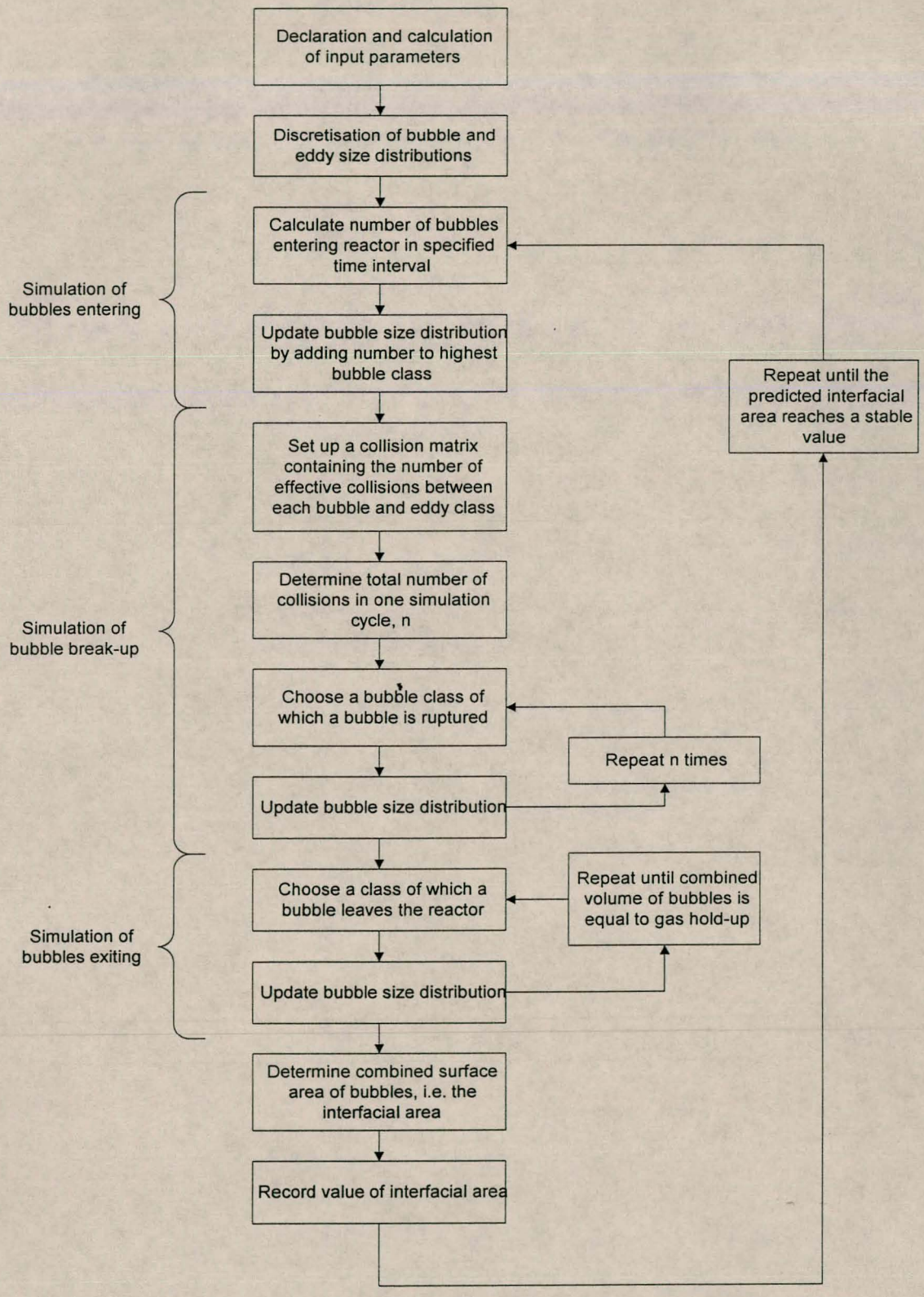

APPENDIX B

ALGORITHM OF MODEL SIMULATION: APPROACH B

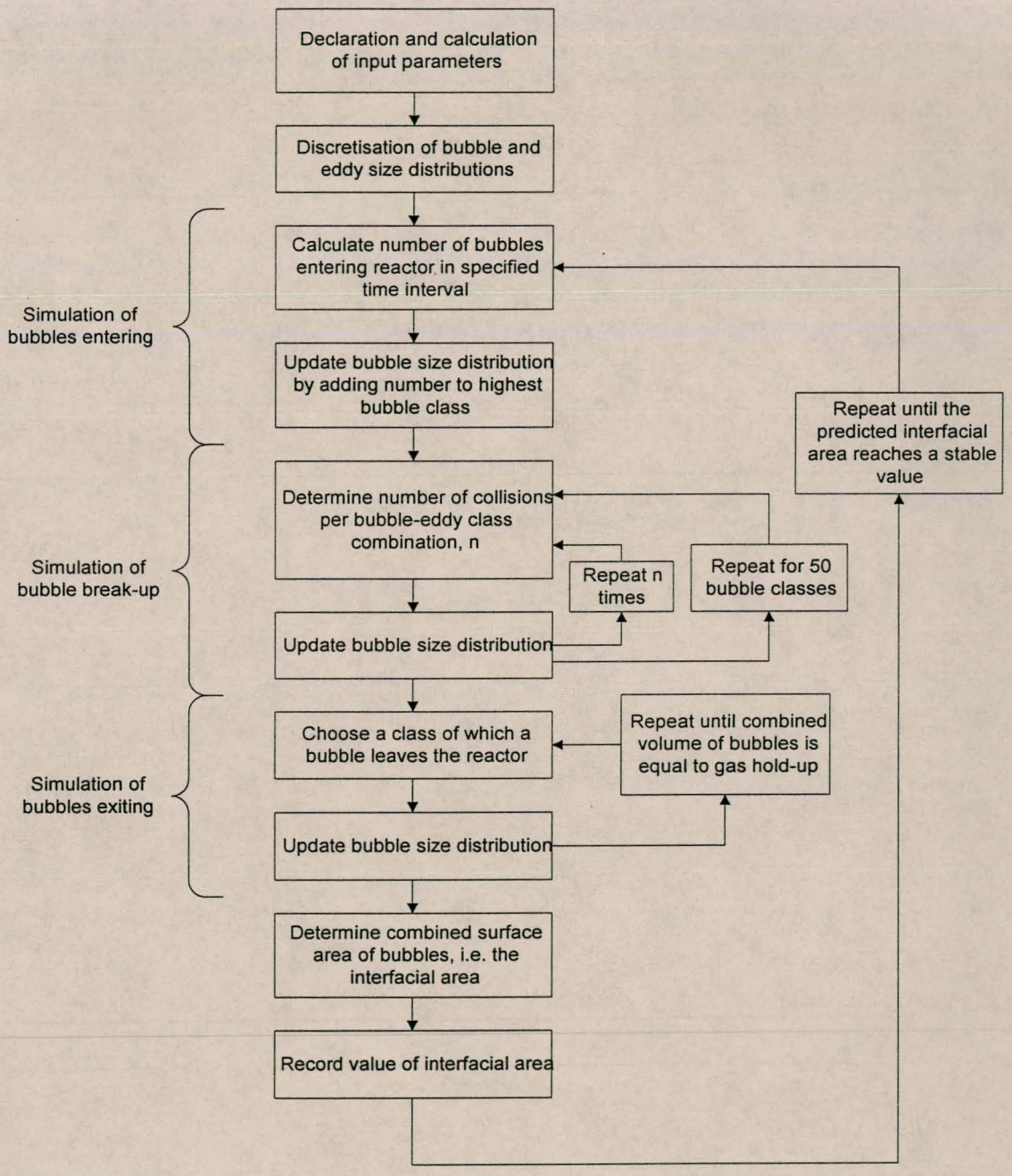

APPENDIX C

TYPICAL EXAMPLE OF THE SIMULATION MODEL

```
Program Model;

Uses CRT32,Math;

const
    bklasse = 50    ;  {number of bubble classes}
    eklasse = 200   ;  {number of eddy classes}
    dbmin  = 0.0001 ;  {smallest bubble diameter}

    rho   = 1000    ;  {liquid density, kg/m^3}
    mul   = 855e-6  ;  {liquid viscosity, N.s/m^2 = Pa.s}
    mug   = 15e-6   ;  {gas viscosity, N.s/m^2 = Pa.s}
    Q     = 717e-4  ;  {liquid surface tension, N/m}

    Vr    = 20e-6   ;  {reactor volume, m^3}
    T     = 298     ;  {temperature in reactor, K}


var
   datfile : text;
   breek : boolean;  {procedure breekeff: true=break, false=does not break}
   Vg,Vl,eps,dklasb,demin,dbin,dtyd,totaal,xbreek,Pg,Vgg,Pl,Kf,dbmax  : real;
   nb,BV : array[1..bklasse] of real;   {amount of bubbles/eddies per class}
   ne,de : array[1..eklasse] of real;
   area : array[1..100] of real;
   BM : array[1..bklasse,1..eklasse] of real;
   b,e,zxz : integer;
   path : string;
```

```
  Vll,Ghold,Ke,Km : real;


Function db(x:integer):real;    {gives bubble diameter for given class number}
   Begin
      db := dbmin - (dklasb/2) + (dklasb * x);
   End;


Function bklas(y:real):integer;
{gives class number for given bubble diameter}
   Begin
      bklas := round( (y - dbmin + (dklasb/2)) / dklasb );
   End;


Function volgas : real;  {determines total volume of gas in reactor}
var
   konst : real;
   i : integer;

   Begin
      konst := 0;
     For i := 1 to bklasse do begin
       konst := konst + ( (PI/6) * db(i)*db(i)*db(i) * nb[i] );
     end;
      volgas := konst;
   End;


Function interarea : real;   {determines interfacial area}
var
   konst : real;
   i : integer;
```

```
  Begin
     konst := 0;
    For i := 1 to bklasse do begin
      konst := konst + ( PI * db(i) * db(i) * nb[i] );
    end;
     interarea := konst;
  End;


Procedure Invoer;   {determines input parameters}
const
     R    = 189      ;   {gas constant, J/kg.K}
     duit = 0.006    ;   {diameter of reactor outlet, m}

var
   Pr,Einl,Eing,rhog,rhogem : real;

  Begin
    Vg := GHold*Vr;              {gas hold-up, m^3}
     Vl := Vr - Vg;              {liquid hold-up, m^3}
     rhog := 1e5 / (R*T);        {gas density, kg/m^3}
     {rhogem := rho*(Vl/Vr) + rhog*(Vg/Vr);  {average density in reactor}
     rhogem := (rho*Vll)/(Vll+Vgg);
     Pr := 1e5 + (rhogem/2)*sqr( (Vgg+Vll) / (0.7854*duit*duit));
     Pr := Pr / 1000;  {pressure in reactor, kPa)}
     Einl := 1000 * (PI - Pr) * Vll;
     Eing := 1e5*Vgg*Ln(Pg/Pr);
     eps := (Einl) / (rho*Vl);  {Energy dissipation / mass liquid, J/kg.s}
  End;


Procedure Verspreidings;   {Fixes initial distribution}
```

```
var
   f,dlaag, dhoog : real;

    Begin
       dbmax := Km * 0.0188 * exp((-0.4)*Ln(eps));
       dklasb := (dbmax - dbmin) / bklasse ;    {class size of bubble}
       demin := dbmin/10;    {smallest eddy diameter which can lead to coll.}
       dlaag := demin;
       f := exp( (Ln(dbmax/demin)) / eklasse );
       dbin := db(bklasse);  {only one bubble size enters reactor}

      For e := 1 to eklasse do begin  {determine ne[e] : stays constant}
       dhoog := f * dlaag;   {borders of eddy classes}
       de[e] := (dlaag + dhoog) / 2;
       ne[e] := (Vl*(0.8/3) * (exp(-3*Ln(dlaag)) - exp(-3*Ln(dhoog))));
       dlaag := dhoog;
       end;

      For b := 1 to bklasse do begin
       nb[b] := 0;          {initially number of bubbles in each class = 0}
      end;

       nb[bklasse] := round(6*Vg / (Pi*dbin*dbin*dbin));
       {Initial bubble size distribution}
    End;


Procedure Botsmatrix;
{Static matrix to reduce number of computations per cycle}
var
   uue,uc,Qe,Qb,Ai,Bi : real;

    Begin
       For b := 2 to bklasse do begin
```

```
          Qb := db(b);

         For e := 1 to eklasse do begin
          Qe := de[e];

          If (Qe > Qb)       {eddy is larger than bubble ...}
{           or ((5*Qe) < Qb)   {bubble more than 5x larger than eddy...}
      {   or ((Qb/1.26) < dbmin)
      {if split up bubble is smaller than smallest class}
          then BM[b,e] := 0

          else begin
          Ai := 0.27768*exp((1/3)*Ln(eps)) / Vr;
          Bi := sqr(Qb+Qe)*sqrt( exp((2/3)*Ln(Qb)) + exp((2/3)*Ln(Qe)) );
          uc := Ke * exp((1/12)*Ln(mul/mug))*exp(0.5*Ln(Q/(rho*Qb)));
          {critical velocity needed for bubble breakup, m/s}
          uue := 2 * exp((2/3)*Ln(eps*Qe));  {u^2 : square of eddy velocity, m/s}
          BM[b,e] := Ai*Bi*exp(-sqr(uc)/uue);   {amount of bubbles that break}
         end;

        end;
       end;
    End;


Procedure InSim;  {simulates bubbles entering the reactor}
const
    aantal = 2    ;   {amount of bubbles entering in time element}

    Begin
       dtyd := (aantal*PI*dbin*dbin*dbin) / (6 * Vgg);
       nb[bklasse] := nb[bklasse] + aantal;
    End;
Procedure Botsvektor;  {initiate collision vector BV[b] }
```

```
var
  deltaBV: real;

   Begin
      totaal := 0;  {total amount of effective collisions per time}
      BV[1] := 0;  {bubbles in smallest class do not lead to effective collisions}

      For b := 2 to bklasse do begin
        BV[b] := 0;

       For e := 1 to eklasse do begin

        deltaBV := nb[b]*ne[e]*BM[b,e];
        BV[b] := BV[b] + deltaBV;
       end;
        totaal := totaal + BV[b];
      end;
   End;


Procedure Klaskies;
{Choose cell from BM proportional to collision probability}
var
  kans : real;

   Begin
     repeat
      kans := totaal * random;
      {kans (chance) = random number between 0 and total}
      b := 1;
     repeat
      b := b + 1 ;
      kans := kans - BV[b];     {subtract cell until kans < 0}
     until (kans < 0);
```

```
  until (nb[b] > 0);
 End;


Procedure BreekSim;  {Simulates bubble break-up}

{One collision matrix is set up and used for the whole cycle, e.g.
collision matrix is not recomputed after each cycle}
var
   bkvoor, bkna : integer;
   botsings, j : longint;
   rand : real;

   Begin
      Botsvektor; {OUTPUT: BV, total}

      botsings := round(dtyd * totaal);
      {Amount of collisions in cycle..e.g. amount of collisions in time dtyd}
      writeln('Collisions =  ',botsings);
     If botsings < 1 then begin
      Writeln('Aantal botsings is kleiner as een: botsings = ',botsings);
      Readkey;
     end;

     For j := 1 to botsings do begin
      Klaskies;     {OUTPUT: b of bubble class associated with collision}
      bkvoor := b;
      rand := random;       {bubble volume is divided into 2 random parts}
      bkna := bklas( db(bkvoor) * exp((1/3)*Ln(rand)) );
     If bkna > 0 then nb[bkna] := nb[bkna] + 1;
      bkna := bklas( db(bkvoor) * exp((1/3)*Ln(1 - rand)) );
     If bkna > 0 then nb[bkna] := nb[bkna] + 1;
      nb[bkvoor] := nb[bkvoor] - 1;
     end;
```

```
End;


Procedure Uitvloei;  {Simulates bubbles exiting the reactor}
var
   chance : real;
   aantalb : array[1..bklasse] of real;

    Begin
       totaal := 0;
      For b := 1 to bklasse do begin

      If nb[b] < 0 then begin
       Writeln('Borrelsel met negatiewe aantal borrels: sel ',b);
       Readkey;
       end;

       aantalb[b] := nb[b];              {determining the total amount}
       totaal := totaal + aantalb[b];    {of bubbles in the reactor}
      end;

      repeat
       chance := totaal * random;
       b := 0;

      repeat
       b := b + 1;
       chance := chance - aantalb[b];
      until (chance < 0);

       If nb[b] > 0 then nb[b] := nb[b] - 1;

     until (volgas < Vg);
   End;
```

```
Procedure Simulasie;
{Calls Insim, Breeksim, Uitvloei & repeat until interfacial area converges}
var
  zz : real;
   zx : integer;

   Begin
     Writeln ('Interfacial area = ', (interarea/Vr):0:0, ' m^2/m^3');

    For zxz := 1 to 10 do begin
     area[zxz] := (interarea/Vr);

     For zx := 1 to 2000 do begin
      Insim;
      Breeksim;
      Uitvloei;
      zz := interarea;
      Writeln ('Interfacial area = ', (zz/Vr):0:0, ' m^2/m^3    ',zx,'/',zxz);
     end;
    end;
   End;


Procedure Lopie;  {simulation of one whole run}
var
  qaz : integer;

Begin
   clrscr;
   Invoer;
   Verspreidings;
   Botsmatrix;
   Randomize;
  For qaz := 1 to 10 do begin
```

```
    area[qaz] := 0;
  end;
    Simulasie;
End;


Procedure Filewrite;  {write output to file}
var
    datdir,savenum,Kes : string;
    qaz,xxx : integer;
    bo, onder, sombo, somonder, sauter : real;

Begin
    xxx := round(Pg-100);
    str(xxx,savenum);
    str(Kfe:3:1,Kes);
    datdir := path+'_'+Kes+'_Kenn'+savenum+'.dat';
    assign(datfile,datdir);
    rewrite(datfile);

  For qaz := 1 to 10 do begin
   Writeln(datfile,round(area[qaz]));
  end;

 Writeln(datfile,'   ');

  For qaz := 1 to bklasse do begin
   Writeln(datfile,db(qaz));
  end;


 Writeln(datfile,'   ');

 For qaz := 1 to bklasse do begin
```

```
  Writeln(datfile,nb[qaz]);
 end;

 Writeln(datfile,'   ');

 sombo:= 0;
 somonder := 0;
 sauter := 0;
 For qaz := 1 to bklasse do begin
  bo := nb[qaz]*(db(qaz))*(db(qaz))*(db(qaz));
  onder := nb[qaz]*(db(qaz))*(db(qaz));
  sombo := sombo + bo;
  somonder := somonder + onder;
 end;
 sauter := sombo/somonder;
 Writeln(datfile,sauter);


 close(datfile);
end;



{-------------------------MAIN PROGRAM-----------------------------}

BEGIN

  Ke := 5;       {Allowed range 4 - 8}
  Kf := 9e-4;
  Km := 1;

  {Liquid 16}
  path := 'c:\ModelOutputs\BREs\CO2-16_' ;
  Vll := 2.0167e-5;
```

```
Pl := 286;
{Gas 10}
Pg := 35 + 100;
Vgg := 0.00016667;
GHold := 0.29;
Lopie;
Filewrite;

{Gas 15}
Pg := 80 + 100;
Vgg := 0.00025;
Ghold := 0.36;
Lopie;
Filewrite;

{Gas 20}
Pg := 140 + 100;
Vgg := 0.0003333;
GHold := 0.43;
Lopie;
Filewrite;


{Liquid 18}
path := 'c:\ModelOutputs\BREs\CO2-18_' ;
Vll := 2.267e-5;
Pl := 341;
{Gas 10}
Pg := 35 + 100;
Vgg := 0.00016667;
GHold := 0.29;
Lopie;
Filewrite;
```

```
{Gas 15}
Pg := 80 + 100;
Vgg := 0.00025;
Ghold := 0.36;
Lopie;
Filewrite;

{Gas 20}
Pg := 140 + 100;
Vgg := 0.0003333;
GHold := 0.43;
Lopie;
Filewrite;


{Liquid 20}
path := 'c:\ModelOutputs\BREs\CO2-20_' ;
Vll := 2.533e-5;
Pl := 376;
{Gas 10}
Pg := 35 + 100;
Vgg := 0.00016667;
GHold := 0.29;
Lopie;
Filewrite;

{Gas 15}
Pg := 80 + 100;
Vgg := 0.00025;
Ghold := 0.36;
Lopie;
Filewrite;

{Gas 20}
```

```
Pg := 140 + 100;
Vgg := 0.0003333;
GHold := 0.43;
Lopie;
Filewrite;


{Liquid 22}
path := 'c:\ModelOutputs\BREs\CO2-22_' ;
Vll := 2.8e-5;
Pl := 445;
{Gas 10}
Pg := 35 + 100;
Vgg := 0.00016667;
GHold := 0.29;
Lopie;
Filewrite;

{Gas 15}
Pg := 80 + 100;
Vgg := 0.00025;
Ghold := 0.36;
Lopie;
Filewrite;

{Gas 20}
Pg := 140 + 100;
Vgg := 0.0003333;
GHold := 0.43;
Lopie;
Filewrite;
{Liquid 24}
path := 'c:\ModelOutputs\BREs\CO2-24_' ;
Vll := 3.1e-5;
```

```
Pl := 514;
{Gas 10}
Pg := 35 + 100;
Vgg := 0.00016667;
GHold := 0.29;
Lopie;
Filewrite;

{Gas 15}
Pg := 80 + 100;
Vgg := 0.00025;
Ghold := 0.36;
Lopie;
Filewrite;

{Gas 20}
Pg := 140 + 100;
Vgg := 0.0003333;
GHold := 0.43;
Lopie;
Filewrite;


{Liquid 26}
path := 'c:\ModelOutputs\BREs\CO2-26_' ;
Vll := 3.4e-5;
Pl := 652;
{Gas 10}
Pg := 35 + 100;
Vgg := 0.00016667;
GHold := 0.29;
Lopie;
Filewrite;
```

```
{Gas 15}
Pg := 80 + 100;
Vgg := 0.00025;
Ghold := 0.36;
Lopie;
Filewrite;

{Gas 20}
Pg := 140 + 100;
Vgg := 0.0003333;
GHold := 0.43;
Lopie;
Filewrite;


END.
```

APPENDIX D

PUBLICATIONS FROM THIS DISSERTATION

The following article was presented at the 4th International Conference on Gas-Liquid and Gas-Liquid-Solid Reactor Engineering at the University of Delft, The Netherlands on 22 – 25 August 1999.

It was also published in *Chemical Engineering Science*, Vol. **54**, November 1999.

THE DEVELOPMENT AND MODELLING OF HIGH INTENSITY IMPINGING STREAM JET REACTORS FOR EFFECTIVE MASS TRANSFER IN HETEROGENEOUS SYSTEMS

A.W. Kleingeld, L. Lorenzen[1], F.G. Botes[2]

Mineral Processing and Environmental Systems Group

Department of Chemical Engineering, University of Stellenbosch

Private Bag X1, Matieland, 7602, Stellenbosch, South Africa

Tel.: +27 (021) 808 4485

Fax: +27 (021) 808 2059

---

[1]Author for correspondence. E-mail address: LL1@ing.sun.ac.za

[2] Present address: Sastech Technology (Pty) Ltd., P.O. Box 1, Sasolburg, 9570, South Africa

Abstract - A novel type of phase contacting device has been researched and is currently being developed at this institution. These high intensity *jet* reactors provide significant improvement over conventional phase contacting equipment due to the impingement of high velocity feed streams upon each other in relatively small reactor volumes, resulting in a highly turbulent mixing of phases. Due to this intimate contact between phases, mass transfer coefficients (k_L) of up to 1.5×10^{-3} [*m/s*] have been realised, which, coupled with values of the specific interfacial area (a) of 8 - 18 000 [m^2/m^3], have yielded volumetric mass transfer coefficients ($k_L a$) of up to 22 [s^{-1}] which are orders of magnitude higher than typical values obtained by conventional systems. A model for the prediction of the interfacial area production in these new reactors has also been proposed. It is implemented in the form of a Monte Carlo simulation, based on the fact that bubble breakup in a turbulent environment is governed by the interactions of bubbles with turbulent eddies. Although the model is only a first attempt, it has proved to be highly practical and flexible, reasonably predicting trends in the experimental data.

Keywords: gas-liquid, impinging streams, mass transfer, bubble size distributions, interfacial area, Monte Carlo simulations.

1. INTRODUCTION

Multiphase reactors, with specific reference to gas-liquid systems, play a key role in chemical (including pharmaceutical and biochemical) process industries as is evident in the application of spray and bubble columns in processes such as gas scrubbing operations and aeration reactions (e.g. fermentation reactions). Most of these systems are characterised by the fact

that transfer rates are limited by the transport of gas to the liquid phase and hence by the overall interfacial area available for mass transfer. These rates in turn limit productivity and are thus a critical design consideration.

Although the introduction of venturi and spray absorbers, as well as a variety of jet loop reactors, have provided better results than the conventional bubble column set-ups to some extent, they have as yet failed to fully realise the advantages of highly turbulent contacting of phases. Research in the field of impinging stream (IS) jet reactors has, however, provided a means to achieve just this. *Elperin* (1972) and *Tamir* (1994) have provided evidence of the intensification of mass and heat transfer processes in heterogeneous systems with the use of IS technology, claiming k_La values of up to 1.22 [s^{-1}], compared to typical values of 0.25 - 0.8 [s^{-1}] for conventional equipment. It has therefore been decided to investigate the intensification of the mechanisms underlying IS technology for maximum interfacial area production and mass transfer.

A fundamental model for the prediction of the interfacial area production in the reactors has been proposed in the form of a Monte Carlo simulation. This paper will focus on its principles and development and compare predicted values with experimental values.

2. EXPERIMENTAL

Setup

The chemical absorption of carbon dioxide into sodium hydroxide solutions was chosen to characterise and quantify the performance of the reactors by way of the following reaction:

$$CO_2 + 2OH^- \Rightarrow CO_3^{2-} + H_2O \qquad (1)$$

A schematic diagram of the experimental setup is shown in *Figure 1*.

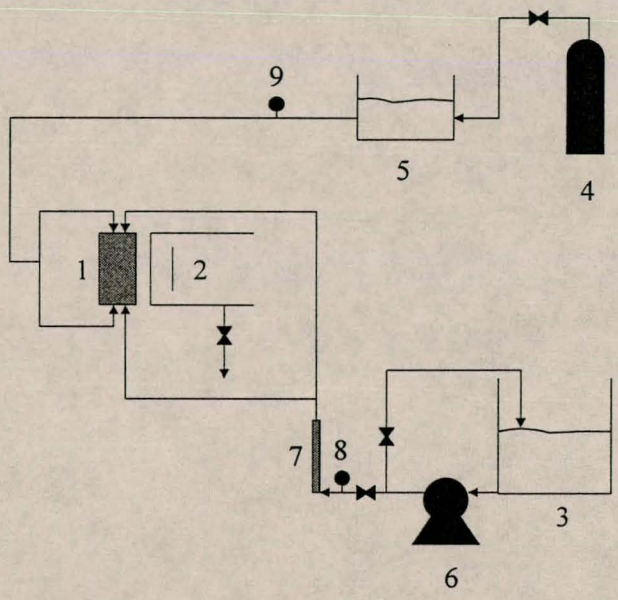

Figure 1 *Diagram of the experimental setup (Refer to text for legend)*

99% pure NaOH pellets were mixed with distilled water (with a conductivity of ~ 1 □mhos) in a *liquid feed mixing tank* (3), after which the *liquid feed pump* (6) was started and the mixing of the contents of the tank continued for 10-15 minutes under full pump recycle to ensure a homogeneous liquid feed concentration. CO_2 gas was supplied from a *feed cylinder* (4) through a coil in

a *water bath* (5) in order to ensure a relatively constant gas feed temperature (measured with a *thermocouple* (9)) in the range of 25 – 27 °C.

After setting the gas flow rate at the required setting, the liquid feed valve to the reactor was opened. A *rotameter* (7) and *liquid pressure gauge* (8) measured the liquid flow rate and pressure. Both liquid and gas feed streams were split up into two and injected into the four impinging streams *reactor* (1) via nozzles. Stainless steel *Spraying Systems* TG-1 nozzles were used for liquid injection and TX-2 nozzles for gas. The two-phase mixture exiting the reactor entered the *phase separator* (2) supplied with a baffle, where a 100 [ml] sample of the liquid was taken for analysis. An excess of barium chloride was added to the sample (to precipitate the carbonate ions formed during reaction) and left to settle, after which the residual NaOH concentration was determined by acid titration with hydrochloric acid using methyl red as indicator.

All reactors were operated in the bubble regime since practically all the resistance to mass transfer is in the liquid phase (hence k_L) and it has been proven by *Tamir* (1994) to exhibit superior performance over spray absorption. The range of operating conditions is as follows:

Table 1 *Range of operating conditions*

Experimental parameter	Range of operating conditions
Reactor volume	8 – 20 *ml*
Liquid flow rate	1.21 – 2.04 *l/min*
Liquid pressure	180 – 550 *kPag*
Gas flow rate	10 – 20 *l/min*
Gas pressure	35 – 140 *kPag*
NaOH feed concentrations	0.25 – 0.5 *M*

It has been found that two (the so-called *kite-shaped* and *π-shaped* reactors: see *Figure 2*) of the seven reactor designs tested as yet have exhibited superior performance over the others. Results for these two reactors will be discussed and compared with model predictions.

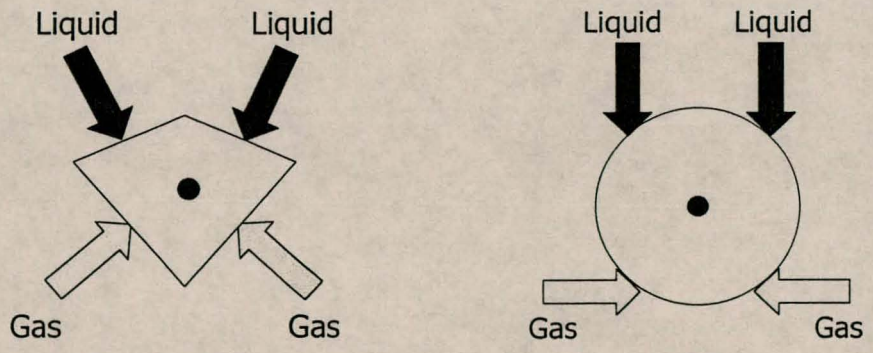

Figure 2 *Simplified diagrams of reactor designs: (A) Kite-shaped reactor (B) π-shaped reactor (Front view).*

Determination of the Mass Transfer Parameters

Mass transfer parameters were determined by way of a new chemical technique proposed by *Botes et al.* (1998) at this institution. The basis of this technique is the determination of the chemical enhancement factor E by way of two chemical absorption experiments at different concentrations but under identical hydrodynamic conditions (which should theoretically yield a single value k_L value for both runs), compared to the method used by *Herskowits et al.* (1990) where *E* is determined by comparing the absorption rate for chemical absorption (CO_2 + NaOH) with that of physical absorption (CO_2 + H_2O).

Although absolute values of the enhancement factor could not be determined, the ratio of *E*-values could be computed from the ratio of absorption rates for the two runs through the following relationship:

$$\left(\frac{E_1}{E_2}\right)=\left(\frac{\dot{N}_1}{\dot{N}_2}\right)\left(\frac{C^*_{A1}}{C^*_{A2}}\right) \qquad (2)$$

Therefore the values of E_1 and E_2 and the value of k_L common to both runs needed to be calculated. However, since the ratio between E_1 and E_2 could experimentally be determined via absorption rates, only two independent variables needed to be solved. The following equation (an approximation to numerical solutions of simultaneous partial differential equations for second order reactions) was employed to find a unique solution for these two variables:

$$E=\frac{\sqrt{M(E_i-E)/(E_i-1)}}{\tanh\sqrt{M(E_i-E)/(E_i-1)}} \qquad (3)$$

where

$$M = \frac{D_A k_2 C_{BO}}{k_L^2} \tag{4}$$

$$E_i = \frac{1}{erf\left(\beta / \sqrt{D_A}\right)} \tag{5}$$

and β is defined by:

$$e^{\beta^2/D_B} erfc\left(\beta/\sqrt{D_B}\right) = \frac{C_{BO}}{zC_A^*}\sqrt{\frac{D_B}{D_A}} e^{\beta^2/D_A} erf\left(\beta/\sqrt{D_A}\right) \tag{6}$$

An iterative mathematical strategy was followed to solve for k_L, E_1 and E_2. At the start of the procedure, k_L was assigned an initial value, after which values for E_1 and E_2 were calculated with equation (3). The ratio of the calculated E values was then compared to the experimentally determined ratio and a better value was assigned to k_L until the system converged. Enhancement factors determined in this way were verified with existing models such as those proposed by *De Coursey* (1974) and *Baldi & Sicardi* (1975): typically *E*-values determined with these explicit models did not deviate from our results by more than 2%.

3. MODELLING

Model development

Since the reactors were always operated in the bubble regime, the total interfacial area could simply be determined from the combined surface area of the bubbles in the reactor. To determine the bubble size distributions present for any given set of hydrodynamic conditions, the simulation had to

account for: (1) the size of bubbles entering the reactor, (2) the processes of bubble break-up and coalescence and (3) the size of bubbles exiting the reactor.

Size of bubbles entering the reactor: Bubble formation from an orifice in turbulent flow was approximated by bubble formation in liquid cross flow, using a simple statistical correlation from *Marshall et al.* (1993). Adapting the numerical coefficient for non-perfect cross flow and incorporating with it the r_o term (since only one type of gas nozzle was used), the equation could be simplified to yield the following (assuming that liquid velocity $\propto$ liquid flow rate):

$$d_{b,i} = K_f \left(\frac{\dot{V}_G}{\dot{V}_L} \right)^{0.36} \tag{7}$$

where K_f is a free parameter which has to be specified when the model is applied.

Bubble coalescence: According to *Craig et al.* (1993), certain electrolytes (including NaOH) have a stabilising effect on bubbles beyond a certain concentration, thereby effectively inhibiting bubble coalescence. Since the NaOH concentrations measured during experimental runs were much higher than transitional concentrations quoted, it was decided not to incorporate bubble coalescence into the model.

Bubble break-up: Bubble break-up was treated analogous to the approach followed by *Prince* (1990) for the modelling of bubble behaviour in bubble

columns. In order to evaluate bubble break-up rates, expressions for both the collision rate/frequency and collision efficiency had to be determined:

Collision rate: Collisions were modelled analogous to the mechanism of particle collisions in an ideal gas (assuming homogeneous isotropic turbulence and eddies in the inertial subrange) where collision rate is a function of bubble and eddy diameters and the energy dissipation in the system:

$$\theta_{b,e} = \frac{\pi}{8\sqrt{2}} \varepsilon^{1/3} n_b n_e \left(d_b + d_e\right)^2 \left(d_b^{2/3} + d_e^{2/3}\right)^{1/2} \tag{8}$$

where the concentration of eddies belonging to a certain diameter can be determined by:

$$n_e = \rho_L \int_{k_1}^{k_2} 0.1 \frac{k^2}{\rho_L} dk = \frac{0.8}{3} \left(d_{low}^{-3} - d_{high}^{-3}\right) \tag{9}$$

Collision efficiency: It was assumed that the fraction of collisions between bubbles and eddies that result in globule break-up, is equal to the fraction of eddies with velocities in excess of the critical velocity. The energy distribution function as provided by *Angelidou et al.* (1979) is used to approximate this fraction:

$$Y = \frac{\int_{E_c}^{\infty} \psi(E) dE}{\int_{0}^{\infty} \psi(E) dE} \tag{10}$$

which, after evaluating the integrals and taking the energy of an eddy as proportional to its velocity, leads to the following expression for the collision efficiency:

$$Y = \exp\left(-\frac{u_c^{\,2}}{\overline{u_e^{\,2}}}\right) \tag{11}$$

where u_c^2 can be determined from the expression for the Weber number:

$$u_c^{\,2} = K_e\left(\frac{\sigma}{\rho_L d_b}\right) \tag{12}$$

and u_e^2 by the following equation:

$$\overline{u_e^{\,2}} = 2\varepsilon^{2/3} d_e^{\,2/3} \tag{13}$$

Model implementation

The model was implemented in the form of a Monte Carlo simulation by discretising bubble and eddy sizes into intervals of equal size. During each step of the simulation, the total amount of effective collisions between bubbles and eddies was determined by summing the collisions in each class whereafter collision efficiencies were calculated to find the total effective bubble break-up rate. Bubbles were then assumed to break into 2 random fractions, after which the bubble size distribution was updated for the next step of the simulation.

4. RESULTS & MODEL EVALUATION

Figure 3 provides a summary of the results obtained for the two mentioned reactors (π and kite) as a function of liquid flow rate. As can be seen, an increase in both the gas and liquid flow rates causes an increase in the volumetric mass transfer coefficient, although the effect of gas flow rate is much more pronounced than that of the liquid flow rate. It was also found that the value of k_L remained relatively constant in the range of liquid flow rates used, but increased markedly with an increase in gas flow rates from $8x10^{-4}$ to $1.5x10^{-3}$ [*m/s*]. These results are in good agreement with results obtained by *Herskowits et al.* (1990) who, for their two-phase impinging jet absorber, have reported that the effect of gas flow rate on interfacial area production is "almost one order of magnitude" higher than for the liquid flow rate.

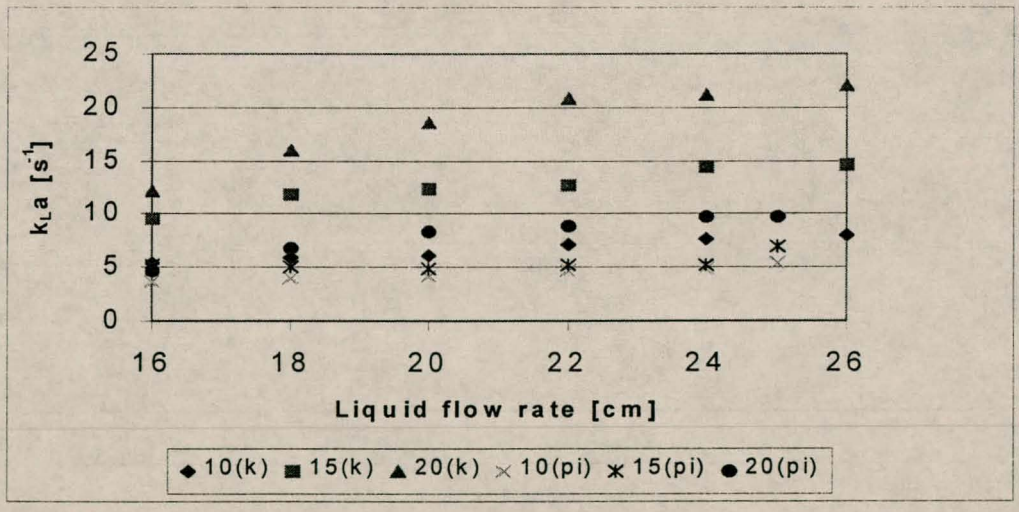

Figure 3 *Volumetric mass transfer coefficient (k_La) vs liquid flow rate (rotameter readings) for the kite (k) and □ (pi)-shaped reactors at different gas flow rates.*

As can be seen from *Figure 4*, experimental data is reasonably well predicted by the model. Close comparison of the predicted and experimental data does, however, show that the model does not satisfactorily predict the strong influence of an increase in gas flow rate on interfacial area *at a constant liquid flow rate* as is illustrated by the difference in gradient between experimental and predicted trends. This can be explained by the fact that the model only takes into account the energy introduced to the system via the liquid feed nozzles. Due to the fact that the mass transfer coefficient is a function of turbulence and liquid parameters, as proposed by *Bouaifi & Roustan* (1998), and the fact that k_L is strongly dependent on gas flow rate (as shown above), one can only conclude that the gas introduced to the system also contributes to the turbulent energy in the reactor and must therefore be incorporated into a future model.

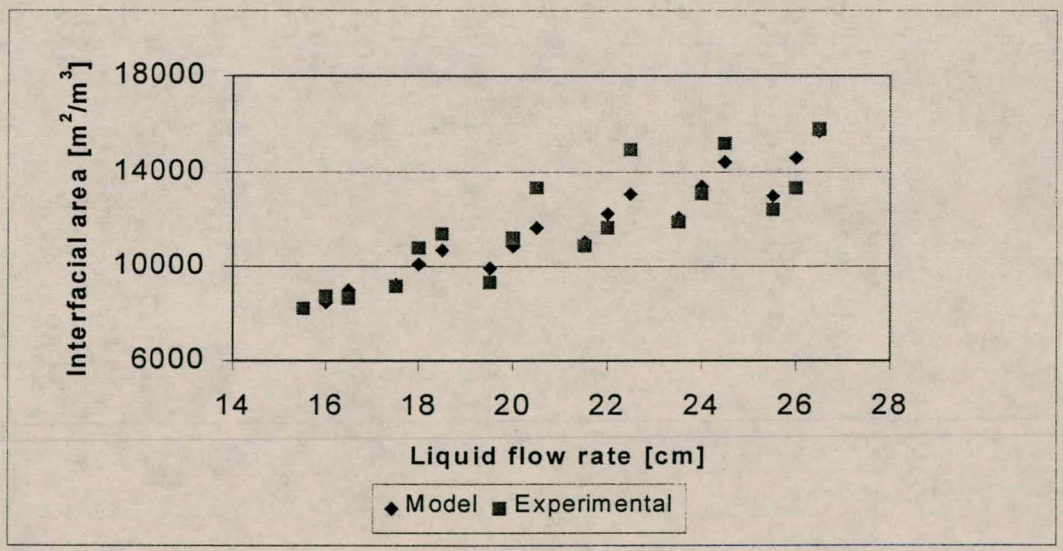

Figure 4 *Model evaluation: Comparison between predicted (Ke: 18 and Kf: $9x10^{-4}$ m) and experimental data (at each liquid flow rate, the gas flow rate is plotted for 10, 15, 20 l/min)*

5. CONCLUSIONS & RECOMMENDATIONS

It has been shown that these newly developed high intensity jet reactors deliver performance figures which are orders of magnitude higher than those achieved by conventional designs. Continued research into these reactors and the intensifying of impinging stream principles is therefore warranted to find an optimum design incorporating the best performance (in terms of interfacial area production and mass transfer) while keeping in mind power consumption.

Although it has been shown that the model reasonably predicts trends in experimental data, certain areas have been identified where the model needs further improvement. The mechanism of bubble coalescence will have to be incorporated into the model for it to be representative of most other gas-liquid systems. Due to the fact that gas introduced into the system has been proven to contribute to the introduction of turbulent energy into the system, it will have to be coupled with the energy introduced by the liquid to obtain an expression for the total energy dissipated in the reactor. Lastly, the model will have to be tested against other gas-liquid systems to verify the fundamental nature and general applicability of the model. Ways of adapting the model for the prediction of interfacial area production in liquid-liquid dispersions can also be investigated.

NOTATION

a	interfacial area [m^2/m^3]
C_A^*	equilibrium concentration of dissolved CO_2 at interface [mol/l]
C_{BO}	Concentration of dissolved NaOH in bulk of liquid [mol/l]
d_b	bubble diameter [m]
$d_{b,i}$	diameter of bubble exiting from nozzle in cross flow [m]
d_e	eddy diameter [m]
d_{low}, d_{high}	upper and lower integration limits for determination of n_e [m]
D_A	diffusivity of dissolved CO_2 [m^2/s]
D_B	diffusivity of reactant NaOH [m^2/s]
E	chemical enhancement factor
E_c	critical energy needed to rupture a bubble [J]
E_i	instantaneous enhancement factor
k_1, k_2	eddy wave numbers, upper and lower integration limits
k_2	second order reaction rate constant [l/mol.s]
K_e	free parameter
K_f	free parameter [m]
k_La	volumetric mass transfer coefficient [s^{-1}]
$\dot{N}$	absorption rate per unit volume of reactor [mol/l.s]
n_b	number (concentration) of bubbles in a class
n_e	number (concentration) of eddies in a class
r_b	radius of bubble exiting nozzle [m]
r_o	radius of nozzle orifice [m]

u_c	critical velocity for bubble break-up [m/s]
u_e	critical eddy velocity [m/s]
$u_{G,o}$	velocity of gas exiting nozzle orifice [m/s]
u_L	velocity of liquid in crossflow [m/s]
V_G	gas flow rate [m^3/s]
V_L	liquid flow rate [m^3/s]
We	Weber number
Y	fraction of eddies with enough energy to rupture a bubble

Greek letters

σ	surface tension [N/m]
$\Psi(E)$	energy distribution function
ρ_L	liquid density [kg/m^3]
$\theta_{b,e}$	collision rate between bubbles and eddies [$m^{-3}s^{-1}$]
ε	energy dissipation rate per mass [J/kg]

REFERENCES

1) Angelidou, C., Psimopoulos, M., Jameson, G.J. (1979) Size distribution functions of dispersions. *Chemical Engineering Science* **34**, pp. 671-676.

2) Baldi, G.C., Sicardi, S. (1975) A model for mass transfer with and without chemical reaction in packed towers. *Chemical Engineering Science* **30**, pp.623.

3) Botes, F.G., Lorenzen, L., Van Deventer, J.S.J. (1998) The Development of High Intensity Gas-Liquid Jet Reactors. *Chemical Engineering Communications* **170**, pp. 217-244.

4) Bouaifi, M., Roustan, M. (1998) Bubble Size and Mass Transfer Coefficients in Dual-Impeller Agitated Reactors. *Canadian Journal of Chemical Engineering* **76**, pp.390-397.

5) Breman, B.B., Beenackers, A.A.C.M., Bouma, M.J. and Van der Werf, M.H. (1996) The Gas-Liquid Mass Transfer Coefficient in the Gas-Liquid Multi-Stage Agitated Contactor (MAC). *Transactions of the Institute of Chemical Engineers* **74**, pp.872-881.

6) Craig, V.S.J., Ninham, B.W., Pashley, R.M. (1993) Effect of electrolytes on bubble coalescence. *Nature* **364**, pp. 317-319.

7) De Coursey, W.J. (1974) Absorption with Chemical Reaction: Development of a New Relation for the Danckwerts model. *Chemical Engineering Science* **29**, p.1867.

8) Herskowits, D., Herskowits, V., Stephan, K., Tamir, A. (1988) Characterization of a two-phase impinging jet absorber - II. Absorption with chemical reaction of CO_2 in NaOH solutions. *Chemical Engineering Science* **45**, pp.1281-1287.

9) Marshall, S.H., Chudacek, M.W., Bagster, D.F. (1993) A model for bubble formation from an orifice in liquid cross flow. *Chemical Engineering Science* **48**, pp. 2049 – 2059.

10) Prince, M.J., Blanch, H.W. (1990) Bubble Coalescence and Break-up in Air-Sparged Bubble Columns. *AIChE Journal* **36**, pp. 1485-1499.

11) Tamir, A. (1994) Impinging-Stream Reactors: Fundamentals and Applications, pp.585-660, Elsevier Science, Amsterdam, The Netherlands.